Investigation of P-H, O-H, and Si-H Oxidative Addition Involving Group 9 Metal PSiP Complexes

by

Fabien Lindeperg

Submitted in partial fulfilment of the requirements
for the degree of Doctor of Philosophy

at

Dalhousie University
Halifax, Nova Scotia
March 2019

Table of Contents

List of Tables ..... **v**

List of Figures ..... **vi**

List of Schemes ..... **viii**

Abstract ..... **xi**

List of Abbreviations and Symbols Used ..... **xii**

Acknowledgements ..... **xiii**

Chapter 1: Introduction **1**

1.1 Overview 1

1.2 Ligand Design 1

1.3 Early Development of Pincer Chemistry 4

1.4 C-H Bond Activation by (PCP)Ir Species 6

1.5 (POCOP) Pincer Complexes: Another Efficient System for the Catalytic Transfer Dehydrogenation of Alkanes 11

1.6 N-H Bond Oxidative Addition by (PCP)Ir Species 13

1.7 Silyl Pincer Complexes: A Different Ligand Design 18

1.8 Further Exploration of E-H Bond Activation at (Cy-PSiP)Ir^{I} 23

Chapter 2: Iridium Mediated P-H Bond Oxidative Addition Leading to Terminal Phosphido Hydride Species Supported by PSiP Ligation **25**

2.1 Introduction 25

2.2 Results and Discussion 28

2.2.1 Synthesis of Ir Phosphido Hydride Complexes *via* Salt Metathesis 28

2.2.2 Attempted Synthesis of Rh Phosphido Complexes *via* Salt Metathesis 40

2.2.3 Ir Phosphido Complexes *via* P-H Oxidative Addition 47

2.2.4 Reactivity of Ir Phosphido Hydride Complexes 48

2.3 Summary and Conclusions 57

2.4 Experimental 58

2.4.1 General Considerations 58

2.4.2 Synthetic Details and Characterization Data 59

2.4.3 Crystallographic Solution and Refinement Details 74

Chapter 3: Synthesis of Coordinatively Unsaturated Aryloxo, Alkoxo, and Hydroxo Iridium Complexes Supported by PSiP Ligation and O-H Bond Oxidative Addition Leading to Aryloxo Hydride Ir^{III} Species 78

3.1 Introduction 78

3.2 Results and Discussion 83

3.2.1 Attempted Synthesis of (Cy-PSiP)Ir(OR)H Complexes *via* Salt Metathesis 83

3.2.2 Synthesis of (Cy-PSiP)Ir(OR)H Complexes *via* Protonolysis of an Ir Amido 85

3.2.3 Attempted Synthesis of (Cy-PSiP)Ir(OR)H Complexes *via* O-H Oxidative Addition 89

3.2.4 Preliminary Reactivity Studies of (Cy-PSiP)Ir(OR)H Complexes 93

3.3 Summary and Conclusions 95

3.4 Experimental 96

3.4.1 General Considerations 96

3.4.2 Synthetic Details and Characterization Data 97

3.4.3 Crystallographic Solution and Refinement Details 104

Chapter 4: Iridium Mediated Si-H Bond Oxidative Addition, Synthesis of (Cy-PSiP)Ir-L Complexes Stabilized by a Neutral L Donor and Synthesis of Cationic Ir^{III} and Rh^{III} Species 107

4.1 Introduction 107

4.2 Results and Discussion 112

4.2.1 Early Attempts at Si-H Bond Activation *via* (Cy-PSiP)Ir^{I} and Rh^{I} 112

4.2.2 Synthesis of (Cy-PSiP)IrCO 120

4.2.3 Synthesis and Reactivity of (Cy-PSiP)Rh(CO) 126

4.2.4 Investigation of Other (Cy-PSiP)Ir-L Complexes 128

4.2.5 Synthesis and Reactivity of (Cy-PSiP)Rh^{III} Cationic Species 131

4.2.6 Attempted Synthesis of (Cy-PSiP)Ir(Me)OTf Complex 135

4.2.7 Synthesis of (Cy-PSiP)Rh(Me)OTf 138

4.2.8 Synthesis of (Cy-PSiP)Ir(PMe_3)(Me)OTf Complex 140

4.2.9 Reactivity of (Cy-PSiP)Ir(PMe_3)(Me)OTf Complex 142

4.2.10 Attempts at the Synthesis of (Cy-PSiP)Ir(PMe_3)$(Me)^{+}[B(C_6F_5)_4]^{-}$ Complex 144

4.3 Summary and Conclusions 146
4.4 Experimental 148
4.4.1 General Considerations 148
4.4.2 Synthetic Details and Characterization Data 149
4.4.3 Crystallographic Solution and Refinement Details 163
Chapter 5: Conclusions and Future Work 166
5.1 Summary and Conclusions 166
5.2 Future Work 169
References 172
Appendix A: Crystallographic Experimental Details 187
Appendix B: Selected NMR Spectra of Reported Compounds 213

List of Tables

Table 2-1. Bond dissociation energies (BDE) and pK_a values for selected amines and phosphines. 28

Table 2-2. Selected NMR spectroscopic data (ppm) for complexes 2-1, 2-2a – c, and 2-3a – d. 30

Table 2-3. Selected crystallographic data – interatomic distances (Å) and bond angles (°) for crystallographically characterized complexes (Cy-PSiP)Ir(H)X (X = Cl, amido, anilido, phosphido). 40

Table 2-4. Selected NMR spectroscopic data (ppm) for complexes 2-4a – e. 41

Table 2-5. Preferential dehydrocoupling of $HPPh_2$ over sp^2-C-P cross-coupling catalyzed by (Cy-PSiP)Rh(Ph)Br (2-5). 46

Table 3-1. Bond dissociation energies (BDE) and pKa values for selected substrates.. 80

Table 3-2. Isolated yields (*via* 3-3) and selected NMR spectroscopic data (ppm; benzene-d_6) for (Cy-PSiP)Ir(OR)H alkoxo/aryloxo/hydroxo-hydride complexes. 85

Table 3-3. Selected crystallographic data – interatomic distances (Å) and bond angles (°) for crystallographically characterized complexes (Cy-PSiP)Ir(H)X (X = Cl, anilido, aryloxo). 88

Table 4-1. Selected interatomic distances (Å) and angles (°) for complexes comparison. 117

Table 4-2. Selected interatomic distances (Å) and angles (°) for 4-13 and 4-14. 134

List of Figures

Figure 1-1. Typical design motifs of LXL pincer ligands. 2

Figure 1-2. PCP pincer complexes synthesized by Shaw and co-workers. 4

Figure 1-3. (A) Design of (^{t}Bu-POCOP)Ir pincers; and (B) complexes resulting from the reaction of 14-electron (^{t}Bu-PCP)Ir^I and (^{t}Bu-POCOP)Ir^I with TBE.. 12

Figure 1-4. Examples of complexes supported by multidentate (phosphino)silyl ligation developed by Stobart and co-workers (A) and bis(quinolyl)silyl (NSiN) metal complexes reported by Tilley and co-workers (B). 19

Figure 1-5. PSiP and PSiN (phosphino)silyl pincer complexes developed in the Turculet group. 20

Figure 2-1. Isolable, mononuclear late transition metal phosphido hydride complexes featuring terminal phosphido ligands. 27

Figure 2-2. Crystallographically determined structure of 2-2c with thermal ellipsoids drawn at the 50% probability level. Most hydrogen atoms have been omitted for clarity. 32

Figure 2-3. Correlation of M-PR_2 bonding in transition metal phosphido complexes with hybridization at phosphorus and ^{31}P NMR chemical shift. 35

Figure 2-4. (A) Distorted trigonal bipyramidal (dist-TBP) and square pyramidal (SP) structures accessible to diamagnetic, five-coordinate d^6 complexes; (B) σ-only frontier MOs associated with such structures (adapted from ref. 82); and (C) orientation of PR_2 phosphido ligand required for π-overlap in the dist-TBP scenario. 37

Figure 2-5. Variable temperature (A) ^{31}P{^{1}H} NMR (121.5 MHz) spectra of 2-3c, showing decoalescence of the Cy-PSiP-phosphino resonance; and (B) ^{1}H NMR (toluene-d_8, 300 MHz) spectra of 2-3c, showing decoalescence of the *ortho*-Me resonance involving the PHMes ligand. 37

Figure 2-6. Crystallographically determined structures of 2-3c (A), 2-3d *major* (B), and 2-3d *minor* (C) shown with thermal ellipsoids drawn at the 50% probability level. Selected P*Cy* carbon atoms and most hydrogen atoms have been omitted for clarity, including the calculated P-*H* of 2-3d *minor*. Only one of the two crystallographically independent molecules of 2-3c is shown. 39

Figure 2-7. ^{31}P{^{1}H} NMR spectra (122.5 MHz, benzene-d_6) of: (A)(Cy-PSiP)Rh(Ph)Br (2-5); (B) (Cy-PSiP)Rh(PPh_3) (2-6); (C) (Cy-PSiP)Rh($PHPh_2$) (2-4b); and (D) reaction mixture resulting from treatment of 2-5 with one equiv. $LiPPh_2$, after 18 h at room temperature, followed by 8 h heating at 65 °C. 43

Figure 2-8. Crystallographically determined structures of 2-8b shown with thermal ellipsoids drawn at the 50% probability level. Most hydrogen atoms have been omitted for clarity. 51

Figure 2-9. Partial ^{1}H NMR (300 MHz, benzene-d_6) spectrum of: (A) (Cy-PSiP)Ir(D)(SiDPh$_2$)(PH$_2$Mes) (2-9-d_2) generated by the reaction of (Cy-PSiP)Ir(H)(PHMes) (2-3c) with D$_2$SiPh$_2$; and (B) (Cy-PSiP)Ir(H)(SiHPh$_2$)(PH$_2$Mes) (2-9) generated by the reaction of (Cy-PSiP)Ir(H)(PHMes) (2-3c) with H$_2$SiPh$_2$..... 56

Figure 2-10. (A) ^{2}H NMR spectrum (46.1 MHz, benzene) and (B) ^{1}H NMR spectrum (300 MHz, benzene-d_6) of partially deuterated (Cy-PSiP)Ir(H/D)$_2$(PH$_2$/D$_2$Mes) (2-10-*d*) generated by the reaction of (Cy-PSiP)Ir(H)(PHMes) (2-3c) with D$_2$; and (C) ^{1}H NMR spectrum (300 MHz, benzene-d_6) of (Cy-PSiP)Ir(H)$_2$(PH$_2$Mes) (2-10) generated by the reaction of 2-3c with H$_2$. 56

Figure 3-1. Transition metal alkoxo, aryloxo, and hydroxo complexes. 78

Figure 3-2. Examples of O-H oxidative addition at Ir to afford alkoxo/aryloxo/hydroxo Ir hydride complexes. 82

Figure 3-3. Crystallographically determined structures of 3-2c (A and B; the structure of 3-2c shown in B is the same approximate view as in A, but shows the hydrogen bonding interactions with the co-crystallized HO(4-^{t}BuC$_6$H$_4$) molecules) and 3-4 (C; only the major contributor of the disordered MeSi(C$_6$H$_4$PCy$_2$)$_2$IrH(OH)$_{0.75}$Cl$_{0.25}$ is depicted) with thermal ellipsoids drawn at the 50% probability level. 88

Figure 4-1. Crystallographically determined structures of 4-1 shown with thermal ellipsoids drawn at the 50% probability level. Most hydrogen atoms have been omitted for clarity. 116

Figure 4-2. The crystallographically determined structure of 4-6 shown with 50% displacement ellipsoids. All H atoms have been omitted for clarity. 124

Figure 4-3. The crystallographically determined structure of 4-7•(OEt$_2$)$_{1.5}$(THF)$_{1.5}$ shown with 50% displacement ellipsoids. All H atoms and selected carbon atoms have been omitted for clarity. 125

Figure 4-4. Crystallographically determined structures of 4-9 shown with thermal ellipsoids drawn at the 50% probability level. Hydrogen atoms have been omitted for clarity. 127

Figure 4-5. Crystallographically determined structures of 4-13 and 4-14 shown with 50% displacement ellipsoids. All non-hydrido H atoms have been omitted for clarity. 134

Figure 4-6. The crystallographically determined structure of 4-15 shown with 50% displacement ellipsoids. All H atoms have been omitted for clarity. 137

List of Schemes

Scheme 1-1. Examples of C-C bond oxidative addition by Milstein and co-workers. 5

Scheme 1-2. Two common pathways for C-H bond activation by a metal center. 6

Scheme 1-3. First examples of metal-mediated C-H bond activation by Bergman (A) and Graham (B) and co-workers..... 7

Scheme 1-4. (A) (PCP)Ir pincer complexes developed by Jensen, Goldman, and co-workers for alkane dehydrogenation; (B) transfer dehydrogenation of COA; (C) acceptorless dehydrogenation of cyclodecane. 8

Scheme 1-5. Proposed mechanism for alkane transfer-dehydrogenation by (^{t}Bu-PCP)IrH_2..... 10

Scheme 1-6. Proposed mechanism for acceptorless catalytic dehydrogenation. 11

Scheme 1-7. N-H bond activation of anline by (^{t}Bu-PCP)Ir..... 14

Scheme 1-8. Formation of (^{t}Bu-PCP)Ir(H)(NH_2) and thermal instability. 15

Scheme 1-9. N-H bond activation of ammonia to form an isolable, monomeric Ir^{III} parent amido complex..... 15

Scheme 1-10. The reaction of (^{t}Bu-POCOP)Ir^I with anilines in benzene solution. 17

Scheme 1-11. Generation of (Cy-PSiP)M^I (1-3, M = Ir; 1-4, M = Rh) and reactivity with sp^2-CH bonds. 22

Scheme 1-12. N-H oxidative addition *via* (Cy-PSiP)M^I (M = Rh, Ir). 23

Scheme 1-13. Summary of bond activation reactivity explored in this thesis. 24

Scheme 2-1. Proposed mechanisms for (A) alkene hydrophosphination and (B) phosphine dehydrocoupling that invoke phosphido hydride complexes as intermediates. 25

Scheme 2-2. Reaction of (Cy-PSiP)Ir(H)Cl (1-1) with lithium phosphide reagents..... 29

Scheme 2-3. Synthesis of (Cy-PSiP)Rh(PHRR') complexes by P-H reductive elimination..... 41

Scheme 2-4. Synthesis of complexes 2-5 and 2-6..... 42

Scheme 2-5. Proposed mechanistic pathways for the formation of 2-6 and 2-4b *via* (Cy-PSiP)Rh(Ph)(PPh_2)..... 45

Scheme 2-6. Proposed mechanism for: (A) Pd-catalyzed C-P cross-coupling of aryl halides and triflates, and (B) dehydrocoupling of $HPPh_2$ by Cp*Rh($PHPh_2$)$_2$..... 46

Scheme 2-7. Synthesis of five-coordinate Ir phosphido hydride complexes *via* P-H oxidative addition 48

Scheme 2-8. Reactivity of (Cy-PSiP)Ir(H)(PHMes) (2-3c) with unsaturated substrates. 50

Scheme 2-9. Possible mechanism for the reaction of an Ir phosphido hydride species with a terminal alkyne to afford an alkynyl hydride complex *via* P-H reductive elimination/*sp*-CH oxidative addition. 53

Scheme 2-10. Reactivity of (Cy-PSiP)Ir(H)(PHMes) (2-3c) towards E-H bonds. 54

Scheme 3-1. General synthetic routes to late transition metal alkoxo/aryloxo/hydroxo complexes by: (A) salt metathesis; (B) protonolysis; and (C) O-H oxidative addition. 79

Scheme 3-2. Oxidative addition of N-H and O-H bonds *via* (Cy-PSiP)Ir^{I} (1-3). 80

Scheme 3-3. Mechanisms proposed for O-H oxidative addition at a late metal center involving either: (A) a concerted pathway *via* a three-centered transition state, or (B) a step-wise pathway *via* protonation at the metal. 81

Scheme 3-4. Synthesis of (Cy-PSiP)Ir(OR)H complexes (3-1a – d, 3-2a – c, 3-4, and 3-4*d*) by salt metathesis or protonolysis routes. 84

Scheme 3-5. Possible outer-sphere (A) and inner-sphere (B) pathways for alcohol dehydrogenation. 89

Scheme 3-6. Reactivity of *in situ* generated (Cy-PSiP)Ir (1-3) with alcohol substrates. 91

Scheme 3-7. Reactivity of (Cy-PSiP)$Ir(H)_4$ (3-5) with alcohol substrates and water. 92

Scheme 3-8. Reactivity of (Cy-PSiP)$Ir(C_2H_4)$ (1-5b) with alcohol substrates and water. 93

Scheme 3-9. Insertion reactions with (Cy-PSiP)Ir(OR)H complexes. 94

Scheme 4-1. Synthesis of $[(^{t}$Bu-POCOP)Ir(H)(acetone)$]^{+}$ for use in alkyl halide reduction catalysis. 108

Scheme 4-2. Proposed catalytic cycle for reduction of amides by (^{t}Bu-POCOP)$IrH_3(SiEt_2H)$. 109

Scheme 4-3. Synthesis of a cationic (PNP)Ir silylene complex active for alkene hydrosilylation catalysis. 110

Scheme 4-4. Proposed mechanism for alkene insertion into a cationic (PNP)Ir silylene (A) and synthesis of a catalytically competent Ir^{V} disilyl intermediate (B). 111

Scheme 4-5. Synthesis of five coordinate Ir silyl hydride complexes *via* Si-H oxidative addition. 114

Scheme 4-6. Suggestion of a transformation leading to an iridium silylene complex. 118

Scheme 4-7. Synthesis of (CyPSiP)IrCO (4-5) complex. 122

Scheme 4-8. Synthesis of 4-6 and 4-7 *via* dehydrohalogenation of 4-4a,b. 123

Scheme 4-9. Synthesis of 4-9 *via* dehydrohalogenation of 4-8a,b and reactivity of 4-9 towards E-H bonds and MeI leading to 4-10. 127

Scheme 4-10. Si-H activation chemistry previously observed for complexes of the type [(Cy-PSiP)IrH]X. 132

Scheme 4-11. Synthesis of (Cy-PSiP)Rh^{III} cation-like complexes (4-13 and 4-14). 133

Scheme 4-12. Examples of (Cy-PSiP) complexes undergoing a structural rearrangement. 137

Scheme 4-13. Proposed mechanism for the formation of 4-15. 138

Scheme 4-14. Synthesis of (Cy-PSiP)Rh(Me)OTf (4-16). 139

Scheme 4-15. Synthesis of (Cy-PSiP)Ir(PMe_3)(Me)OTf (4-17) and selected $^{31}P\{^1H\}$; ^1H NMR spectroscopic features of 4-17. 140

Scheme 4-16. Stability of 4-17 and attempt at C-H bond activation of benzene. 141

Scheme 4-17. Synthesis of (Cy-PSiP)Ir(Me)(CO)$(PMe_3)^+(OTf)^-$ (4-19), (Cy-PSiP)Ir(Me)$(NH_3)(PMe_3)^+(OTf)^-$ (4-20) and (Cy-PSiP)Ir(PMe_3)(CC^tBu)(OTf) (4-21). 143

Scheme 4-18. Synthesis of iridium methyl (4-22) and hydride (4-23) cations. 145

Scheme 4-19. Proposed mechanism for the slow transformation of 4-22 overtime. 146

Scheme 5-1. Proposed synthetic strategy for (Cy-PSiP)Ir(H)(=SiR_2) species. 169

Scheme 5-2. Proposal of different ligand variations in backbone, flanking phosphines design and silicon-bound substituents. 170

Abstract

Group 9 transition metal pincer complexes have shown remarkable reactivity with respect to E-H (E = main group element) bond activation chemistry. In this context, this research focuses on developing new Ir and Rh complexes supported by bis(phosphino)silyl ligands of the type[κ^3-(2-$Cy_2PC_6H_4)_2SiMe]^-$ (Cy-PSiP). A prominent feature of this ligand is the presence of a highly *trans*-labilizing and electron donating silyl group located at the central anionic position. These properties may allow for the stabilization of reactive, coordinatively unsaturated compounds. This document details the synthesis of neutral and cationic (Cy-PSiP)M (M = Ir, Rh) complexes, and their application towards E-H bond oxidative addition (E = P, O, and Si) reactions.

With the goal of observing E-H bond oxidative addition mediated by the (Cy-PSiP)M system, considerable progress has been made in isolating unusual monomeric phosphido-hydride, alkoxy-hydride, and silyl-hydride species. In particular, several examples of successful Ir-mediated P-H, O-H and Si-H bond oxidative addition were demonstrated. Furthermore, phosphido-hydride species showed interesting reactivity in subsequent E-H bond activation featuring alkynes, hydrosilanes, and H_2. Migratory insertions of CO_2 and isocyanates involving alkoxy-hydride complexes were also observed.

Efforts were undertaken to generate silylene species (Cy-PSiP)Ir(H)(=SiR_2) from complexes of the type (Cy-PSiP)Ir(H)(SiRR') (R = H, Cl; R' = Ph, Mes). While such silylene species remain elusive, a better understanding of the behaviour of Ir-silyl complexes was garnered.

Lastly, syntheses of cationic M^{III} complexes of the type [(Cy-PSiP)MR]$^+X^-$ (M = Ir, Rh, R = H, Me; X = OTf, BF_4, $B(C_6F_5)_4$) were explored. Challenges were encountered, associated with either the reactivity or the stability of the synthesized complexes. The inclusion of a neutral L donor resulting in complexes of the type [(Cy-PSiP)MRL]$^+X^-$ (L = PMe_3) afforded increased stability, allowing for the isolation of Ir-methyl cations.

List of Abbreviations and Symbols Used

Å = Angstrom
° = degree
δ **=** chemical shift
Δ = difference
η **=** hapticity (contiguous donor atoms)
κ **=** hapticity (non-contiguous donor atoms)
Σ< = sum of the angles
λ = wavelength
Ad = adamantyl
Anal. Calcd. = analysis calculated
BDE = Bond Dissociation Energy
br = broad
cm^{-1} = wavenumber
COA = cyclooctane
COE = cyclooctene
COSY = *CO*rrelation *S*pectroscop*Y*
Cp* = pentamethylcyclopentadienyl
Cy = cyclohexyl
d = doublet
DEPT = *D*istortionless *E*nchancement by *P*olarization *T*ransfer
DFT = *D*ensity *F*unctional *T*heory
dist-TBP = distorted trigonal bipyramidal
dist-SP = distorted square planar
DMSO = dimethyl sulfoxide
dt = doublet of triplets
E = main group element
equiv = equivalent
h = hour
HMBC = *H*eteronuclear *M*ultiple *B*ond *C*orrelation
HMQC = *H*eteronuclear *M*ultiple *Q*uantum *C*orrelation
HSQC = *H*eteronuclear *S*ingle *Q*uantum *C*orrelation
Hz = Hertz
^{i}Pr = isopropyl
m = multiplet
Mes = mesityl (2,4,6-trimethylphenyl)
min = minute
$^{n}J_{XX'}$ = n bond coupling constant between atom X and atom X'
K = Kelvin
kcal = kilocalorie
kJ = kilojoule
L = neutral donor
m = meta
m = multiplet
min = minutes
MO = molecular orbitals
[NSiN] =

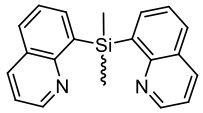

o = ortho
ORTEP = Oak Ridge Thermal Ellipsoid Plot
OTf = triflate (trifluoromethylsulfonate)
p = para
(PCP) =

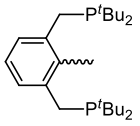

(POCOP) =

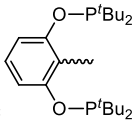

(R-PSiP) =

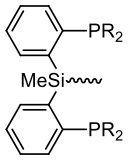

ppm = parts per million
NMR = Nuclear Magnetic Resonance
NOESY = *N*uclear *O*verhauser *E*ffect *S*pectroscop*Y*
(NSiN) =
t = triplet
TBE = *tert*-butylethylene
^{t}Bu = *tert*-butyl
THF = tetrahydrofuran
X = anionic donor

Acknowledgments

First, I would like to thank my supervisor, Dr. Laura Turculet, for all the precious advice, guidance and wisdom throughout the years. Her support, supervision and knowledge have helped to make all this work possible, and provided me with an appreciation of my future career opportunities as a chemist, and a researcher.

The members of the Turculet group, past and present, Sophie, Casper, Colin, Dylan, Helia, Hiko, and Luke with whom I spent countless hours working with, and also sharing good moments that made this experience one to remember. Not to forget friendly moments shared with members of the Stradiotto and Speed groups.

I would also like to thank the members of my supervisory committee, Drs. Fran Cozens, Alex Speed and Mark Stradiotto for helpful discussions and meetings held over the course of my degree, as well as my external examiner Dr. Lisa Rosenberg for taking the time to review and evaluate my work.

Also, collaborators, including Drs. Robert McDonald, Michael Ferguson and Yuqiao Zhou of the University of Alberta must be acknowledged for their outstanding work with regards to X-ray data collection and refinement of the structure presented in this document. Also, Dr. Mike Lumsden of NMR^3 for his insights and expertise concerning NMR data acquisition and interpretation.

Lastly, I would like to thank my parents Michelle and Jean, as well as my family for their support. Despite being thousand miles away, they provided an uninterrupted source of encouragement throughout my years at Dalhousie. It helped me a lot during the toughest moments, but also made me feel proud to be part of a loving family. Thank you.

To my beloved aunt, Annie.

Chapter 1: Introduction

1.1 Overview

A leading goal of modern organometallic chemistry is to develop transition metal complexes that can catalyze targeted chemical reactions with high efficiency and selectivity.[1] The tremendous utility of organometallic catalysts has been highlighted by the 2001, 2005, and 2010 Nobel Prizes in Chemistry for advances in asymmetric catalysis,[2] olefin metathesis,[3] and palladium catalyzed cross-coupling,[4] respectively. While catalysts of this type have numerous impressive applications in chemical synthesis, the development of new catalytic methodology is rooted in the synthesis of new types of transition metal complexes and in developing a fundamental understanding of the reactivity of such complexes.

With respect to preparing new types of reactive complexes, while the choice of the metal is limited by the periodic table, the design of the ancillary ligand is widely variable and provides many opportunities for innovation. In this regard, the research described in this thesis details the synthesis and reactivity of transition metal complexes supported by bis(phosphino)silyl 'pincer'-type ancillary ligands. In particular, the synthesis of Rh and Ir complexes is investigated, and their respective reactivity towards P-H, O-H and Si-H bonds will be explored.

1.2 Ligand Design

Ancillary ligand design plays a major role in the advancement of organometallic chemistry, as such ligands, while not typically being directly involved in bond-making and -breaking steps at the metal center, can still have a pronounced effect on the reactivity,

structure, and electronic properties of the metal complex. The steric and electronic features of the ancillary ligand are thus of key importance, as they influence the properties of the complex. In this respect, the aim of modern research is to design ancillary ligands that can help stabilize reactive metal fragments, while allowing for empty coordination sites at the metal center where bond making/breaking can occur at reasonable rates and with desirable selectivity. Modularity is an important element of ancillary ligand design, as it allows for tuning of the reactivity at the metal center to achieve optimum performance.

Pincer ligands are a specific class of highly modular ancillary ligands that have emerged as a versatile platform for the synthesis of highly reactive organometallic complexes.[5] Pincers are tridentate ligands that coordinate to the metal center *via* three donor groups connected to each other by an organic backbone, and they typically feature an LXL-type (X = anionic donor, L = neutral donor) donor motif (Figure 1-1). Although traditionally pincer ligands were shown to coordinate to a metal center in a planar, meridional manner, examples of more flexible ligands that can also adopt a facial binding mode have been reported.[5] Given the modular nature of pincer ligands, the reactivity of the ensuing metal complexes can be readily tuned by modifying substituents on the ligand backbone, the types of neutral and anionic donors, and the substitution on the donor atoms themselves.[6]

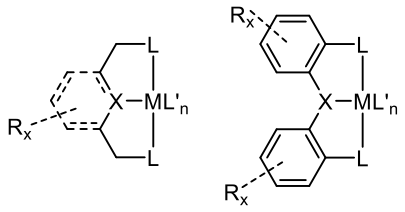

X = anionic donor (C, N, Si)
L = neutral donor (R_2N, R_2P, etc.)
R_x = substituents on ligand backbone

Figure 1-1. Typical design motifs of LXL pincer ligands.

Given the tridentate design of pincer ligands, coordination to a metal center leads to the formation of complexes featuring two fused metallacycles (Figure 1-1). The composition of the ligand backbone dictates the size of the metallacycle that is formed, with five-membered rings being the most popular design choice.[7] The chelating nature of pincer ligands leads to enhanced stability in the corresponding metal complexes relative to related complexes that feature monodentate ligation. This additional stabilization can lead to new reactivity, as has been observed in the case of catalytic alkane dehydrogenation, where the thermal stability of Ir pincer complexes facilitated a catalytic process that was not accessible to less stable non-pincer Ir species.[8] Aspects of this reactivity are discussed in more detail in sections 1.4 and 1.5 of this document.

One of the most attractive features of pincer ligands is their exceptional tunability. Both the neutral donor groups (L) and central anionic donor (X) can be changed, as well as the ligand backbone itself. Such modifications will have a noticeable effect on the chemistry of the pincer metal complex.[9] A large range of neutral L donors have been studied; while the most commonly employed donors are phosphine[10] and amine[11] groups, it is also possible to use other species such as O-[12], S-[13], Se-[14], Si-[15], Ge-[16] and C-based[17] donors. With respect to the central anionic X donor, pincers have largely been limited to carbon (aliphatic or aromatic)[5,18] and nitrogen (amido)[19] donors at this position, with phenylene-bridged silicon (silyl)[20,21] pincers having emerged only recently, although other pincer classes do exist.[22,23,24] Lastly, the ligand backbone is typically an aromatic or aliphatic scaffold. The choice of this framework will have a direct impact on the rigidity, flexibility, and crystallinity of the pincer complex. The backbone also has a direct influence on the donor capabilities of the L and X donors, which can impact the reactivity of the

overall complex.[25] Furthermore, it is also possible to incorporate electron withdrawing or donating groups within the ligand backbone, which will also allow for fine-tuning the electronic features of the pincer metal complex.[25]

Despite the many design possibilities offered by the pincer platform, research in this area has largely been focused on PCP-type complexes, which were among the first reported examples of pincer species. Such PCP-supported complexes have become ubiquitous in organometallic chemistry and have been utilized for numerous applications, including catalysis,[26] bond activation,[5] and the synthesis of new functional materials.[8]

1.3 Early Development of Pincer Chemistry

The synthesis of PCP pincer metal complexes was pioneered by Shaw in the early 1970s.[27] The original impetus of this work was to use the bis-phosphino ligand framework in order to promote a chelate assisted C-H bond (either aliphatic or aromatic) oxidative addition to a metal center, with Shaw's primary focus being the observation of C-H bond activation chemistry. Interestingly, the newly synthesized PCP pincer complexes (Figure 1-2) were significantly more stable than analogous complexes with monodentate phosphine ligands. Since these initial reports, pincer chemistry has become a field of research in and of itself.

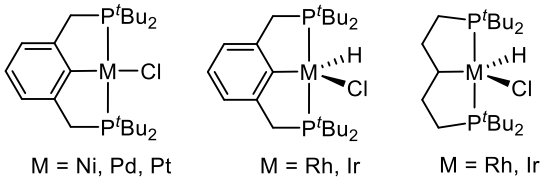

Figure 1-2. PCP pincer complexes synthesized by Shaw and co-workers.

The chelate assisted cyclometalation path remains a popular method for the synthesis of PCP pincer complexes.[5] Species featuring κ^2-P,P bidentate coordination of the

pro-ligand have been proposed as intermediates in such processes, and in some cases complexes of this type have been isolated.[28] The C-H bond activation step of the pincer metalation can be somewhat difficult to achieve and often requires high temperatures and long reaction times to reach completion. The phosphino donors are generally alkyl substituted and thus strongly electron donating, thereby promoting the challenging oxidative addition step.[18b]

In subsequent early studies of PCP late metal complexes, Milstein and co-workers utilized a similar cyclometalation strategy to prepare (PCP)Rh complexes *via* a sp^2-sp^3 C-C bond cleavage strategy, which represents a rare example of net C-C bond oxidative addition (Scheme 1-1).[29]

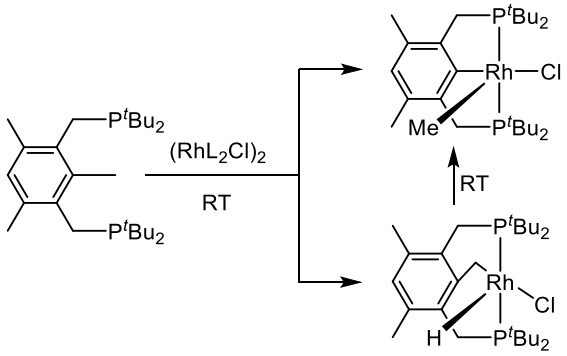

Scheme 1-1. Examples of C-C bond oxidative addition by Milstein and co-workers.

Methylene transfer into Si-H, Si-Si, and C-H bonds could also be achieved in such systems.[30] These studies are remarkable given the relatively inert nature of C-C bonds, and they served to establish late transition metal pincer complexes as a versatile platform for the study of challenging bond activation processes. In particular, significant research efforts have focused on the study of E-H (E = main group element) bond activation involving preformed platinum group metal PCP pincer complexes. As a background to the work presented in this thesis, and to highlight examples of challenging transformations

enabled by use of such pincer complexes, the following sections feature a discussion of C-H and N-H bond activation chemistry.

1.4 C-H Bond Activation by (PCP)Ir Species

The selective activation of C-H bonds in hydrocarbons is a key objective of modern organometallic chemistry, whereby a metal center inserts into a C-H bond of a substrate molecule. Two common mechanisms for such transformations include: (a) the oxidative addition of a C-H bond to the metal center, which raises the metal oxidation state by two units (Scheme 1-2A); or, (b) a σ-bond metathesis pathway, whereby no change in the metal oxidation state occurs (Scheme 1-2B). Such C-H bond cleavage processes represent key steps toward achieving what some have referred to as a "holy grail" of synthetic chemistry, the selective, catalytic functionalization of unactivated alkanes under mild conditions.[31]

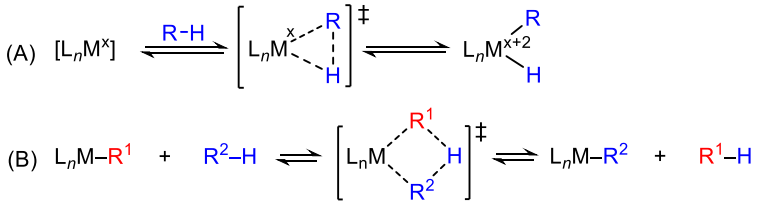

Scheme 1-2. Two common pathways for C-H bond activation by a metal center.

Simple alkanes are extremely stable and unreactive molecules, and are therefore exceedingly challenging to functionalize in a selective manner. However, in the early 1980s, Bergman and Graham concurrently reported the first examples of metal mediated intramolecular sp^3-hybridized C-H bond oxidative addition (Scheme 1-3).[32] In both cases an unsaturated Ir^I species was generated photochemically and underwent subsequent C-H bond oxidative addition to afford an Ir^{III} alkyl hydride complex. This alkane C-H activation was performed under stoichiometric conditions[31a] and is therefore not suitable for a

practical industrial application. However, this reactivity demonstrated the potential of coordinatively unsaturated late metal fragments, such as Cp*IrL (L = PMe_3, CO; Cp* = C_5Me_5) to undergo challenging oxidative addition processes.

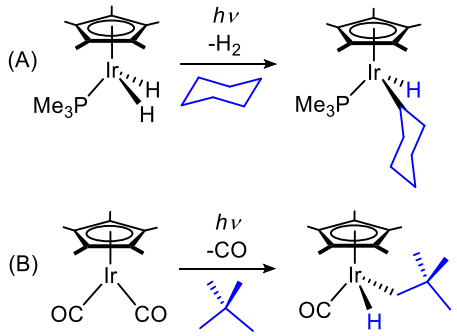

Scheme 1-3. First examples of metal-mediated C-H bond activation by Bergman (A) and Graham (B) and co-workers.

Since the pioneering studies of Bergman and Graham, numerous examples of metal mediated C-H bond activation have been reported.[33] As such, current focus in this research area is on the development of catalytic processes that utilize such C-H bond cleavage steps. One such process that has been investigated is the transfer-dehydrogenation of an alkane to afford a terminal alkene, which is a highly desirable synthon for the preparation of more complex molecules.[34] The first reports of homogeneous catalytic alkane transfer-dehydrogenation were published concurrently by Felkin[34a,35] and Crabtree,[34b,36] with bis(trialkylphosphine) complexes of Ir being among the best performing catalysts. Crabtree also reported that $IrH_2(O_2CR)(PCy_3)_2$ catalyzed the *acceptorless* dehydrogenation of cyclooctane (COA), to give up to 36 turnovers of cyclooctene (COE) in 48 h.[37] However, turnover numbers were typically limited in these systems by catalyst decomposition at the high temperatures required for reactivity.[38] By comparison, Goldman and co-workers reported that while $Rh(PMe_3)_2(CO)Cl$ is a robust catalyst for photochemical alkane dehydrogenation,[39] under thermal conditions the transfer dehydrogenation reaction only

proceeds under an atmosphere of H_2, which severely limits the utility of this catalyst.[40]

Given the high thermal stability of pincer complexes and the established effectiveness of Rh and Ir bis-(trialkylphosphine) complexes in catalytic alkane dehydrogenation, the investigation of pincer-ligated complexes for this type of reactivity was actively pursued. The first studies detailing the reactivity of (PCP)RhH_2 and (PCP)IrH_2 complexes in the dehydrogenation of alkanes were reported concurrently by Jensen, Kaska and co-workers,[41] and Goldman and co-workers,[9,42] in the late 1990s (Scheme 1-4).

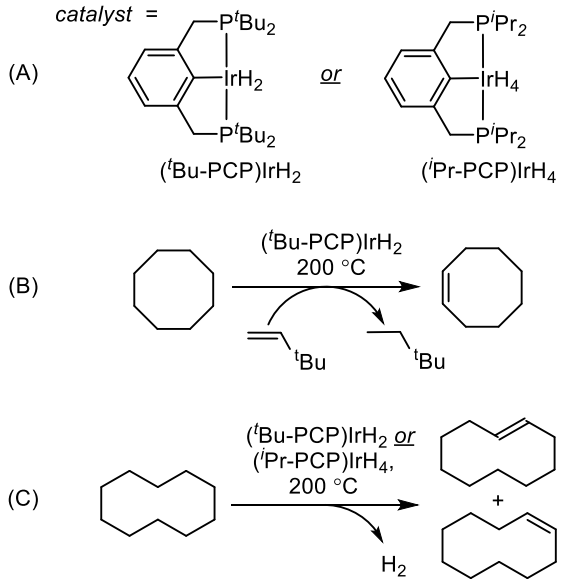

Scheme 1-4. (A) (PCP)Ir pincer complexes developed by Jensen, Goldman, and co-workers for alkane dehydrogenation; (B) transfer dehydrogenation of COA; (C) acceptorless dehydrogenation of cyclodecane.

The Ir pincer complex (^{t}Bu-PCP)IrH_2 displayed high activity for the transfer dehydrogenation of COA in the presence of the sacrificial hydrogen acceptor *tert*-butylethylene (TBE), affording 12 turnovers/min and no observable decomposition over one week at 200 °C (Scheme 1-4).[41a] Subsequently, Kaska and Jensen reported that other cycloalkanes such as cyclohexane, methylcyclohexane, and decalin were also efficiently dehydrogenated by (^{t}Bu-PCP)IrH_2.[41b] The analogous Rh complex (^{t}Bu-PCP)RhH_2 and the

less sterically encumbered dimethylphosphino derivative (Me-PCP)RhH_2 were found to be poor catalysts, yielding <1 turnover/h under the same conditions and undergoing decomposition after a day at 200 °C.[41a,42a] These observations illustrate the important interplay of metal choice and ligand design in achieving desirable reactivity.

Pincer Ir complexes of the type depicted in Scheme 1-4 were also applied in the acceptorless dehydrogenation of alkanes (Scheme 1-4c). This reaction is thermodynamically uphill, which is why a sacrificial hydrogen acceptor is typically used to shift the equilibrium towards the desired alkene products. However, given the high thermal stability of the pincer catalysts, the reaction can be carried out at reflux in a high boiling alkane solvent, such as cyclodecane (boiling point = 201 °C), with liberated H_2 being removed from the reaction mixture by a purge of Ar. Under these conditions, utilizing (^{t}Bu-PCP)IrH_2 as the catalyst resulted in cyclodecene formation with 360 turnovers observed after 24 h.[42b] By comparison, use of the less bulky catalyst (^{i}Pr-PCP)IrH_4 (effectively a source of (^{i}Pr-PCP)IrH_2) under these conditions afforded close to 1000 turnovers in the dehydrogenation of cyclodecane and the first reported example of acceptorless dehydrogenation of an acyclic alkane (*n*-undecane).[9] These results highlight the importance of tuning substituents in such pincer systems in order to optimize catalytic results.

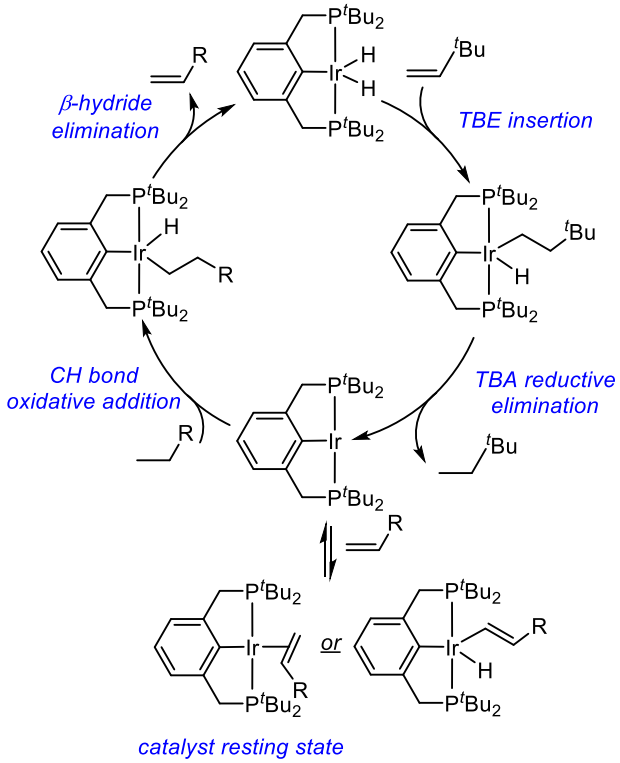

Scheme 1-5. Proposed mechanism for alkane transfer-dehydrogenation by (^{t}Bu-PCP)IrH$_2$.

Detailed kinetic studies of catalytic transfer-dehydrogenation of alkenes by (^{t}Bu-PCP)IrH$_2$ in the presence of TBE were carried out, and the proposed mechanism of this reaction is depicted in Scheme 1-5.[43] The involves initial step is coordination of TBE to Ir and subsequent insertion into an Ir-H bond. Subsequent reductive elimination of the corresponding alkane (*tert*-butylethane, TBA) generates a reactive, coordinatively unsaturated (^{t}Bu-PCP)Ir^I species with a low electron count (14 electrons). Oxidative addition of the alkane follows, to form a hydrido alkyl Ir^{III} complex. Finally, β-hydride elimination releases the product alkene and regenerates (^{t}Bu-PCP)IrH$_2$. Off-cycle C-H bond activation of an alkene as well as alkene coordination to Ir^I also occur, however these species are in rapid equilibrium with the catalytically active 14-electron (^{t}Bu-PCP)Ir^I species.[44] Experimental results also suggest that the alkene adduct is the resting state of the catalyst. Thus, alkene (either the desired product or the sacrificial acceptor) can

significantly inhibit catalytic activity. In the case of acceptorless dehydrogenation, the proposed mechanism is similar, with the exception that the 14-electron species (^{t}Bu-PCP)Ir^I is generated by thermal extrusion of H_2 from (^{t}Bu-PCP)IrH_2 (Scheme 1-6).[45] This represents the turnover-limiting step of the cycle, in the limit of effective H_2 removal from the system.

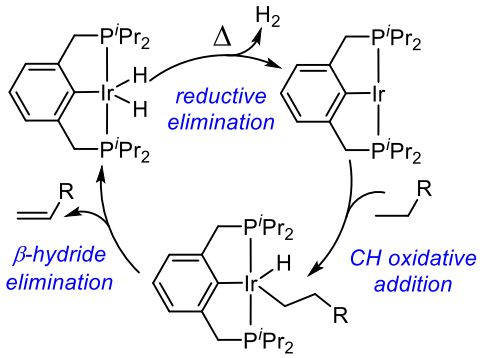

Scheme 1-6. Proposed mechanism for acceptorless catalytic dehydrogenation.

1.5 (POCOP) Pincer Complexes: Another Efficient System for the Catalytic Transfer Dehydrogenation of Alkanes

In an effort to develop more active catalysts for alkane dehydrogenation, a variety of PCP derivatives have been screened over the years.[46] One the most notable to emerge is the bis(phosphinite) POCOP Ir pincer system, independently developed by Jensen[47] and Brookhart[48] (Figure 1-3). Although at first glance the bis(phosphinite) ligation appears electron withdrawing relative to the bis(phosphine) PCP system, DFT calculations show that the oxygen atoms donate substantial π-electron density to the aryl ring in the ^{t}Bu-POCOP ligand.[46b] As a result, the metal center in (^{t}Bu-POCOP)Ir is calculated to be marginally more electron-rich than that in (^{t}Bu-PCP)Ir. While electronic effects therefore do not figure significantly in the reactivity differences between these classes of pincers, pronounced geometric differences appear to play a more decisive role. The metal center in

(^{t}Bu-POCOP)Ir is much less sterically hindered than that of (^{t}Bu-PCP)Ir, as indicated by DFT calculations as well as X-ray crystallographic data, largely due to shorter P-O and C-O bonds and wider P-O-C bond angles in the bis(phosphinite) complex relative to the analogous metrical parameters in the PCP system.[46c] As such, one can envision that the Ir center should be sterically more accessible for substrate binding in (^{t}Bu-POCOP)Ir relative to (^{t}Bu-PCP)Ir. Indeed, (POCOP)Ir-derived catalysts have displayed higher catalytic activity in COA/TBE transfer dehydrogenation reactions than (^{t}Bu-PCP)IrH_2.

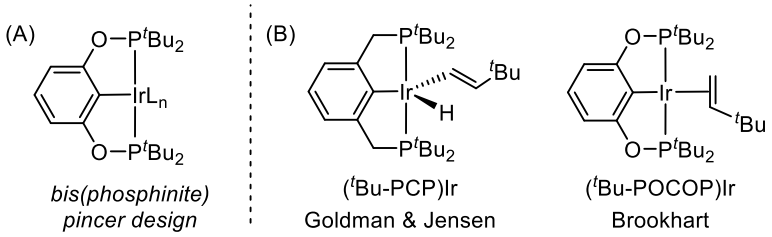

Figure 1-3. (A) Design of (^{t}Bu-POCOP)Ir pincers; and (B) complexes resulting from the reaction of 14-electron (^{t}Bu-PCP)Ir^I and (^{t}Bu-POCOP)Ir^I with TBE.

In the case of (^{t}Bu-POCOP)Ir the catalytically active species is easily generated *in situ* from the reaction of air-stable (^{t}Bu-POCOP)Ir(H)Cl with NaO^{t}Bu.[46c,48-49] Upon addition of COA and the hydrogen acceptor TBE, (^{t}Bu-POCOP)Ir catalyzes the desired dehydrogenation to COE with turnover numbers up to 2200 and turnover frequencies of up to 2.4 s^{-1} at 200°C.[48b] In comparison, (^{t}Bu-PCP)Ir was ca. ten times less efficient under similar conditions, thus showcasing the greater efficiency of bis(phosphinite) Ir catalysts.

With respect to the mechanism of COA dehydrogenation, (^{t}Bu-POCOP)Ir is proposed to operate in a similar manner to (^{t}Bu-PCP)Ir (Scheme 1-4). However, these complexes do display a difference in the preferred coordination mode of TBE. Whereas Goldman and Jensen's (^{t}Bu-PCP)Ir^I undergoes oxidative addition of the sp^2-CH bond of TBE to form a vinyl complex, Brookhart's (^{t}Bu-POCOP)Ir^I coordinates the olefin in a π-

bonding fashion (Figure 1-3).[48a] As well, the rate of alkene hydrogenation by (^{t}Bu-POCOP)IrH_2 is much faster than that of (^{t}Bu-PCP)IrH_2.

Although (PCP)Ir species have demonstrated remarkable C-H bond activation chemistry, which can be influenced by the design features of the pincer pincer ligand structure, the reactivity of such species is not limited to C-H bond activation and functionalization. As described below, complexes of this type have also proven adept at a number of other E-H bond cleavage reactions, such as N-H bond oxidative addition.

1.6 N-H Bond Oxidative Addition by (PCP)Ir Species

Due to to the prevalence of amino functional groups in pharmaceuticals, fine chemicals and other synthetic targets, the development of new transition metal catalyzed amination reactions is highly desirable and as such, research in this area has been pursued extensively.[50] Interestingly, while a number of high profile metal-catalyzed reactions, such as hydrogenation, hydrosilylation, and hydroboration, proceed by E-H (E = H, Si, or B, respectively) bond oxidative addition to the metal center,[51] well-documented examples of N-H bond oxidative addition of amines are exceedingly rare.[52] This scarcity is a result of the inherent ability of amines to form stable Werner-type coordination complexes resulting from the dative interaction between the nitrogen lone pair and the metal atom.[53] The development of facile N-H bond oxidative addition of simple amines thus represents an opportunity to exploit such reactivity in new catalytic amination protocols.

In recent years, PCP-type Ir pincer complexes have demonstrated a relative aptitude for N-H bond oxidative addition.[54] Zhao, Goldman, and Hartwig explored the reactivity of the previously described (^{t}Bu-PCP)IrH_2 with ammonia and aniline.[52g] Having established in the course of alkane dehydrogenation chemistry that the highly reactive (^{t}Bu-PCP)Ir^I 14-

electron species undergoes facile C-H bond activation, it was proposed that this coordinatively unsaturated intermediate would be a good candidate to react *in situ* with the N-H bonds of amines. Indeed, facile N-H bond oxidative addition of aniline was observed at room temperature to afford (^{t}Bu-PCP)Ir(H)(NHPh) (Scheme 1-7).

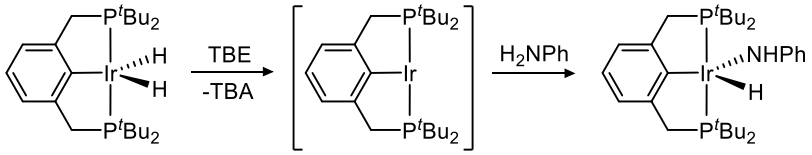

Scheme 1-7. N-H bond activation of anline by (^{t}Bu-PCP)Ir.

The analogous parent amido complex resulting from N-H bond cleavage in ammonia proved to be thermodynamically less stable than the reductive elimination product, (^{t}Bu-PCP)Ir(NH_3) (Scheme 1-8). Further attempts to synthesize the Ir^{III} parent amido hydride complex by adding ammonia to (^{t}Bu-PCP)Ir(H)Cl followed by dehydrohalogenation did lead to formation of the desired (^{t}Bu-PCP)Ir(H)(NH_2) complex; however, this compound was shown to reductively eliminate ammonia at temperatures above -10 °C. In addition, exposure of (^{t}Bu-PCP)Ir(H)(NHPh) to benzene resulted in the formation of an equilibrium mixture containing the anilido complex and the phenyl hydride species resulting from reductive elimination of aniline and oxidative addition of a benzene C-H bond. These results indicate that although N-H bond oxidative addition occurs in this system, the reaction is readily reversible, which complicates the development of subsequent reactions involving the Ir-NHR fragment.

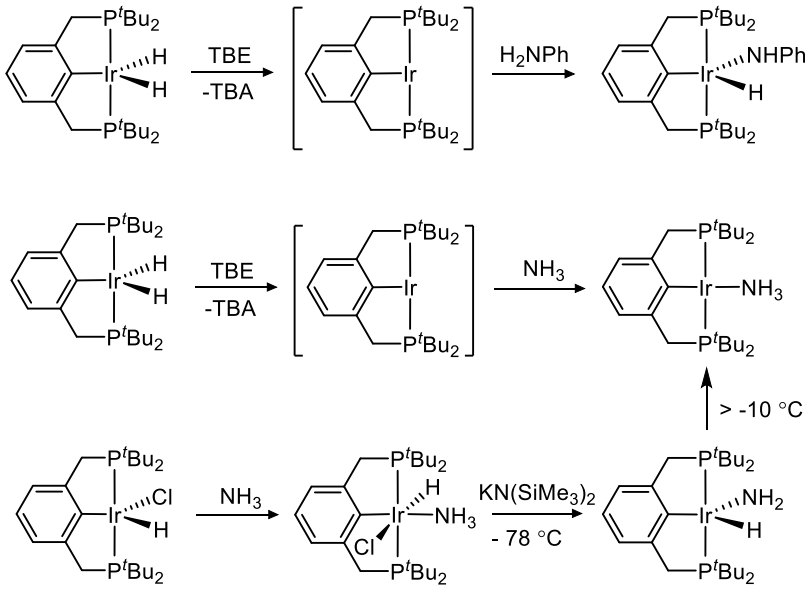

Scheme 1-8. Formation of (^{t}Bu-PCP)Ir(H)(NH_2) and thermal instability.

In an effort to achieve the NH oxidative addition of ammonia, a highly desirable substrate, Goldman, Hartwig and co-workers subsequently targeted a more electron-rich (PCP)Ir fragment that would help stabilize the higher oxidation state of the amido hydride reaction product (Scheme 1-8).[52i] A related Ir^I complex featuring an aliphatic pincer ligand backbone, [(^{t}Bu$_2$P(CH$_2$)$_2$)$_2$CH]Ir(CH$_2$=CHMe), was reacted with ammonia at room temperature to generate the desired Ir^{III} parent amido complex upon liberation of propene (Scheme 1-9). The latter complex is a rare example of an isolable, monomeric amido hydride complex resulting from N-H bond oxidative addition of ammonia.

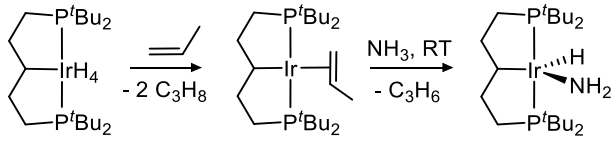

Scheme 1-9. N-H bond activation of ammonia to form an isolable, monomeric Ir^{III} parent amido complex.

Hartwig and co-workers sought to further determine the stability of the amido hydride complex relative to the corresponding Ir^I alkene complex [(^{t}Bu$_2$P(CH$_2$)$_2$)$_2$CH]Ir(1-

pentene).[55] Upon combining ammonia, 1-pentene, and [(^{t}Bu$_2$P(CH$_2$)$_2$)$_2$CH]Ir(1-pentene) (0.03 M in diethyl ether-d_{10}) in a 15:30:1 ratio, an equilibrium constant of 9 was determined for the conversion of the alkene complex to the amido hydride species. By comparison, the reaction of the alkene complex with H$_2$N(3,5-Me$_2$C$_6$H$_3$) revealed that the formation of the hydrido arylamide oxidative addition product was thermodynamically less favorable than the analogous reaction with ammonia, with an equilibrium constant of 0.09. This result is somewhat surprising given the lower N-H bond strength (BDE of NH_3 = 450.08±0.24 kJ mol^{-1}, *vs*. BDE of H$_2$NPh = 375.3 kJ mol^{-1}) and greater acidity (in DMSO pK_a of NH_3 = 41, *vs*. pK_a of H$_2$NPh = 30.6) of the aromatic amine.[56]

The mechanism of the ammonia activation reaction was probed using isotopic labeling studies with ND_3 and the results were consistent with a mechanism involving oxidative addition of ammonia to a [(^{t}Bu$_2$P(CH$_2$)$_2$)$_2$CH]Ir^I intermediate, with deuterium incorporation only observed at the Ir-*H* and Ir-N*H*$_2$ positions.[54] Kinetic studies indicated that the rate of the reaction is dependent on the concentration of alkene, which is consistent with a dissociative mechanism in which the alkene first dissociates from the Ir center to generate a three-coordinate [(^{t}Bu$_2$P(CH$_2$)$_2$)$_2$CH]Ir^I species that subsequently reacts with ammonia.

In a similar vein, having examined the reactivity of bis(phosphinite) Ir pincer complexes in C-H bond activation chemistry (*vide supra*), Brookhart and co-workers sought to apply (^{t}Bu-POCOP)Ir toward the activation of the N-H bonds. Their study revealed that (^{t}Bu-POCOP)Ir^I (generated by the reaction of (^{t}Bu-POCOP)Ir(H)Cl with NaO^{t}Bu) reacted with the N-H bonds of anilines in benzene solution to produce three products in equilibrium – (^{t}Bu-POCOP)Ir(H)Ph, (^{t}Bu-POCOP)Ir(H)(NHAr) and the Lewis

base adduct (^{t}Bu-POCOP)Ir(NH_2Ar) (Scheme 1-10, Ar = *p*-X-C_6H_3; X = OMe, Me, H, Cl, or CF_3).[52j] The complex (^{t}Bu-POCOP)Ir(H)Ph was formed by the reaction of (^{t}Bu-POCOP)Ir^I with the benzene solvent, while (^{t}Bu-POCOP)Ir(H)(NHAr) and (^{t}Bu-POCOP)Ir(NH_2Ar) result from the reaction of (^{t}Bu-POCOP)Ir^I with aniline. Equilibrium constants for these processes were determined to be dependent on the nature of the *para*-substituent on the aniline. Thus, more electron-donating *para*-substituents led to increased fomation of the aniline adduct (^{t}Bu-POCOP)Ir(NH_2Ar), while more electron-withdrawing groups led to formation of the aniline oxidative addition product (^{t}Bu-POCOP)Ir(H)(NHAr) as the major product. The former effect can be attributed to the increased Lewis basicity of the anline, while Brookhart and co-workers propose that the latter effect is due to decreased repulsion between filled metal d_π–orbitals and N p-orbitals.

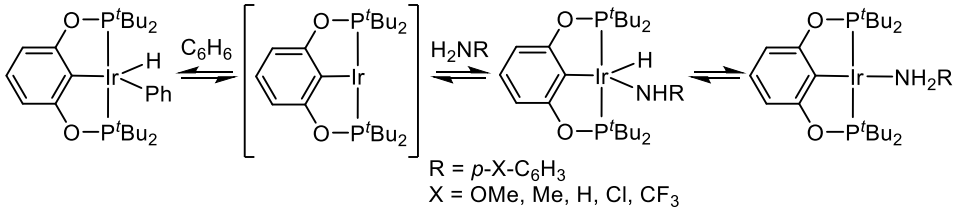

Scheme 1-10. The reaction of (^{t}Bu-POCOP)Ir^I with anilines in benzene solution.

The rates of reductive elimination from (^{t}Bu-POCOP)Ir(H)(NHAr) were measured by heating the Ir^{III} complexes in the presence of ethylene as a trapping ligand for (^{t}Bu-POCOP)Ir^I. The reductive elimination barriers fall in the range of 21-22 kcal mol^{-1} and increase with the electron-withdrawing ability of the aniline employed. By comparison, the barrier of C-H bond reductive elimination from (^{t}Bu-POCOP)Ir(H)Ar (Ar = 3,5-$Me_2C_6H_3$) was determined to be 14.1 kcal mol^{-1}.

The work of Hartwig, Brookhart and co-workers has established the aptitude of PCP-type pincer Ir species to undergo NH bond activation processes. It is anticipated that

the design of new types of highly reactive pincer complexes that can undergo N-H bond oxidative addition reactions will facilitate the development of useful organic transformations that incorporate such N-H bond activation steps.

1.7 Silyl Pincer Complexes: A Different Ligand Design

As discussed in the previous sections, a large majority of reported pincer chemistry involves PCP and PNP derived ligands. However, the LXL ligand design is highly modular and can accommodate a variety of neutral (L) and anionic (X) donors. While numerous studies have explored changing the nature of the L donors, the identity of the central anionic donor has been held relatively constant. Recently examples of pincer ligation where X = P,[22] B,[23] Sn,[24] Ge[24] and Si[20,21] have appeared, with the latter silyl based pincers being the most extensively explored. These novel ligand designs are predicted to engender new reactivity in the ensuing pincer complexes due to the influence of the central donor on the electronic features of the metal center.

In comparing traditional PCP pincers with analogous platinum group metal PSiP complexes, the reduced electronegativity of Si relative to C (Pauling electronegativity of C = 2.55 while that of Si = 1.90) is anticipated to lead to a more electron rich metal center, hence facilitating oxidative addition reactions and increasing reactivity. In addition, the stronger trans-labilizing ability of Si can better promote the generation of coordinatively unsaturated complexes, thus offering increased opportunities for reactivity at the metal center.[57]

Multidentate (phosphino)silyl ligands were first reported by Stobart and co-workers in the 1980s (Figure 1-4A).[58] These early studies primarily addressed the fundamental

coordination chemistry of such chelating silyl ligands. Tilley and co-workers subsequently reported on the synthesis of late metal complexes supported by tridentate bis(quinolyl)silyl (NSiN) ligation (Figure 1-4B).[59] Tridentate coordination of NSiN to Rh, Ir, and Pt has been achieved, affording both neutral and cationic complexes. Such complexes typically exhibit *fac*-NSiN coordination, although square planar (NSiN)PtCl has also been isolated.[59d] The Ir^{III} triflate complex (NSiN)Ir(H)(OTf)(COE) (COE = cyclooctene) catalyzes both aryl silane redistribution and the dehydrogenative silylation of arenes, albeit with low activity and low yields.[59c] While increased reactivity might be accessed in such pincer systems by tuning the ligand steric and electronic features, the substitution at nitrogen in such quinolyl-derived ligands is not readily modified. Furthermore, N-based peripheral donors are anticipated to afford late metal complexes that are not very electron-rich, and thus may not readily undergo oxidative addition reactions.

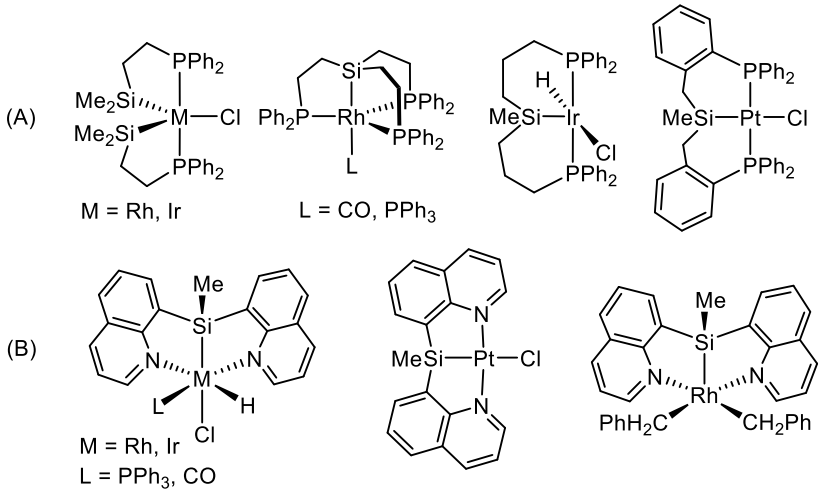

Figure 1-4. Examples of complexes supported by multidentate (phosphino)silyl ligation developed by Stobart and co-workers (A) and bis(quinolyl)silyl (NSiN) metal complexes reported by Tilley and co-workers (B).

More recently, the Turculet group has developed PSiP[60] (as well as PSiN)[61] ligation featuring a phenylene backbone ($[\kappa^3$-(2-$R_2PC_6H_4)_2Si$Me$]^-$ = R-PSiP, R = alkyl or aryl;

Figure 1-5),[62] as well as derivatives that feature an indolyl backbone,[63] and has explored the reactivity and catalytic activity of such late metal PSiP species.[20,21,64,65] Such complexes lack β-hydrogens in the ligand backbone, which removes the possibility of β-hydride elimination from the PSiP backbone. Although these somewhat rigid phenylene-based ligands feature an sp^3-hybridized central silyl donor, examples of both meridional and facial binding to a metal have been observed. The reduced conformational flexibility associated with the *ortho*-phenylene backbone is anticipated to also provide enhanced stability and selectivity in metal-mediated substrate transformations. Furthermore, such PSiP ligation offers the opportunity to readily tune the steric and electronic properties of the phosphino donors.

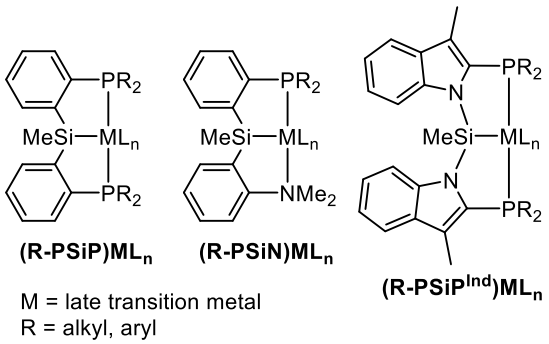

Figure 1-5. PSiP and PSiN (phosphino)silyl pincer complexes developed in the Turculet group.

Thus far, metal complexes supported by R-PSiP ligation have displayed aggressive reactivity in challenging E-H bond activation reactions, including examples of Ir-mediated arene C-H[20b] and amine N-H bond activation.[52k] As well, Cy-PSiP ligation has been shown to stabilize unusual low-coordinate metal species, such as 14-electron, four-coordinate Ru complexes that adopt an unusual trigonal pyramidal coordination geometry.[20e] Lastly, R-PSiP complexes have been shown to be catalytically active in reactions such as the transfer hydrogenation of ketones,[20a] and the reduction of CO_2 with either hydrosilanes[20f] or

boranes.[63] Such silyl pincer ligands have also recently been shown to support catalytically active first row transition metal complexes,[64b,c] including an example of a highly active (Cy-PSiP)Fe catalyst for alkene hydrogenation.

In the context of Group 9 metal chemistry, five-coordinate Rh^{III} and Ir^{III} complexes of the type (Cy-PSiP)M(H)Cl (**1-1**, M = Ir; **1-2**, M = Rh; Scheme 1-11) proved readily accessible *via* Si-H oxidative addition of the tertiary silane pro-ligand.[20b] Complexes **1-1** and **1-2** can be dehydrohalogenated *in situ* to provide access to reactive (Cy-PSiP)M^{I} (**1-3**, M = Ir; **1-4**, M = Rh) species that have thus far resisted isolation attempts. While such 14-electron species are not isolable, they can be trapped as 16-electron complexes of the type (Cy-PSiP)ML (**1-5a**, M = Ir, L = PMe_3; **1-5b**, M = Ir, L = C_2H_4; **1-6**, M = Rh, L = PMe_3; Scheme 1-11).[52k] In the case of *in situ* generated **1-3**, evidence for a possible Ir-*H* was observed by ^{1}H NMR spectroscopy in cyclohexane-d_{12} solution, suggesting that reversible metalation of the Cy-PSiP ligand may play a role in the reactivity of this highly reactive complex. In the presence of benzene, complex **1-3** undergoes sp^2-CH bond activation to afford (Cy-PSiP)IrH(Ph) (**1-7**), which also undergoes facile arene exchange. The Rh analogue **1-4** proved unreactive toward such arene substrates. Following these initial reports from the Turculet group, Shimada and co-workers[21d] demonstrated that complexes of the type (R-PSiP)$Ir(H)_4$ (**1-8**; R = Cy, ^{i}Pr, ^{t}Bu) also undergo benzene C-H bond activation in the presence of an alkene H_2 acceptor.

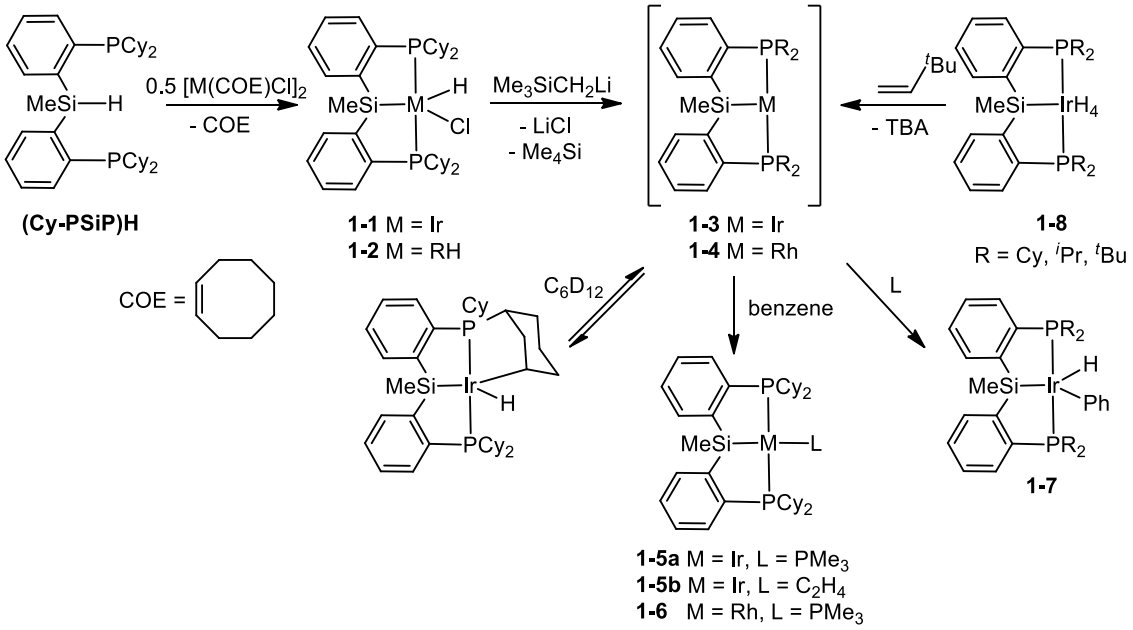

Scheme 1-11. Generation of (Cy-PSiP)M^{I} (**1-3**, M = Ir; **1-4**, M = Rh) and reactivity with sp^2-CH bonds.

The Turculet group extended the reactivity of (Cy-PSiP)M (M = Rh, Ir) species to the oxidative addition of N-H bonds (Scheme 1-12).[52k,66] *In situ* generated **1-3** was found to undergo N-H bond oxidative addition of anilines, alkylamines lacking β-hydrogen substituents (e.g., H_2N^tBu), and ammonia under mild conditions, resulting in the formation of mononuclear Ir^{III} amido hydride complexes of the type (Cy-PSiP)Ir(H)(NHR) (**1-9**, R = aryl, alkyl, or H), which could be readily isolated. Unlike previously reported (PCP)Ir and (POCOP)Ir systems, complexes **1-9** proved to be resistant to N-H bond reductive elimination. Subsequent work further revealed that **1-3** also mediates the oxidative addition of N-H bonds in hydrazine derivatives H_2N-NR'$_2$ (R'$_2$ = C_5H_{10}, $(CH_2CH_2)_2NMe$) and benzamides $H_2N(C{=}O)R$" (R" = Ph, C_6F_5).[66] In the case of Rh, while complexes of the type (Cy-PSiP)Rh(H)(NHR) (**1-10**, R = aryl) proved isolable when prepared by treatment of **1-2** with LiNHR reagents, such complexes could not be prepared by N-H oxidative addition to *in situ* generated **1-4**. Rather, treatment of **1-4** with various amines led to the

formation of the corresponding Rh^{I} adducts (Cy-PSiP)Rh(NH_2R') (**1-11**, R' = aryl, alkyl, H).[52k]

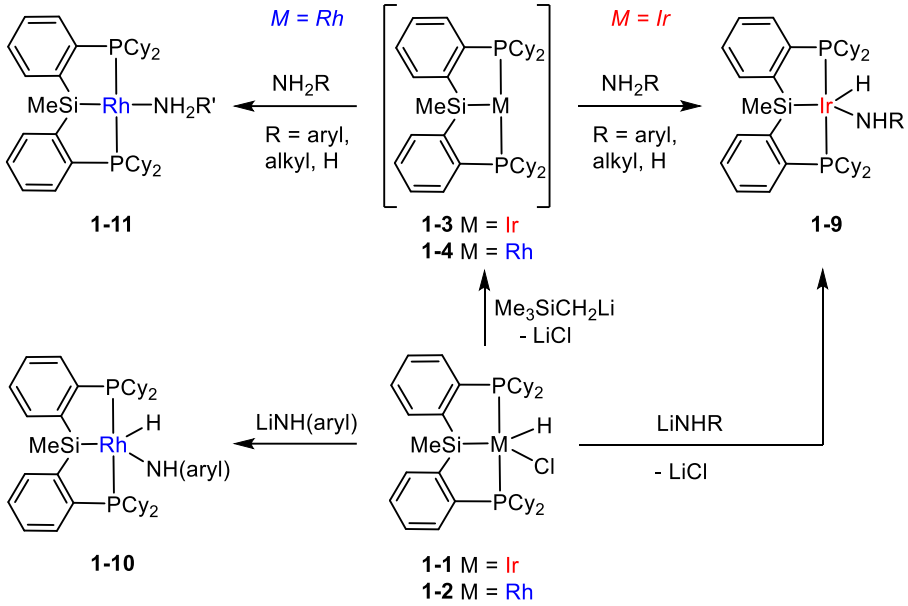

Scheme 1-12. N-H oxidative addition *via* (Cy-PSiP)M^{I} (M = Rh, Ir).

1.8 Further Exploration of E-H Bond Activation at (Cy-PSiP)Ir^{I}

Having established that Cy-PSiP ligation provides access to Ir complexes that can engage in challenging oxidative addition processes, such as N-H oxidative addition of ammonia, a significant area of inquiry involves outlining the scope of E-H bond activation by such complexes. The oxidative addition of E-H bonds is a key component of numerous catalytic process that have emerged as important synthetic tools, including hydroboration[63,65b,67] and hydrosilylation[68] catalysis, and there is significant interest in developing new reactivity involving challenging N-H and O-H activation steps for processes such as amination[69] and water splitting.[70] In this regard, the work described in this thesis builds on previous work from the Turculet group dealing with the synthesis and reactivity of (Cy-PSiP)Ir pincer complexes. The synthetic studies presented herein will

address the extension of bond activation studies to new types of E-H bonds, including P-H, O-H and Si-H bonds (Scheme 1-13). The synthesis and characterization of new and unusual coordinatively unsaturated late metal phosphido, aryloxo, alkoxo, hydroxo, and silyl complexes will be detailed. The development of new reactive platforms for studying such bond activation processes will also be addressed, including cationic (Cy-PSiP)M(Me)^{III} species (M = Rh or I). These studies contribute to further understanding of the range of oxidative addition processes that can be accessed with late transition metals, as well as understanding of how pincer ligation strategies support highly reactive metal complexes.

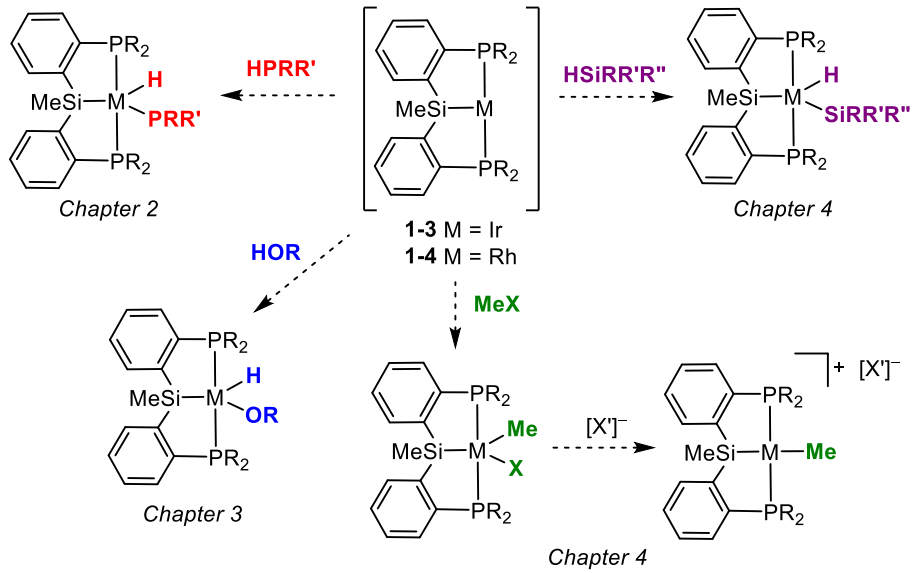

Scheme 1-13. Summary of bond activation reactivity explored in this thesis.

Chapter 2: Iridium Mediated P-H Bond Oxidative Addition Leading to Terminal Phosphido Hydride Species Supported by PSiP Ligation

2.1 Introduction

The oxidative addition of P-H bonds in hydrophosphines to generate transition metal phosphido species (eq 2-1) has been implicated as a key step in late transition metal catalyzed processes for the formation of new phosphorus-element bonds, such as alkene/alkyne hydrophosphination and dehydrocoupling (Scheme 2-1).[71] While this mechanistic step is often invoked in such contexts, examples of well-defined, mononuclear transition metal phosphido hydride complexes that represent the product of such an oxidative addition process are surprisingly rare.

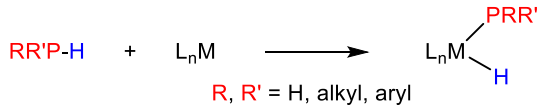

(2-1)

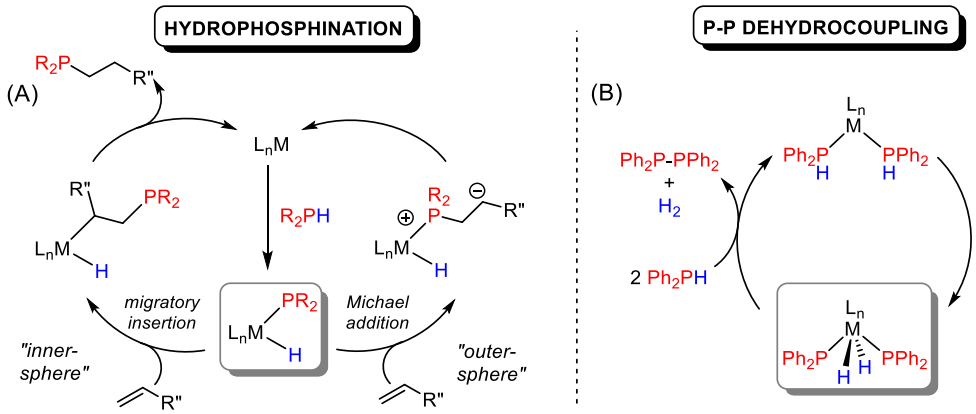

Scheme 2-1. Proposed mechanisms for (A) alkene hydrophosphination and (B) phosphine dehydrocoupling that invoke phosphido hydride complexes as intermediates.

With regard to late transition metals, a handful of such isolable phosphido hydride species involving Group 9 and 10 metals have been reported in recent years (Figure 2-1). Glueck and co-workers demonstrated that P-H oxidative addition by the Pt^0 complex (Me-DuPhos)Pt(*trans*-stilbene) affords a square-planar Pt^{II} phosphido hydride complex **A** that

was shown to engage in catalytic hydrophosphination involving activated (electron-poor) alkene substrates.[72] Manners and co-workers subsequently demonstrated that treatment of the Pt^{II} complex (dcype)PtH_2 (dcype = $Cy_2PCH_2CH_2PCy_2$) with primary and secondary phosphines led to formation of the corresponding *cis*-phosphido-hydride Pt^{II} complexes **B**, with evolution of H_2.[73] In a related example involving Ni, Miluykov, Latypov, and co-workers reported that *in situ* generated (dtbe)Ni^0 (dtbe = $^tBu_2PCH_2CH_2P^tBu_2$) reacts with the bulky primary phosphine $H_2P(2,6\text{-}Mes_2C_6H_3)$ (Mes = $2,4,6\text{-}Me_3C_6H_2$) to afford the mononuclear complex (dtbe)NiH[$PH(2,6\text{-}Mes_2C_6H_3)$] (**C**), the first example of a terminal phosphido hydride Ni species that was also shown to be a viable intermediate in alkene hydrophosphination.[74] In the context of Group 9 chemistry, following early reports from Schunn,[75] as well as Ebsworth and co-workers[76] on the synthesis Ir(H)(PH_2) complexes, Tejel and co-workers[77] have more recently prepared and structurally characterized examples of coordinatively saturated Rh^{III} and Ir^{III} diphenylphosphido hydride complexes supported by tris(pyrazolyl)borate (**D**) or hybrid scorpionate ligation (**E**), respectively. These represent rare examples of terminal Group 9 metal phosphido hydride complexes formed by P-H oxidative addition. The Rh phosphido complex proved to be catalytically active for alkene hydrophosphination as well as dehydrogenative coupling of $HPPh_2$. Less bulky primary phosphines, such as H_2PPh resulted in the formation of phosphido-bridged dinuclear Rh complexes that proved inactive under comparable catalytic conditions.

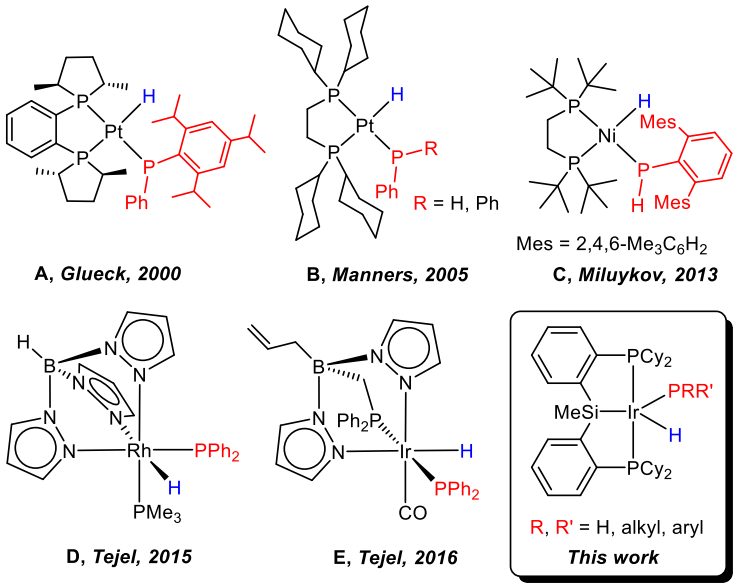

Figure 2-1. Isolable, mononuclear late transition metal phosphido hydride complexes featuring terminal phosphido ligands.

Previous work from the Turculet group has shown that coordinatively unsaturated Ir^{I} species supported by bis(phosphino)silyl ligation of the type κ^3-(2-$Cy_2PC_6H_4)_2SiMe$(Cy-PSiP) can mediate both C-H and N-H bond oxidative addition to afford Ir^{III} species of the type (Cy-PSiP)Ir(H)X (X = aryl, anilido, amido).[20b,52k,66] While five-coordinate Ir aryl hydride complexes of this type are generally not isolable and undergo facile arene exchange reactions,[20b] analogous anilido and amido complexes resulting from N-H bond activation are isolable and highly resistant to N-H reductive elimination.[52k,66] Related Rh anilido hydride complexes are also isolable and thermally stable, however such complexes could not be accessed by an N-H oxidative addition route and were prepared by the metathesis reaction of (Cy-PSiP)Rh(H)Cl (**1-2**) with LiNH(aryl) reagents.[52k,66] In an effort to further explore the reactivity of (Cy-PSiP)M (M = Rh, Ir) towards E-H (E = main group element) bond oxidative addition, reactions with hydrophosphines were pursued with the goal of accessing coordinatively unsaturated

terminal phosphido hydride complexes related to the amido and anilido species previously reported by the Turculet group.

A comparison of N-H bonds in anilines and amines with P-H bonds in hydrophosphines (Table 2-1) reveals that P-H bonds in hydrophosphines are, on average, weaker and more acidic than N-H bonds in comparable amines. As such, P-H bond cleavage is anticipated to be more facile than analogous N-H bond cleavage reactivity. Indeed, the results outlined herein indicate that (Cy-PSiP)Ir readily undergoes P-H oxidative addition reactions with a variety of hydrophosphines to afford rare examples of isolable, coordinatively unsaturated phosphido hydride Ir^{III} complexes that feature terminal phosphido groups. Such phosphido hydride complexes were not observed for Rh, where both P-H and P-C reductive elimination occur rapidly to preferentially form Rh^{I} phosphine adducts. This chapter details these synthetic investigations, as well as the structural characterization of the ensuing complexes, and an exploration of their reactivity.

Table 2-1. Bond dissociation energies (BDE)[56e] and pK_a values[56b,d] for selected amines and phosphines.

	H–NH_2	**H–PH_2**	**H–NHMe**	**H–PHMe**	**H–NHPh**	**H–PHPh**
BDE (kJ mol^{-1})	450.08±0.24	351.0±2.1	425.1±8.4	322.2±12.6	375.3	319.34[a]
pK_a (DMSO)	41	24.1[b]	N/A	29.6[b]	30.6	22.4[b] (24.5) [c]

[a]Calculated (DFT) value.[56c] [b]Calculated value.[56d] [c]Experimental value in THF.[56a]

2.2 Results and Discussion

2.2.1 Synthesis of Ir Phosphido Hydride Complexes *via* Salt Metathesis

In order to study P–H activation *via* (Cy-PSiP)Ir, the viability of Ir phosphido hydride complexes was probed initially by targeting the direct synthesis of such complexes utilizing a salt metathesis approach. In this regard, the Ir^{III} precursor (Cy-PSiP)Ir(H)Cl (**1-**

1) was treated with a variety of lithium phosphido reagents that can be prepared readily by the reaction of commercially available hydrophosphines with ^{n}BuLi (Scheme 2-2). The reaction of **1-1** with one equiv. $LiPPh_2$ led to the quantitative (by ^{31}P NMR) formation of a new complex assigned as the phosphido hydride complex (Cy-PSiP)Ir(H)(PPh_2) (**2-1**). Complex **2-1** was isolated in 83% yield. The formulation of **2-1** was determined on the basis of characteristic NMR data (Table 2-2), including $^{31}P\{^{1}H\}$ NMR resonances at 107.2 (t, 1 P, $^{2}J_{PP}$ = 33 Hz) and 56.7 (d, 2 P, $^{2}J_{PP}$ = 37 Hz) ppm corresponding to the Ir-phosphido (PPh_2) and Ir-phosphino (PCy_2R) groups, respectively. In addition, the ^{1}H NMR spectrum (benzene-d_6) of isolated **2-1** features an Ir-hydride resonance at -15.37 ppm (dt, $^{2}J_{HPCy2}$ = 18 Hz, $^{2}J_{HPPh2}$ = 75 Hz). These data are consistent with a C_s-symmetric five-coordinate structure similar to those observed for **1-1** and related (Cy-PSiP)Ir(H)(anilido) species,[52k,66] where the chemically equivalent Cy-PSiP phosphino donors are *trans*-disposed, and mutually *cis* relative to the Ir-PPh_2 ligand. Complex **2-1** is stable at room temperature both in solution and in the solid state, and upon heating a sample at 70 °C over the course of 18 h in benzene solution no evidence of P-H reductive elimination or decomposition was observed.

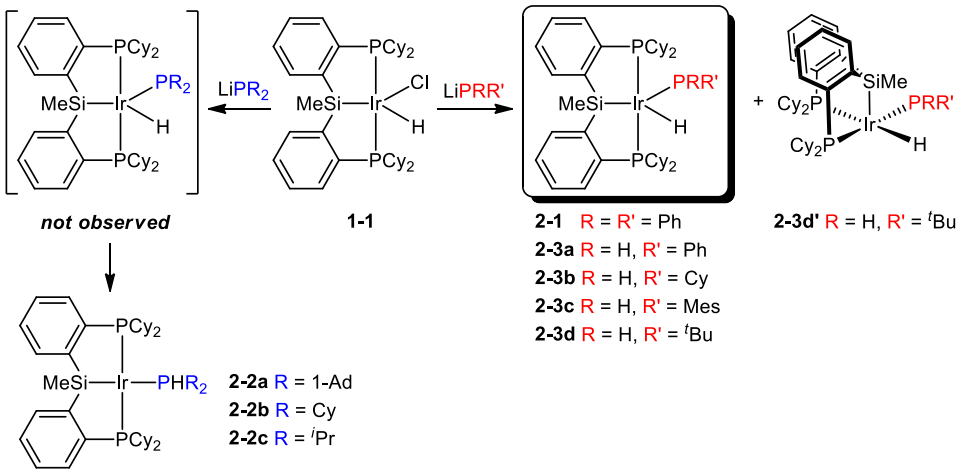

Scheme 2-2. Reaction of (Cy-PSiP)Ir(H)Cl (**1-1**) with lithium phosphide reagents.

Table 2-2. Selected NMR spectroscopic data (ppm) for complexes **2-1**, **2-2a** - **c**, and **2-3a** – **d**.

Complex	^{1}H NMR[a] Ir-*H*	^{31}P{^{1}H} NMR[b] Ir-*phosphido*	^{31}P{^{1}H} NMR[b] Ir-*phosphine*	^{31}P{^{1}H} NMR[b] *parent phosphine*	Δ ^{31}P NMR[c]	^{29}Si NMR[d]
(Cy-PSiP)Ir(H)Cl[20b]	-23.79 (t)	-	-	-	-	7.7
(Cy-PSiP)Ir(H)(NHPh)[52k]	-21.16 (t)	-	-	-	-	13.3
Ir-phosphino complexes						
(Cy-PSiP)Ir(PMe$_3$)[52k]	-	-	-21.2 (t)	-62.6	41	68.0
(Cy-PSiP)Ir[PH(1-Ad)$_2$] (**2-2a**)	-	-	51.4 (br m)	18.1	33	62.8
(Cy-PSiP)Ir(PHCy$_2$) (**2-2b**)	-	-	21.6 (t)	-28.1	50	68.6
(Cy-PSiP)Ir(PH^{i}Pr$_2$) (**2-2c**)	-	-	34.6 (t)	-16.5	51	68.3
Ir-phosphido complexes						
(Cy-PSiP)Ir(H)(PPh$_2$) (**2-1**)	-15.37 (dt)	107.2 (t)	-	-40.6	148	30.8
(Cy-PSiP)Ir(H)(PHPh) (**2-3a**)	-13.51 (dt)	20.8 (t)	-	-122.1	143	24.4
(Cy-PSiP)Ir(H)(PHCy) (**2-3b**)	-14.00 (dt)	69.4 (t)	-	-111.8	181	28.6
(Cy-PSiP)Ir(H)(PHMes) (**2-3c**)	-12.05 (dt)	0.2 (t)	-	-154.8	155	24.0
(Cy-PSiP)Ir(H)(PH^{t}Bu) (**2-3d**)	-14.96 (dt)	99.7 (t)	-	-80.1	180	29.4
(Cy-PSiP)Ir(H)(PH^{t}Bu) (**2-3d'**)	-5.92 (dt)	130.5 (dd)	-	-80.1	211	25.8

[a]Benzene-d_6. [b]Relative to 85% H_3PO_4. [c]Downfield shift of ^{31}P NMR resonance upon complexation of *parent phosphine* to Ir as either Ir-*phosphido* or Ir-*phosphine*. [d] ^{1}H-^{29}Si HMBC.

Encouraged by this result, the reactivity of **1-1** with other phosphido reagents derived from secondary phosphines was evaluated (Scheme 2-2). Unlike in the case of **2-1**, treatment of **1-1** with one equiv. of either LiP(1-Ad)$_2$, LiPCy$_2$, or LiP(^{i}Pr)$_2$ led to quantitative (by ^{31}P NMR) formation of the corresponding Ir^{I} phosphine adduct (Cy-PSiP)Ir(PHR$_2$) (Scheme 2-2; **2-2a**, R' = 1-Ad; **2-2b**, R = Cy; **2-2c**, R = ^{i}Pr), presumably as a result of P-H reductive elimination from Ir^{III} phosphido hydride intermediates. The formation of **2-2a** – **c** was generally complete within 30 min. of mixing, with no evidence for phosphido hydride intermediate species observed spectroscopically (by ^{31}P or ^{1}H NMR) over the course of the reaction. Characteristic of the formulation of **2-2a** – **c** as secondary phosphine adducts, the ^{1}H NMR spectra of these complexes (benzene-d_6) each feature a P-

H resonance at 5.64 (dt, $^{1}J_{HP}$ = 295 Hz, $^{2}J_{HP}$ = 13 Hz), 5.17 (dm, $^{1}J_{HP}$ = 292 Hz), and 5.19 (dm, $^{1}J_{HP}$ = 290 Hz) ppm, respectively, rather than an Ir-*H* resonance. In the case of **2-2b** and **c**, two resonances were observed by $^{31}P\{^{1}H\}$ NMR spectroscopy (for **2-2b**, δ 63.1 (d, 2 P, $^{2}J_{PP}$ = 11 Hz), 21.6 (t, 1 P, $^{2}J_{PP}$ = 11 Hz); for **2-2c**, δ 63.3 (d, 2 P, $^{2}J_{PP}$ = 10 Hz), 34.6 (t, 1 P, $^{2}J_{PP}$ = 10 Hz)), corresponding to chemically equivalent Cy-PSiP phosphino donors and the secondary phosphine ligand, respectively (Table 2-2). These data are consistent with C_s-symmetric, square-planar Ir species in solution, similar to that previously noted for (Cy-PSiP)Ir(PMe_3). By comparison, in the case of **2-2a**, the Cy-PSiP phosphino donors give rise to an AB multiplet (δ_A = 67.2, δ_B = 51.9, $^{2}J_{AB}$ = 278 Hz), likely due to hindered rotation involving the very bulky HP(1-Ad)$_2$ ligand. No appreciable change in these ^{31}P NMR features was observed when the spectrum was acquired at 80°C, suggesting that the barrier for rotation about the Ir−PH(1-Ad)$_2$ bond is relatively high.

The solid-state structure of **2-2c** was obtained by use of single crystal X-ray diffraction techniques and is in agreement with the formulation of this complex as an Ir^{I} phosphine adduct. The complex adopts distorted square planar geometry in the solid state, with the HP^{i}Pr$_2$ ligand coordinated to Ir trans to Si. The P1-Ir-P2 and P3-Ir-Si bond angles of 149.47(8) and 151.57(8)°, respectively, are comparable to those reported previously for the related complex (Cy-PSiP)Rh(PMe_3).[52k]

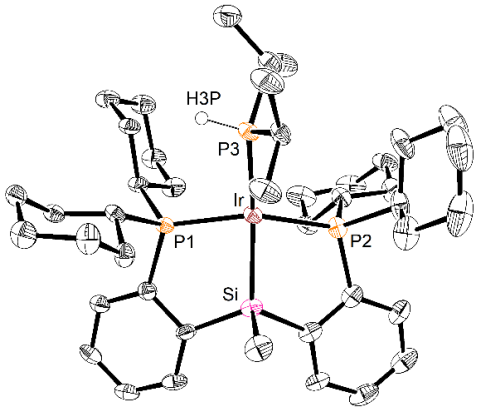

Figure 2-2. Crystallographically determined structure of **2-2c** with thermal ellipsoids drawn at the 50% probability level. Most hydrogen atoms have been omitted for clarity. Selected interatomic distances (Å) and angles (°): Ir-P1 2.255(2), Ir-P2 2.279(2), Ir-P3 2.320(2), Ir-Si 2.314(2), P3-H3P 1.19(10), P1-Ir-P2 149.47(8), P1-Ir-P3 97.22(8), P2-Ir-P3 108.74(8), P1-Ir-Si 82.33(8), P2-Ir-Si 82.23(8), P3-Ir-Si 151.57(8).

In an effort to prevent P-H reductive elimination, Ir phosphido hydride complexes derived from primary phosphines were targeted, with the consideration that steric effects may play an important role in facilitating such reductive elimination reactions. Indeed, treatment of **1-1** with lithium phosphide reagents derived from primary phosphines led to quantitative (by ^{31}P NMR) formation of the corresponding Ir^{III} phosphido complexes (Cy-PSiP)Ir(H)(PHR') (Scheme 2-2; **2-3a**, R' = Ph; **2-3b**, R' = Cy; **2-3c**, R' = Mes; **2-3d**, R' = ^{t}Bu), all of which proved isolable and resistant to reductive elimination (including upon heating in benzene solution at 75 – 80 °C over the course of 18 h), as in the case of **2-1**. The ^{1}H NMR spectra of complexes **2-3a** – **d** (benzene-d_6) each feature Ir-*H* resonances, consistent with their formulation as Ir^{III} phosphido hydride species (Table 2-2). A selective 1D NOESY experiment (25 °C; relaxation delay = 1.0 s; mixing time = 0.5 s) was carried out in the case of **2-3c**, and no response was observed in the P-*H* resonance upon irradiation of the Ir-*H* resonance. In the case of **2-3d**, two such Ir-*H* resonances were observed (δ -14.96 (dt, $^{2}J_{HP}$ = 66 Hz, $^{2}J_{HP}$ = 18 Hz and -5.92 (dt, 1 H, $^{2}J_{HP}$ = 99 Hz, $^{2}J_{HP}$ = 24 Hz; *ca.* 1:1 ratio), indicative of isomeric Ir phosphido hydride species in solution. This proposal is

supported by the $^{31}P\{^{1}H\}$ NMR spectrum of this complex, which contains resonances that can be assigned to two such isomers: **2-3d**, which features chemically equivalent *trans*-disposed Cy-PSiP phosphino groups giving rise to a single $^{31}P\{^{1}H\}$ NMR resonance at 57.7 ppm, and **2-3d'**, which features inequivalent *cis*-disposed phosphino groups (δ 55.3 (d, $^{2}J_{PP trans}$ = 152 Hz) and 50.2 (d, $^{2}J_{PP cis}$ = 32 Hz)), consistent with a square pyramidal structure where Si is coordinated in the apical position (Scheme 2-2).

The ^{31}P NMR shifts of complexes **2-1** and **2-3a** – **d** are shown in Table 2-2, and range in value from 130.5 ppm (for **2-3d'**) to 0.2 ppm (for **2-3c**). It has been noted that the ^{31}P NMR chemical shift of terminal phosphido ligands correlates with sp^2-hybridization at phosphorus accompanied by P→M π-donation, such that ^{31}P chemical shifts that are significantly downfield (relative to the parent phosphine, often on the order of 150 - 300 ppm difference) are associated with significant M-P π-bonding and planarity at the phosphido P donor (Figure 2-3).[78] Conversely, ^{31}P chemical shifts that are not significantly downfield relative to either the parent phosphine, or a structurally related metal-phosphino precursor, are associated with an absence of significant M-P π-bonding and pyramidal geometry at the predominantly sp^3-hybridized phosphido P donor. An evaluation of the change in ^{31}P NMR chemical shift in the phosphido hydride species **2-1** and **2-3a** – **d** relative to the respective parent phosphines (Table 2-2) indicates a downfield shift (Δ ^{31}P NMR) ranging from 143 (for **2-3a**, *cf.* free H_2PPh) – 211 ppm (for **2-3d'**, *cf.* free $H_2{}^{t}Bu$). The magnitude of this downfield shift suggests that moderate to significant P→M π-donation may be invoked for **2-1** and **2-3a** – **d**, with more pronounced π-interaction in the case of alkyl phosphido donors such as PHCy and $PH{}^{t}Bu$. This is in accord with the coordinatively and electronically unsaturated nature of such complexes. By comparison, Δ

^{31}P NMR in the case of the secondary phosphino derivatives **2-2a** – **c** ranges from 33 to 51 ppm, and is comparable in magnitude to that of 41 ppm previously reported for (Cy-PSiP)Ir(PMe_3).[52k] Further comparison to previously reported terminal phosphido complexes of Ir shows that in the case of the coordinatively saturated Ir(H)(PPh_2) complex previously reported by Tejel and co-workers (**E**, Figure 2-1),[77a] the ^{31}P NMR resonance of the phosphido ligand appears at 4.2 ppm, corresponding to a downfield shift of 45 ppm relative to $HPPh_2$. X-Ray crystallographic characterization of the latter complex confirm that the phosphido ligand is pyramidal at P, with a sum of bond angles at P of 318.92°.[77a] While the latter complex is coordinatively saturated, more closely related five-coordinate Ir^{III} phosphido methyl complexes of the type (PNP)Ir(Me)(PRR') (PNP = κ^3-*N*($SiMe_2CH_2$*P*Ph_2)$_2$) have been reported by Fryzuk and co-workers.[79] The ^{31}P NMR chemical shift of the phosphido ligands in such complexes is closely matched to that observed for the PSiP-supported phosphido complexes reported herein (*e.g.*, δ 26.95 for R = H, R' = Ph,[79a] *cf.* 20.8 for **2-3a**; δ 105.65 for R = R' = Ph,[79b] *cf.* 107.2 for **2-1**). However, the X-ray crystal structure of (PNP)Ir(Me)(PPh_2) revealed pyramidal geometry at the phosphido P in the solid state (Σ< at P = 326.4°), in conjunction with a planar amido donor in the PNP ligand backbone.[79a] This latter observation suggests that the correlation between Δ ^{31}P NMR (M-phosphido *cf.* parent phosphine) and hybridization at phosphorus/M-phosphido π-bonding may not be as direct as initially anticipated.

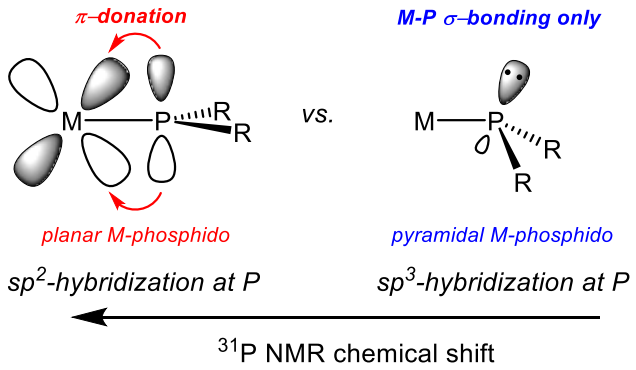

Figure 2-3. Correlation of M-PR_2 bonding in transition metal phosphido complexes with hybridization at phosphorus and ^{31}P NMR chemical shift.

In order for P→M π-donation, the metal center must have empty, low-lying acceptor orbitals of appropriate symmetry. In the case of diamagnetic, five-coordinate d^6 metal complexes that feature a π-donor X, detailed theoretical analyses of metal-ligand bonding interactions have shown that such complexes adopt distorted ("Y-shaped" in the equatorial plane) trigonal bipyramidal (dist-TBP, Figure 2-4) structures of the type previously observed for (Cy-PSiP)Ir(H)X (X = Cl, amido, anilido), which facilitate the overlap of π-donor orbitals on X with the metal d_{xy} orbital that lies in the trigonal plane.[80] As such, P→M π-donation in (Cy-PSiP)Ir(H)(phosphido) complexes is indeed feasible, and the ensuing complexes are anticipated to adopt similarly distorted trigonal bipyramidal structures. Notably, in order for such π-overlap to occur, a fixed orientation of the planar phosphido ligand orthogonal to the Y-distorted trigonal plane is required (Figure 2-4C). In the case of unsymmetrically substituted phosphido ligands, such as is the case for **2-3a** – **d**, this orientation should give rise to chemically inequivalent Cy-PSiP phosphino donors in the absence of rapid rotation about the Ir-phosphido linkage. Analysis of the room temperature $^{31}P\{^1H\}$ NMR spectra of **2-3a** – **c** reveals that the pincer phosphino donors give rise to a single, somewhat broad resonance in each case, consistent with a relatively

low barrier to inversion/rotation about the Ir-phosphido bond, which leads to averaged Cy-PSiP phosphorus environments. Variable temperature $^{31}P\{^{1}H\}$ NMR analysis for **2-3c** revealed that the resonance attributed to the Cy-PSiP-phosphino donors decoalesces (at T_c = 273K), such that at the low temperature limit an AB pattern is observed (δ_A 59.7, δ_B 55.8, J_{AB} = 273 Hz), consistent with the proposed dist-TBP static structure (Figure 2-5A). The $\Delta G^{\ddagger}$ associated with this process was determined to be 12.2 kcal mol^{-1}, which falls well within the range of barriers (ca. 11 – 16 kcal mol^{-1}) reported previously for inversion/rotation at phosphorus in pyramidal phosphido ligands.[81] Variable temperature ^{1}H NMR analysis for **2-3c** (toluene-d_8) revealed that the *ortho*-Me protons of the P*Mes* substituent also give rise to an averaged ^{1}H NMR resonance at high temperature, and this resonance decoalesces at 288K with $\Delta G^{\ddagger}$ = 13.6 kcal mol^{-1} (Figure 2-5B). This barrier is associated with inversion/rotation involving the P-C_{ipso} linkage of the PHMes ligand. These observations indicate that although P→Ir π-donation in **2-3c** and related complexes is feasible based on orbital considerations, phosphido π-contribution is likely minimal. Interestingly, in the case of (Cy-PSiP)Ir(H)(PH^{t}Bu), ^{31}P and ^{1}H NMR analysis revealed an apparent 1:1 mixture of the predicted dist-TBP species (**2-3d**) and a square pyramidal isomer with Si in the apical position (**2-3d'**). While electronic considerations suggest that the dist-TBP structure should be preferred, it is possible that the steric demand of the PH^{t}Bu ligand perturbs this bonding model.

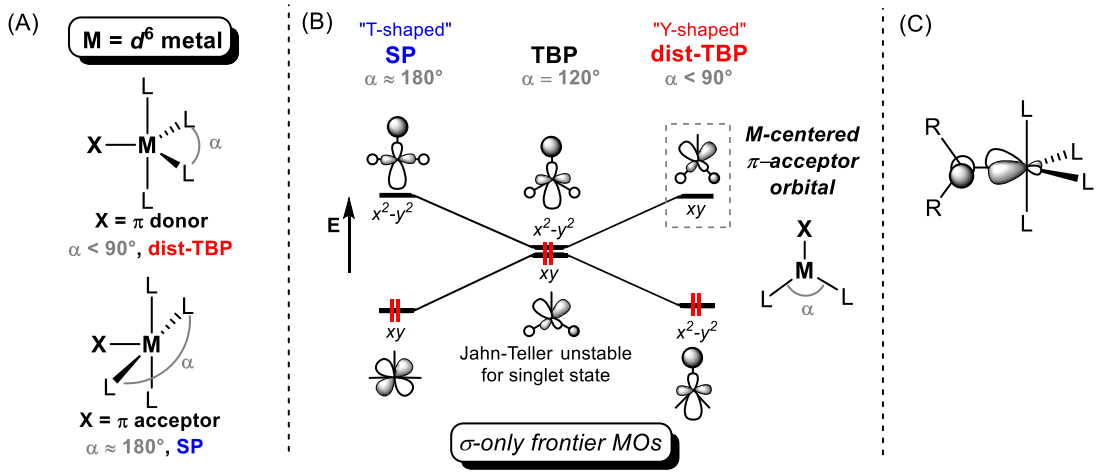

Figure 2-4. (A) Distorted trigonal bipyramidal (dist-TBP) and square pyramidal (SP) structures accessible to diamagnetic, five-coordinate d^6 complexes; (B) σ-only frontier MOs associated with such structures (adapted from ref. 80); and (C) orientation of PR_2 phosphido ligand required for π-overlap in the dist-TBP scenario.

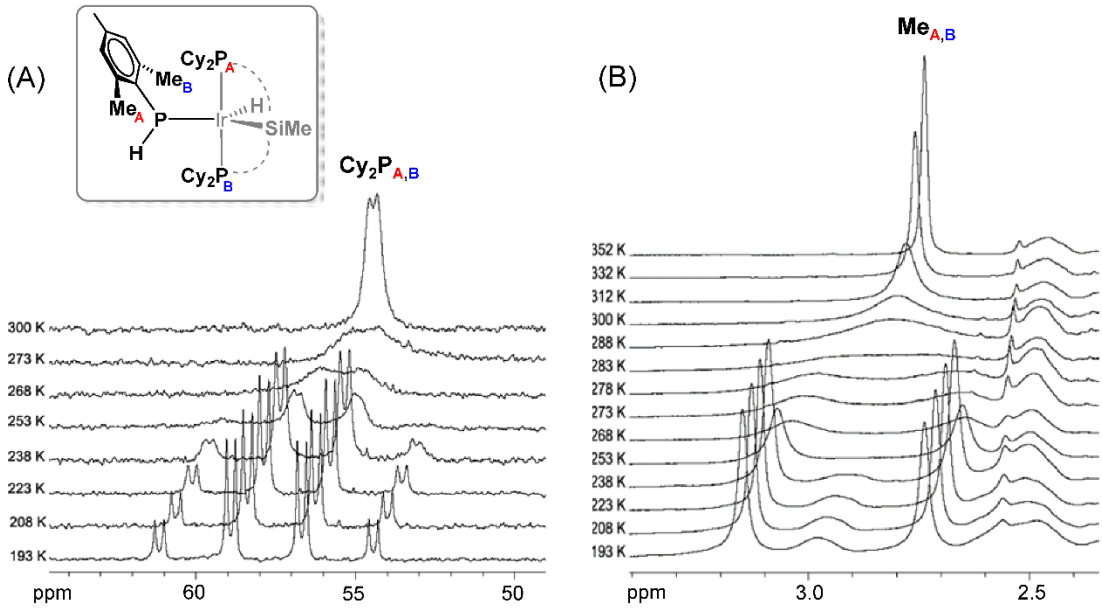

Figure 2-5. Variable temperature (A) $^{31}P\{^1H\}$ NMR (121.5 MHz) spectra of **2-3c**, showing decoalescence of the Cy-PSiP-phosphino resonance; and (B) ^1H NMR (toluene-d_8, 300 MHz) spectra of **2-3c**, showing decoalescence of the *ortho*-Me resonance involving the PHMes ligand.

The solid-state structures of **2-3c** and **2-3d** were determined by use of single crystal X-ray diffraction techniques, confirming the proposed formulation of these complexes as

five-coordinate Ir species with terminal phosphido ligands (Figure 2-6). Complex **2-3c** features dist-TBP coordination geometry at Ir with *trans*-disposed PSiP-phosphino groups (P1-Ir-P2 156.65(5)°), consistent with solution NMR data. The trigonal plane contains Si, the phosphido P (P3), as well as the Ir-*H* (H1), with an acute Si-Ir-H1 angle of 82.5(14)°, which is consistent with the predicted Y-shaped distortion (*vide supra*). The sum of bond angles at P3 is 347.8°, which is intermediate in value between 360° (planar P) and the values obtained for the Ir(H)(PPh_2) complex previously reported by Tejel and co-workers (**E**, Figure 2-1; 318.92°)[77a] and Fryzuk's (PNP)Ir(Me)(PPh2) complex (326.4°).[79a] Thus it appears that although the barrier to inversion/rotation at the phosphido donor in **2-3c** is relatively low (12.2 kcal mol^{-1}, *vide supra*), the geometry at phosphorus in the solid state is significantly closer to planar than has been observed previously for terminal Ir^{III} phosphido complexes. The Ir-P3 distance of 2.2672(16) Å is significantly shorter than that of 2.436(1) Å reported by Tejel and co-workers for the Ir-PPh_2 distance in complex **E** (Figure 2-1),[77a] but closer in value to that of 2.297(2) Å reported by Fryzuk and co-workers[79a] for the Ir-PPh_2 distance in five-coordinate (PNP)Ir(Me)(PPh_2). In the case of complex **2-3d**, the PH^{t}Bu ligand is disordered over two positions, with the major contributor (**2-3d *major***, 85% occupancy, Figure 2-6B) adopting analogous coordination geometry to **2-3c**. The sum of bond angles at the phosphido P3A is 354.3°, which is slightly closer to planarity than in **2-3c**, and the Ir-P3A distance of 2.2544(8) Å is slightly shorter. The orientation of the PH^{t}Bu ligand is nearly perpendicular to the Y-distorted trigonal plane (Si-Ir-P3A-C2A-77.1(3)°), positioning the phosphido group for π-overlap with the Ir d_{xy} orbital. Conversely, the minor contributor (**2-3d *minor***, 15% occupancy, Figure 2-6C) features square pyramidal coordination at Ir, with Si in the apical position and the PH^{t}Bu

ligand coordinated *trans* to hydride (P3B-Ir-H1 170.4(12)°, *cf.* 147.1(11)° for P3A-Ir-H1). Notably, this square pyramidal component is different from the square pyramidal isomer **2-3d'**, which features the phosphido ligand coordinated *cis* to the Ir-*H* and has effective C_1 symmetry in solution. The Ir-P3B distance of 2.302(5)Å is slightly elongated relative to the Ir-P3A distance. The phosphido ligand is oriented such that the P-^{t}*Bu* group is *anti*-relative to the Ir-*Si* (Si-Ir-P3B-C2B-177.7(19)°), which corresponds to a rotation of the phosphido ligand along Ir-P of *ca*. 100°.

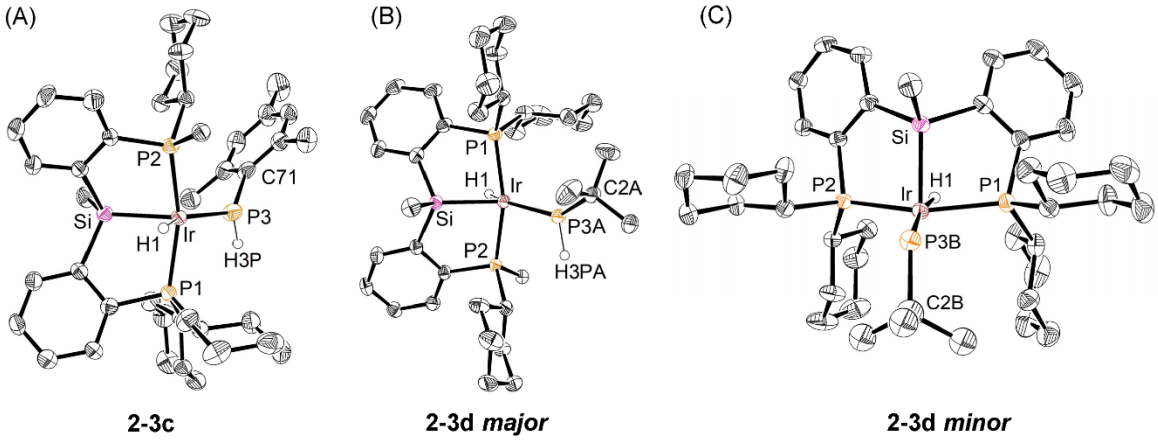

Figure 2-6. Crystallographically determined structures of **2-3c** (A), **2-3d *major*** (B), and **2-3d *minor*** (C) shown with thermal ellipsoids drawn at the 50% probability level. Selected P*Cy* carbon atoms and most hydrogen atoms have been omitted for clarity, including the calculated P-*H* of **2-3d *minor***. Only one of the two crystallographically independent molecules of **2-3c** is shown. Selected interatomic distances (Å) and angles (°): for **2-3c** Ir-H1 1.501(5), Ir-P1 2.2901(14), Ir-P2 2.2892(13), Ir-P3 2.2672(16), Ir-Si 2.2869(15), P3-C71 1.839(6), P1-Ir-P2 156.65(5), P3-Ir-Si 127.16(6), P3-Ir-H1 150.0(14), Si-Ir-H1 82.5(14), P3-Ir-Si 127.16(6), Ir-P3-H3P 121(3), Ir-P3-C71 132.8(2), C71-P3-H3P 94(3); for **2-3d *major*** Ir-H1 1.47(3), Ir-P1 2.2998(7), Ir-P2 2.2865(7), Ir-P3A 2.2544(8), Ir-Si 2.3100(7), P3A-C2A 1.872(4), P1-Ir-P2 154.98(2), P3A-Ir-Si 133.48(3), P3A-Ir-H1 147.1(11), Si-Ir-H1 78.7(11), Ir-P3A-H3PA 118(2), Ir-P3A-C2A 141.55(15), C2A-P3A-H3PA 95(2); for **2-3d *minor*** Ir-P3B 2.302(5), P3B-Ir-Si 105.30(12), P3B-Ir-H1 170.4(12), Ir-P3B-C2B 122.8(15).

The dist-TBP structures observed for **2-3c** and **2-3d *major*** are comparable to those of related amido and anilido complexes supported by Cy-PSiP ligation (Table 2-3).[52k,66] One notable difference is the trend of short Ir-N distances (2.056(2) Å for (Cy-

PSiP)Ir(H)(NHPh), 2.077(3) Å for (Cy-PSiP)Ir(H)[NH(2,6-$Me_2C_6H_3$)], and 2.018(2) Å for (Cy-PSiP)Ir(H)[NH(1-Ad)]) by comparison with Ir-P (phosphido) distances, which is in accordance with the smaller size of N *vs*. P. In solution, $^{31}P\{^1H\}$ NMR analysis for such anilido and amido complexes indicates a single resonance in each cases, consistent with averaged phosphine environments due to rapid inversion/rotation involving the Ir-N bond, similar to the observations made for the related phosphido hydride complexes reported herein.

Table 2-3. Selected crystallographic data – interatomic distances (Å) and bond angles (°) for crystallographically characterized complexes (Cy-PSiP)Ir(H)X (X = Cl, amido, anilido, phosphido).

Complex	Ir-X distance	P-Ir-P (PSiP) Angle	Si-Ir-X Angle	X-Ir-H Angle	Si-Ir-H Angle
(Cy-PSiP)Ir(H)(PHMes) (**2-3c**)	2.2672(16)	156.65(5)	127.13(6)	150.0(14)	82.5(14)
(Cy-PSiP)Ir(H)(PH^{t}Bu) (**2-3d *major***)	2.2544(8)	154.98(2)	133.48(3)	147.1(11)	78.7(11)
(Cy-PSiP)Ir(H)Cl[20b]	2.4143(12)	166.07(4)	130.64(5)	160.6(18)	68.7(18)
(Cy-PSiP)Ir(H)(NHPh)[52k]	2.056(2)	158.06(3)	137.35(8)	154.4	67.5
(Cy-PSiP)Ir(H)[NH(2,6-$Me_2C_6H_3$)][52k]	2.077(3)	162.01(3)	129.72(11)	160.7	68.8
(Cy-PSiP)Ir(H)[NH(1-Ad)][66]	2.018(2)	154.61(2)	131.03(7)	153.7	72.6

2.2.2 Attempted Synthesis of Rh Phosphido Complexes *via* Salt Metathesis

Having successfully prepared a series of mononuclear Ir phosphido hydride complexes by a salt metathesis route, the synthesis of related Rh species was also attempted (Scheme 2-3). In all such attempts, treatment of the hydrido chloride Rh precursor **1-2** with a range of different lithium phosphide reagents (*e.g.*, LiPHCy, $LiPPh_2$, LiP^iPr_2, LiPHMes) resulted in quantitative formation of the corresponding Rh^I phosphine complexes (Cy-PSiP)Rh(PHRR') (**2-4a** R = H, R = Cy; **2-4b** R = R' = Ph; **2-4c** R = R' = ^{i}Pr; **2-4d** R = H, R' = Mes), which can be isolated in high yield. Monitoring of these reaction mixtures by ^{31}P and ^1H NMR spectroscopy revealed no evidence for the formation of intermediate

phosphido hydride species. As in the case of **2-2a** – **c**, the ^{1}H NMR spectra of complexes **2-4a** – **e** do not feature a characteristic Ir-*H* resonance, which is the most telling indicator of P-H reductive elimination. Rather, a downfield P-*H* resonance is observed, which is readily identified by the characteristic large $^{1}J_{PH}$ coupling constant (Table 2-4).

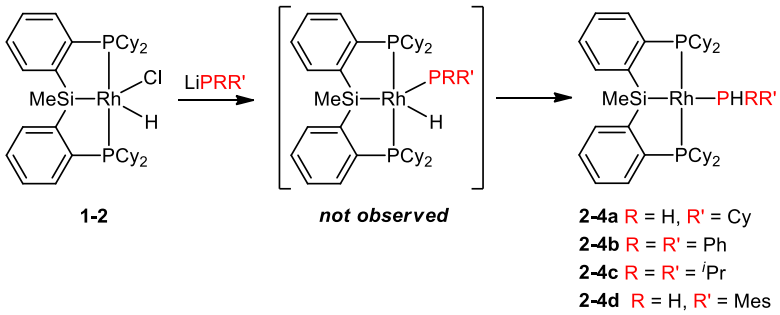

Scheme 2-3. Synthesis of (Cy-PSiP)Rh(PHRR') complexes by P-H reductive elimination.

Table 2-4. Selected NMR spectroscopic data (ppm) for complexes **2-4a** – **e**.

Complex	^{1}H NMR[a] P-*H*	$^{1}J_{PH}$ (Hz)	^{31}P{^{1}H} NMR[b] Rh-*phosphino*	^{31}P{^{1}H} NMR[b] *parent phosphine*	Δ ^{31}P NMR[c]	^{29}Si NMR[d]
(Cy-PSiP)Rh(PMe_3)[52k]	-	-	-21.2 (t)	-62.6	41	68.0
(Cy-PSiP)Rh(PPh_3) (**2-6**)	-	-	20.8 (dt)	-5.0	26	68.8
(Cy-PSiP)Rh(PH_2Cy) (**2-4a**)	4.73 (dm)	264	-50.6 (dt)	-111.8	61	70.2
(Cy-PSiP)Rh($PHPh_2$) (**2-4b**)	7.15 (dt)	290	-5.9 (dt)	-40.6	35	69.6
(Cy-PSiP)Rh(PH^iPr_2) (**2-4c**)	4.50 (dm)	269	26.6 (dt)	-16.5	43	69.5
(Cy-PSiP)Rh(PH_2Mes) (**2-4d**)	6.50 (br d)	282	-103.5 (br d)	-154.8	51	68.8

[a]Benzene-d_6. [b]Relative to 85% H_3PO_4. [c]Downfield shift of ^{31}P NMR resonance upon complexation of *parent phosphine* to Rh. [d]^{1}H-^{29}Si HMBC.

The apparently facile P-H reductive elimination in the case of (Cy-PSiP)Rh(H)(phosphido) species stands in contrast to the resistance to N-H reductive elimination of the analogous anilido Rh species. Both (Cy-PSiP)Rh(H)(NHPh) and (Cy-PSiP)Rh(H)[NH(2,6-$Me_2C_6H_3$)] are isolable complexes that are stable both in solution and in the solid state.[52k] As such, while steric factors seemed to play a role in the propensity of (Cy-PSiP)Ir(H)(phosphido) complexes to undergo reductive elimination, it does not appear

that steric considerations factor as significantly in the observed reductive elimination at Rh. From a thermodynamic perspective, Rh^{I}-phosphino complexes are anticipated to be relatively more stable than Rh^{I}-aniline adducts, which have been observed in the case of Cy-PSiP ligation only in the presence of excess aniline and are not isolable.[52k] However, the kinetic barrier to reductive elimination must also be considered, and appears to generally be lower in the case of Rh P-H reductive elimination than Ir.

In an effort to access low-coordinate terminal Rh phosphido complexes, alternative Rh precursors were sought. In this regard, the phenyl complex (Cy-PSiP)Rh(Ph)Br (**2-5**) was prepared by treatment of **1-2** first with $LiCH_2SiMe_3$, and subsequently with PhBr (Scheme 2-4).

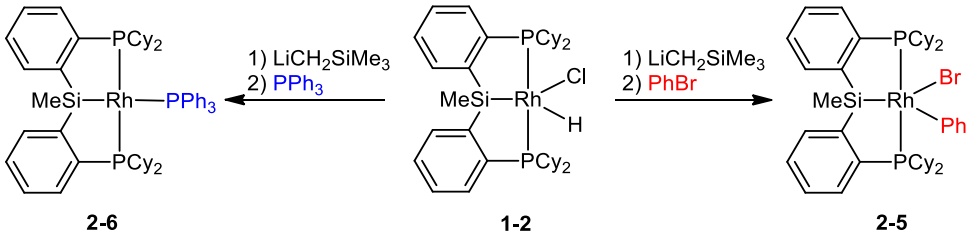

2-6 **1-2** **2-5**

Scheme 2-4. Synthesis of complexes **2-5** and **2-6**.

Complex **2-5** was isolated in 93% yield and gives rise to a single $^{31}P\{^{1}H\}$ NMR resonance at 45.9 ppm (d, $^{1}J_{PRh}$ = 117 Hz), consistent with a C_s-symmetric structure in solution. Treatment of **2-5** with one equiv. $LiPPh_2$ in benzene solution led to the full consumption of **2-5** and formation of two products (by ^{31}P NMR) in a ca. 2:1 ratio (after 18 h at room temperature, followed by 8 h heating at 65 °C), as well as trace PPh_3 (Figure 2-7). The major product is (Cy-PSiP)Rh(PPh_3) (**2-6**), resulting from P-Ph reductive elimination. The assignment of **2-6** was confirmed by the independent synthesis of this complex (Scheme 2-4, Table 2-4). No evidence for the formation of a phosphido phenyl

intermediate on the path to **2-6** was detected by monitoring of this reaction using $^{31}P\{^{1}H\}$ NMR techniques. A second minor product observed (*ca*. 25%) in this reaction corresponds to the *diphenyl*phosphino adduct **2-4b**, assigned on the basis of ^{1}H and ^{31}P NMR analysis. The possibility of **2-4b** resulting from the reaction of $LiPPh_2$ with a protic impurity in the reaction mixture was considered, but the formation of this complex proved reproducible in numerous subsequent experiments where the purity of reagents and the solvent was rigorously confirmed. Furthermore, samples of **2-6** prepared independently do not generate **2-4b** over time. As such, the formation of **2-4b** appears to be endemic to the reaction of **2-5** with $LiPPh_2$, implying that the unobserved intermediate (Cy-PSiP)Rh(Ph)(PPh_2) (**2-7**) may be involved.

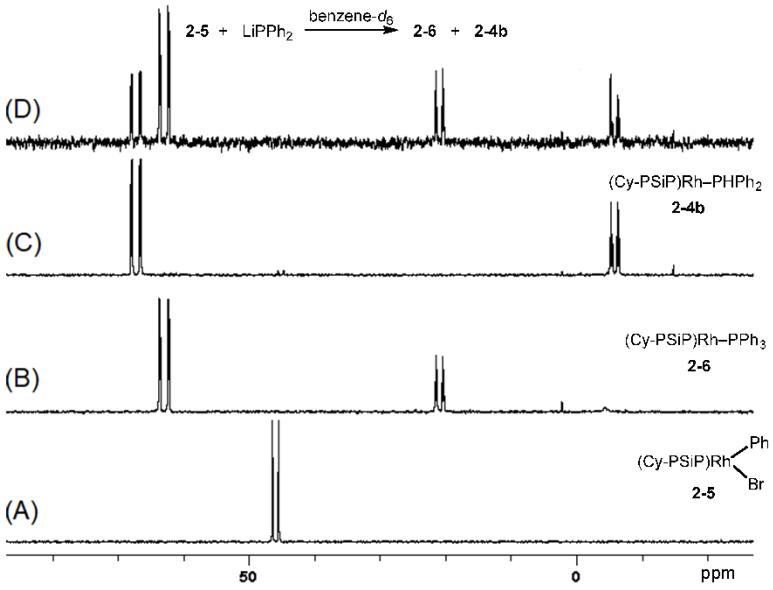

Figure 2-7. $^{31}P\{^{1}H\}$ NMR spectra (122.5 MHz, benzene-d_6) of: (A)(Cy-PSiP)Rh(Ph)Br (**2-5**); (B) (Cy-PSiP)Rh(PPh_3) (**2-6**); (C) (Cy-PSiP)Rh($PHPh_2$) (**2-4b**); and (D) reaction mixture resulting from treatment of **2-5** with one equiv. $LiPPh_2$, after 18 h at room temperature, followed by 8 h heating at 65 °C.

Mechanistic possibilities for the formation of **2-4b** in this context include: (A) reactivity with the benzene solvent, (B) β-H elimination involving a P*Cy* substituent, or

(C) ligand metalation involving the P*Cy* substituents (Scheme 2-5). With respect to pathway (A), one can envision reactivity with benzene *via* a σ-bond metathesis-like pathway involving a benzene sp^2-C-H bond and either the Rh-Ph or Rh-PPh_2 linkages. Concerning the latter option, the intramolecular addition of an sp^2-C-H bond across a terminal metal-phosphido ligand has been previously reported,[83] including by Peters and co-workers in a related tetradentate tris(phosphino)silyl Ru^{II} system.[62b] Experiments conducted in benzene-d_6 did not reveal ^2H incorporation at the P-H position in **2-4b** in a manner that would be consistent with a benzene activation pathway (A). As well, the formation of **2-4b** was reproduced when the reaction was carried out in either cyclohexane or THF solution, confirming that benzene is not necessary for this reactivity. In pathway (B), *β*-H elimination involving a P*Cy* substituent[83] would generate P=Cy fragments, which should be readily observable by ^{31}P NMR spectroscopic analysis. As this spectroscopic feature is absent in the $^{31}P\{^1H\}$ NMR spectra of **2-4b** formed in this context, pathway (B) is likely not operational. Lastly, pathway (C) involving P*Cy* metalation, followed by β-hydride elimination, and final P-H reductive elimination, remains as the most plausible mechanistic pathway for the formation of **2-4b** *via* **2-7**. The metalation of P*Cy* substituents has been well-documented,[84] and a Ru^{II} cyclohexenyl species derived from such Cy-PSiP activation has been previously reported.[64a] While PCy metalation and subsequent *β*-hydride elimination should generate a P-cyclohexenyl fragment that may be detected by ^1H and ^{13}C NMR spectroscopic techniques, no such olefinic resonances were observed for the minor species **2-4b** formed in this reaction. However, this apparent discrepancy may be attributed to the formation of a mixture of isomeric species (**2-4b'**), wherein the position of C=C bond is varied within the four (formerly) P*Cy* groups. Attempts to vary the phosphido lithium

reagent resulted in the formation of complex reaction mixtures from which no pure material could be isolated.

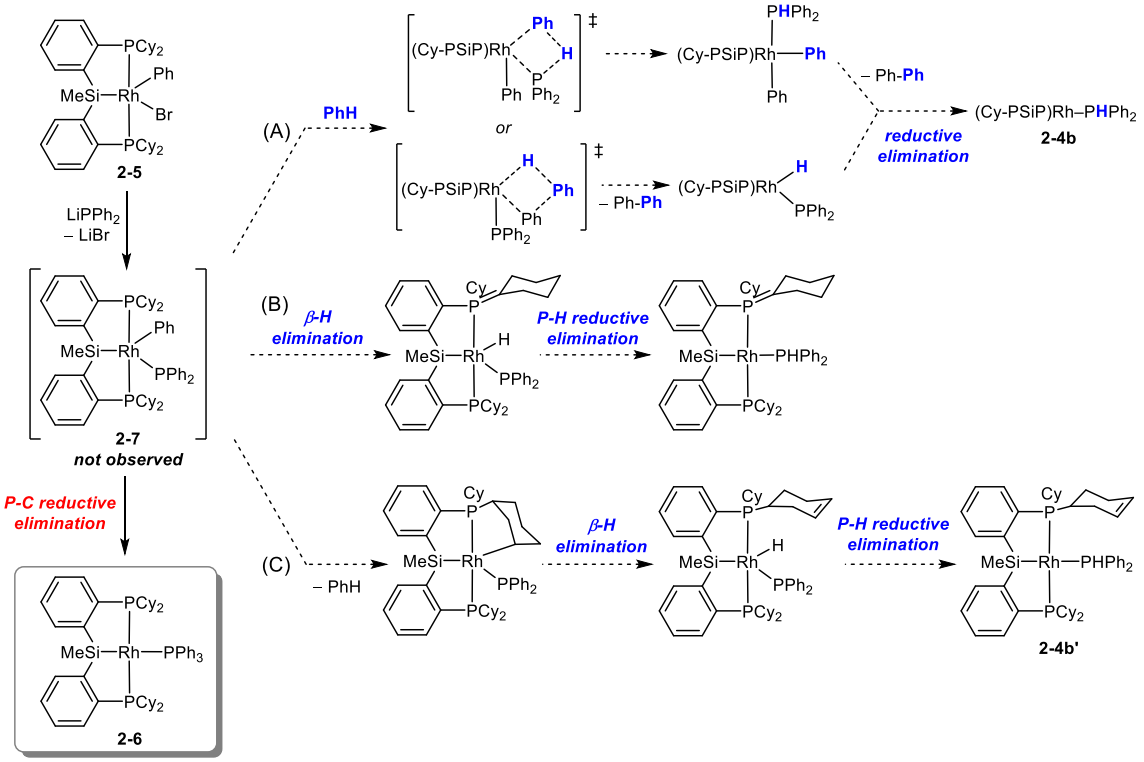

Scheme 2-5. Proposed mechanistic pathways for the formation of **2-6** and **2-4b** *via* (Cy-PSiP)Rh(Ph)(PPh_2).

The formation of **2-6** *via* sp^2-C-P reductive elimination is a commonly invoked step in C-P cross-coupling catalysis, where Pd catalysts are commonly employed (Scheme 2-6A).[71b,85] In this context, C-P reductive elimination of arylphosphines from arylpalladium phosphido complexes is generally considered to be much faster than reductive eliminations of arylamines from arylpalladium amides.[86] In an effort to gauge the propensity of (Cy-PSiP)Rh to facilitate sp^2-C-P cross-coupling, a catalytic amount (10 mol%) of **2-5** was treated with PhBr and $HPPh_2$ in the presence of base (Table 2-5). While no conversion was observed (by ^{31}P NMR) at room temperature in benzene solution after 48 h in the presence of either NaO^tBu or Cs_2CO_3, heating of these reaction mixtures at 75 °C for 24 h resulted

in *ca*. 50% conversion to tetraphenyldiphosphine (Ph_2P-PPh_2), the product of $HPPh_2$ dehydrocoupling, with no trace of Ph_3P observed. Additional heating at this temperature did not result in further conversion to either PPh_3 or Ph_2P-PPh_2. The control reaction (reaction without **2-5**) did not show any conversion, either for P–C or P–P coupling.

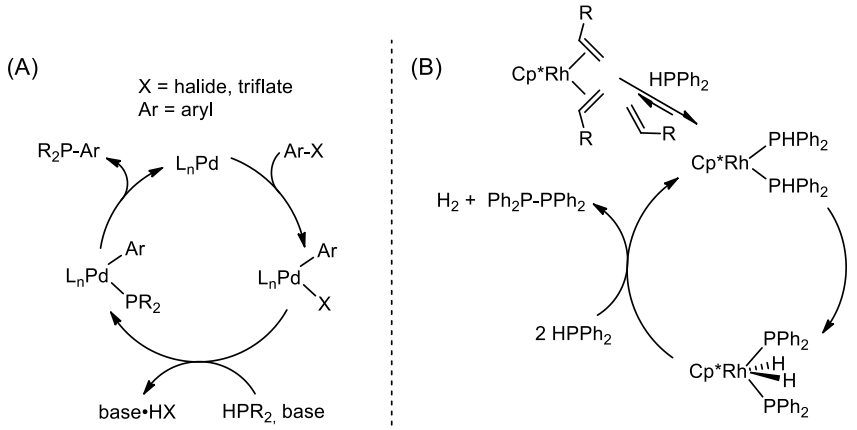

Scheme 2-6. Proposed mechanism for: (A) Pd-catalyzed C-P cross-coupling of aryl halides and triflates, and (B) dehydrocoupling of $HPPh_2$ by $Cp^*Rh(PHPh_2)_2$.[87]

Table 2-5. Preferential dehydrocoupling of $HPPh_2$ over sp^2-C-P cross-coupling catalyzed by (Cy-PSiP)Rh(Ph)Br (**2-5**).

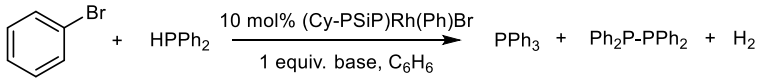

Entry	Base	Temp (°C)	Time	Conversion to PPh_3 (%)[a]	Conversion to Ph_2P-PPh_2 (%)[a]
1	Cs_2CO_3	25	48 h	0	0
2	NaO^{t}Bu	25	48 h	0	0
3	Cs_2CO_3	75	24 h	0	50
4	NaO^{t}Bu	75	24 h	0	54
5	Cs_2CO_3	75	5 d	0	52
6	NaO^{t}Bu	75	5 d	0	59

[a]Conversion based on initial $HPPh_2$ concentration as determined by $^{31}P\{^1H\}$ NMR spectroscopy.

The groups of Brookhart,[87] Tilley,[88] and Tejel[77b] have each previously reported on Rh-catalyzed dehydrocoupling of phosphines, including $HPPh_2$. Han and Tilley reported 91% yield of Ph_2P-PPh_2 (based on ^{31}P NMR) after 8 h at 70 °C (benzene solution) in the presence of 5 mol% (dippe)Rh(η^3-Bz) (generated *in situ*; dippe = $^i Pr_2PCH_2CH_2P^i Pr_2$).[88a]

By comparison, Böhm and Brookhart reported that at a 7.8 mol% loading of Cp*Rh(CH_2=$CHSiMe_3$)$_2$, 60% yield of Ph_2P-PPh_2 (based on ^{31}P NMR) was obtained after 27 h at 70 °C (benzene solution) in the presence of 1.1 equiv. CH_2=CH^tBu, which functions as an H_2 acceptor (Scheme 2-6b).[87] Similarly, Tejel and co-workers reported that at 5 mol% loading, the Rh phosphido complex **D** (Figure 2-1) achieves 51% conversion to Ph_2P-PPh_2 (based on ^{31}P NMR) after 13 h at 80 °C (toluene solution).[77b] The latter reaction achieved >95% conversion to Ph_2P-PPh_2 after 5 h at 80 °C under an atmosphere of ethylene (6 bar). The example reported herein is closely related to these previous examples, in that all involve a Rh^I fragment that likely undergoes P-H oxidative addition to generate phosphido intermediates that can engage in dehydrogenative P-P coupling. In the case of (Cy-PSiP)Rh, such P-H oxidative addition is apparently more facile than oxidative addition of PhBr.

2.2.3 Ir Phosphido Complexes *via* P-H Oxidative Addition

Having established the viability of five-coordinate Ir phosphido species supported by Cy-PSiP ligation (*vide supra*), the generation of such complexes by P-H oxidative addition of hydrophosphines to unsaturated Ir^I species was pursued. Previous work from the Turculet group has demonstrated that dehydrohalogenation of (Cy-PSiP)Ir(H)Cl (**1-1**) provides *in situ* access to a highly reactive Ir^I source equivalent to (Cy-PSiP)Ir (**1-3**), which can subsequently engage in intermolecular C-H and N-H oxidative addition reactions.[20b,52k] In this regard, P-H oxidative addition to **1-3** was pursued (Scheme 2-7). Treatment of **1-1** with one equiv. $LiCH_2SiMe_3$ in cyclohexane solution generated **1-3**, which was confirmed in each instance by ^{31}P NMR analysis. Subsequent addition of one equiv. HPRR' resulted in the quantitative (by ^{31}P NMR) formation of the corresponding phosphido hydride

species(Cy-PSiP)Ir(H)(PRR') (R = R' = Ph, **2-1**; R = H, R' = Ph, **2-3a**;R = H, R' = Cy, **2-3b**; R = H, R' = Mes, **2-3c**; R = H, R' = ^{t}Bu, **2-3d**), which could be isolated in high yield (63 – 91%, depending on R, R') *via* this route. These oxidative addition reactions generally occurred within 10 min. of mixing, with no evidence observed spectroscopically for intermediate Ir^I-phosphino species. By comparison, analogous N-H oxidative addition processes were significantly more sluggish. While the formation of **2-3a** *via* P-H activation of H_2PPh was complete within minutes at room temperature, the generation of (Cy-PSiP)Ir(H)(NHPh) by related N-H activation of H_2NPh required heating at 65 °C for 16 h to reach completion.[52k] Similarly, the formation of **2-3c** by a P-H activation route was equally rapid to that of **2-3a**, whereas the analogous N-H activation of $H_2N(2,6\text{-}Me_2C_6H_3)$ to generate (Cy-PSiP)Ir(H)[NH(2,6-$Me_2C_6H_3$)] required 20 equiv. of $H_2N(2,6\text{-}Me_2C_6H_3)$ and heating at 65°C for 72 h to reach completion.[52k]

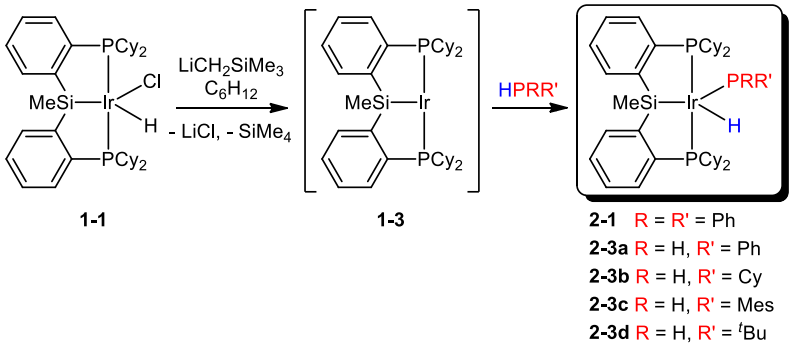

Scheme 2-7. Synthesis of five-coordinate Ir phosphido hydride complexes *via* P-H oxidative addition.

2.2.4 Reactivity of Ir Phosphido Hydride Complexes

Having prepared a series of coordinatively unsaturated Ir phosphido hydride species, the reactivity of these complexes in stoichiometric reactions with various small molecules was probed. Complex **2-3c** was utilized primarily for these studies, due largely to its ease of synthesis. Initial attempts in this vein focused on unsaturated substrates,

including alkenes and alkynes. Primarily in the context of hydrophosphination catalysis involving late transition metal species, the reactivity of terminal phosphido ligands towards substrates of this type has been classified as either "inner-sphere", referring to migratory insertion reactions involving the metal-phosphido linkage (Scheme 2-1A), or "outer-sphere", referring to Michael-type nucleophilic attack of the phosphido group on electrophilic substrates (Scheme 2-1B).[71a,89] In the case of phosphido hydride species, the additional possibility of migratory insertion reactions involving the metal hydride is also a consideration, and a mechanism of this type has been invoked in the context of hydrophosphination catalysis.[74b,77b,90]

Upon exposure of a benzene-d_6 solution of **2-3c** to 1 atm of CO, $^{31}P\{^1H\}$ NMR analysis of the resulting reaction mixture indicated the formation of free H_2PMes as well as a new major Cy-PSiP-containing product that features a single ^{31}P NMR resonance at 48.2 ppm. The latter is consistent with the dicarbonyl complex (Cy-PSiP)Ir$(CO)_2$ (**4-6**; *vide infra*), which has been prepared independently. This result indicates that the coordination of CO to the Ir center in **2-3c** promotes P-H reductive elimination. By comparison, treatment of **2-3c** with one equiv. of xylyl isocyanide resulted in a complex mixture of products from which no pure material could be isolated. Conversely, no reaction was observed upon exposure of a benzene-d_6 solution of **2-3c** to 1 atm of CO_2, including after heating the mixture at 80 °C for several days. This same result was obtained under analogous conditions when **2-3c** was exposed to 1 atm of ethylene. Complex **2-3c** proved similarly unreactive toward various other alkenes (1 – 20 equiv.), such as *tert*-butyl ethylene, 1-octene, *cis*-4-octene and norbornene, including after heating at 80 °C over the course of several days. Complex **2-3c** does react with 5 equiv. of the activated alkene

acrylonitrile, which is typically reactive with late metal phosphido species, to afford a complex mixture of products, including unreacted **2-3c**, after 48 h at room temperature in benzene-d_6 solution. ^{1}H NMR analysis of the reaction mixture indicated that all of the acrylonitrile was consumed in this process.

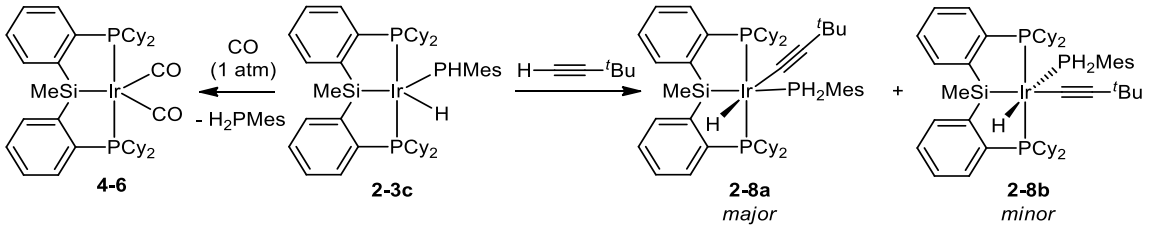

Scheme 2-8. Reactivity of (Cy-PSiP)Ir(H)(PHMes) (**2-3c**) with unsaturated substrates.

The reactivity of alkyne substrates with **2-3c** was also investigated. While diphenylacetylene (1 – 20 equiv.) proved unreactive (up to 80 °C in benzene), the terminal alkyne 3,3-dimethyl-1-butyne (two equiv.) reacted with **2-3c** over the course of 3 days at room temperature to afford a mixture of two products (**2-8a** and **b**, *ca*. 3:1 ratio, by ^{31}P and ^{1}H NMR). The ^{1}H and ^{31}P{^{1}H} NMR data obtained for **2-8a**,**b** are consistent with the formulation of these complexes as isomeric six-coordinate Ir alkynyl hydride species resulting from net deprotonation of the terminal alkyne by the Ir-phosphido ligand, which remains coordinated to Ir as the corresponding phosphine (Scheme 2-8). The ^{1}H NMR spectrum of the mixture of isomers (benzene-d_6) features two Ir-*H* resonances at -14.71 (m, **2-8a**) and -14.02 ppm (dt, $^2J_{HP}$ = 131 Hz, $^2J_{HP}$ = 18 Hz, **2-8b**), as well as two resonances corresponding to Ir-P*H*$_2$Mes at 5.75 (dm, $^1J_{PH}$ = 334 Hz, **2-8a**) and 5.83 ppm (dm, $^1J_{PH}$ = 337 Hz, **2-8b**). The ^{31}P{^{1}H} NMR spectrum of the product mixture features two sets of resonances, the first at 31.5 (d, $^2J_{PP}$ = 20 Hz, *P*Si*P*) and -119.9 ppm (t, $^2J_{PP}$ = 20 Hz, *P*H$_2$Mes) corresponding to the major isomer **2-8a**, and the second at 30.1 (d, $^2J_{PP}$ = 17 Hz) and -120.7 ppm (m) corresponding to the minor species **2-8b**. On the basis of these data,

the major isomer **2-8a** is assigned as the *mer*-κ^3-Cy-PSiP complex with the alkynyl ligand coordinated *cis* to Si, while **2-8b** is assigned as the *mer*-Cy-PSiP isomer with the alkynyl coordinated *trans* to Si. While attempts to selectively crystallize the major isomer **2-8a** on a preparative scale were unsuccessful, a minute amount of crystalline material was isolated from a mixture of **2-8a**,**b**. Single crystal X-ray diffraction analysis of this sample revealed the minor isomer **2-8b**, with the alkynyl group *trans* to Si (Si-Ir-C1 169.56(5)°; Figure 2-8).

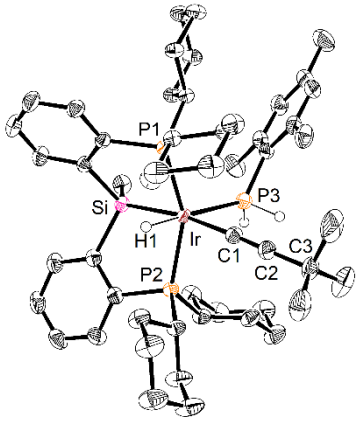

Figure 2-8. Crystallographically determined structures of **2-8b** shown with thermal ellipsoids drawn at the 50% probability level. Most hydrogen atoms have been omitted for clarity. Selected interatomic distances (Å) and angles (°): Ir-P1 2.3137(4), Ir-P2 2.3271(4), Ir-P3 2.3535(5), Ir-Si 2.3633(5), Ir-C1 2.0836(19), Ir-H1 1.53(3), C1-C2 1.200(3), P1-Ir-P2 151.992(15), Si-Ir-C1 169.56(5), P3-Ir-H1 175.2(10), Si-Ir-H1 78.8(10), P3-Ir-C1 83.24(5), Ir-C1-C2 170.11(17), C1-C2-C3 176.5(2).

While the strong Brønsted basicity of late metal phosphido ligands is well established,[78,91] the net insertion of terminal alkynes into late transition metal-phosphido linkages is also precedented,[92] including examples of terminal alkyne hydrophosphination *via* phosphido intermediates.[90b,93] Furthermore, while isolable phosphido hydride late metal complexes are relatively rare, computational studies by Beletskaya and co-workers suggest that insertion into the metal hydride is likely to be more facile relative to an analogous process involving the metal phosphido linkage.[90c,d] As such, the net

deprotonation of 3,3-dimethyl-1-butyne by **2-3c** is somewhat surprising. Interestingly, Rosenberg and co-workers[91a] have reported that coordinatively unsaturated Ru phosphido species of the type (η^5-indenyl)Ru(PPh_3)(PR_2) (R = Cy, ^{i}Pr) are basic enough to deprotonate acetonitrile (pK_a of 31.3 in DMSO), despite the presence of substantial Ru-phosphido double bond character. Yet, such Ru phosphido species undergo formal [2+2] cycloaddition with terminal alkynes such as phenylacetylene (pK_a of 28.8 in DMSO) and 1-hexyne to afford phosphametallacyclobutene species as the major product, forming only minute amounts of alkynyl phosphine species derived from alkyne deprotonation.[92] The authors conclude that such results point to a significantly higher rate for the cycloaddition process relative to deprotonation. The results detailed herein thus suggest that this scenario may be reversed for (Cy-PSiP)Ir-phosphido species, such that deprotonation is the favored pathway. However, no intermediates associated with alkyne insertion into the Ir-*H* were observed, which is surprising, given the low barriers typically associated with such processes. As such, it may be that the formation of **2-8a**,**b** involves an initial P-H reductive elimination upon coordination of the alkyne substrate to the Ir center in **2-3c**, and this is followed by *sp*-C-H oxidative addition of the alkyne to afford the final alkynyl products (Scheme 2-9). Such a mechanism would be in accord with the observation that P-H reductive elimination occurs upon addition of CO to **2-3c**, and that P-H reductive elimination in such five-coordinate Ir phosphido complexes is highly sensitive to steric influence. The *sp*-C-H oxidative addition process would produce the minor isomer **2-8b**, which indicates that this species undergoes a subsequent isomerization to form **2-8a**.

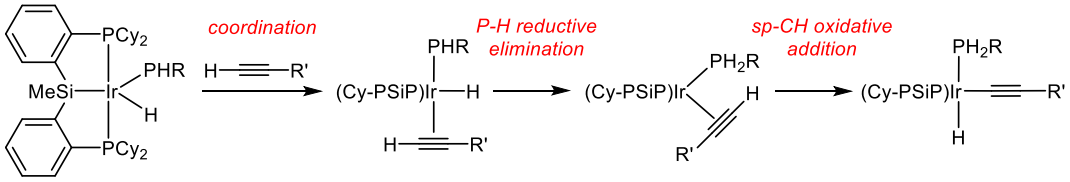

Scheme 2-9. Possible mechanism for the reaction of an Ir phosphido hydride species with a terminal alkyne to afford an alkynyl hydride complex *via* P-H reductive elimination/*sp*-CH oxidative addition.

Given the possibility that **2-8a**,**b** forms *via* a C-H oxidative addition pathway, the reactivity of **2-3c** with H_2, hydrosilanes, and benzaldehyde was also investigated (Scheme 2-10). In the latter case, no reaction was observed upon treatment of **2-3c** from 1 equiv. up to 10 equiv. of benzaldehyde in benzene solution, even after heating at 80 °C for 2 days. Tertiary silanes, such as triphenylsilane, triethylsilane, and diphenylmethylsilane, proved equally unreactive. Conversely, treatment of **2-3c** with 1 equiv. of phenylsilane resulted in the formation of a complex mixture of unidentified products (by $^{31}P\{^1H\}$ NMR) within 20 min of addition. By comparison, treatment of **2-3c** with 1.1 equiv. of diphenylsilane led to the generation of a new major product tentatively assigned as the silyl hydride complex (Cy-PSiP)Ir(H)($SiHPh_2$)(PH_2Mes) (**2-9**) on the basis of *in situ* ^1H and $^{31}P\{^1H\}$ NMR data (>90% conversion to **2-9** over the course of 5 h at room temperature). The isolation and characterization of **2-9** is complicated by the formation of several side-products, including species subsequently identified as (Cy-PSiP)Ir($H)_2$(PH_2Mes) (**2-10**) and (Cy-PSiP)Ir(H)($SiHPh_2$) (**4-1**; *vide infra*). Heating of this reaction mixture did not result in the clean formation of **2-9**. In addition, the formation of **2-10** was favored when excess diphenylsilane was utilized in this reaction, presumably due to a background silane dehydrocoupling process. Complex **2-9** gives rise to three $^{31}P\{^1H\}$ NMR resonances at 36.5 (apparent t, $^2J_{PP}$ = 21 Hz), 13.6 (br s), and -128.7 ppm (apparent t, $^2J_{PP}$ = 24 Hz) in a 1:1:1 ratio. Complex **2-9** also gives rise to an Ir-*H* ^1H NMR resonance at -13.13 ppm

(apparent dt, $^{2}J_{HP}$ = 99 and 19 Hz, respectively), as well as an Ir-Si*H*Ph$_2$ resonance at 5.25 ppm (ddd, $^{3}J_{PH}$ = 26, 8, and 3 Hz, respectively), and two resonances corresponding to the diastereotopic Ir-P*H*$_2$Mes protons at 5.51 (dm, $^{1}J_{PH}$ = 316 Hz) and 5.67 ppm (dm, $^{1}J_{PH}$ = 357 Hz). These data are consistent with a formulation of **2-9** as a six-coordinate silyl hydride complex featuring *fac*-κ^3-Cy-PSiP coordination, where the PH$_2$Mes ligand is coordinated *trans* to Si (Scheme 2-10).

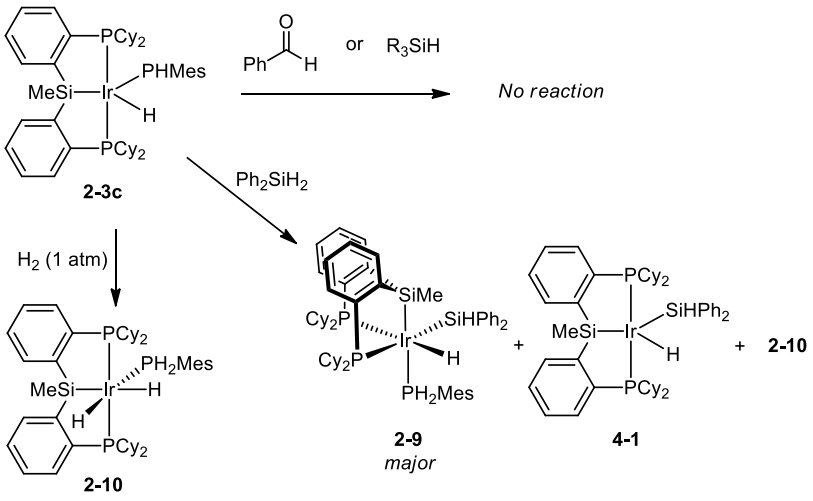

Scheme 2-10. Reactivity of (Cy-PSiP)Ir(H)(PHMes) (**2-3c**) towards E-H bonds.

Treatment of a benzene-d_6 solution of **2-3c** with H_2 (1 atm) resulted in the rapid (within 10 min.) and quantitative (by ^{1}H and ^{31}P NMR) formation of a new species assigned as the dihydride complex (Cy-PSiP)Ir(H)$_2$(PH$_2$Mes) (**2-10**, Scheme 2-10). The ^{31}P{^{1}H} NMR spectrum of **2-10** feature two signals 47.0 (d, $^{2}J_{PP}$ = 18 Hz) and -136.8 ppm (m). The ^{1}H NMR spectrum of **2-10** (benzene-d_6) features two Ir-*H* resonances at -10.70(m) and -14.82 ppm (apparent dt, $^{2}J_{PH}$ = 118 and 19 Hz, respectively), as well as one resonance corresponding to the Ir-P*H*$_2$Mes protons centered at 5.50 ppm (dm, $^{1}J_{PH}$ = 330 Hz). These data are consistent with an Ir dihydride complex featuring *mer*-κ^3-Cy-PSiP coordination,

with one hydride ligand coordinated *trans* to Si (Scheme 2-10). The difference in the structures of complexes **2-9** (*fac*-κ^3-Cy-PSiP, PH_2Mes *trans* to Si) and **2-10** (*mer*-κ^3-Cy-PSiP, PH_2Mes *cis* to Si) in solution is likely due to steric preferences involving the relatively bulky $SiHPh_2$ ligand in **2-9** *vs*. a hydride ligand in **2-10**.

In an effort to gain further understanding of the reactivity of **2-3c** with H_2SiPh_2 and H_2, the analogous reactions with D_2SiPh_2 and D_2 were pursued. In the case of D_2SiPh_2, evaluation of the ^{1}H NMR spectrum (benzene-d_6) of the resulting Ir silyl product revealed approximately quantitative ^{2}H incorporation at the Ir-*H* and Si-*H* positions in **2-9**, with no ^{2}H incorporation in the P*H*$_2$Mes ligand (Figure 2-9). The ^{31}P NMR spectrum of the resulting complex revealed a complex multiplet at -128.7 ppm, indicative of one-bond P-H coupling to the diastereotopic P-*H* protons of the PH_2Mes ligand in **2-9**-d_2. These data are consistent with a mechanism involving P-H reductive elimination in **2-3c**, followed by Si-D oxidative addition of D_2SiPh_2. In the reaction of **2-3c** with D_2 (1 atm), ^{1}H NMR analysis (benzene-d_6) of the reaction mixture indicates that partial ^{2}H incorporation has occurred at both the Ir-*H* positions, as well as the P-*H* of the PH_2Mes ligand in **2-10**. This observation was confirmed by ^{2}H NMR analysis (benzene) of the reaction mixture (Figure 2-10). These observations suggest that in the case of H_2/D_2, H-D scrambling involving the Ir-phosphido complex can also occur. Interestingly, a previous study involving the reaction of H_2 and Et_3SiH with the phosphido complex (η^5-indenyl)Ru(PPh_3)(=PCy_2) afforded Ru^{II}-$PHCy_2$ products consistent with net 1,2-addition of an E-H bond across the $Ru^{\delta+}$=$P^{\delta-}$ double bond.[83] The results presented herein suggest that such a process is not operational in the case of **2-3c** reacting with Ph_2SiH_2, but it cannot be discounted in the case of the analogous reaction with D_2, given the observed incorporation of ^{2}H at the Ir-$PH_2(D_2)$Mes position.

The reaction of (PNP)Ir(Me)(PPh_2) (PNP = κ^3-*N*($SiMe_2CH_2PPh_2$)$_2$) with H_2 to afford Ir-$PHPh_2$ species has also been reported, however this reactivity was complicated by apparent α-hydride abstraction by the Ir-phosphido from the Ir-Me to generate a phosphino methylidene species.[79c]

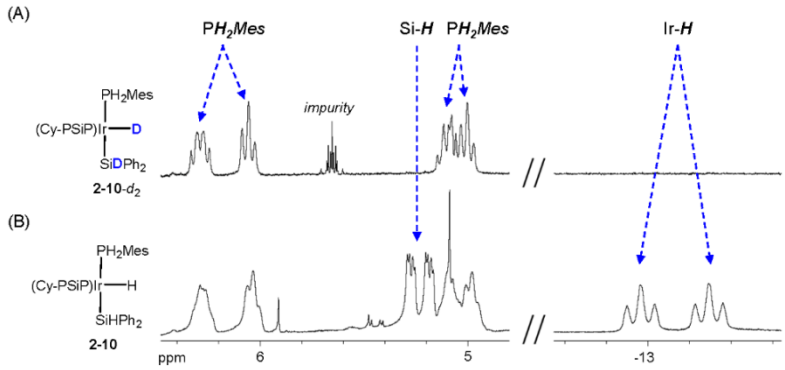

Figure 2-9. Partial ^{1}H NMR (300 MHz, benzene-d_6) spectrum of: (A) (Cy-PSiP)Ir(D)($SiDPh_2$)(PH_2Mes) (**2-9**-d_2) generated by the reaction of (Cy-PSiP)Ir(H)(PHMes) (**2-3c**) with D_2SiPh_2; and (B) (Cy-PSiP)Ir(H)($SiHPh_2$)(PH_2Mes) (**2-9**) generated by the reaction of (Cy-PSiP)Ir(H)(PHMes) (**2-3c**) with H_2SiPh_2.

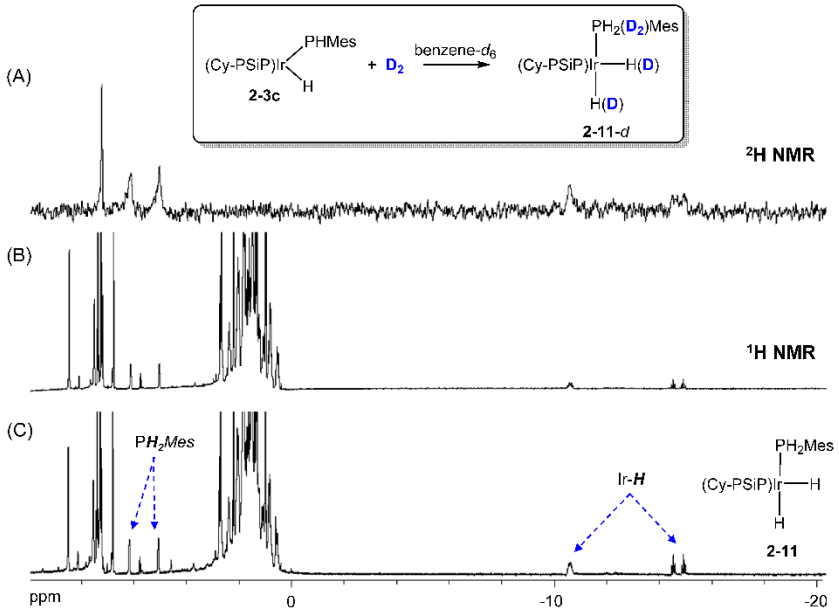

Figure 2-10. (A) ^{2}H NMR spectrum (46.1 MHz, benzene) and (B) ^{1}H NMR spectrum (300 MHz, benzene-d_6) of partially deuterated (Cy-PSiP)Ir(H/D)$_2$(PH_2/D_2Mes) (**2-10**-*d*) generated by the reaction of (Cy-PSiP)Ir(H)(PHMes) (**2-3c**) with D_2; and (C) ^{1}H NMR spectrum (300 MHz, benzene-d_6) of (Cy-PSiP)Ir(H)$_2$(PH_2Mes) (**2-10**) generated by the reaction of **2-3c** with H_2.

2.3 Summary and Conclusions

The results detailed in this chapter demonstrate that rare examples of mononuclear, coordinatively unsaturated pincer Ir phosphido hydride complexes featuring terminal phosphido ligands are synthetically accessible, including *via* P-H oxidative addition to (Cy-PSiP)Ir^{I}. This P-H oxidative addition reactivity complements studies previously reported by the Turculet group on N-H oxidative addition of ammonia, amines, and anilines.

As in the case of related five-coordinate amido and anilido hydride Ir complexes, phosphido species of the type (Cy-PSiP)Ir(H)(PHR) (R = aryl or alkyl) are isolable and adopt distorted trigonal bipyramidal structures. While the phosphido group in crystallographically characterized complexes of this type is close to trigonal planar geometry, solution NMR studies indicate that the barrier to rotation about the Ir-phosphido bond is relatively low, implying that P→Ir π-donation is minimal.

Although isolated phosphido complexes of this type that feature primary phosphido ligation are relatively resistant to P-H reductive elimination, facile P-H reductive elimination was noted in the case of secondary phosphido groups, leading to the exclusive formation of Ir-secondary-phosphine adducts, with no observed intermediates. This observation suggests that such P-H reductive elimination is sensitive to steric pressure. Interestingly, analogous Rh phosphido complexes supported by Cy-PSiP ligation are not isolable, and appear to undergo facile P-H reductive elimination in the case of both primary and secondary phosphido groups to afford Rh-phosphine adducts. As in the case of P-H reductive elimination at Ir, no intermediates were observed in these Rh-mediated reductive elimination processes. This observation stands in contrast to previous reports from the

Turculet group that complexes of the type (Cy-PSiP)Rh(H)(NHR) (R = aryl) are isolable and resistant to N-H reductive elimination. Evidence of relatively facile sp^2-CP reductive elimination was also observed in the case of Rh.

The reactivity of (Cy-PSiP)Ir(H)(PHR) species with respect to unsaturated substrates such as alkenes, and alkynes was evaluated. In a general sense, it appears that migratory insertion reactions of such substrates into the Ir-phosphido linkage are not accessible. As well, it appears that substrates that contain reactive E-H σ-bonds, such as hydrosilanes, terminal alkynes, and H_2 react *via* a pathway involving likely P-H reductive elimination/E-H oxidative addition. These studies provide new insights into the reactivity of late transition metal terminal phosphido hydride species, a class of compounds that are often invoked as intermediates in P-C and P-P bond formation reactions.

2.4 Experimental

2.4.1 General Considerations

All experiments were conducted under nitrogen in an MBraun glovebox or using standard Schlenk techniques. Dry, oxygen-free solvents were used unless otherwise indicated. Tetrahydrofuran and diethyl ether were distilled from Na/benzophenone ketyl. Benzene, toluene, and pentane were sparged with nitrogen and dried by subsequent passage through a double-column solvent purification system (one activated alumina column and one column packed with activated Q-5). All purified solvents were stored over 4 Å molecular sieves. Benzene-d_6, cyclohexane-d_{12}, and dichloromethane-d_2 were degassed *via* three freeze-pump-thaw cycles and stored over 4 Å molecular sieves. The compounds (Cy-PSiP)Ir(H)Cl (**1-1**) and (Cy-PSiP)Rh(H)Cl (**1-2**),[20b] as well as phosphido lithium reagents,[94] and D_2SiPh_2[95] were prepared according to literature procedure. All other

reagents were purchased from commercial suppliers and used without further purification. Unless otherwise stated, ^{1}H, ^{13}C, ^{31}P, and ^{29}Si NMR characterization data were collected at 300K on a Bruker AV-300 spectrometer operating at 300.1, 75.5, 121.5, and 59.6 MHz (respectively) with chemical shifts reported in parts per million downfield of $SiMe_4$ (for ^{1}H, ^{13}C, and ^{29}Si) or 85% H_3PO_4 in D_2O (for ^{31}P). ^{1}H and ^{13}C NMR chemical shift assignments are based on data obtained from ^{13}C-DEPTQ, ^{1}H-^{1}H COSY, ^{1}H-^{13}C HSQC, and ^{1}H-^{13}C HMBC NMR experiments. ^{29}Si NMR assignments are based on ^{1}H-^{29}Si HMQC and ^{1}H-^{29}Si HMBC experiments. In some cases, fewer than expected unique ^{13}C NMR resonances were observed, despite prolonged acquisition times. X-ray data collection, solution, and refinement were carried out by Drs. Robert MacDonald, Michael J. Ferguson, and Yuqiao Zhou at the University of Alberta X-ray Crystallography Laboratory, Edmonton, Alberta.

2.4.2 Synthetic Details and Characterization Data

(Cy-PSiP)Ir(H)(PPh_2) (2-1). A solution of **1-1** (0.025 g, 0.031 mmol) in ca. 7 mL of cyclohexane was treated with $(THF)_2LiPPh_2$ (0.010 g, 0.031 mmol). The resulting orange reaction mixture was allowed to stand at room temperature for 1 h, at which point the volatile components of the reaction mixture were removed *in vacuo*. The remaining residue was extracted with ca. 5 mL of pentane, and the pentane extracts were filtered through Celite. The filtrate solution was collected and dried under vacuum to afford **2-1** (0.024 g, 83%) as an orange solid. ^{1}H NMR (benzene-d_6): δ 8.19 (d, 2 H, J = 7 Hz, H_{arom}), 7.94 (t, 4 H, J = 7 Hz, H_{arom}), 7.41 (m, 2 H, H_{arom}), 7.24 (t, 2 H, J = 7 Hz, H_{arom}), 7.12 – 6.88 (overlapping resonances, 8 H, H_{arom}), 2.49 - 2.16 (overlapping resonances, 6 H, PCy), 1.98 (m, 2 H, P*Cy*), 1.78 - 0.90 (overlapping resonances, 30 H, P*Cy* + Si*Me*; the Si-*Me*

resonance was identified at 1.26 ppm in a ^{1}H-^{13}C HSQC experiment), 0.74 – 0.43 (overlapping resonances, 6 H, P*Cy*), -15.37 (dt, 1 H, $^{2}J_{HP}$ = 75 Hz, $^{2}J_{HP}$ = 18 Hz, Ir*H*). ^{13}C{^{1}H} NMR (benzene-d_6): δ 158.7 (C_{arom}), 154.5 (C_{arom} P*Ph*$_2$), 144.8 (C_{arom}), 133.7 (d, J = 9 Hz, CH$_{arom}$), 132.3 (apparent t, J = 9 Hz, CH$_{arom}$), 129.2 (m, CH$_{arom}$), 127.7 (CH$_{arom}$), 127.0 (CH$_{arom}$), 126.5 (m, CH$_{arom}$), 33.9 – 33.0 (overlapping resonances CH$_{Cy}$), 30.6 (CH$_{2Cy}$), 29.7 (CH$_{2Cy}$), 29.2 (CH$_{2Cy}$), 27.8 –26.1 (overlapping resonances, CH$_{2Cy}$), 8.0 (Si*Me*). ^{31}P{^{1}H} NMR (benzene-d_6): δ 107.2 (t, 1 P, $^{2}J_{PP}$ = 33 Hz, Ir-*P*Ph$_2$), 56.7 (d, 2 P, $^{2}J_{PP}$ = 37 Hz, *P*Si*P*). ^{29}Si NMR (benzene-d_6): δ 30.8. Anal. Calcd for $C_{49}H_{66}IrP_3Si$: C, 60.78; H, 6.87. Found: C, 60.65; H, 6.72.

(Cy-PSiP)Ir(PH(1-Ad)$_2$) (2-2a). A solution of **1-1** (0.030 g, 0.037 mmol) in ca. 7 mL of cyclohexane was treated with (Et$_2$O)LiP(1-Ad)$_2$ (0.014 g, 0.037 mmol). The resulting dark red reaction mixture was allowed to stand at room temperature for 1.5 h, at which point the volatile components of the reaction mixture were removed *in vacuo*. The remaining residue was extracted with ca. 5 mL of pentane, and the pentane extracts were filtered through Celite. The filtrate solution was collected and dried under vacuum to afford **2-2a** (0.035 g, 90%) as a red solid.^{1}H NMR (300 MHz, benzene-d_6): δ 8.37 (d, 2 H, J = 7 Hz, H_{arom}), 7.78 (m, 1 H, H_{arom}), 7.67 (m, 1 H, H_{arom}), 7.40 – 7.20 (m, 4 H, H_{arom}), 5.64 (dt, 1 H, $^{1}J_{HP}$ = 295 Hz, $^{3}J_{HP}$ = 13 Hz, P*H*(1-Ad)$_2$), 2.80 – 0.90 (overlapping resonances, 74 H, P*Cy* + P(*1-Ad*)$_2$), 0.83 (s, 3 H, Si*Me*). ^{13}C{^{1}H} NMR (300 K, 75.5 MHz, benzene-d_6): δ 160.0 (C_{arom}), 148.5 – 147.9 (overlapping resonances, C_{arom}), 132.6 (d, J = 16 Hz, CH$_{arom}$), 132.3 (d, J = 17 Hz, CH$_{arom}$), 129.8 (CH$_{arom}$), 129.2 (CH$_{arom}$), 129.0 (CH$_{arom}$), 128.5 (CH$_{arom}$), 127.5 (d, J = 5 Hz, CH$_{arom}$), 127.3 (d, J = 6 Hz, CH$_{arom}$), 44.4 (CH$_{2Ad}$), 43.8 (CH$_{2Ad}$), 42.2 (d, $^{1}J_{CP}$ = 28 Hz, CH$_{Cy}$), 38.20 (d, $^{1}J_{CP}$ = 28 Hz, CH$_{Cy}$), 37.2 (CH$_{2Ad}$), 37.1

(CH_{2Ad}), 30.7 – 26.7 (overlapping resonances, CH_{2Cy} + CH_{Ad}), 7.1 (Si*Me*). $^{31}P\{^{1}H\}$ NMR (300 K, 121.5 MHz, benzene-d_6): δ AB pattern 67.3 (dd, 1 P, $^{2}J_{PP}$ = 278 Hz, $^{2}J_{PP}$ = 3 Hz, *P*Si*P*) and 51.8 (dd, 1 P, $^{2}J_{PP}$ = 278 Hz, $^{2}J_{PP}$ = 8 Hz, *P*Si*P*), 51.4 (br m, 1 P, Ir-*P*H(1-Ad)$_2$). ^{29}Si NMR (59.6 MHz, benzene-d_6): δ 62.8. Anal. Calcd for $C_{57}H_{86}IrP_3Si$: C, 63.13; H, 7.99. Found: C, 63.16; H, 8.51.

(Cy-PSiP)Ir(PHCy$_2$) (2-2b). A solution of **1-1** (0.027 g, 0.033 mmol) in ca. 6 mL of diethyl ether was treated with (THF)LiPCy$_2$ (0.009 g, 0.033 mmol). The resulting red reaction mixture was allowed to stand at room temperature for 30 min., at which point the volatile components of the reaction mixture were removed *in vacuo*. The remaining residue was extracted with ca. 5 mL of pentane, and the pentane extracts were filtered through Celite. The filtrate solution was collected and dried under vacuum to afford **2-2b** (0.025 g, 82%) as a red solid. ^{1}H NMR (benzene-d_6): δ 8.41 (apparent d, 2 H, J = 7 Hz, H_{arom}), 7.70 (apparent d, 2 H, J = 7 Hz, H_{arom}), 7.38 (apparent t, 2 H, J = 7 Hz, H_{arom}), 7.27 (apparent t, 2 H, J = 7 Hz, H_{arom}), 5.17 (dm, 1 H, $^{1}J_{HP}$ = 292 Hz, Ir-P*H*Cy$_2$), 2.64– 0.98 (overlapping resonances, 66 H, P*Cy$_2$*), 0.75 (s, 3 H, Si*Me*). $^{13}C\{^{1}H\}$ NMR (benzene-d_6): δ 160.8 (C_{arom}), 147.7 (C_{arom}), 132.9 (apparent t, J = 10 Hz, C_{arom}), 129.8 (CH_{arom}), 129.3 (CH_{arom}), 127.2 (CH_{arom}), 40.5 – 38.8 (overlapping resonances, CH_{Cy}), 35.1 (d, J = 6 Hz, CH_{2Cy}), 33.9 (d, J = 6 Hz, CH_{2Cy}), 31.0– 26.8 (overlapping resonances, CH_{2Cy}), 8.1 (Si*Me*). $^{31}P\{^{1}H\}$ NMR (benzene-d_6): δ 63.1 (d, 2 P, $^{2}J_{PP}$ = 11 Hz, *P*Si*P*), 21.6 (t, 1 P, $^{2}J_{PP}$ = 11 Hz, Ir-*P*HCy$_2$). ^{29}Si NMR (benzene-d_6): δ 68.6. Anal. Calcd for $C_{49}H_{78}IrP_3Si$: C, 60.03; H, 8.02. Found: C, 59.70; H, 7.98.

(Cy-PSiP)Ir(PH^{i}Pr$_2$) (2-2c). A solution of **1-1** (0.060 g, 0.073 mmol) in ca. 10 mL of THF was treated with (THF)LiP^{i}Pr$_2$ (0.014 g, 0.073 mmol). The resulting dark red

reaction mixture was allowed to stand at room temperature for 30 min., at which point the volatile components of the reaction mixture were removed *in vacuo*. The remaining residue was extracted with ca. 5 mL of benzene, and the benzene extracts were filtered through Celite. The filtrate solution was collected and dried under vacuum. The remaining residue was triturated with 3 × 5 mL pentane and subsequently dried under vacuum to afford **2-2c** (0.057 g, 99%) as a red solid.^{1}H NMR (500 MHz, benzene-d_6): δ 8.40 (apparent d, 2 H, J = 8 Hz, H_{arom}), 7.69 (apparent d, 2 H, J = 8 Hz, H_{arom}), 7.38 (apparent t, 2 H, J = 8 Hz, H_{arom}), 7.26 (apparent t, 2 H, J = 8 Hz, H_{arom}), 5.19 (dm, 1 H, $^{1}J_{PH}$ = 291 Hz, Ir-PH^{i}Pr$_2$), 2.54 (m, 2 H, CH_{Cy}), 2.44 (m, 2 H, CH_{Cy}), 2.30 (m, 2 H, PH(CHMe$_2$)$_2$), 2.18 (m, 4 H, CH_{2Cy}), 1.83– 0.95 (overlapping resonances, 48 H, PCy + PH(CHMe_2)$_2$), 0.77 (s, 3 H, SiMe). ^{13}C{^{1}H} NMR (125.8 MHz, benzene-d_6): δ 160.7 (C_{arom}), 147.9 (C_{arom}), 133.2 (apparent t, J = 8 Hz, CH_{arom}), 130.1 (CH_{arom}), 129.6 (CH_{arom}), 127.6 (CH_{arom}), 40.2 (apparent t, J = 17 Hz, CH_{Cy}), 39.5 (apparent t, J = 13 Hz, CH_{Cy}), 31.3– 29.7 (overlapping resonances, CH_{2Cy}), 29.2 (d, $^{1}J_{CP}$ = 21 Hz, PCHMe$_2$), 28.2 – 27.2 (overlapping resonances, CH_{2Cy}), 24.7 (PCHMe_2), 23.9 (PCHMe_2), 8.6 (SiMe). ^{31}P{^{1}H} NMR (202.5 MHz, benzene-d_6): δ 63.3 (d, 2 P, $^{2}J_{PP}$ = 10 Hz, PSiP), 34.6 (t, 1 P, $^{2}J_{PP}$ = 10 Hz, Ir-PH^{i}Pr$_2$). ^{29}Si NMR (99.4 MHz, benzene-d_6): δ 68.3. Anal. Calcd for $C_{43}H_{70}IrP_3Si$: C, 57.37; H, 7.84. Found: C, 57.03; H, 7.89. Crystals suitable for X-ray diffraction analysis were obtained from a concentrated pentane solution of **2-2c** at room temperature.

(Cy-PSiP)Ir(H)(PHPh) (2-3a). A solution of **1-1** (0.060 g, 0.073 mmol) in ca. 7 mL of benzene was treated with (Et$_2$O)LiPHPh (0.014 g, 0.073 mmol). The resulting orange reaction mixture was allowed to stand at room temperature for 1 h, at which point the volatile components of the reaction mixture were removed *in vacuo*. The remaining

residue was extracted with ca. 5 mL of pentane, and the pentane extracts were filtered through Celite. The filtrate solution was collected and dried under vacuum to afford **2-3a** (0.041 g, 63%) as an orange solid.^{1}H NMR (benzene-d_6): δ 8.11 (d, 2 H, J = 7 Hz, H_{arom}), 7.97 (dt, 1 H, $^{1}J_{HP}$ = 283 Hz, $^{3}J_{HP}$ = 8 Hz, Ir-P*H*Ph), 7.92 (apparent t, 2 H, J = 8 Hz, H_{arom}), 7.48 (m, 2 H, H_{arom}), 7.23 (apparent t, 2 H, J = 7 Hz, H_{arom}), 7.14 –7.06 (overlapping resonances, 4 H, H_{arom}), 7.02 (m, 1 H, H_{arom}), 2.64 – 0.55 (overlapping resonances, 47 H, P*Cy* + Si*Me*; the Si-*Me* resonance was identified at 0.97 ppm in a ^{1}H-^{13}C HSQC experiment), -13.51 (dt, 1 H, $^{2}J_{HP}$ = 58 Hz, $^{2}J_{HP}$ = 16 Hz, Ir*H*). ^{13}C{^{1}H} NMR (benzene-d_6): δ 159.0 (C_{arom}), 149.0 (C_{arom} PH*Ph*), 143.4 (C_{arom}), 133.2 (d, J = 9 Hz, *C*H$_{arom}$), 132.1 (apparent t, J = 9 Hz, *C*H$_{arom}$), 129.6 (*C*H$_{arom}$), 129.0 (*C*H$_{arom}$), 128.4 (*C*H$_{arom}$), 126.5 (*C*H$_{arom}$), 126.0 (*C*H$_{arom}$), 33.2 – 32.7 (overlapping resonances, *C*H$_{Cy}$), 31.0 (*C*H$_{2Cy}$), 30.2 – 29.9 (overlapping resonances, *C*H$_{2Cy}$), 27.6 – 26.6 (overlapping resonances, *C*H$_{2Cy}$), 8.0 (Si*Me*). ^{31}P{^{1}H} NMR (benzene-d_6): δ 58.6 (d, 2 P, $^{2}J_{PP}$ = 34 Hz, *P*Si*P*), 20.8 (t, 1 P, $^{2}J_{PP}$ = 34 Hz, Ir-*P*HPh). ^{29}Si NMR (benzene-d_6): δ 24.4.

(Cy-PSiP)Ir(H)(PHCy) (2-3b). A solution of **1-1** (0.060 g, 0.073 mmol) in ca. 7 mL of benzene was treated with (Et$_2$O)LiPHCy (0.014 g, 0.073 mmol). The resulting orange reaction mixture was allowed to stand at room temperature for 30 min., at which point the volatile components of the reaction mixture were removed *in vacuo*. The remaining residue was extracted with ca. 5 mL of pentane, and the pentane extracts were filtered through Celite. The filtrate solution was collected and dried under vacuum to afford **2-3b** (0.060 g, 91%) as an orange solid. ^{1}H NMR (benzene-d_6): δ 8.17 (d, 2 H, J = 7 Hz, H_{arom}), 7.51 (m, 2 H, H_{arom}), 7.32 (apparent dq, 1 H, $^{1}J_{HP}$ = 277 Hz, $^{3}J_{HP}$ = 9 Hz, P*H*Cy), 7.25 (apparent t, 2 H, J = 7 Hz, H_{arom}), 7.13 (apparent t, 2 H, J = 7 Hz, 2 H, H_{arom}), 2.79

(m, 2 H, P*Cy*), 2.38 (m, 6 H, P*Cy*), 2.19– 1.09 (overlapping resonances, 43 H, P*Cy*), 1.04 (s, 3 H, Si*Me*), 0.91 – 0.64 (overlapping resonances, 4 H, P*Cy*), -14.00 (dt, 1 H, $^{2}J_{HP}$ = 65 Hz, $^{2}J_{HP}$ = 17 Hz, Ir*H*). $^{13}C\{^{1}H\}$ NMR (benzene-d_6): δ 159.3 (C_{arom}), 143.6 (C_{arom}), 132.8 (apparent t, J = 9 Hz, CH_{arom}), 130.0 (CH_{arom}), 129.5 (CH_{arom}), 126.8 (CH_{arom}), 33.0 (apparent t, J = 16 Hz, CH_{Cy}), 31.0 (CH_{2Cy}), 29.3 –26.9 (overlapping resonances, CH_{2Cy}), 7.8 (Si*Me*). $^{31}P\{^{1}H\}$ NMR (benzene-d_6): δ 69.4 (t, 1 P, $^{2}J_{PP}$ = 36 Hz, Ir-*P*HCy), 59.6 (d, 2 P, $^{2}J_{PP}$ = 33 Hz, *P*Si*P*). ^{29}Si NMR (benzene-d_6): δ 28.6. Anal. Calcd for $C_{43}H_{68}IrP_3Si$: C, 57.50; H, 7.63. Found: C, 57.18; H, 7.66.

(Cy-PSiP)Ir(H)(PHMes) (2-3c). A solution of **1-1** (0.038 g, 0.046 mmol) in ca. 7 mL of cyclohexane was treated with $(THF)_2$LiPHMes (0.014 g, 0.046 mmol), The resulting orange reaction mixture was allowed to stand at room temperature for 90 min., at which point the volatile components of the reaction mixture were removed *in vacuo*. The remaining residue was extracted with ca. 5 mL of pentane, and the pentane extracts were filtered through Celite. The filtrate solution was collected and dried under vacuum to afford **2-3c** (0.037 g, 86%) as an orange solid. ^{1}H NMR (500 MHz, benzene-d_6): δ 8.11 (apparent d, 2 H, J = 8 Hz, H_{arom}), 7.48 (m, 2 H, H_{arom}), 7.36 (dt, 1 H, $^{1}J_{HP}$ = 280 Hz), 7.22 (apparent t, 2 H, J = 8 Hz, H_{arom}), 7.12 (apparent t, 2 H, J = 8 Hz, H_{arom}), 6.92 (s, 2 H, H_{arom}), 2.87 (br, 6 H, *o*-C*Me*), 2.60 – 0.95 (overlapping resonances, 41 H, P*Cy* + *p*-C*Me*; the *p*-C*Me* resonance was identified at 2.44 ppm in a ^{1}H-^{13}C HSQC experiment), 1.00 (s, 3 H, Si*Me*), 0.85 – 0.52 (overlapping resonances, 6 H, P*Cy*), -12.05 (dt, 1 H, $^{2}J_{HP}$ = 58 Hz, $^{2}J_{HP}$ = 16 Hz, Ir*H*). $^{13}C\{^{1}H\}$ NMR (125.8 MHz, benzene-d_6): δ 158.3 (C_{arom}), 143.5 (C_{arom}), 141.6 (C_{arom}), 135.7 (C_{arom}), 131.9 (apparent t, J = 9 Hz, CH_{arom}), 129.3 (CH_{arom}), 128.8 (CH_{arom}), 128.5 (CH_{arom}), 126.5 (CH_{arom}), 33.8 (apparent t, J = 18 Hz, CH_{Cy}), 30.6– 30.2 (overlapping

resonances, CH_{2Cy}), 29.4 (CH_{2Cy}), 27.8– 26.6 (overlapping resonances, CH_{2Cy}), 24.1 (d, J = 10 Hz, *o*-C*Me*), 21.1 (*p*-C*Me*), 7.7 (Si*Me*). $^{31}P\{^{1}H\}$ NMR (202.5 MHz, benzene-d_6): δ 58.0 (br d, 2 P, $^{2}J_{PP}$ = 32 Hz, *P*Si*P*), 0.2 (t, 1 P, $^{2}J_{PP}$ = 35 Hz, Ir-*P*HMes).^{31}P NMR (202.5 MHz, benzene-d_6): δ 58.0 (br s, 2 P, *P*Si*P*), 0.2 (ddt, 1 P, $^{1}J_{PH}$ = 280 Hz, $^{2}J_{PH}$ = 58 Hz, $^{2}J_{PP}$ = 35 Hz, Ir-*P*HMes). ^{29}Si NMR (99.4 MHz, benzene-d_6): δ 24.0. Anal. Calcd for $C_{46}H_{68}IrP_3Si$: C, 59.14; H, 7.34. Found: C, 59.03; H, 7.28. Crystals of **2-3c** suitable for X-ray diffraction analysis were obtained from a concentrated Et_2O solution at -35 ºC.

(Cy-PSiP)Ir(H)(PH^{t}Bu) (2-3d, d'). A solution of **1-1** (0.019 g, 0.023 mmol) in ca. 7 mL of benzene was treated with $(Et_2O)LiPH^tBu$ (0.004 g, 0.023 mmol). The resulting orange reaction mixture was allowed to stand at room temperature for 30 min., at which point the volatile components of the reaction mixture were removed *in vacuo*. The remaining residue was extracted with ca. 5 mL of pentane, and the pentane extracts were filtered through Celite. The filtrate solution was collected and dried under vacuum to afford **2-3d** (0.014 g, 70%) as an orange solid. NMR analysis indicates that this complex forms a 1:1 mixture of isomers, identified as **2-3d** and **2-3d'**. Due to the complexity of the ^{1}H and $^{13}C\{^{1}H\}$ NMR spectra associated with this mixture of isomers, assignments are only provided for characteristic resonances; the corresponding spectra are provided in Appendix B15. ^{1}H NMR (benzene-d_6): δ 7.76 (dt, 1 H, $^{1}J_{HP}$ = 280 Hz, P*H*^{t}Bu, **2-3d**; the P*H* resonance associated with **2-3d'** is only partially visible (br m at 8.31 ppm) due to significant overlap in the aromatic region), 1.57 (d, 9 H, $^{3}J_{PH}$ = 13 Hz, PH^t*Bu*, **2-3d**), 1.55ppm (d, 9 H, $^{3}J_{PH}$ = 14 Hz, PH^t*Bu*, **2-3d'**), 1.10 (s, 3 H, Si*Me*, **2-3d**), 1.06 (s, 3 H, Si*Me*, **2-3d'**), -5.92 (dt, 1 H, $^{2}J_{HP}$ = 99 Hz, $^{2}J_{HP}$ = 24 Hz, Ir*H*, **2-3d'**), -14.96 (dt, 1 H, $^{2}J_{HP}$ = 66 Hz, $^{2}J_{HP}$ = 18 Hz, Ir*H*, **2-3d**).$^{13}C\{^{1}H\}$ NMR (benzene-d_6): δ 33.6 (PH(C*Me*$_3$), **2-3d**), 32.9 (PH(C*Me*$_3$), **2-3d'**), 7.6

(Si*Me*, **2-3d**), 3.7 (Si*Me*, **2-3d'**). $^{31}P\{^{1}H\}$ NMR (benzene-d_6): δ 130.5 (dd, 1 P, $^{2}J_{PPcis}$ = 34 Hz, $^{2}J_{PPtrans}$ = 154 Hz, Ir-*P*H^{t}Bu, **2-3d'**), 99.7 (t, 1 P, $^{2}J_{PP}$ = 36 Hz, Ir-*P*H^{t}Bu, **2-3d**), 57.7 (br m, 2 P, *P*Si*P*, **2-3d**), 55.3 (d, 1 P, $^{2}J_{PPtrans}$ = 152 Hz, *P*Si*P*, **2-3d'**), 50.2 (d, 1 P, $^{2}J_{PPcis}$ = 32 Hz, *P*Si*P*, **2-3d'**). ^{29}Si NMR (benzene-d_6): δ 29.4 (**2-3d**), 25.8 (**2-3d'**). Crystals of **2-3d** suitable for X-ray diffraction analysis were obtained from a concentrated pentane solution at -35 ºC.

General Procedure for the Generation of Ir Phosphido Hydride Complexes *via* P-H Oxidative Addition – *NMR-scale*. In a typical experiment, a room temperature solution of $LiCH_2SiMe_3$ (0.0011 g, 0.012 mmol) in ca. 0.4 mL of cyclohexane-d_{12} was added to a solution of **1-1** (0.010 g. 0.012 mmol) in ca. 0.4 mL of cyclohexane-d_{12}. An immediate color change from yellow to bright orange was observed. After 15 min. at room temperature the reaction mixture was analyzed by ^{1}H and $^{31}P\{^{1}H\}$ NMR spectroscopy to confirm the complete consumption of **1-1**. The reaction mixture was then treated with one equiv. of a hydrophosphine. Conversion to the corresponding phosphido complex was complete within 10 min. of phosphine addition, as confirmed by ^{1}H and $^{31}P\{^{1}H\}$ NMR analysis.

General Procedure for the Generation of Ir Phosphido Hydride Complexes *via* P-H Oxidative Addition – *Preparative-scale*. In a typical experiment, a room temperature solution of $LiCH_2SiMe_3$ (0.006 g, 0.065 mmol) in ca. 2 mL of cyclohexane was added to a solution of **1-1** (0.053 g. 0.065 mmol) in ca. 3 mL of cyclohexane. An immediate color change from yellow to bright orange was observed. After 15 min. at room temperature an aliquot of the reaction mixture was analyzed by ^{1}H and $^{31}P\{^{1}H\}$ NMR spectroscopy to confirm the complete consumption of **1-1**. The reaction mixture was then filtered through

Celite, and subsequently treated with one equiv. of H_2PMes (0.010 g, 0.065 mmol) and allowed to stir at room temperature for 10 min. The volatile components of the reaction mixture were then removed in vacuo, to afford **2-3c** (0.052 g, 86%) as an orange solid.

(Cy-PSiP)Rh(PH_2Cy) (2-4a). A solution of **1-2** (0.050 g, 0.068 mmol) in ca. 7 mL of cyclohexane was treated with $(Et_2O)LiPHCy$ (0.013 g, 0.068 mmol) was added to the mixture. The resulting red-orange reaction mixture was allowed to stand at room temperature for 1 h, at which point the volatile components of the reaction mixture were removed *in vacuo*. The remaining residue was extracted with ca. 5 mL of pentane, and the pentane extracts were filtered through Celite. The filtrate solution was collected and dried under vacuum to afford **2-4a** (0.043 g, 77%) as an orange solid. ^{1}H NMR (benzene-d_6): δ 8.36 (d, 2 H, J = 7 Hz, H_{arom}), 7.64 (m, 2 H, H_{arom}), 7.39 (apparent t, 2 H, J = 7 Hz, H_{arom}), 7.28 (apparent t, 2 H, J = 7 Hz, H_{arom}), 4.73 (dm, 2 H, $^1J_{PH}$ = 264 Hz, Rh-PH_2Cy), 2.52 – 1.03 (overlapping resonances, 44 H, P*Cy*), 0.99 (s, 3 H, Si*Me*). $^{13}C\{^1H\}$ NMR (benzene-d_6): δ 160.8 (C_{arom}), 146.7 (C_{arom}), 132.9 (apparent t, J = 11 Hz, CH_{arom}), 130.2 (CH_{arom}), 129.2 (CH_{arom}), 127.1 (CH_{arom}), 39.9 (apparent t, J = 8 Hz, CH_{Cy}), 38.6 (apparent t, J = 11 Hz, CH_{Cy}), 36.3 (CH_{2Cy}), 35.5 (d, $^1J_{CP}$ = 19 Hz, CH_{Cy}), 31.9 (CH_{2Cy}), 30.6 (CH_{2Cy}), 29.3 (CH_{2Cy}), 28.5–27.5 (overlapping resonances, CH_{2Cy}), 27.3 (CH_{2Cy}), 26.8 (CH_{2Cy}), 26.4 (CH_{2Cy}), 9.0 (Si*Me*). ^{31}P NMR (benzene-d_6): δ 69.8 (dd, 2 P, $^1J_{PRh}$ = 161 Hz, $^2J_{PP}$ = 27 Hz, *P*Si*P*), -50.6 (dt, 1 P, $^1J_{PRh}$ = 121 Hz, $^2J_{PP}$ = 27 Hz, Rh-*P*H_2Cy). ^{29}Si NMR (benzene-d_6): δ 70.2.

(Cy-PSiP)Rh($PHPh_2$) (2-4b). A solution of **1-2** (0.050 g, 0.068 mmol) in ca. 7 mL of benzene was treated with $(THF)_2LiPPh_2$ (0.023 g, 0.068 mmol). The resulting orange reaction mixture was allowed to stand at room temperature for 15 min., at which point the

volatile components of the reaction mixture were removed *in vacuo*. The remaining residue was extracted with ca. 5 mL of pentane, and the pentane extracts were filtered through Celite. The filtrate solution was collected and dried under vacuum to afford **2-4b** (0.058 g, 97%) as an orange solid. ^{1}H NMR (benzene-d_6): δ 8.37 (apparent d, 2 H, J = 7 Hz, H_{arom}), 7.82 (apparent t, 4 H, J = 7 Hz, H_{arom}), 7.60 (m, 2 H, H_{arom}), 7.40 (apparent t, 2 H, J = 7 Hz, H_{arom}), 7.26 (apparent t, 2 H, J = 7 Hz, H_{arom}), 7.15 (dt, 1 H, $^{1}J_{HP}$ = 290 Hz, $^{3}J_{HP}$ = 10 Hz, Rh-P*H*Ph$_2$), 7.15– 7.00 (overlapping resonances, 6 H, H_{arom}), 2.27 (m, 2 H, P*Cy*), 2.08 – 1.88 (overlapping resonances, 6 H, P*Cy*), 1.79 - 0.72 (overlapping resonances, 35 H, P*Cy* + Si*Me*; the Si*Me* resonance was identified at 0.92 ppm in a ^{1}H-^{13}C HSQC experiment). ^{13}C{^{1}H} NMR (benzene-d_6): δ 159.9 (C_{arom}), 146.4 (C_{arom}), 138.3 (C_{arom}), 134.7 (d, J = 12 Hz, CH$_{arom}$), 132.9 (apparent t, J = 12 Hz, CH$_{arom}$), 130.2 (CH$_{arom}$), 129.3 (CH$_{arom}$), 128.7 (CH$_{arom}$), 128.3 (CH$_{arom}$), 127.4 (CH$_{arom}$), 39.7 – 39.0 (overlapping resonances, CH$_{Cy}$), 31.7 (CH$_{2Cy}$), 30.8 (CH$_{2Cy}$), 30.3 (CH$_{2Cy}$), 29.5 (CH$_{2Cy}$), 28.0 – 27.1 (overlapping resonances, CH$_{2Cy}$), 26.7 (CH$_{2Cy}$), 9.4 (Si*Me*). ^{31}P{^{1}H} NMR benzene-d_6): δ 67.18 (dd, 2 P, $^{2}J_{PP}$ = 25 Hz, $^{1}J_{PRh}$ = 162 Hz, *P*Si*P*), -5.9 (dt, 1 P, $^{2}J_{PP}$ = 25 Hz, $^{1}J_{PRh}$ = 128 Hz, Rh-*P*HPh$_2$). ^{31}P NMR (benzene-d_6): δ 67.18 (br dd, 2 P, $^{2}J_{PP}$ = 25 Hz, $^{1}J_{PRh}$ = 162 Hz, *P*Si*P*), -5.9 (br dd, 1 P, $^{1}J_{PH}$ = 291 Hz, $^{1}J_{PRh}$ = 129 Hz, Rh-*P*HPh$_2$). ^{29}Si NMR (benzene-d_6): δ 69.6. Anal. Calcd for $C_{49}H_{66}RhP_3Si$: C, 66.96; H, 7.57. Found: C, 66.58; H, 7.49.

(Cy-PSiP)Rh(PH*i*Pr$_2$) (2-4c). A solution of **1-2** (0.015 g, 0.021 mmol) in ca. 5 mL of THF was treated with (THF)LiP*i*Pr$_2$ (0.004 g, 0.021 mmol). The resulting dark red reaction mixture was allowed to stand at room temperature for 15 min., at which point the volatile components of the reaction mixture were removed *in vacuo*. The remaining residue was extracted with ca. 5 mL of benzene, and the benzene extracts were filtered through

Celite. The filtrate solution was collected and dried under vacuum. The remaining residue was triturated with 3 × 5 mL pentane and subsequently dried under vacuum to afford **2-4c** (0.012 g, 62%) as a red solid. ^{1}H NMR (500 MHz, benzene-d_6): δ 8.37 (apparent d, 2 H, J = 7 Hz, H_{arom}), 7.68 (apparent d, 2 H, J = 7 Hz, H_{arom}), 7.40 (apparent t, 2 H, J = 7 Hz, H_{arom}), 7.29 (apparent t, 2 H, J = 7 Hz, H_{arom}), 4.50 (dm, 1 H, $^{1}J_{HP}$ = 269 Hz, Rh-PH^{i}Pr$_2$), 2.42 – 2.11 (overlapping resonances, 10 H, PCy + PH(CHMe$_2$)$_2$), 1.89 – 0.97 (overlapping resonances, 48 H, PCy + PH(CHMe_2)$_2$), 0.78 (s, 3 H, SiMe). ^{13}C{^{1}H} NMR (125.8 MHz, benzene-d_6): δ 160.8 (C_{arom}), 147.3 (C_{arom}), 133.15 (apparent t, J = 10 Hz, CH$_{arom}$), 130.2 (CH$_{arom}$), 129.5 (C_{arom}), 127.5 (C_{arom}), 39.8 (apparent t, J = 10 Hz, CH$_{Cy}$), 38.9 (apparent t, J = 11 Hz, CH$_{Cy}$), 31.9 (CH$_{2Cy}$), 31.3 (CH$_{2Cy}$), 30.2 (CH$_{2Cy}$), 29.6 (CH$_{2Cy}$), 28.3–27.3 (overlapping resonances, CH$_{2Cy}$ + PH(CHMe$_2$)$_2$), 24.5 (PH(CHMe_2)$_2$), 23.9 (PH(CHMe_2)$_2$), 9.6 (SiMe). ^{31}P NMR (202.5 MHz, benzene-d_6): δ 65.7 (dd, 2 P, $^{2}J_{PP}$ = 24 Hz, $^{1}J_{PRh}$ = 166 Hz, PSiP), 26.6 (dt, 1 P, $^{2}J_{PP}$ = 24 Hz, $^{1}J_{PRh}$ = 121 Hz, Rh-PH^{i}Pr$_2$). ^{29}Si NMR (99.4 MHz, benzene-d_6): δ 69.5.

(Cy-PSiP)Rh(PH$_2$Mes) (2-4d). A solution of **1-2** (0.12 g, 0.16 mmol) in ca. 10 mL of THF was treated with (THF)$_2$LiPHMes (0.048 g, 0.16 mmol). The resulting dark red reaction mixture was allowed to stand at room temperature for 15 min., at which point the volatile components of the reaction mixture were removed *in vacuo*. The remaining residue was extracted with ca. 5 mL of benzene, and the benzene extracts were filtered through Celite. The filtrate solution was collected and dried under vacuum. The remaining residue was triturated with 3 × 5 mL pentane and subsequently dried under vacuum to afford **2-4d** (0.13 g, 97%) as a red solid. ^{1}H NMR (500 MHz, benzene-d_6): δ 8.33 (apparent d, 2 H, J = 7 Hz, H_{arom}), 7.58 (apparent d, 2 H, J = 7 Hz, H_{arom}), 7.38 (apparent t, 2 H, J = 7 Hz, H_{arom}),

7.25 (apparent t, 2 H, J = 7 Hz, H_{arom}), 6.77 (s, 2 H, H_{arom}), 6.5 (br d, 2 H, $^{1}J_{HP}$ = 282 Hz, Rh-PH_2Mes), 2.64 (s, 6 H, *o*-C*Me*), 2.32 (m, 2 H, P*Cy*), 2.13 (s, 3 H, *p*-C*Me*), 2.08 - 1.00 (overlapping resonances, 42 H, P*Cy*), 0.88 (s, 3 H, Si*Me*). $^{13}C\{^{1}H\}$ NMR (125.8 MHz, benzene-d_6): δ 160.6 (C_{arom}), 146.9 (C_{arom}), 140.5 (d, J = 8 Hz, C_{arom}), 137.8 (C_{arom}), 133.2 (apparent t, J = 14 Hz, CH_{arom}), 130.4 (CH_{arom}), 129.7 (d, J = 7 Hz, CH_{arom}), 129.6 (CH_{arom}), 127.6 (CH_{arom}), 39.6 (br, CH_{Cy}), 38.7 (br, CH_{Cy}), 31.5–26.8 (overlapping resonances, CH_{2Cy}), 24.4 (*o*-C*Me*), 21.4 (*p*-C*Me*), 10.1 (Si*Me*). $^{31}P\{^{1}H\}$ NMR (202.5 MHz, benzene-d_6): δ 68.7 (dd, 2 P, $^{2}J_{PP}$ = 27 Hz, $^{1}J_{PRh}$ = 162 Hz, *P*Si*P*), -103.5 (br d, 1 P, $^{1}J_{PRh}$ = 115 Hz, Rh-*P*H_2Mes). ^{29}Si NMR (99.4 MHz, benzene-d_6): δ 68.8.

(Cy-PSiP)Rh(Ph)Br (2-5). A solution of **1-2** (0.038 g, 0.052 mmol) in ca. 7 mL of fluorobenzene was treated with $LiCH_2SiMe_3$ (0.005 g, 0.052 mmol). The resulting orange solution was allowed to stand at room temperature for 15 min., and was subsequently filtered through Celite. The filtrate solution was treated with PhBr (0.008 mL, 0.078 mmol). The resulting pale yellow reaction mixture was allowed to stand at room temperature for 15 min., and the volatile components were then removed in vacuo. The remaining solid was triturated with 3 × 5 mL pentane and subsequently dried under vacuum to afford **2-5** (0.041 g, 93%) as a pale yellow solid. ^{1}H NMR (dichloromethane-d_2): δ 7.93 (apparent d, 2 H, J = 7 Hz, H_{arom}), 7.67 – 7.64 (overlapping resonances, 3 H, H_{arom}), 7.43 – 7.30 (overlapping resonances, 5 H, H_{arom}), 7.00 (m, 2 H, H_{arom}), 6.83 (apparent t, 1 H, J = 7 Hz, H_{arom}), 3.07 (m, 2 H, P*Cy*), 2.74 (m, 2 H, P*Cy*), 2.40 (m, 2 H, P*Cy*), 2.04 (m, 2 H, P*Cy*), 1.96 – 0.66 (overlapping resonances, 37 H, P*Cy* + Si*Me*; the Si*Me* resonance was identified at 0.82 ppm in a ^{1}H-^{13}C HSQC experiment), 0.24 (m, 2 H, P*Cy*). $^{13}C\{^{1}H\}$ NMR (dichloromethane-d_2): δ 156.7 (C_{arom}), 143.7 (C_{arom}), 139.0 (CH_{arom}), 131.1 (apparent t, J =

10 Hz, CH$_{arom}$), 130.5 (CH$_{arom}$), 128.9 (CH$_{arom}$), 128.2 (CH$_{arom}$), 124.9 (CH$_{arom}$), 124.5 (CH$_{arom}$), 121.9 (CH$_{arom}$), 39.6 (apparent t, J = 12 Hz, CH$_{Cy}$), 38.5 (apparent t, J = 11 Hz, CH$_{Cy}$), 33.4 (CH$_{2Cy}$), 30.5 (CH$_{2Cy}$), 28.6–27.3 (overlapping resonances, CH$_{2Cy}$), 26.7 (CH$_{2Cy}$), 25.9 (CH$_{2Cy}$), 8.7 (Si*Me*). ^{31}P{^{1}H} NMR (dichloromethane-d_2): δ 45.9 (d, 2 P, $^{1}J_{PRh}$ = 117 Hz). ^{29}Si NMR (dichloromethane-d_2): δ 46.6.

(Cy-PSiP)Rh(PPh$_3$) (2-6). A solution of **1-2** (0.050 g, 0.068 mmol) in ca. 7 mL of cyclohexane was treated with LiCH$_2$SiMe$_3$ (0.006 g, 0.068 mmol). Triphenylphoshine (0.018 g, 0.068 mmol) was added to the reaction mixture. The resulting bright orange solution was allowed to stand at room temperature for 15 min., at which point the volatile components of the reaction mixture were removed *in vacuo*. The remaining residue was extracted with ca. 5 mL of pentane, and the pentane extracts were filtered through Celite. The filtrate solution was collected and dried under vacuum to afford **2-6** (0.058 g, 90%) as an orange solid. ^{1}H NMR (benzene-d_6): δ 8.41 (apparent d, 2 H, J = 7 Hz, H_{arom}), 8.00 (apparent t, 6 H, J = 8 Hz, H_{arom}), 7.53 (apparent d, 2 H, J = 7 Hz, H_{arom}), 7.39 (apparent t, 2 H, J = 7 Hz, H_{arom}), 7.24 (apparent t, 2 H, J = 7 Hz, H_{arom}), 7.17 – 6.98 (overlapping resonances, 9 H, H_{arom}), 2.20 (m, 2 H, P*Cy*), 1.94 (m, 2 H, P*Cy*), 1.72– 0.78 (overlapping resonances, 41 H, P*Cy* + Si*Me*; the Si*Me* resonance was identified at 1.13ppm in a ^{1}H-^{13}C HSQC experiment), 0.64 (m, 2 H, P*Cy*). ^{13}C{^{1}H} NMR (benzene-d_6): δ 159.6 (C_{arom}), 146.6 (C_{arom}), 142.1 (C_{arom}), 135.3 (d, J = 14 Hz, CH$_{arom}$), 132.7 (apparent t, J = 11 Hz, CH$_{arom}$), 130.0 (CH$_{arom}$), 129.1 (CH$_{arom}$), 128.8 (CH$_{arom}$), 127.9 (CH$_{arom}$), 127.0 (CH$_{arom}$), 37.9 (apparent t, J = 10 Hz, CH$_{Cy}$), 37.4 (apparent t, J = 10 Hz, CH$_{Cy}$), 31.5 (CH$_{2Cy}$), 30.7 (CH$_{2Cy}$), 30.1 (CH$_{2Cy}$), 28.4 (CH$_{2Cy}$), 28.1 – 26.9 (overlapping resonances, CH$_{2Cy}$), 26.4 (CH$_{2Cy}$), 9.1 (Si*Me*). ^{31}P{^{1}H} NMR (benzene-d_6): δ 62.8 (dd, 2 P, $^{2}J_{PP}$ = 20 Hz, $^{1}J_{PRh}$ = 166

Hz, *P*Si*P*), 20.8 (dt, 1 P, $^{2}J_{PP}$ = 20 Hz, $^{1}J_{PRh}$ = 129 Hz, Rh-*P*Ph$_3$). ^{29}Si NMR (benzene-d_6): δ 68.8. Anal. Calcd for $C_{55}H_{70}RhP_3Si$: C, 69.17; H, 7.39. Found: C, 69.52; H, 7.48.

General Procedure for Attempted *sp*^{2}-CP Cross-coupling Catalyzed by (Cy-PSiP)Rh(Ph)Br (2-5). In a typical experiment a 1-dram glass vial was charged with $HPPh_2$ (0.036 g, 0.034 mL, 0.19 mmol) and PhBr (0.030 g, 0.020 mL, 0.19 mmol), and diluted with 1.5 mL of benzene. This solution was added to another vial containing one equiv. of base (either NaOtBu or Cs_2CO_3; 0.19 mmol). The pre-catalyst **2-5** (0.016 g, 0.019 mmol) was then added to the mixture as a stock solution in benzene. Conversion to products was estimated on the basis of $^{31}P\{^{1}H\}$ NMR analysis of the reaction mixture.

(Cy-PSiP)Ir(H)(C≡C*t*Bu)(PH$_2$Mes) (2-8a, b). A solution of **2-3c** (0.062 g, 0.066mmol) in ca. 7 mL of benzene was treated with 3,3-dimethyl-1-butyne (0.011 g, 0.13mmol). The orange reaction mixture was allowed to stand at room temperature 72 h, at which point $^{31}P\{^{1}H\}$ NMR analysis of an aliquot indicated that **2-3c** was fully consumed. The volatile components of the reaction mixture were then removed under vacuum, and the remaining yellow residue was triturated with 3 × 5 mL pentane and subsequently dried under vacuum to afford **2-8** (0.062 g, 93%) as a pale-yellow solid. NMR analysis of this material indicates that **2-8** is formed as a ca. 3:1 mixture of two isomers, **2-8a** and **b**. Due to the complexity of the ^{1}H and $^{13}C\{^{1}H\}$ NMR spectra associated with this mixture of isomers, assignments are only provided for characteristic resonances; the corresponding spectra are provided in Appendix B29. ^{1}H NMR (benzene-d_6): δ 5.83 (dm, 2H, $^{1}J_{PH}$ = 337 Hz, Ir-P*H*$_2$Mes, **2-8b**), 5.75 (dm, 2H, $^{1}J_{PH}$ = 334 Hz, Ir-P*H*$_2$Mes, **2-8a**), 2.65 (s, 6 H, *o*-C*Me*, **2-8b**), 2.54 (s, 6 H, *o*-C*Me*, **2-8a**), 2.11 (s, 3 H, *p*-C*Me*, **2-8a**), 2.09 (s, 3 H, *p*-C*Me*, **2-8b**), 1.56 (s, 9 H, CC*tBu*, **2-8b**), 1.55 (s, 9 H, CC*tBu*, **2-8a**), 1.05 (s, 3 H, Si*Me*, **2-8b**),

1.00 (s, 3 H, Si*Me*, **2-8a**), -14.02 (dt, 1 H, $^{2}J_{HP}$ = 131 Hz, $^{2}J_{HP}$ = 18 Hz, Ir*H*, **2-8b**), -14.71 (m, 1 H, Ir*H*, **2-8a**). $^{13}C\{^{1}H\}$ NMR (benzene-d_6): δ 33.9 (C≡C^{t}*Bu*, **2-8a**), 33.6 (C≡C^{t}*Bu*, **2-8b**), 23.6 (d, *J* = 6 Hz, *o*-C*Me*, **2-8b**), 23.2 (d, *J* = 8 Hz, *o*-C*Me*, **2-8a**), 21.1 (*p*-C*Me*, **2-8a**), 20.9 (*p*-C*Me*, **2-8b**), 8.8 (Si*Me*, **2-8a**), 7.6 (Si*Me*, **2-8b**). $^{31}P\{^{1}H\}$ NMR (benzene-d_6): δ 31.5 (d, 2 P, $^{2}J_{PP}$ = 20 Hz, *P*Si*P*, **2-8a**), 30.1 (d, 2 P, $^{2}J_{PP}$ = 17 Hz, *P*Si*P*, **2-8b**), -119.9 (t, 1 P, $^{2}J_{PP}$ = 20 Hz, Ir-*P*H$_2$Mes, **2-8a**), -120.7 (m, 1 P, Ir-*P*H$_2$Mes, **2-8b**). ^{29}Si NMR (benzene-d_6): δ 44.7 (**2-8a**), 29.2 (**2-8b**). Crystals of **2-8b** suitable for X-ray diffraction analysis were obtained from a concentrated pentane solution at -35 ºC.

Generation of (Cy-PSiP)Ir(H)(SiHPh$_2$)(PH$_2$Mes) (2-9). A solution of **2-3c** (0.028 g, 0.030 mmol) in ca. 7 mL of benzene-d_6 was treated with H$_2$SiPh$_2$ (0.006 g, 0.033 mmol). The resulting orange reaction mixture was allowed to stand at room temperature for 5 h, over the course of the course of which a color change to bright yellow was observed. ^{1}H and $^{31}P\{^{1}H\}$ NMR analysis of this reaction mixture indicated >90% conversion of **2-3c** to **2-9**. ^{1}H NMR (benzene-d_6): δ 7.97 (apparent d, 2 H, *J* = 8 Hz, *H*$_{arom}$), 7.83 (apparent d, 1 H, *J* = 7 Hz, *H*$_{arom}$), 7.68 (apparent d, 1 H, *J* = 7 Hz, *H*$_{arom}$), 7.59 (m, 2 H, *H*$_{arom}$), 7.50 (m, 2 H, *H*$_{arom}$), 7.27 – 6.95 (overlapping resonances, 10 H, *H*$_{arom}$), 6.67 (s, 2 H, *H*$_{arom}$), 5.67 (dm, 1H, $^{1}J_{PH}$ = 357 Hz, Ir-P*H*$_2$Mes), 5.51 (dm, 1H, $^{1}J_{PH}$ = 316 Hz, Ir-P*H*$_2$Mes), 5.25 (ddd, 1H, $^{3}J_{PH}$ = 26, 8, and 3 Hz, Ir-Si*H*Ph$_2$), 3.03 (m, 1 H, P*Cy*), 2.41 – 0.94 (overlapping resonances, 51 H, P*Cy* + *o*-C*Me* + *p*-C*Me* + Si*Me*; singlet resonances at 2.24, 2.08, and 0.99 ppm were identified as corresponding to the *o*-C*Me*, *p*-C*Me*, and Si*Me* groups, respectively, in a ^{1}H-^{13}C HMQC experiment), 0.72 – 0.48 (overlapping resonances, 3 H, P*Cy*), -0.35 (m, 1 H, P*Cy*), -13.14 (dt, 1 H, $^{2}J_{HP}$ = 99 Hz, $^{2}J_{HP}$ = 19 Hz, Ir*H*). $^{13}C\{^{1}H\}$ NMR (benzene-d_6): δ 161.7 (*C*$_{arom}$), 158.0 (*C*$_{arom}$), 145.9 (*C*$_{arom}$), 144.1 (*C*$_{arom}$), 140.8 (*C*$_{arom}$),

138.5 (C_{arom}), 138.1 (CH_{arom}), 136.9 (CH_{arom}), 133.8 (d, J_{CP} = 18 Hz, CH_{arom}), 133.1 (d, J_{CP} = 20 Hz, CH_{arom}), 131.4 (CH_{arom}), 129.5 (CH_{arom}), 128.9 (CH_{arom}), 127.3 (CH_{arom}), 126.8 (CH_{arom}), 126.6 (CH_{arom}), 125.9 (CH_{arom}), 42.4 – 41.6 (overlapping resonances, CH_{Cy}), 36.8 (d, J_{CP} = 9 Hz, CH_{Cy}), 32.4 (CH_{2Cy}), 31.9 (CH_{2Cy}), 30.0 – 26.2 (overlapping resonances, CH_{2Cy}), 22.7 (*o*-C*Me*), 21.0 (*p*-C*Me*), 3.24 (Si*Me*). $^{31}P\{^{1}H\}$ NMR (benzene-d_6): δ 36.5 (apparent t, 1 P, $^{2}J_{PP}$ = 21Hz, *P*Si*P*), 13.6 (br s, 1 P, *P*Si*P*), -128.7 (apparent t, 1 P, $^{2}J_{PP}$ = 24 Hz, Ir-*P*H_2Mes).

Generation of (Cy-PSiP)Ir(H)$_2$(PH$_2$Mes) (2-10). A J-Young NMR tube was charged with a solution of **2-3c** (0.020 g, 0.021 mmol) in ca. 0.75 mL benzene-d_6. The solution was degassed *via* three freeze-pump-thaw cycles, and H_2 (1 atm) was introduced. An immediate color change to pale yellow was observed. The mixture was allowed to react at room temperature for 10 min., at which point ^{1}H and $^{31}P\{^{1}H\}$ NMR analysis indicated quantitative conversion to **2-10**. ^{1}H NMR (benzene-d_6): δ 8.37 (apparent d, 2 H, *J* = 7 Hz, H_{arom}), 7.42 (m, 2 H, H_{arom}), 7.27 (apparent t, 2 H, *J* = 7 Hz, H_{arom}), 7.11 (apparent t, 2 H, *J* = 7 Hz, H_{arom}), 6.68 (s, 2 H, H_{arom}), 5.50 (dm, 2 H, $^{1}J_{HP}$ = 330 Hz, Ir-P*H*$_2$Mes), 2.57 (s, 6 H, *o*-C*Me*), 2.27 (m, 2 H, P*Cy*), 2.10 (s, 3 H, *p*-C*Me*), 2.02 – 0.90 (overlapping resonances, 39 H, P*Cy* + Si*Me*; the Si*Me* resonance was identified at 1.20 ppm), 0.71 (m, 4 H, P*Cy*), 0.43 (m, 2 H, P*Cy*), -10.70 (m, 1 H, Ir*H*), -14.84 (dt, 1 H, $^{2}J_{HP}$ = 118 Hz, $^{2}J_{HP}$ = 19 Hz, Ir*H*). $^{31}P\{^{1}H\}$ NMR (benzene-d_6): δ 47.0 (d, 2 P, $^{2}J_{PP}$ = 18 Hz, *P*Si*P*), -136.8 (m, 1 P, Ir-*P*H_2Mes).

2.4.3 Crystallographic Solution and Refinement Details

Crystallographic data for each of **2-2c**, **2-3c**, **2-3d**, and **2-8b** were obtained at 173(±2)K on a Bruker D8/APEX II CCD diffractometer using either graphite-

monochromated Mo Kα (λ = 0.71073 Å) radiation (for **2-2c**) or CuKα (λ =1.54178 Å, microfocus source) radiation (for **2-3c**, **2-3d**, and **2-8b**), employing a sample that was mounted in inert oil and transferred to a cold gas stream on the diffractometer. Programs for diffractometer operation, data collection, and data reduction (including SAINT) were supplied by Bruker. Gaussian integration (face-indexed) was employed as the absorption correction method for **2-3d** and **2-8b**, and multi-scan (TWINABS) was used for **2-2c** and **2-3c**. The structure of **2-2c** was solved by direct methods, while **2-3c** and **2-3d** were solved by use of the Patterson search/structure expansion, and **2-8b** was solved by use of intrinsic phasing methods. All structures were refined by use of full-matrix least-squares procedures (on F^2) with R_1 based on $F_o^2 \geq 2\sigma(F_o^2)$ and wR_2 based on $F_o^2 \geq -3\sigma(F_o^2)$.

In the case of **2-2c**, the crystal used for data collection was found to display non-merohedral twinning. Both components of the twin were indexed with the program *CELL_NOW* (Bruker AXS Inc., Madison, WI, 2004). The second twin component can be related to the first component by 180º rotation about the [$^2/_5$ $^1/_2$ 1] axis in real space and about the [0 0 1] axis in reciprocal space. Integrated intensities for the reflections from the two components were written into a *SHELXL-97* HKLF 5 reflection file with the data integration program *SAINT* (version 7.68A), using all reflection data (exactly overlapped, partially overlapped and non-overlapped). The refined value of the twin fraction (*SHELXL-97* BASF parameter) was 0.4315(10). Anisotropic displacement parameters were employed for the non-hydrogen atoms. The P-*H* hydrogen atom H3P was located in the difference Fourier map and refined with a fixed isotropic displacement parameter. All remaining hydrogen atoms for **2-2c** were added at calculated positions and refined by use of a riding model employing isotropic displacement parameters based on the isotropic

displacement parameter of the attached atom.

For **2-3c**, the crystal used for data collection was also found to display non-merohedral twinning. Both components of the twin were indexed with the program *CELL_NOW* (Bruker AXS Inc., Madison, WI, 2004). The second twin component can be related to the first component by 180º rotation about the [1 0 $^{-1}/_{4}$] axis in real space and about the [–1 1 0] axis in reciprocal space. Integrated intensities for the reflections from the two components were written into a *SHELXL-97* HKLF 5 reflection file with the data integration program *SAINT* (version 7.68A), using all reflection data (exactly overlapped, partially overlapped and non-overlapped). The refined value of the twin fraction (*SHELXL-97* BASF parameter) was 0.4605(7). Two independent molecules of (Cy-PSiP)Ir(H)(PHMes) (A and B) were located in the asymmetric unit; for convenience, only molecule A is discussed in the text. Anisotropic displacement parameters were employed for the non-hydrogen atoms. The Ir-*H* (H1) and P-*H* (H3P) hydrogen atoms were located in the difference Fourier map; H1 was refined with a fixed isotropic displacement parameter, and H3P was refined with a common isotropic displacement parameter. The Ir–H1 distances in both crystallographically-independent molecules were constrained to be 1.50(1) Å. The P1···H1 and P2···H1 distances were constrained to be equal (within 0.003 Å) during refinement ($d(P1\cdots H1)_A = d(P2\cdots H1)_A$; $d(P1\cdots H1)_B = d(P2\cdots H1)_B$). As well, the Si–H1 distances in both molecules were constrained to be equal (within 0.003 Å) during refinement ($d(Si\cdots H1)_A = d(Si\cdots H1)_B$), as were the P3–H3P distances in both molecules ($d(P3–H3P)_A = d(P3–H3P)_B$). All remaining hydrogen atoms for **2-3c** were added at calculated positions and refined by use of a riding model employing isotropic displacement parameters based on the isotropic displacement parameter of the attached atom.

For **2-3d**, disorder involving the PH^{t}Bu group was observed. The constituent atoms were modelled over two positions (A and B), such that P3A, C2A, C3A, C4A, and C5A were refined with an occupancy factor of 0.85, while P3B, C2B, C3B, C4B, and C5B were refined with an occupancy factor of 0.15. The P3B–C2B distance was constrained to be 1.85(1) Å during refinement. The atoms C2B, C3B, C4B, and C5B were refined with a common isotropic displacement parameter. Anisotropic displacement parameters were employed for all remaining non-hydrogen atoms. The Ir-*H* (H1) and P-*H* (H3PA) hydrogen atoms were located in the difference Fourier map and were refined isotropically. The P-*H* hydrogen atom H3PB was generated assuming an idealized sp^2 hybridization of P3B, a fixed P3B–H3PB distance of 1.33 Å, and an isotropic displacement parameter 120% of the U_{eq} for P3B. All remaining hydrogen atoms for **2-3d** were added at calculated positions and refined by use of a riding model employing isotropic displacement parameters based on the isotropic displacement parameter of the attached atom.

For **2-8b**, disorder involving the alkynyl ^{t}Bu substituent was observed. This disorder was addressed satisfactorily by modelling two of the ^{t}Bu methyl groups (corresponding to C4 and C6) over two positions (A and B), each with 50% occupancy. Anisotropic displacement parameters were employed for all the non-hydrogen atoms in **2-8b**. The P-*H* hydrogen atoms H3PA and H3PB were located in the difference Fourier map and were refined isotropically. All remaining hydrogen atoms for **2-8b** were added at calculated positions and refined by use of a riding model employing isotropic displacement parameters based on the isotropic displacement parameter of the attached atom. Additional crystallographic information is provided in Appendix A.

Chapter 3: Synthesis of Coordinatively Unsaturated Aryloxo, Alkoxo, and Hydroxo Iridium Complexes Supported by PSiP Ligation and O-H Bond Oxidative Addition Leading to Aryloxo Hydride Ir^{III} Species

3.1 Introduction

The synthesis and reactivity of late transition metal alkoxo, aryloxo, and hydroxo complexes (Figure 3-1) has attracted substantial interest,[96] as such complexes have been implicated in numerous metal-mediated processes,[97] including the Wacker process for olefin oxidation,[98] catalytic transfer hydrogenation[99] and related processes involving dehydrogenation of alcohols,[100] C-H bond activation,[96d,101] cross-coupling,[50c,102] and water splitting.[70c,103] Although numerous examples of high oxidation state early metal complexes of this type are known,[104] electron-rich late metal variants have generally proven more challenging to access. It has been proposed that reactivity differences between early and late metal alkoxo/aryloxo/hydroxo species arise from a number of factors, including hard-soft mismatch between the hard O-donors and soft late metal centers, and d_π-p_π repulsion involving lone pairs on the O-donors and late metal *d*-electrons.[105] While the effects of such factors on late metal-alkoxo/aryloxo/hydroxo bond dissociation energies have been debated,[106] ultimately, late metal variants display significant nucleophilicity and basic character at the O-donor[96a,c,d] due to greatly diminished O→M π-donation.[107] As such, the reactivity properties of late metal alkoxo/aryloxo/hydroxo complexes has been compared to that of alkali metal analogues.[96c]

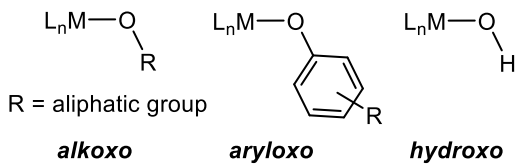

Figure 3-1. Transition metal alkoxo, aryloxo, and hydroxo complexes.

The majority of examples of late transition metal alkoxo/aryloxo/hydroxo complexes have been prepared by a salt metathesis route, whereby a metal halide or triflate complex is treated with an alkali metal alkoxide/aryloxide/hydroxide reagent (Scheme 3-1A).[96a-d] A protonolysis route, whereby an X ligand bound to a metal center functions as a Brønsted base toward an alcohol or water, has also been utilized effectively in this regard (Scheme 3-1B).[96a-d,100h,103i,108,109] By comparison, while the oxidative addition of an O-H bond to a low valent species has been invoked as a route to generate late metal alkoxo/aryloxo/hydroxo species (Scheme 3-1C), relatively few examples of such reactivity are well-known.[96a,110]

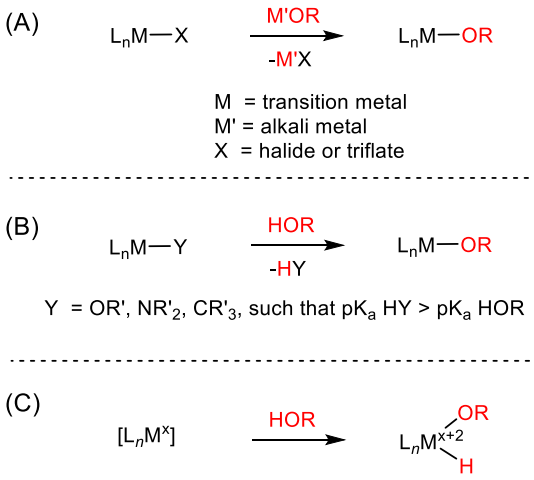

Scheme 3-1. General synthetic routes to late transition metal alkoxo/aryloxo/hydroxo complexes by: (A) salt metathesis; (B) protonolysis; and (C) O-H oxidative addition.

Having previously observed that in situ generated (Cy-PSiP)Ir^{I} species (**1-3**) derived from dehydrohalogenation of (Cy-PSiP)Ir(H)Cl (**1-1**) can undergo N-H bond oxidative addition of ammonia and alkylamines to afford isolable five-coordinate amido hydride complexes,[52k,66] the extension of this reactivity to the activation of O-H bonds in alcohols became of interest (Scheme 3-2). A comparison of bond dissociation energy (BDE) and pK$_a$ values for O-H and N-H containing species is shown in Table 3-1. For the

range of substrates indicated, BDE values of O-H bonds are generally higher than for N-H bonds in analogous species, and both exhibit similar trends, with phenol and aniline displaying BDE values at the low end of the series, while Me and ^{t}Bu substituted species feature appreciably larger X-H BDE's (X = N or O). The BDE of the O-H bond in water is the largest in the series at 497.10 ± 0.29 kJ mol^{-1}. From the perspective of thermodynamic feasibility, the O-H bond strength has to be compared with the Ir-O and Ir-H bonds formed as a result of O-H oxidative addition. While such BDE values involving (Cy-PSiP)Ir species have not been determined, it has been demonstrated that M-X bond dissociation energies are generally well-correlated with H-X BDE's,[106g] suggesting that O-H oxidative addition of aliphatic alcohols and phenols by **1-3** may be favorable. As expected, pK_a values trend lower for O-H bonds relative to N-H bonds in related species, and in accordance, evidence for an O-H oxidative addition mechanism involving initial protonation at the late metal center has been reported (Scheme 3-3).[110k,r]

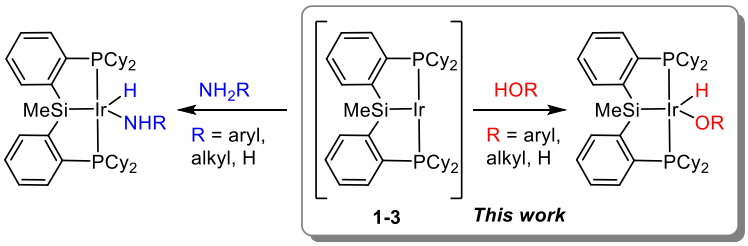

Scheme 3-2. Oxidative addition of N-H and O-H bonds *via* (Cy-PSiP)Ir^I (**1-3**).

Table 3-1. Bond dissociation energies (BDE)[56e] and pK_a values[56b,d,111] for selected substrates.

	H–OH	**H–OMe**	**H–O^{t}Bu**	**H–OPh**
BDE (kJ mol^{-1})	497.10±0.29	440.2±3	444.9±2.8	362.8±2.9
pK$_a$ (DMSO)	31.2	29.0	29.4	18.0
	H–NH$_2$	**H–NHMe**	**H–NH^{t}Bu**	**H–NHPh**
BDE (kJ mol^{-1})	450.08±0.24	425.1±8.4	397.5±8.4	375.3
pK$_a$ (DMSO)	41	42.9[a]	N/A	30.6

[a]Calculated value.[56d]

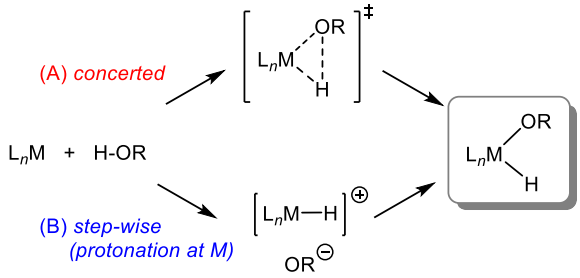

Scheme 3-3. Mechanisms proposed for O-H oxidative addition at a late metal center involving either: (A) a concerted pathway *via* a three-centered transition state, or (B) a step-wise pathway *via* protonation at the metal.

In the context of Group 9 transition metals, a handful of examples of O-H oxidative addition of aliphatic alcohols, phenols, and water at Ir metal centers have been previously reported (Figure 3-2). Milstein and co-workers were among the earliest to report O-H oxidative addition involving cationic $[(Me_3P)_4Ir]^+$ species[110c,d] (Figure 3-2A) and related neutral $(Me_3P)_3IrCl$ analogues[110e] (Figure 3-2B). In the former case, evidence for a concerted oxidative addition process involving a 14-electron $[(Me_3P)_3Ir]^+$ intermediate species was obtained. While O-H activation of water affords the cationic hydroxo complex, in the case of methanol facile β-hydride elimination was observed, leading to formation of a cationic Ir^{III} dihydride complex. Such β-elimination reactivity is often encountered in coordinatively unsaturated alkoxo complexes, and represents a common decomposition pathway. Oxidative addition involving the neutral complex $(Me_3P)_3IrCl$ was proposed to proceed by a concerted pathway involving nucleophilic attack of Ir on the O-H proton of the alcohol. Merola and co-workers targeted O-H oxidative addition *via* a related $[Ir(COD)(PMe_3)_3]Cl$ complex (COD = 1,5-cyclooctadiene; Figure 3-2C).[110k] While primary alcohols containing β-hydrogens generally led to the formation of multiple products, oxidative addition of phenols was observed at moderate temperatures (60 – 80 °C). A stepwise oxidative addition mechanism involving protonation at Ir, followed by

nucleophilic attack of both RO^- and Cl^- on the Ir center, was proposed. In the case of ^{t}BuOH, isobutene elimination was observed, leading to formation of an Ir hydroxo complex.

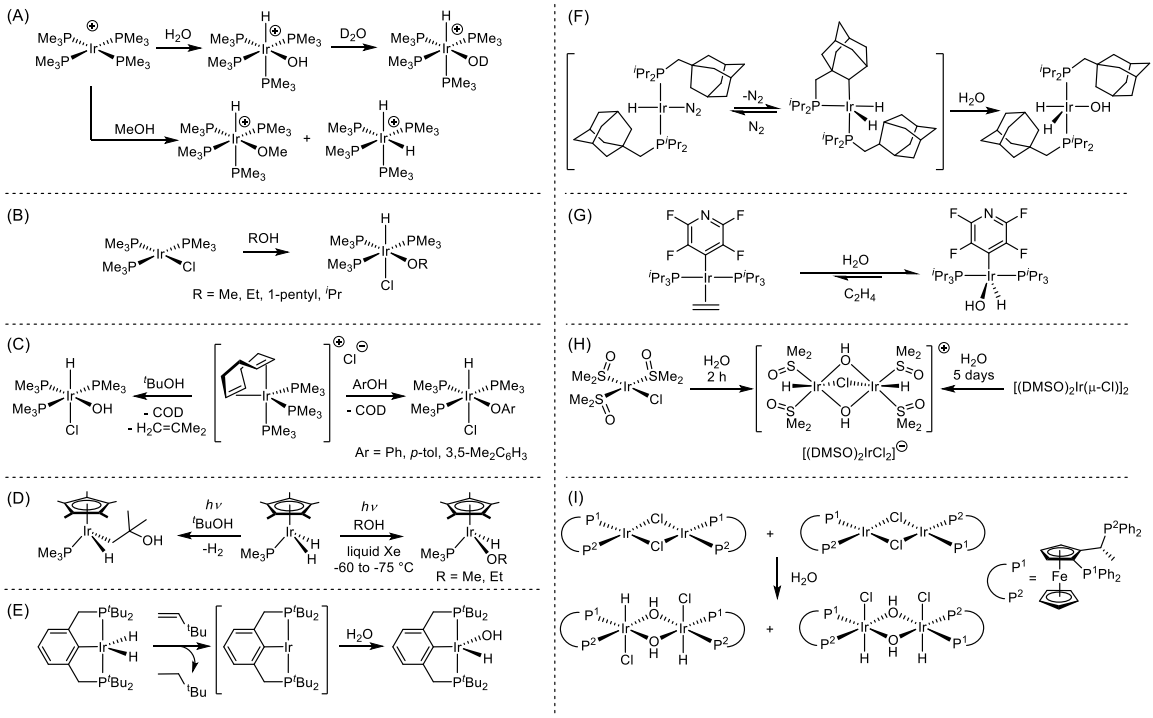

Figure 3-2. Examples of O-H oxidative addition at Ir to afford alkoxo/aryloxo/hydroxo Ir hydride complexes.

Bergman and co-workers reported that photolysis of $Cp^*Ir(PMe_3)(H)_2$ ($Cp^* = \eta^5$-C_5Me_5) in either neat ^{t}BuOH or in liquid xenon at -60 to -75 °C in the presence of ^{t}BuOH led exclusively to C-H oxidative addition upon H_2 elimination (Figure 3-2D).[110g,112] Conversely, when $Cp^*Ir(PMe_3)(H)_2$ was irradiated with UV light in liquid xenon at -60 to -75 °C in the presence of MeOH or EtOH, O-H oxidative addition was observed to afford the corresponding Ir^{III} alkoxo hydride complexes.[110g]

Perhaps most relevant to the work described herein is a report by Jensen and co-workers involving of O-H oxidative addition of water by ^{t}Bu-PCP ligated Ir pincer species (Figure 3-2E).[110l] This reaction is proposed to follow a pathway involving oxidative

addition to a 14-electron Ir^{I} intermediate, and affords a rare example of a 16-electron Ir hydroxo hydride complex. The latter complex is a pre-catalyst for alkane dehydrogenation, which implies that O-H reductive elimination, the reverse of oxidative addition, is also facile in this instance. More recent examples of O-H oxidative addition of water to form 16-electron hydroxo hydride complexes have also been reported by Figueroa[110m] (Figure 3-2F) and Braun[110n] (Figure 3-2G), respectively. The former report F is a unique example of a dihydride-hydroxo complex, and is remarkably resistant to O-H reductive elimination upon heating to 90 °C for as long as one week in benzene solution. Lastly, examples of O-H oxidative addition leading to dinuclear Ir^{III} complexes featuring bridging hydroxo ligands have also been reported (Figure 3-2H and I).[110o,p]

In an effort to assess the capability of (Cy-PSiP)Ir (**1-3**) to undergo O-H oxidative addition of alcohols, this chapter details synthetic investigations targeting alkoxo/aryloxo/hydroxo complexes of the type (Cy-PSiP)Ir(OR)H (R = alkyl, aryl, or H). The preparation of such compounds was initially attempted by salt metathesis and protonolysis routes, the latter of which proved to be the most facile approach for the isolation of a wide range of the targeted Ir^{III} alkoxo/aryloxo/hydroxo hydride complexes. Having observed that these five-coordinate species are indeed isolable, their preparation by O-H oxidative addition was attempted.

3.2 Results and Discussion

3.2.1 Attempted Synthesis of (Cy-PSiP)Ir(OR)H Complexes *via* Salt Metathesis

Salt metathesis, whereby a metal halide or triflate complex is treated with an alkali metal alkoxide/aryloxide/hydroxide reagent, is the most commonly employed route for the

synthesis of late transition metal alkoxo/aryloxo/hydroxo complexes (Scheme 3-1A). In this regard, initial efforts to prepare complexes of the type (Cy-PSiP)Ir(OR)H (R = alkyl, aryl, or H) focused on treatment of (Cy-PSiP)Ir(Cl)H (**1-1**) with alkoxide and aryloxide salts, such as NaOtBu and LiOPh (Scheme 3-4). Although no reaction was observed upon treatment of **1-1** with up to 20 equiv. NaO^{t}Bu in benzene solution at room temperature, heating of the mixture at 65 ºC for 8 h resulted in complete conversion (by ^{31}P NMR) to a new product assigned as (Cy-PSiP)Ir(O^{t}Bu)H (**3-1a**) on the basis of ^{1}H and ^{31}P{^{1}H} NMR analysis (benzene-d_6). Complex **3-1a** gives rise to a single ^{31}P{^{1}H} NMR resonance at 56.5 ppm, consistent with a C_s-symmetric structure in solution (Table 3-2). The ^{1}H NMR spectrum of **3-1a** features a characteristic Ir-*H* resonance at -25.12 ppm (t, $^2J_{HP}$ = 17 Hz), which indicates that no O-H reductive elimination has occurred.

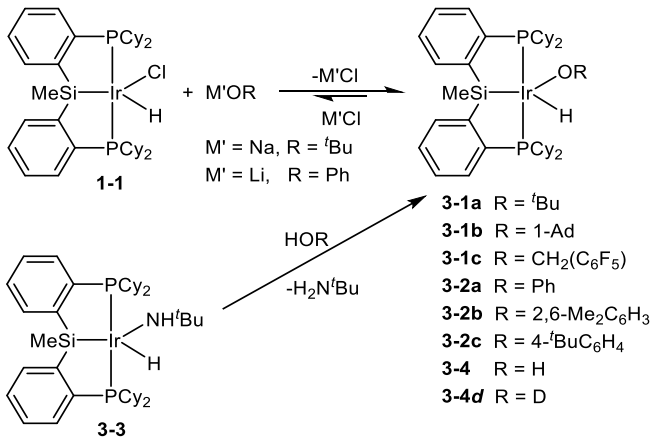

Scheme 3-4. Synthesis of (Cy-PSiP)Ir(OR)H complexes (**3-1a** – **d**, **3-2a** – **c**, **3-4**, and **3-4*d***) by salt metathesis or protonolysis routes.

By comparison, treatment of **1-1** with five equiv. LiOPh in THF solution resulted in ca. 50% conversion (by ^{31}P NMR) to a new product assigned as (Cy-PSiP)Ir(OPh)H (**3-2a**). Complex **3-2a** features similar spectroscopic features to **3-1a**, including an Ir-*H* ^{1}H NMR resonance at -25.82 ppm (t, $^2J_{HP}$ = 15 Hz). Additional reaction time or the use of up

to 20 equiv. LiOPh did not result in significantly higher conversion to **3-2a**. While it is possible that this reaction requires more forcing conditions to reach completion, the possibility of an equilibrium between **3-2a** and the starting complex **1-1** in the presence of LiCl must also be considered. Such metathesis reactions involving related Rh and Ir hydroxo complexes reacting with an alkali metal halide have been observed previously.[113] While such reactivity may be reduced in less polar solvents (*vide supra*), the poor solubility of alkali metal alkoxo/aryloxo/hydroxo salts in such solvents also presents a synthetic challenge. As such, a protonolysis route was pursued as an alternative strategy for the direct synthesis of (Cy-PSiP)Ir(OR)H.

Table 3-2. Isolated yields (*via* **3-3**) and selected NMR spectroscopic data (ppm; benzene-d_6) for (Cy-PSiP)Ir(OR)H alkoxo/aryloxo/hydroxo-hydride complexes.

Complex	Isolated Yield (%)	$^{31}P\{^1H\}$ NMR[a]	^1H NMR Ir-*H*	$^2J_{PH}$ (Ir-*H*)	^{29}Si NMR[b]
(Cy-PSiP)Ir(Cl)H (**1-1**)[20b]		61.1 (s)	-23.79 (t)	14	7.7
(Cy-PSiP)Ir(NH^{t}Bu)H (**3-3**)[66]		52.0 (s)	-20.78 (t)	19	16.7
(Cy-PSiP)Ir(OH)H (**3-4**)	78	57.9 (s)	-23.92 (t)	15	8.5
(Cy-PSiP)Ir(O^{t}Bu)H (**3-1a**)	92	56.5 (s)	-25.12 (t)	17	7.1
(Cy-PSiP)Ir[O(1-Ad)]H (**3-1b**)	83	56.7 (s)	-25.05 (t)	17	7.5
(Cy-PSiP)Ir[$OCH_2(C_6F_5)$]H (**3-1c**)	72	59.2 (s)	-25.26 (t)	15	7.7
(Cy-PSiP)Ir(OPh)H (**3-2a**)	86	59.1 (s)	-25.82 (t)	15	7.6
(Cy-PSiP)Ir[O(2,6-$Me_2C_6H_3$)]H (**3-2b**)	95	57.5 (s)	-26.44 (t)	15	6.8
(Cy-PSiP)Ir[O(4-^{t}BuC_6H_4)]H (**3-2c**)	72	58.9 (s)	-25.76 (t)	15	7.4

[a]Relative to 85% H_3PO_4. [b] ^1H-^{29}Si HMBC.

3.2.2 Synthesis of (Cy-PSiP)Ir(OR)H Complexes *via* Protonolysis of an Ir Amido

In order to optimize the formation of Ir alkoxo/aryloxo/hydroxo complexes *via* a protonolysis route involving the reaction of M-Y with HOR, the relative pK_a's of the YH species and the reacting alcohol must be considered. In this regard, the alkylamido complex (Cy-PSiP)Ir(NH^{t}Bu)H (**3-3**) was chosen as suitable starting material for this effort, as it is

readily prepared from **1-1** and LiNH^{t}Bu,[66] and the pK_a of H_2N^tBu is anticipated to be significantly higher (*cf.* the pK_a of H_2NMe, calculated value of 42.9)[56d] than that of most alcohols of interest (Table 3-1), as well as higher than the pK_a of water.

Treatment of **3-3** with a variety of alcohols, phenols, as well as water led to the evolution of H_2N^tBu and concomitant formation of the corresponding (Cy-PSiP)Ir(OR)H complexes (Scheme 3-4; **3-1a** R = ^{t}Bu, **3-1b** R = 1-Ad, **3-1c** R = $CH_2(C_6F_5)$, **3-2a** R = Ph, **3-2b** R = 2,6-$Me_2C_6H_3$, **3-2c** R = 4-^{t}BuC_6H_4, **3-4** R = H), which were readily isolated. $^{31}P\{^1H\}$ NMR analysis of the reaction mixtures indicated that all reactions proceeded to quantitative conversion at room temperature within an hour of mixing, with no observable intermediates. All such (Cy-PSiP)Ir(OR)H complexes exhibit similar spectroscopic features consistent with their formulation as C_s-symmetric five-coordinate species in solution (Table 3-2). Namely, as was previously observed for related amido and anilido hydride complexes of the type (Cy-PSiP)Ir(NHR)H, each complex gives rise to a single $^{31}P\{^1H\}$ NMR resonance, as well as an Ir-*H* ^{1}H NMR resonance that exhibits $^2J_{HP}$ coupling (ca. 15–17 Hz) consistent with *cis*-coordination relative to the magnetically equivalent Cy-PSiP phosphino donors. In the case of **3-2c**, the ^{1}H NMR spectrum of the isolated complex indicates that *ca*. 2 equiv. of HO(4-^{t}BuC_6H_4) are associated with the aryloxo complex, likely *via* hydrogen bonding interactions. Related examples of hydrogen bonding involving late metal alkoxo, aryloxo, and hydroxo complexes have been previously reported.[52d,110f,j] In the case of **3-4**, the ^{1}H NMR spectrum of the isolated complex features a broad resonance at 3.65 ppm (1 H) that corresponds to the Ir-O*H* proton. When **3-3** was treated with D_2O in place of H_2O, ^{2}H incorporation was observed exclusively at the Ir-O*H* position, affording the hydrido complex **3-4*d*** as would be anticipated for a protonolysis reaction.

The solid state structure of **3-2c** was determined by use of X-ray crystallographic techniques and confirms the formulation of this complex as a five-coordinate aryloxo hydride complex (Figure 3-3A, B). Two molecules of HO(4-^{t}BuC$_6$H$_4$) co-crystallize with the Ir complex and are involved in hydrogen bonding *via* the aryloxo ligand, which is consistent with the solution NMR data for **3-2c**. The complex adopts a distorted trigonal bipyramidal structure in the solid state that is analogous to that previously observed for related five coordinate Cy-PSiP complexes, including (Cy-PSiP)Ir(Cl)H (**1-1**)[20b] and (Cy-PSiP)Ir(NHPh)H (Table 3-3).[52k,66] The Cy-PSiP phosphino groups occupy the apical positions (P1-Ir1-P2 160.96(2)°), while the Y-distorted equatorial positions are taken up by the silyl, aryloxo, and hydride donors, with an acute H1-Ir1-Si1 angle of H(1)-Ir-Si 67.5(1)°. The theoretical underpinnings for such a Y-distortion involving five-coordinate d^6 metal complexes that feature a potential π-donor ligand have been addressed previously.[80] The Ir-O distance of 2.1234(16) is relatively long by comparison with Ir-O distances in previously reported Ir aryloxo complexes, which include *trans*-(Ph$_3$P)$_2$Ir(CO)(OPh) (2.049(4) Å),[114] *trans*-(Ph$_3$P)$_2$Ir(CO)(OC$_6$F$_5$) (2.058(3) Å),[115] (Ph$_3$P)$_2$Ir(CO)(OPh)(TCNE) (2.057(8) Å),[116] and *mer*-(Me$_3$P)$_3$Ir(H)(Cl)(O(3,5-Me$_2$C$_6$H$_3$)] (2.109(5) Å).[110k] The solid state structure of **3-4** was also determined (Figure 3-3C). However, this complex was found to co-crystallize with (Cy-PSiP)Ir(Cl)H, resulting in disorder (25% Cl site occupancy). Although disordered, this structure does confirm the connectivity in the targeted hydroxo complex. This observation also highlights the extreme sensitivity of such Ir hydroxo/aryloxo/alkoxo to halide impurities.

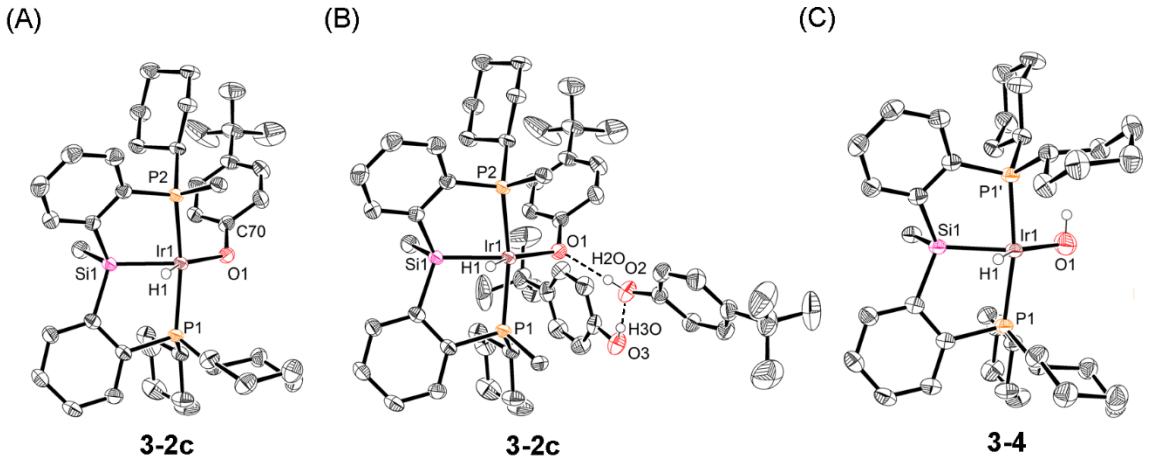

Figure 3-3. Crystallographically determined structures of **3-2c** (A and B; the structure of **3-2c** shown in B is the same approximate view as in A, but shows the hydrogen bonding interactions with the co-crystallized HO(4-^{t}BuC$_6$H$_4$) molecules) and **3-4** (C; only the major contributor of the disordered MeSi(C$_6$H$_4$PCy$_2$)$_2$IrH(OH)$_{0.75}$Cl$_{0.25}$ is depicted) with thermal ellipsoids drawn at the 50% probability level. Selected P*Cy* carbon atoms and most hydrogen atoms have been omitted for clarity. Selected interatomic distances (Å) and angles (°): for **3-2c** Ir1-P1 2.3071(6), Ir1-P2 2.3139(6), Ir1-O1 2.1234(16), Ir1-Si1 2.2762(6), Ir1-H1 1.46(1), O2-H2O 0.78(3), H2O···O1 1.89(3), O2···O1 2.664(3), O3-H3O 0.77(4), H3O···O2 2.01(4), O3···O2 2.770(3), P1-Ir1-P2 160.96(2), O1-Ir1-Si1 139.06(5), H1-Ir1-Si1 67.5(1), O1-Ir1-H1 153.2(1), O2-H2O···O1 174(3), O3-H3O···O2 170(5); for **3-4** Ir1-P1 2.2956(5), Ir1-Si1 2.2791(7), Ir1-O1 2.030(6), Ir1-H1 1.42(3), P1-Ir1-P1' 166.38(3), O1-Ir1-Si1 138.48(18), H1-Ir1-Si1 73.1(12), O1-Ir1-H1 148.4(12).

Table 3-3. Selected crystallographic data – interatomic distances (Å) and bond angles (°) for crystallographically characterized complexes (Cy-PSiP)Ir(H)X (X = Cl, anilido, aryloxo).

Complex	Ir-X distance	P-Ir-P (PSiP) Angle	Si-Ir-X Angle	X-Ir-H Angle	Si-Ir-H Angle
(Cy-PSiP)Ir[O(4-^{t}BuC$_6$H$_4$)]H (**3-2c**)	2.1234(16)	160.96(2)	139.06(5)	153.2(1)	67.5(1)
(Cy-PSiP)Ir(Cl)H (**1-1**)[20b]	2.4143(12)	166.07(4)	130.64(5)	160.6(18)	68.7(18)
(Cy-PSiP)Ir(NHPh)H[52k,66]	2.056(2)	158.06(3)	137.35(8)	154.4	67.5
(Cy-PSiP)Ir[NH(2,6-Me$_2$C$_6$H$_3$)]H[52k,66]	2.077(3)	162.01(3)	129.72(11)	160.7	68.8

In an effort to evaluate the reactivity of **3-3** with relatively bulky substrates, treatment with up to 10 equiv. of (2,6-^{t}Bu$_2$-4-MeC$_6$H$_3$)OH resulted in no reaction even with heating up to 75 ºC. Alcohols containing β-hydrogen substituents were also evaluated in such protonolysis reactions. In all cases, treatment of **3-3** with either methanol,

cyclohexanol, or 1-butanol led to the formation of (Cy-PSiP)Ir(H)$_4$, (**3-5**) which has been previously reported by Shimada and co-workers.[21d] The formation of **3-5** likely involves facile dehydrogenation of the aliphatic alcohol,[100] which may proceed by either an outer- (*e.g. via* a concerted transfer of H^+ to Ir-NH^{t}Bu and H^- to Ir) or inner-sphere (*e.g. via* β-hydride elimination from an Ir-alkoxo species) mechanism (Scheme 3-5). No evidence for the formation of aldehydes was observed *in situ* by ^{1}H NMR spectroscopic analysis of the reaction mixtures. Interestingly, similar formation of **3-5** was observed in the reaction of **3-3** with HOCH$_2$Ph, while treatment of **3-3** with the fluorinated HOCH$_2$(C$_6$F$_5$) cleanly afforded the corresponding Ir alkoxo complex **3-1c**, which reflects the diminished reactivity of the benzylic H's in HOCH$_2$(C$_6$F$_5$). By comparison, treatment of *in situ* generated (Cy-PSiP)Ir (**1-3**) with H$_2$NCH$_2$Ph resulted in exclusive C-H activation at the *ortho* position of the aromatic ring.[66]

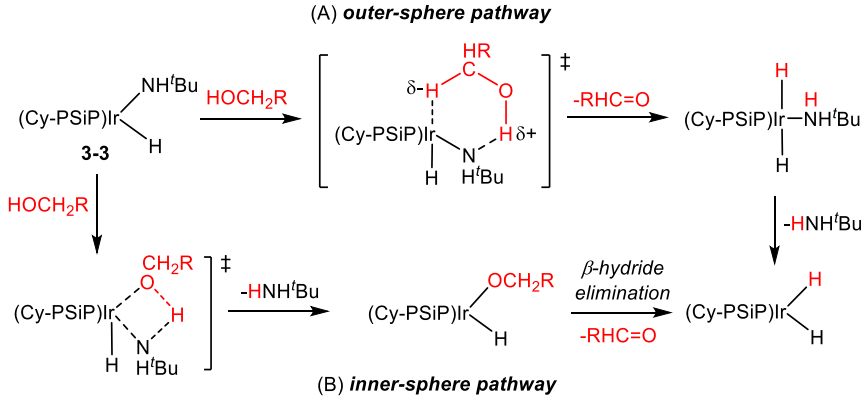

Scheme 3-5. Possible outer-sphere (A) and inner-sphere (B) pathways for alcohol dehydrogenation.

3.2.3 Attempted Synthesis of (Cy-PSiP)Ir(OR)H Complexes *via* O-H Oxidative Addition

Having demonstrated that complexes of the type (Cy-PSiP)Ir(OR)H (R = alkyl, aryl, or H) are synthetically accessible, the synthesis of such alkoxo/aryloxo/hydroxo

species by an O-H oxidative addition pathway was targeted. Initial attempts toward this goal utilized the route previously employed for the synthesis of related amido and anilido hydride Ir complexes via N-H oxidative addition of the corresponding amines/anilines (Scheme 3-2).[52k,66] Thus, treatment of **1-1** with $LiCH_2SiMe_3$ in cyclohexane solution affords in situ access to the highly reactive Ir^I species (Cy-PSiP)Ir (**1-3**), which undergoes N-H oxidative addition upon subsequent treatment with amines/anilines. Given the observed sensitivity of the Ir-OR linkage to metathesis processes with alkali metal halides, *in situ* generated **1-3** in cyclohexane solution was filtered through a glass microfiber filter (0.7 μm pore size) prior to treatment with alcohols, with the hope that precipitated LiCl may be removed from the reaction mixture by this approach. Treatment of **1-3** generated *via* this process with one equiv. of either HOPh, $HO(2,6\text{-}Me_2C_6H_3)$, or $HOCH_2(C_6F_5)$, respectively, led to the partial generation of the corresponding (Cy-PSiP)Ir(OR)H complex, as well as significant quantities of **1-1** (*ca*. 3:1 ratio of **3-2a** to **1-1**, and *ca*. 3:2 ratio for each of **3-2b** or **3-1c** to **1-1**; by ^{31}P NMR; Scheme 3-6) after 2 h at room temperature. *In situ* spectroscopic analysis of **1-3** prior to the addition of the alcohol confirmed that no unreacted **1-1** remained in solution, thus the presence of **1-1** in the final mixture is tentatively attributed to the metathesis reaction of (Cy-PSiP)Ir(OR)H with LiCl persisting in solution. In a similar reaction where **1-3** was treated with two equiv. of HO^{t}Bu, quantitative conversion to **1-1** was observed after 2 h at room temperature. When **1-3** was treated with DO^{t}Bu in an analogous manner, quantitative formation of (Cy-PSiP)Ir(Cl)D (**1-1*d***) was obtained. Treatment of **1-1** with 50 equiv. of DO^{t}Bu in benzene-d_6 solution does not lead to any ^2H incorporation into **1-1** after 1 h at room temperature, which suggests that the targeted (Cy-PSiP)Ir(O^{t}Bu)(H/D) complex **3-1a** may indeed be an intermediate in this

process, but it is quickly reverted to **1-1** in the presence of persistent LiCl impurities.

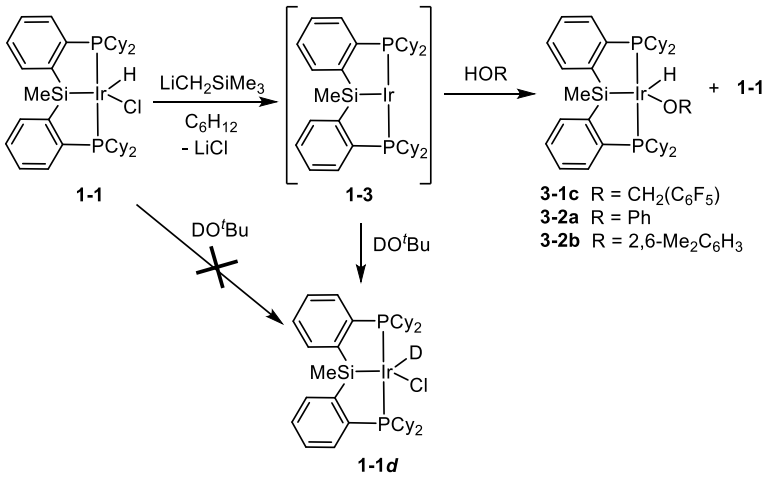

Scheme 3-6. Reactivity of *in situ* generated (Cy-PSiP)Ir (**1-3**) with alcohol substrates.

In an effort to avoid the generation of LiCl or related halide salts in the generation of **1-3**, the reactivity of (Cy-PSiP)Ir(H)$_4$ (**3-5**) with alcohols was examined with and without added *tert*-butylethylene (TBE) as a hydrogen acceptor. In related reactivity, Jensen and co-workers previously demonstrated that dehydrogenation of (^{t}Bu-PCP)Ir(H)$_2$ (^{t}Bu-PCP = 2,6-(^{t}Bu$_2$PCH$_2$)$_2$C$_6$H$_3$) with TBE in the presence of water (165 equiv.) led to the quantitative formation of the hydroxo complex (^{t}Bu-PCP)Ir(OH)H via O-H oxidative addition to a 14-electron (^{t}Bu-PCP)Ir intermediate (Figure 3-2E).[110l] As well, Shimada and co-workers[21d] have previously reported that **3-5** is readily dehydrogenated by TBE in benzene solution to afford (Cy-PSiP)Ir(Ph)H (**1-7**), presumably via the intermediate generation of **1-3**. In this regard, treatment of **3-5** with one equiv. of HOPh in benzene-d_6 solution afforded 81% conversion (by ^{1}H and ^{31}P NMR) to **3-2a** within ten minutes of mixing, in the absence of TBE (Scheme 3-7). Analogous reactions with HO^{t}Bu and water (2 equiv. in each case) did not result in any conversion of **3-5**, even upon heating at 75 °C for 24 h. Treatment of **3-5** with 5 equiv. of TBE, followed by addition of one equiv. of

HO^{t}Bu also did not afford any conversion to the Ir alkoxo complex **3-1a**.

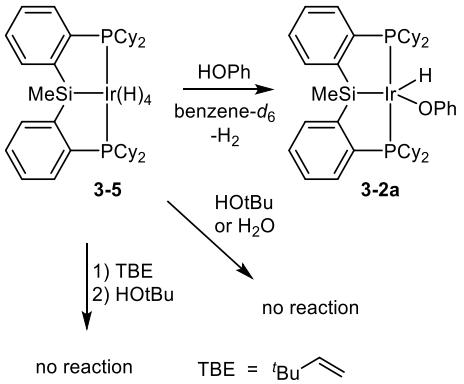

Scheme 3-7. Reactivity of (Cy-PSiP)Ir(H)$_4$ (**3-5**) with alcohol substrates and water.

The reactivity of (Cy-PSiP)Ir(C_2H_4) (**1-5b**) with alcohols was also examined. In related reactivity, Bergman and co-workers have previously reported that the Ru complex (PMe_3)$_4$Ru(C_2H_4) reacts with one equiv. of water at room temperature to afford (PMe_3)$_4$Ru(OH)H.[110f] Complex **1-5b** was previously reported in the context of trapping *in situ* generated **1-3** by the coordination of C_2H_4,[52k] and is a readily accessible (Cy-PSiP)Ir^I complex that can be isolated in high yield by treatment of **1-1** with $LiCH_2SiMe_3$ under an atmosphere of C_2H_4. Unlike (PMe_3)$_4$Ru(C_2H_4), **1-5b** does not appear to react with water, and as such, the isolated complex can be washed with degassed water to remove any residual LiCl. Upon treatment of **1-5b** with 1 - 10 equiv. of HOR (R = ^{t}Bu, 1-Ad, Ph, 2,6-$Me_2C_6H_3$, 4-^{t}BuC_6H_4, or $CH_2(C_6F_5)$) no reaction was observed at room temperature over a period of 3 days. Heating a toluene solution of **1-5b** and 10 equiv. of HOPh at 80 ºC for 2 h afforded quantitative (by ^{31}P NMR) conversion to the aryloxo-hydride complex **3-2a** (Scheme 3-8). In the case of HO(2,6-$Me_2C_6H_3$), heating to 110 ºC for 18 h was necessary to achieve quantitative (by ^{31}P NMR) conversion to the corresponding aryloxo **3-2b**. By comparison, under similar conditions the reaction of **1-5b** with five equiv. $HOCH_2(C_6F_5)$ afforded a complex mixture of products from which no pure material could be isolated after

heating for 8 h at 65 ºC. No reaction was observed upon treatment of **1-5b** with 1-20 equiv. of either HO^{t}Bu, HO(1-Ad), or water followed by heating of the reaction mixtures up to 90 ºC.

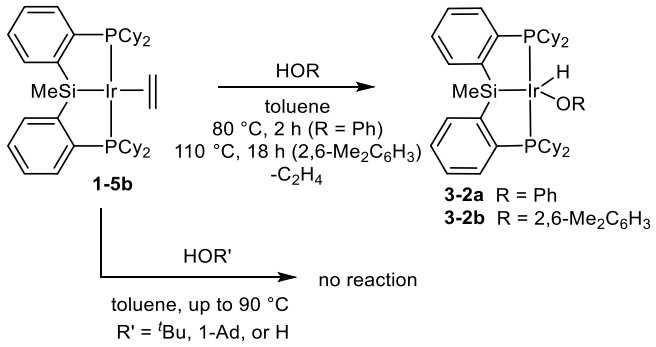

Scheme 3-8. Reactivity of (Cy-PSiP)Ir(C_2H_4) (**1-5b**) with alcohol substrates and water.

3.2.4 Preliminary Reactivity Studies of (Cy-PSiP)Ir(OR)H Complexes

Previous reports regarding the reactivity of late metal alkoxo/hydroxo complexes have established that due to the nucleophilic nature of the O-donor ligands, unsaturated substrates such as CO_2 and RNCO insert readily into the M-O bonds.[96a,104] In several examples where both alkoxo/hydroxo and hydride ligands are present, preferential insertion at the M-O linkage was observed,[52d,110j,n,117] despite the fact that formal insertion of such unsaturated substrates into late transition metal hydrides is also a known process.

The reaction of **3-4** with CO_2 (1 atm) occurs readily upon mixing in benzene-d_6 solution to afford a new product tentatively formulated as the bicarbonato complex (Cy-PSiP)Ir(κ^2-O_2COH)H (**3-6**; Scheme 3-9). Complex **3-6** gives rise to a single new $^{31}P\{^1H\}$ NMR resonance at 53.2 ppm, as well as a new Ir-*H* ^{1}H NMR resonance at -27.71 ppm (t, $^2J_{HP}$ = 15 Hz). The broad Ir-O*H* ^{1}H NMR resonance at 3.66 ppm associated with **3-4** is no longer observed following CO_2 addition, rather a broad resonance centered at 12.40 ppm is assigned to the proton of the Ir-bicarbonato group. The IR spectrum of **3-6** (thin film)

features a broad absorption at 2650 cm^{-1}, characteristic of the O-H vibration of the Ir-bicarbonato. Similar ν_{OH} values have previously been reported for related Os-, Rh-, and Ir-bicarbonato species.[110n,117-118] Additional characteristic absorptions for the bicarbonato ligand were observed at 1579 and 1474 cm^{-1}. Preliminary results indicate that while (Cy-PSiP)Ir(O^{t}Bu)H (**3-1a**) undergoes a related insertion process with CO_2 to afford a carbonate complex, the phenoxo analogue (**3-2a**) does not react with CO_2 (1 – 5 atm) under analogous conditions.

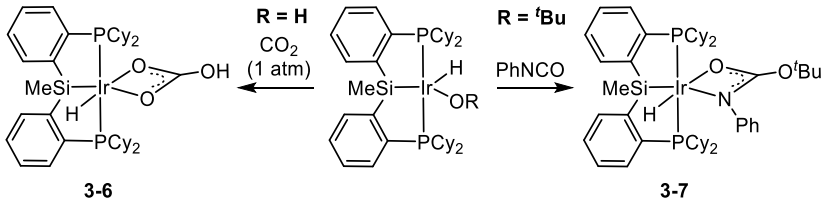

Scheme 3-9. Insertion reactions with (Cy-PSiP)Ir(OR)H complexes.

Complex **3-1a** reacted with phenyl isocyanate (1 equiv.) to afford an isolable insertion product assigned as the hydrido-Ir *tert*-butyl *N*-phenylcarbamato complex (Cy-PSiP)Ir(κ^2-*O*(*N*Ph)CO^{t}Bu)H (**3-7**; Scheme 3-9). This complex gives rise to a single $^{31}P\{^1H\}$ NMR resonance at 48.1 ppm, as well as an Ir-*H* ^{1}H NMR resonance at -23.30 ppm (t, $^2J_{HP}$ = 16 Hz) ppm. The IR spectrum of **3-7** does not feature any strong absorption bands above 1600 cm^{-1} that can be assigned to a carbonyl stretching band, consistent with κ^2-coordination mode of the *N*-phenylcarbamato group where the Ir-(κ^2-*O*-C(O^{t}Bu)=*N*Ph) resonance form is a significant contributor.

3.3 Summary and Conclusions

The synthesis and characterization of a series of coordinatively unsaturated alkoxo, aryloxo, and hydroxo Ir hydride complexes supported by bis(phosphino) silyl (PSiP) pincer ligation were described. Such mononuclear, coordinatively unsaturated alkoxo/aryloxo/hydroxo late transition metal complexes are relatively rare. The studies detailed in this chapter demonstrate that complexes of the type (Cy-PSiP)Ir(OR)H (R = alkyl, aryl, or H) are isolable and do not undergo O-H reductive elimination under typical conditions. While apparently resistant to O-H reductive elimination, such complexes are highly sensitive to alkali metal halide impurities, and readily undergo metathesis reactions with halide salts to afford (Cy-PSiP)Ir(X)H (X = halide). As such, (Cy-PSiP)Ir(OR)H complexes are most readily prepared by protonolysis reactions, such as the treatment of (Cy-PSiP)Ir(NH^{t}Bu) (**3-3**) with the corresponding alcohol HOR. Preliminary studies indicate that (Cy-PSiP)Ir(OR)H complexes undergo formal insertion preferentially into the Ir-O bond with substrates such as CO_2 and phenyl isocyanate to form Ir κ^2-*O*,*O*-bicarbonato (for R = H) and κ^2-*N*,*O*-*tert*-butyl-*N*-phenylcarbamato (for R = ^{t}Bu) complexes.

Attempts to prepare (Cy-PSiP)Ir(OR)H complexes by an O-H oxidative addition pathway proved significantly more challenging than analogous reactivity involving N-H oxidative addition of amines, anilines, and ammonia. While dehydrohalogenation of (Cy-PSiP)Ir(Cl)H (**1-1**) with alkyllithium reagents in cyclohexane solution served as a convenient route to access 14-electron species of the type (Cy-PSiP)Ir (**1-3**) that went on to active N-H bonds and readily afford (Cy-PSiP)Ir(NHR)H complexes, in the presence of alcohol substrates LiCl generated in the dehydrohalogenation step led to significant regeneration of **1-1**. Attempts to filter such LiCl impurities away from the reaction mixtures

containing **1-3** were not successful, and due to the highly reactive nature of the intermediate **1-3**, this species is not amenable to more rigorous isolation and purification protocols (*e.g.*, recrystallization). When **1-3** generated *via* this route was treated with DO^{t}Bu, ^{2}H incorporation was observed at the Ir-*H* position, affording exclusively (Cy-PSiP)Ir(Cl)D (**1-1*d***). As complex **1-1** does not itself appear to undergo H/D exchange with DO^{t}Bu, these results suggest that **1-3** does indeed mediate O-H/D oxidative addition of the aliphatic alcohol substrate, but the resulting Ir-alkoxo complex is readily intercepted by LiCl to reform **1-1**/**1-1*d***. Attempts to observe (Cy-PSiP)Ir-mediated O-H oxidative addition of HOR substrates via alternative source of **1-3**, such as (Cy-PSiP)Ir(H)$_4$ (**3-5**) and (Cy-PSiP)Ir(C_2H_4) (**1-5b**), were partly successful, leading to O-H oxidative addition of phenol substrates to afford Ir aryloxo hydride complexes, but did not mediate O-H bond activation of aliphatic alcohols or water. These studies provide new insights into the chemistry of coordinatively unsaturated late transition metal alkoxo/aryloxo/hydroxo species, and further inform the understanding of O-H oxidative addition processes mediated by transition metal pincer complexes.

3.4 Experimental

3.4.1 General Considerations

All experiments were conducted under nitrogen in an MBraun glovebox or using standard Schlenk techniques. Dry, oxygen-free solvents were used unless otherwise indicated. Tetrahydrofuran and diethyl ether were distilled from Na/benzophenone ketyl. Benzene, toluene, and pentane were sparged with nitrogen and dried by subsequent passage through a double-column solvent purification system (one activated alumina column and

one column packed with activated Q-5). All purified solvents were stored over 4 Å molecular sieves. Benzene-d_6, cyclohexane-d_{12}, and dichloromethane-d_2 were degassed via three freeze-pump-thaw cycles and stored over 4 Å molecular sieves. The compounds (Cy-PSiP)Ir(Cl)H (**1-1**),[21] (Cy-PSiP)Ir(NH^{t}Bu)H (**3-3**),[16b] and (Cy-PSiP)Ir(H)$_4$ (**3-5**)[27] were prepared according to literature procedure. All other reagents were purchased from commercial suppliers and used without further purification. Unless otherwise stated, ^{1}H, ^{13}C, ^{31}P, ^{19}F, and ^{29}Si NMR characterization data were collected at 300K on a Bruker AV-300 spectrometer operating at 300.1, 75.5, 121.5, 282.4, and 59.6 MHz (respectively) with chemical shifts reported in parts per million downfield of $SiMe_4$ (for ^{1}H, ^{13}C, and ^{29}Si) or 85% H_3PO_4 in D_2O (for ^{31}P). ^{1}H and ^{13}C NMR chemical shift assignments are based on data obtained from ^{13}C-DEPTQ, ^{1}H-^{1}H COSY, ^{1}H-^{13}C HSQC, and ^{1}H-^{13}C HMBC NMR experiments. ^{29}Si NMR assignments are based on ^{1}H-^{29}Si HMQC and ^{1}H-^{29}Si HMBC experiments. In some cases, fewer than expected unique ^{13}C NMR resonances were observed, despite prolonged acquisition times. X-ray data collection, solution, and refinement were carried out by Drs. Robert MacDonald, Michael J. Ferguson, and Yuqiao Zhou at the University of Alberta X-ray Crystallography Laboratory, Edmonton, Alberta.

3.4.2 Synthetic Details and Characterization Data

(Cy-PSiP)Ir(C_2H_4) (1-5b). A resealable, thick-walled reaction vessel equipped with a Teflon stopcock was charged with solution of **1-1** (0.085 g, 0.10 mmol) in ca. 10 mL of diethyl ether. The solution was degassed by three freeze-pump-thaw cycles and an atmosphere of ethylene was introduced. Under a purge of ethylene, a solution of $LiCH_2SiMe_3$ (0.010 g, 0.10 mmol) in ca. 2 mL of pentane was added by syringe. The solution immediately turned bright orange in color. After 15 minutes at room temperature,

the volatile components of the reaction mixture were removed under vacuum. The remaining residue was extracted with ca. 10 mL of benzene, and the benzene extracts were filtered through Celite. The filtrate solution was collected and the volatile components were removed *in vacuo*. The remaining residue was triturated with pentane (3 × 5 mL) and dried under vacuum to afford **1-5b** as an orange powder (0.090 g, 91%). NMR spectroscopic data for **1-5b** obtained by this route is in agreement with previously reported data.[16b] ^{1}H NMR (500 MHz, benzene-d_6): δ 8.24 (apparent d, 2 H, J = 7 Hz, H_{arom}), 7.52 (m, 2 H, H_{arom}), 7.32 (apparent t, 2 H, J = 7 Hz, H_{arom}), 7.18 (apparent t, 2 H, J = 7 Hz, H_{arom}), 2.68 (s, 4 H, C_2H_4), 2.59 (m, 4 H, P*Cy*), 2.05 – 1.98 (overlapping resonances, 6 H, P*Cy*), 1.73 – 1.04 (overlapping resonances, 30 H, P*Cy*), 0.88 – 0.79 (overlapping resonances, 7 H, P*Cy* + Si*Me*; Si*Me* at 0.86 ppm). ^{31}P{^{1}H} NMR (202.5 MHz, benzene-d_6): δ 65.4.

(Cy-PSiP)Ir(O^{t}Bu)H (3-1a). A solution of **3-3** (0.020 g, 0.023 mmol) in ca. 7 mL of pentane was treated with ^{t}BuOH (0.002 g, 0.023 mmol). The color of the solution changed from orange to bright yellow upon addition. The resulting reaction mixture was allowed to stand at room temperature for 1 h, at which point the volatile components were removed *in vacuo*. The remaining residue was triturated with 3 × 3 mL of pentane and dried under vacuum to afford **3-1a** (0.018 g, 92%) as an orange solid. ^{1}H NMR (benzene-d_6): δ 8.10 (apparent d, 2 H, J = 7 Hz, H_{arom}), 7.47 (m, 2 H, H_{arom}), 7.20 (apparent t, 2 H, J = 7 Hz, H_{arom}), 7.12 (apparent t, 2 H, J = 7 Hz, H_{arom}), 2.88 (m, 2 H, CH_{Cy}), 2.66 (m, 2 H, CH_{Cy}), 2.48 (m, 2 H, P*Cy*), 2.18– 0.64 (overlapping resonances, 45 H, P*Cy* + O^{t}Bu; the O^{t}Bu resonance was identified at 1.61 ppm in a ^{1}H-^{13}C HSQC experiment), 0.90 (s, 3 H, Si*Me*), 0.73 (m, 2 H, P*Cy*), -25.11 (t, 1 H, $^{2}J_{HP}$ = 17 Hz, Ir*H*). ^{13}C{^{1}H} NMR (benzene-d_6): δ 158.7 (C_{arom}), 144.1 (C_{arom}), 131.8 (apparent t, J = 9 Hz, CH$_{arom}$), 130.2 (CH$_{arom}$), 128.8

(CH_{arom}), 126.8 (CH_{arom}), 73.5 ($OCMe_3$), 36.0 ($OCMe_3$), 34.5 (apparent t, J = 15 Hz, CH_{Cy}), 33.9 (apparent t, J = 16 Hz, CH_{Cy}), 30.4 (CH_{2Cy}), 30.2 (CH_{2Cy}), 29.9 (CH_{2Cy}), 28.0 - 26.7 (overlapping resonances, CH_{2Cy}), 4.4 (Si*Me*). $^{31}P\{^1H\}$ NMR (benzene-d_6): δ 56.5. ^{29}Si NMR (benzene-d_6): δ 7.1.

(Cy-PSiP)Ir[O(1-Ad)]H (3-1b). A solution of **3-3** (0.026 g, 0.030 mmol) in ca. 7 mL of pentane was treated with 1-AdOH (0.005 g, 0.030 mmol). The resulting reaction mixture was allowed to stand at room temperature for 1 h, at which point the volatile components were removed *in vacuo.* The remaining residue was triturated with 3 × 3 mL of pentane and dried under vacuum to afford **3-1b** (0.024 g, 83%) as a yellow solid. ^1H NMR (benzene-d_6): δ 8.11 (apparent d, 2 H, J = 7 Hz, H_{arom}), 7.48 (m, 2 H, H_{arom}), 7.24 (apparent t, 2 H, J = 7 Hz, H_{arom}), 7.14 (m, 2 H, H_{arom}), 2.97 (m, 2 H, C*H*$_{Cy}$), 2.68 (m, 2 H, C*H*$_{Cy}$), 2.51 (m, 2 H, P*Cy*), 2.37 (m, 3 H, C*H*$_{Ad}$), 2.19 – 0.98 (overlapping resonances, 48 H, P*Cy* + *1-Ad*), 0.91 (s, 3 H, Si*Me*), 0.74 (m, 2 H, P*Cy*), -25.05 (t, 1 H, $^2J_{HP}$ = 17 Hz, Ir*H*). $^{13}C\{^1H\}$ NMR (benzene-d_6): δ 158.8 (C_{arom}), 144.0 (C_{arom}), 131.8 (apparent t, J = 8 Hz, CH_{arom}), 130.2 (CH_{arom}), 128.8 (CH_{arom}), 126.8 (CH_{arom}), 71.3 (C_{Ad}), 50.9 (CH_{2Ad}), 37.8 (CH_{2Ad}), 34.4 (m, CH_{Cy}), 32.5 (CH_{Ad}), 30.5 (CH_{2Cy}), 30.2 (CH_{2Cy}), 29.9 (CH_{2Cy}), 28.2 - 26.7 (overlapping resonances, CH_{2Cy}), 4.1 (Si*Me*).$^{31}P\{^1H\}$ NMR (benzene-d_6): δ 56.7. ^{29}Si NMR (benzene-d_6): δ 7.4.

(Cy-PSiP)Ir[OCH$_2$(C$_6$F$_5$)]H (3-1c). A solution of **3-3** (0.033 g, 0.038 mmol) in ca. 7 mL of THF was treated with $HOCH_2(C_6F_5)$ (0.008 g, 0.038 mmol). The color of the solution changed from orange to bright yellow upon addition. The resulting reaction mixture was allowed to stand at room temperature for 2 h, at which point the volatile components were removed *in vacuo*. The remaining residue was triturated with 3 × 3 mL

of pentane and dried under vacuum to afford **3-1c** (0.027 g, 72%) as a yellow solid. ^{1}H NMR (benzene-d_6): δ 8.05 (apparent d, 2 H, J = 7 Hz, H_{arom}), 7.39 (m, 2 H, H_{arom}), 7.21 (apparent t, 2 H, J = 7 Hz, H_{arom}), 7.10 (apparent t, 2 H, J = 7 Hz, H_{arom}), 5.36 (br, 2 H, OCH_2(C_6F_5)), 2.67 – 2.41 (overlapping resonances, 6 H, P*Cy*), 2.17 (m, 2 H, P*Cy*), 2.00– 0.74 (overlapping resonances, 39 H, P*Cy* + Si*Me*; the Si-*Me* resonance was identified at 0.90 ppm in a ^{1}H-^{13}C HSQC experiment), -25.25 (t, 1 H, $^{2}J_{HP}$ = 15 Hz, Ir*H*). ^{13}C{^{1}H} NMR (benzene-d_6): δ 159.0 (C_{arom}), 143.1 (C_{arom}), 131.9 (apparent t, J = 9 Hz, CH$_{arom}$), 130.8 (CH$_{arom}$), 129.1 (CH$_{arom}$), 127.0 (CH$_{arom}$), 35.2 (apparent t, J = 11 Hz, CH$_{Cy}$), 34.7 (apparent t, J = 15 Hz, CH$_{Cy}$), 30.1 (CH$_{2Cy}$), 29.6 (CH$_{2Cy}$), 28.1 (CH$_{2Cy}$), 27.8 (CH$_{2Cy}$), 27.2 (CH$_{2Cy}$), 26.4 (CH$_{2Cy}$), 4.6 (Si*Me*). ^{31}P{^{1}H} NMR (benzene-d_6): δ 59.2. ^{19}F{^{1}H} NMR (benzene-d_6) δ -146.2 (br, 2 F, *o*-C_6F_5), -159.2 (br, 1 F, *p*-C_6F_5), -163.9 (br, 2 F, *m*-C_6F_5). ^{29}Si NMR (benzene-d_6): δ 7.5.

(Cy-PSiP)Ir(OPh)H (3-2a). A solution of **3-3** (0.031 g, 0.037 mmol) in ca. 7 mL of THF was treated with HOPh (0.004 g, 0.038 mmol). The color of the solution changed from orange to bright yellow upon addition. The resulting reaction mixture was allowed to stand at room temperature for 1 h, at which point the volatile components were removed *in vacuo*. The remaining residue was triturated with 3 × 3 mL of pentane and dried under vacuum to afford **3-2a** (0.029 g, 89%) as an orange solid. ^{1}H NMR (benzene-d_6): δ 8.03 (apparent d, 2 H, J = 7 Hz, H_{arom}), 7.38 (m, 2 H, H_{arom}), 7.24 – 7.16 (overlapping resonances, 4 H, H_{arom}), 7.08 (apparent t, 2 H, J = 7 Hz, H_{arom}), 6.90 (d, 2 H, H_{arom}), 6.76 (t, 1 H, O*PhH*$_{arom}$), 2.58 (m, 2 H, CH_{Cy}), 2.38 (m, 2 H, P*Cy*), 2.27– 0.76 (overlapping resonances, 43 H, P*Cy* + Si*Me*; the Si-*Me* resonance was identified at 0.94 ppm in a ^{1}H-^{13}C HSQC experiment), -25.82 (t, 1 H, $^{2}J_{HP}$ = 15 Hz, Ir*H*). ^{13}C{^{1}H} NMR (benzene-d_6): δ 168.6

(C_{arom}), 158.6 (C_{arom}), 143.3 (C_{arom}), 132.1 (apparent t, J = 8 Hz, CH_{arom}), 131.0 (CH_{arom}), 129.9 (CH_{arom}), 129.6 (CH_{arom}), 127.7 (CH_{arom}), 119.6 (CH_{arom}), 117.1 (CH_{arom}), 35.6 (apparent t, J = 16 Hz, CH_{Cy}), 34.9 (apparent t, J = 16 Hz, CH_{Cy}), 30.9 (CH_{2Cy}), 30.7 (CH_{2Cy}), 29.8 (CH_{2Cy}), 28.2 (CH_{2Cy}), 27.8 - 27.2 (overlapping resonances, CH_{2Cy}), 26.7 (CH_{2Cy}), 25.9 (CH_{2Cy}), 4.9 (Si*Me*). $^{31}P\{^{1}H\}$ NMR (benzene-d_6): δ 59.1. ^{29}Si NMR (benzene-d_6): δ 7.6.

(Cy-PSiP)Ir[O(2,6-Me$_2$C$_6$H$_3$)]H (3-2b). A solution of **3-3** (0.026 g, 0.030 mmol) in ca. 7 mL of pentane was treated with HO(2,6-$Me_2C_6H_3$) (0.004 g, 0.030 mmol). The resulting reaction mixture was allowed to stand at room temperature for 1 h, at which point the volatile components were removed *in vacuo*. The remaining residue was triturated 3 × 3 mL of pentane and dried under vacuum to afford **3-2b** (0.026 g, 95%) as a yellow solid. ^{1}H NMR (benzene-d_6): δ 8.05 (apparent d, 2 H, J = 7 Hz, H_{arom}), 7.40 (m, 2 H, H_{arom}), 7.26 – 7.16 (overlapping resonances, 4 H, H_{arom}), 7.11 (m, 2 H, H_{arom}), 6.77 (t, 1 H, J = 7 Hz, H_{arom}), 2.66 (s, 3 H, 2,6-*Me*$_2$C$_6$H$_3$), 2.54 (s, 3 H, 2,6-*Me*$_2$C$_6$H$_3$), 2.34– 0.75 (overlapping resonances, 47 H, P*Cy* + Si*Me*; the Si-*Me* resonance was identified at 0.93 ppm in a ^{1}H-^{13}C HSQC experiment), -26.44 (t, 1 H, $^{2}J_{HP}$ = 15 Hz, Ir*H*). $^{13}C\{^{1}H\}$ NMR (benzene-d_6): δ 172.8 (C_{arom}), 158.6 (C_{arom}), 143.6 (C_{arom}), 131.8 (apparent t, J = 8 Hz, CH_{arom}), 131.6 (CH_{arom}), 130.3 (CH_{arom}), 129.1 (CH_{arom}), 128.6 (CH_{arom}), 126.9 (C_{arom}), 115.4 (CH_{arom}), 35.7 (apparent t, J = 16 Hz, CH_{Cy}), 34.5 (apparent t, J = 16 Hz, CH_{Cy}), 27.7 (apparent t, J = 16 Hz, CH_{2Cy}), 27.6–27.0 (overlapping resonances, CH_{2Cy}), 26.5 (CH_{2Cy}), 18.7 (2,6-*Me*$_2$C$_6$H$_3$), 17.9 (2,6-*Me*$_2$C$_6$H$_3$), 4.9 (Si*Me*). $^{31}P\{^{1}H\}$ NMR (benzene-d_6): δ 57.5. ^{29}Si NMR (benzene-d_6): δ 6.8.

(Cy-PSiP)Ir[O(4-^{t}Bu(C$_6$H$_4$)]H·[HO(4-^{t}BuC$_6$H$_4$)]$_2$ (3-2c·[HO(4-^{t}BuC$_6$H$_4$)]$_2$). A

solution of **3-3** (0.026 g, 0.030 mmol) in ca. 7 mL of benzene was treated with HO[4-^{t}Bu(C_6H_4)] (0.020 g, 0.150 mmol). The color of the solution changed from orange to bright yellow upon addition. The resulting reaction mixture was allowed to stand at room temperature for 1 h, at which point the volatile components were removed *in vacuo*. The remaining residue was triturated with 3 × 3 mL of pentane and dried under vacuum to afford **3-2c** (0.027 g, 72%) as a yellow solid. ^{1}H NMR (500 MHz, benzene-d_6): δ 8.05 (apparent d, 2 H, J = 7 Hz, H_{arom}), 7.39 (m, 2 H, H_{arom}), 7.25 – 7.16 (overlapping resonances, 8 H, H_{arom}), 7.11 (apparent t, 2 H, J = 7 Hz, H_{arom}), 6.84 (br s, 6 H, H_{arom}), 2.58 (m, 2 H, CH_{Cy}), 2.38 (m, 2 H, CH_{Cy}), 2.30 – 2.17 (overlapping resonances, 4 H, P*Cy*), 2.03 (m, 2 H, P*Cy*), 1.88 (m, 2 H, P*Cy*), 1.78 (m, 2 H, P*Cy*), 1.71– 0.81 (overlapping resonances, 60 H, P*Cy* + ^{t}*Bu* + Si*Me*; the ^{t}*Bu* and Si-*Me* resonances were identified at 1.34 and 0.95 ppm, respectively, in a ^{1}H-^{13}C HSQC experiment), -25.72 (t, 1 H, $^2J_{HP}$ = 15 Hz, Ir*H*). ^{13}C{^{1}H} NMR (125.8 MHz, benzene-d_6): δ 158.5 (apparent t, J = 20 Hz, C_{arom}), 143.1 (apparent t, J = 27 Hz, C_{arom}), 138.5 (br, *C*-^{t}Bu), 131.8 (apparent t, J = 9 Hz, *C*H$_{arom}$), 130.6 (*C*H$_{arom}$), 129.1 (*C*H$_{arom}$), 127.3 (*C*H$_{arom}$), 126.6 (br, *C*H$_{arom}$), 119.7 (br, *C*H$_{arom}$), 35.1 (apparent t, J = 14 Hz, *C*H$_{Cy}$), 34.3 (apparent t, J = 10 Hz, *C*H$_{Cy}$), 34.0 (*C*Me$_3$), 32.1 (C*Me*$_3$), 30.5 (*C*H$_{2Cy}$), 30.4 (*C*H$_{2Cy}$), 29.4 (*C*H$_{2Cy}$), 27.9 (*C*H$_{2Cy}$), 27.6 (*C*H$_{2Cy}$), 27.3 – 26.9 (overlapping resonances, *C*H$_{2Cy}$), 26.4 (*C*H$_{2Cy}$), 4.7 (Si*Me*). ^{31}P{^{1}H} NMR (202.5 MHz, benzene-d_6): δ 58.8. ^{29}Si NMR (99.4 MHz, benzene-d_6): δ 7.4.

(Cy-PSiP)Ir(OH)H (3-4). A solution of **3-3** (0.055 g, 0.064 mmol) in ca. 7 mL of pentane was treated with degassed water (0.001 mg, 0.064 mmol). The color of the solution changed from orange to yellow upon addition. The resulting reaction mixture was allowed to stand at room temperature for 1 h, at which point the volatile components were removed

in vacuo. The remaining residue was triturated with 3 × 3 mL of pentane and dried under vacuum to afford **3-4** (0.040 g, 78%) as a yellow solid. ^{1}H NMR (benzene-d_6): δ 8.09 (apparent d, 2 H, J = 7 Hz, H_{arom}), 7.42 (m, 2 H, H_{arom}), 7.23 (apparent t, 2 H, J = 7 Hz, H_{arom}), 7.11 (apparent t, 2 H, J = 7 Hz, H_{arom}), 3.65 (br s, 1 H, O*H*), 2.63 - 2.47 (overlapping resonances, 6 H, P*Cy*), 2.20 - 0.97 (overlapping resonances, 38 H, P*Cy*), 0.94 (s, 3 H, Si*Me*), -23.92 (t, 1 H, $^{2}J_{HP}$ = 15 Hz, Ir*H*). ^{13}C{^{1}H} NMR (benzene-d_6): δ 159.3 (C_{arom}), 143.5 (C_{arom}), 131.9 (apparent t, J = 8 Hz, CH$_{arom}$), 130.7 (CH$_{arom}$), 129.0 (CH$_{arom}$), 127.0 (CH$_{arom}$), 35.4 – 34.7 (overlapping resonances, CH$_{Cy}$), 30.2 (CH$_{2Cy}$), 30.0 (CH$_{2Cy}$), 28.4 (CH$_{2Cy}$), 27.5 - 26.4 (CH$_{2Cy}$), 4.8 (Si*Me*). ^{31}P{^{1}H} NMR (benzene-d_6): δ 57.9. ^{29}Si NMR (benzene-d_6): δ 8.5.

(Cy-PSiP)Ir[κ^2-*O*(*N*Ph)CO^{t}Bu]H (3-7). A solution of **3-1a** (0.027 g, 0.032 mmol) in ca. 7 mL of pentane was treated with PhNCO (0.004 g, 0.032 mmol), added as a stock solution in pentane (1 M concentration). The color of the solution changed from orange to pale yellow upon addition. The resulting reaction mixture was allowed to stand at room temperature for 2 h, at which point the volatile components were removed *in vacuo*. The remaining residue was triturated with 3 × 3 mL of pentane and dried under vacuum to afford **3-7** (0.025 g, 80%) as an off-white solid. ^{1}H NMR (benzene-d_6): δ 8.16 (apparent d, 2 H, J = 7 Hz, H_{arom}), 7.73 (d, 2 H, J = 7 Hz, H_{arom}), 7.51 (m, 2 H, H_{arom}), 7.31 – 7.22 (overlapping resonances, 4 H, H_{arom}), 7.15 (m, 2 H, H_{arom}), 6.88 (t, 1 H, J = 7 Hz, H_{arom}), 2.73 (m, 2 H, CH_{Cy}), 2.39 – 0.66 (overlapping resonances, 54 H, P*Cy* + ^{t}*Bu* + Si*Me*; the ^{t}*Bu* and Si-*Me* resonances were identified at 1.62 and 1.00 ppm, respectively, in a ^{1}H-^{13}C HSQC experiment), -23.30 (t, 1 H, $^{2}J_{HP}$ = 16 Hz, Ir*H*). ^{13}C{^{1}H} NMR (benzene-d_6): δ 159.8 (apparent t, J = 21 Hz, C_{arom}), 157.5 (OC(O^{t}Bu)N), 146,8 (C_{arom}), 144.8 (apparent t, J = 31

Hz, C_{arom}), 132.2 (apparent t, J = 9 Hz, CH_{arom}), 129.4 (CH_{arom}), 129.0 (CH_{arom}), 128.2 (CH_{arom}), 124.6 (CH_{arom}), 120.6 (CH_{arom}), 79.0 ($OCMe_3$), 37.2 (apparent t, J = 14 Hz, CH_{Cy}), 36.7 (apparent t, J = 12 Hz, CH_{Cy}), 30.1 (CH_{2Cy}), 29.5 ($OCMe_3$), 29.3 (CH_{2Cy}), 29.0 (CH_{2Cy}), 28.0 – 26.9 (overlapping resonances, CH_{2Cy}), 26.2 (CH_{2Cy}), 5.2 (Si*Me*). $^{31}P\{^1H\}$ NMR (benzene-d_6): δ 48.0. ^{29}Si NMR (benzene-d_6): δ 4.7.

3.4.3 Crystallographic Solution and Refinement Details

Crystallographic data for **3-2c** was obtained at 193(±2)K on a Bruker PLATFORM/APEX II CCD diffractometer using graphite-monochromated Mo Kα (λ = 0.71073 Å) radiation, employing a sample that was mounted in inert oil and transferred to a cold gas stream on the diffractometer. Crystallographic data for **3-4** was obtained at 173(±2)K on a Bruker D8/APEX II CCD diffractometer using CuKα (λ =1.54178 Å, microfocus source) radiation, employing a sample that was mounted in inert oil and transferred to a cold gas stream on the diffractometer. Data for **3-4** were collected with the detector set at three different positions. Low-angle (detector 2θ = –33º) data frames were collected using a scan time of 5 s, medium-angle (detector 2θ = 75º) frames using a scan time of 10 s, and high-angle (detector 2θ = 117º) frames using a scan time of 10 s. Programs for diffractometer operation, data collection, and data reduction (including SAINT) were supplied by Bruker. Gaussian integration (face-indexed) was employed as the absorption correction method. Both structures were solved by use of intrinsic phasing methods and were refined by use of full-matrix least-squares procedures (on F^2) with R_1 based on $F_o^2 \geq 2\sigma(F_o^2)$ and wR_2 based on $F_o^2 \geq -3\sigma(F_o^2)$.

In the case of **3-2c**, two equiv. of hydrogen bonded HO(4-^{t}BuC$_6$H$_4$) and one equiv. of pentane were located in the asymmetric unit. One of the HO(4-^{t}BuC$_6$H$_4$) molecules

contains a ^{t}Bu substituent that is disordered over two positions. The corresponding carbon atoms were modeled over two positions (A and B), with refined occupancies of 0.726(7) for C96A – C99A (refined anisotropically) and 0.274(7) for C96B – C99B (refined isotropically). The C–C distances of the disordered ^{t}Bu group were restrained to be approximately the same by use of the *SHELXL* **SADI** instruction. The pentane solvate is also disordered over two positions (A and B), with refined occupancies of 0.496(7) for C1SA – C5SA and 0.504(7) for C1SB – C5SB. The 1,2 and 1,3 C–C and C···C distances within the disordered solvent pentane molecule were restrained to be approximately the same by use of the *SHELXL* **SADI** instruction. All the carbon atoms of the pentane solvate were refined isotropically. Anisotropic displacement parameters were employed for all remaining non-hydrogen atoms. The Ir-*H* (H1) and O-*H* hydrogen atoms of the two hydrogen bonded HO(4-^{t}BuC$_6$H$_4$) molecules (H2O and H3O) were located in the difference Fourier map and were refined isotropically. All remaining hydrogen atoms for **3-2c** were added at calculated positions and refined by use of a riding model employing isotropic displacement parameters based on the isotropic displacement parameter of the attached atom.

The structure of **3-4** is disordered as a result of co-crystallized (Cy-PSiP)Ir(OH)H and (Cy-PSiP)Ir(Cl)H. The site occupancy of O1 and H1O (Ir-*OH*) was optimized to 75% and the occupancy of Cl1 (Ir-*Cl*) was optimized to 25%. The disordered molecule lies on a crystallographic symmetry element, such that one portion (corresponding to primed atoms) is related to the other by the operation (x, y,$^{-}$+3/2, z). Two equiv. of diethyl ether were located in the asymmetric unit and were refined in a satisfactory manner. Anisotropic displacement parameters were employed for all non-hydrogen atoms. The Ir-*H* (H1) and

O-*H* (H1O) hydrogen atoms were located in the difference Fourier map and were refined isotropically. All remaining hydrogen atoms for **3-4** were added at calculated positions and refined by use of a riding model employing isotropic displacement parameters based on the isotropic displacement parameter of the attached atom. Additional crystallographic information is provided in Appendix A.

Chapter 4: Iridium Mediated Si-H Bond Oxidative Addition, Synthesis of (Cy-PSiP)Ir-L Complexes Stabilized by a Neutral L Donor and Synthesis of Cationic Ir^{III} and Rh^{III} Species

4.1 Introduction

In addition to further bond activation chemistry, Chapter 4 focuses on the development of cationic species capable of Si-H bond activation. In order to understand why such studies are important, it is crucial to acknowledge how previous contributions to this type of chemistry constitute a solid base for the work described herein. Pioneering work by Bergman and co-workers have shown cationic 16-electron Ir^{III} complexes of the type $[Cp^*(PMe_3)Ir(R)]^+$ (R = H, Me) to be highly reactive towards E-H bond activation chemistry, including alkane CH bond activation[119] and Si-H bond activation to form unusual $Ir{=}SiR_2$ silylene species.[120] In an effort to develop related 16-electron cationic Ir^{III} pincer species, Brookhart and co-workers synthesized the bis(phosphinite) pincer complex $[(^tBu\text{-}POCOP)Ir(H)(acetone)]^+[B(C_6F_5)_4]^-$ by treatment of $[POCOP]Ir(H)_2$ with $(Ph_3C)[B(C_6F_5)_4]$ in acetone (Scheme 4-1).[121] This complex was shown to be a highly active catalyst for the reduction of primary, secondary and tertiary alkyl and halides to alkanes employing Et_3SiH as the reductant (Scheme 4-1).[121-122] Catalyst loadings as low as 0.01% were used and reactions could be carried out under solvent-free conditions. A proposed catalytic cycle for this process involves generation of a highly electrophilic σ-silane species that transfers Et_3Si^+ to the alkyl halide to form a silyl-substituted halonium ion, Et_3SiXR^+ (X = Cl, Br, I, F), which subsequently reacts with an equivalent of $(^tBu\text{-}POCOP)Ir(H)_2$ to produce the reduced alkane and $XSiEt_3$ (Scheme 4-1). Interestingly, isolation of the proposed σ-silane intermediate revealed an unusual end-on η^1-SiH coordination mode, likely adopted due to steric pressure from the bulky $^tBu_2P$ donors which

prevents the more conventional η^2-SiH binding.[123]

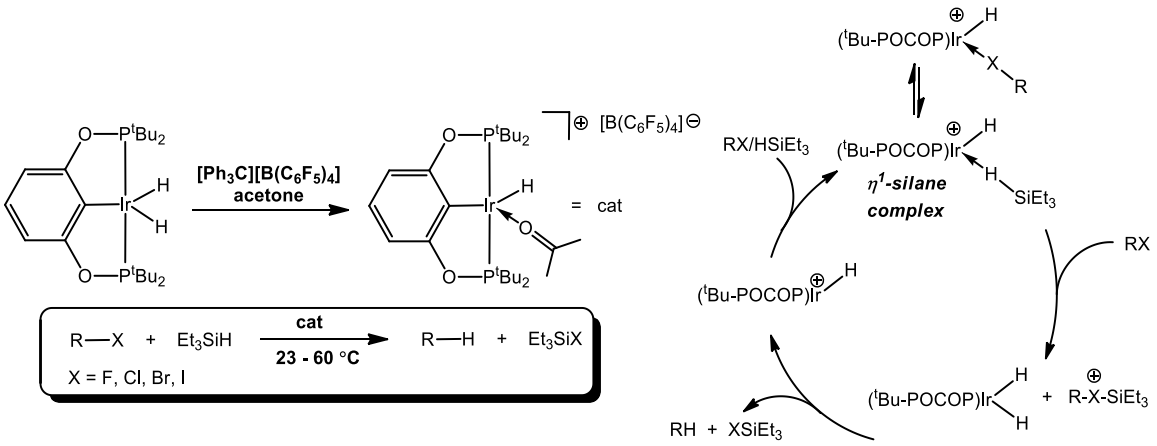

Scheme 4-1. Synthesis of [(^{t}Bu-POCOP)Ir(H)(acetone)]$^+$ for use in alkyl halide reduction catalysis.

The chemistry of [(^{t}Bu-POCOP)Ir(H)(acetone)]$^+$ has been extended to a variety of other applications, such as the reduction of ethers (including primary, secondary, and tertiary alkyl ethers as well as aryl alkyl ethers and poly(ethylene)glycol) in the presence of Et_3SiH (*via* generation of oxonium ions),[124] the hydrosilylation of carbonyl compounds (ketones, aldehydes, esters and amides) by Et_3SiH (*via* generation of oxocarbenium ions),[125] and the reduction of CO_2 to methane with trialkylsilanes (*via* generation of a formoxysilane).[126] These transformations are all proposed to involve generation of an electrophilic η^1-silane complex of the type [(^{t}Bu-POCOP)Ir(H)(η^1-HSiR$_3$)]$^+$. By comparison, the reduction of tertiary amides to amines with the secondary silane Et_2SiH_2 was proposed to follow a very different mechanism involving an Ir^V silyl hydride intermediate (Scheme 4-2).

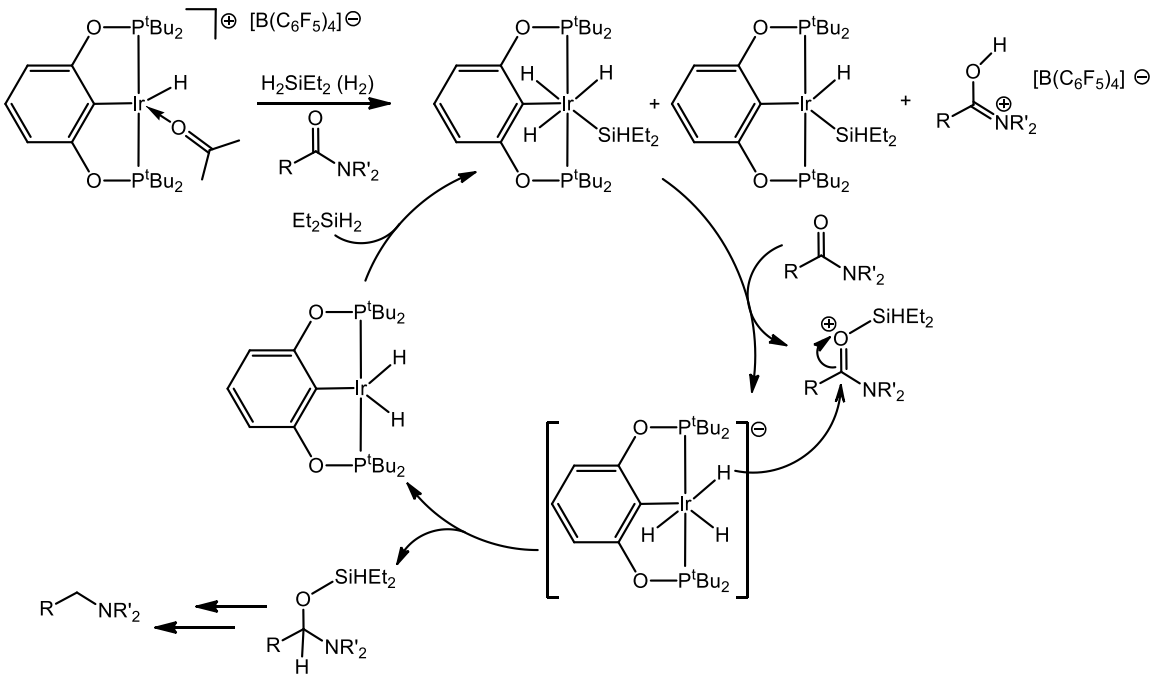

Scheme 4-2. Proposed catalytic cycle for reduction of amides by (^{t}Bu-POCOP)IrH$_3$(SiEt$_2$H).

Initial studies found that the combination of [(^{t}Bu-POCOP)Ir(H)(acetone)]$^+$ (0.5 mol %) with Et$_2$SiH$_2$ (3 equiv.) at 60 ºC enabled the catalytic reduction of aromatic, aliphatic, heteroaromatic and heterocyclic amides to tertiary amines. An equilibrium mixture of the neutral Ir^{III} complex (^{t}Bu-POCOP)Ir(H)(SiEt$_2$H) and the Ir^V species (^{t}Bu-POCOP)Ir(H)$_3$(SiEt$_2$H) (from the reaction of (^{t}Bu-POCOP)Ir(H)(SiEt$_2$H) with H$_2$ formed by the reaction of Et$_2$SiH$_2$ and adventitious water) was found to be the resting state during catalysis (Scheme 4-2). Transfer of Et$_2$SiH$^+$ from (^{t}Bu-POCOP)Ir(H)$_3$(SiEt$_2$H) to the amide substrate leads to formation of an oxocarbenium intermediate and [(^{t}Bu-POCOP)Ir(H)$_3$]$^-$, which can subsequently react to yield a hemiaminal and (^{t}Bu-POCOP)Ir(H)$_2$. The neutral Ir dihydride complex can reenter the catalytic cycle by reacting with Et$_2$SiH$_2$ to regenerate (^{t}Bu-POCOP)Ir(H)$_3$(SiEt$_2$H). The hemiaminal reacts with a weak acid (the conjugate acid of the amide/amine) to generate an iminium ion that is then further reduced to the amine

by Et_2SiH_2. This study further demonstrates the rich chemistry that cationic Ir pincer species can undergo with silanes of varied substitution.

The silane activation chemistry of cationic Ir pincer complexes has also been studied by Tilley and co-workers[127] who utilized a (PNP)Ir derivative, $(PNP)IrH_2$ (PNP = $[N(2\text{-}P^iPr_2\text{-}4\text{-}Me\text{-}C_6H_3)_2]^-$; Scheme 4-3), initially developed by Ozerov and co-workers.[128] Treatment of $(PNP)Ir(H)_2$ with the primary silane H_3SiMes (Mes = $2,4,6\text{-}Me_3C_6H_2$) led to formation of the Ir silyl complex $(PNP)Ir(H)(SiH_2Mes)$ (Scheme 4-3). Treatment of the later complex with $[Ph_3C][B(C_6F_5)_4]$ resulted in hydride abstraction and formation of the readily isolabe cationic Ir silylene species $[(PNP)Ir(H)(=SiHMes)][B(C_6F_5)_4]$. This complex catalyzes the exclusively anti-Markovnikov hydrosilylation of a variety of unhindered alkenes with aryl and alkyl-substituted primary silanes (5 mol % catalyst, 60 °C), and produces disubstituted silanes that are inactive toward further hydrosilylation.

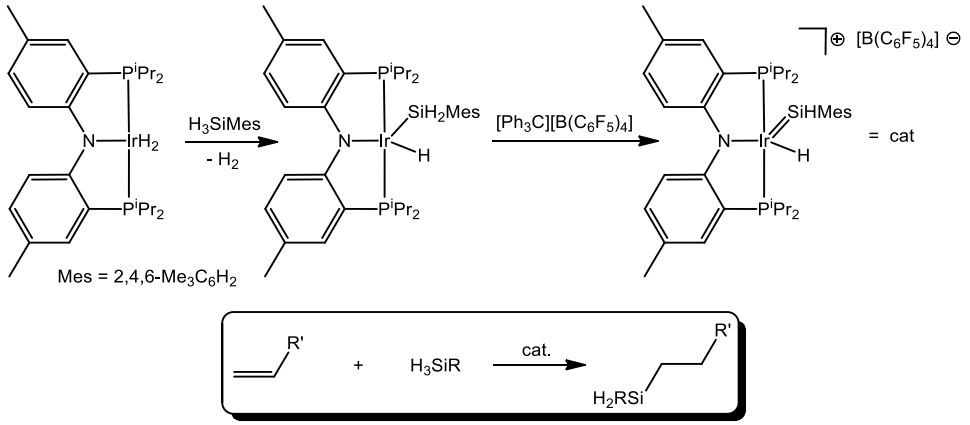

Scheme 4-3. Synthesis of a cationic (PNP)Ir silylene complex active for alkene hydrosilylation catalysis.

The anti-Markovnikov displayed by this (PNP)Ir pincer catalyst is similar to that observed for the related cationic silylene complex $[Cp^*(^iPr_3P)H_2Ru(=SiHPh)][B(C_6F_5)_4]$,[129] and a similar mechanism was proposed (Scheme 4-4A). The first step of the proposed mechanism involves formation of a disubstituted

silylene complex *via* reaction of an H-substituted Ir silylene complex with an alkene. This is thought to occur *via* direct insertion of the alkene into the Si-H bond to regenerate a new alkyl substituted silylene ligand. Subsequent migration of a hydride ligand to Si generates a new Ir silyl species. In the case of $[Cp^*(^iPr_3P)H_2Ru(=SiHPh)]^+$ computational studies suggest that product release and regeneration of the silylene ligand occur by subsequent low-barrier rearrangements involving several intermediates that contain silyl and hydride groups, and exhibits nonclassical Si-H interactions.[130] Interestingly, in the case of (PNP)Ir, treatment of $(PNP)Ir(H)(=SiPh_2)^+$ with an excess of Ph_2SiH_2 resulted in the formation of the Ir^V disilyl complex $(PNP)(SiPh_2)Ir(SiPh_2H)(H)_2^+$, that possesses a Si-N bond and is catalytically competent towards alkene hydrosilylation (Scheme 4-4B).[127b] As such, Tilley proposes that the amido donor of Ir PNP complexes may play an important role in the mechanism of substrate activation, particularly invoking the migration of hydride or silyl ligands to the N atom.[131] This work further highlights the unique reactivity of cationic Ir pincer species with hydrosilanes.

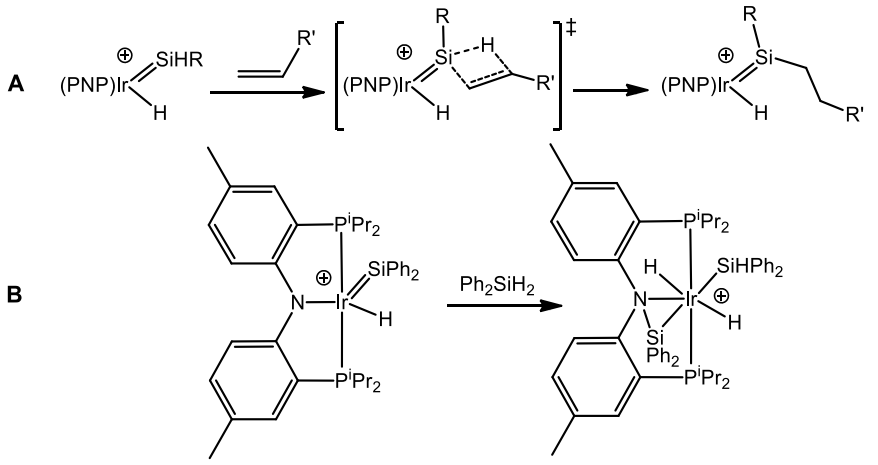

Scheme 4-4. Proposed mechanism for alkene insertion into a cationic (PNP)Ir silylene (A) and synthesis of a catalytically competent Ir^V disilyl intermediate (B).

Chapter 4 will present progress towards preparation of iridium and rhodium silyl-hydride species, as well efforts towards the generation of silylene complexes. Alternative routes towards the generation and isolation of Ir^{I} species stabilized with neutral L donors as well as reactive cationic Ir^{III} species are also included.

4.2 Results and Discussion

4.2.1 Early Attempts at Si-H Bond Activation *via* (Cy-PSiP)Ir^{I} and Rh^{I}

Based on results compiled from the study of phosphido-hydride and alkoxy-hydride complexes, investigation of the reactivity of (Cy-PSiP)Ir^{I} towards Si–H bonds was also proved interesting. The activation of Si–H bonds is typically more facile than analogous C–H bonds and Si–H bonds. Due to the high electropositivity of Si, Si-H bonds are typically hydridic in contrast to the acidic nature of C-H bonds. The nature of these bonds presents a synthetic challenge, as the generation of silyl anions is notoriously difficult, precluding the use of salt metathesis as a synthetic strategy towards silyl hydride complexes. As an entry point for the generation of silyl-hydride complexes, *in situ* generation of (Cy-PSiP)M^{I} (M= Ir (**1-3**), Rh (**1-4**)) was performed through the reaction of (Cy-PSiP)M(H)Cl (M = Ir (**1-1**), Rh (**1-2**)) with $LiCH_2SiMe_3$ in C_6H_{12} over the course of 15 min at room temperature. Subsequent treatment with one equivalent of tertiary silanes such as $Me_2{}^{i}PrSiH$, $Me_2{}^{t}BuSiH$, Et_3SiH or Ph_3SiH did not show any evidence of oxidative addition of the Si–H bond by ^{31}P NMR. Further reactions were attempted in cyclohexane, employing 1 to 10 equivalents of tertiary silane, as well as attempts where the reaction was left overnight at room temperature or stirred for several hours at temperatures up to 65 °C.

In all cases, the decomposition of (Cy-PSiP)M^{I} was observed, leading to complex mixtures of unidentifiable products by ^{31}P NMR from which no clean products could be observed or isolated.

Due to the lack of reactivity found with tertiary silanes, investigation into the reactivity of secondary and primary silanes was performed. The treatment of **1-3** and **1-4** with $PhSiH_3$ or Et_2SiH_2 in C_6H_{12} at room temperature over the course of 1 h led to a quick color change from dark orange to light orange-yellow. In each reaction the $^{31}P\{^{1}H\}$ NMR spectra shows the generation of multiple products. The ^{1}H NMR spectra of these reactions feature multiple signals associated with hydrosilanes, and as such it can be postulated that substituent redistribution or dehydrocoupling reactions of the silanes may take place, generating several unidentified products. As previously discussed in Chapter 2, sterics are seemingly a major factor in the stability and reactivity of these complexes, and has led to reactions employing bulkier secondary silanes.

Accordingly, the treatment of (Cy-PSiP)Ir^{I} (**1-3**) with one equivalent of Ph_2SiH_2, Mes_2SiH_2 or Mes_2SiHCl in C_6H_{12} at room temperature over an hour showed complete conversion to (Cy-PSiP)Ir(H)($SiHPh_2$) (**4-1**), (Cy-PSiP)Ir(H)($SiHMes_2$) (**4-2**) and (Cy-PSiP)Ir(H)($SiClMes_2$) (**4-3**) respectively (Scheme 4-5). The formation of **4-2** and **4-3** was quantitative by $^{31}P\{^{1}H\}$ NMR analysis of the crude reaction mixtures (by monitoring consumption of **1-3**) and both complexes were isolated as yellow powder in 81% and 78% yield, respectively. Discussion of **4-1** will be presented further in this document (*vide infra*). Identical reactions were repeated with (Cy-PSiP)Rh^{I} (**1-4**) and one equivalent of Ph_2SiH_2, Mes_2SiH_2 or Mes_2SiHCl in C_6H_{12} at room temperature over an hour, but only led to intractable mixtures from which no clean material could be recovered.

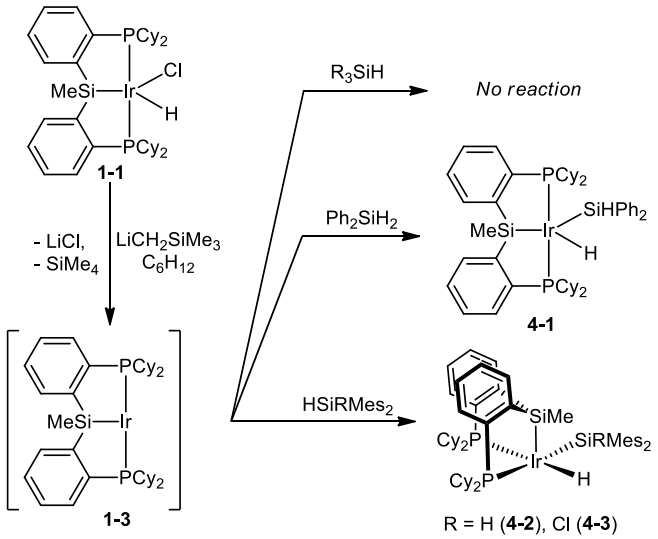

Scheme 4-5. Synthesis of five coordinate Ir silyl hydride complexes *via* Si-H oxidative addition.

Complexes **4-2** and **4-3** share spectroscopic similarities with the (Cy-PSiP) ligand coordinated in a facial geometry with an overall square pyramidal geometry. The presence of two distinct resonances by $^{31}P\{^{1}H\}$ NMR demonstrates magnetically inequivalent phosphorus atoms due to the loss of C_s symmetry in the complex. Each signal presents as a doublet at 60.2 and 43.2 ppm ($^{2}J_{PP\textit{cis}}$ = 11 Hz) for **4-2**, as well as 59.4 and 42.5 ppm ($^{2}J_{PP\textit{cis}}$ = 12 Hz) for **4-3**. The ^{1}H NMR spectrum shows a doublet of doublets corresponding to a hydride at –7.96 ppm ($^{2}J_{PH\textit{cis}}$ = 19 Hz, $^{2}J_{PH\textit{trans}}$ = 100 Hz) for **4-2** and –8.42 ppm ($^{2}J_{PH\textit{cis}}$ = 19 Hz, $^{2}J_{PH\textit{trans}}$ = 99 Hz) for **4-3**. The multiplicity of the signal is indicative of the relative position of the (Cy-PSiP) ligand compared to the hydride ligand and allows confident assertion of the general geometry of the complexes. Another notable spectroscopic feature in complex **4-2** is the resonance corresponding to the proton from the –Si*H*Mes$_2$ fragment. This signal shows coupling to the phosphine ligand moieties and appears as a doublet of doublets. The associated $^{3}J_{PH}$ coupling constants are 12 Hz and 9 Hz for each of the phosphines. The $^{3}J_{HH}$ coupling between the –SiHMes$_2$ proton and the Ir–*H* hydride has not

been observed, likely due to the coupling being too small to observe. Additionally, hydride signals from complexes **4-2** and **4-3** have similar multiplicity, further contributing to the argument that the $^{3}J_{HH}$ coupling is too small to be observed.

The synthesis of (Cy-PSiP)Ir(H)($SiHPh_2$) (**4-1**) can be achieved through two synthetic rouges. The dehydrohalogenation of **1-1** by $LiCH_2SiMe_3$ in cyclohexane at room temperature over the course of 15 min generates **1-3** *in situ*, which can be subsequently treated with 1.1 equiv. H_2SiPh_2 to form **4-1** over the course of 30 min and shows partial consumption of starting material (by ^{31}P NMR) and *ca*. 12% unreacted **1.3**, only 36% conversion to **4-1**. The remaining 53% of the reaction mixture was composed of unidentified products. While this method did not lead to a clean isolation of **4-1**, the generation of (Cy-PSiP)Ir(H)(NH^{t}Bu) (**3-3**) by reaction of **1-1** with LiNH^{t}Bu in benzene and subsequent treatment with one equivalent of H_2SiPh_2 shows complete conversion to **4-1** by $^{31}P\{^{1}H\}$ NMR. Contrary to **4-2** where the –PCy_2 moities are inequivalent due to the *fac*-κ^3-(Cy-PSiP) geometry of the ligand around iridium, **4-1** shows a single resonance at 42.0 ppm which accounts for both phosphines. This suggests that the ligand phosphines are in equivalent environments and that the complex adopts a *mer*-κ^3-(Cy-PSiP) geometry. The structural difference between these complexes is likely due to the steric difference between –$SiHPh_2$ and –$SiHMes_2$, with the reduced size of the –SiHPh2 fragment being enough to allow the complex to adopt a distorted trigonal bipyramidal geometry instead of distorted square pyramidal. In the ^{1}H NMR spectra of **4-2** and **4-3**, the metal-hydride resonance is well resolved and shows as a sharp doublet of doublets. This multiplicity can be explained due to the geometry of each complex and the electronic environment around the hydride. For complex for **4-1**, only a broad resonance is visible at –9.36 ppm accounting

for one proton (Ir-*H*). At room temperature, standard ^{1}H NMR experiments were not able to resolve distinct splitting patterns for the Ir-*H* resonance. The broadness of the signal could be due to a dynamic process involving this hydride. In order to gather more structural information about this complex, crystals suitable for X-ray diffraction analysis were obtained from a concentrated solution of the complex in pentane at -35°C.

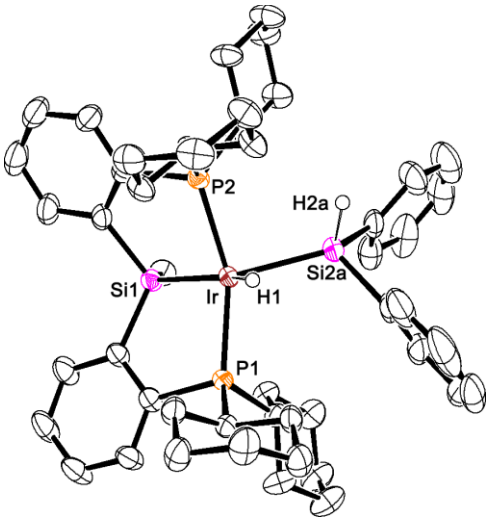

Figure 4-1. Crystallographically determined structures of **4-1** shown with thermal ellipsoids drawn at the 50% probability level. Most hydrogen atoms have been omitted for clarity. Selected interatomic distances (Å) and angles (°): Ir-P(1) 2.3184(6), Ir-P(2) 2.3085(6), Ir-H(1) 1.45(4), Ir-Si(1) 2.3829(7), Ir-Si(2A) 2.4266(9), Si(2A)-H(2A) 1.40(4), P(1)-Ir-P(2) 158.86(2), P(1)-Ir-Si(2A) 107.89(3), P(2)-Ir-Si(2A) 91.97(3), P(1)-Ir-Si(1) 84.42(2), P(2)-Ir-Si(1) 84.39(2), Si(1)Ir-Si(2A) 141.34(3), Ir-Si(2A)-H(2A) 109.5(17).

The crystallographic features of **4-1** are similar to those of **1-1** (Table 4-1), as both feature a distorted trigonal bipyramidal geometry. An exception to this similarity is the Ir-*H* (H1) which leans towards SiA2 from the –$SiHPh_2$ moiety, whereas the hydride in complex **1-1** leans towards the silicon atom from the (Cy-PSiP) ligand backbone.

Table 4-1. Selected interatomic distances (Å) and angles (°) for complexes comparison.

Complex	Ir-X distance	P-Ir-P (PSiP) Angle	Si-Ir-X Angle	X-Ir-H Angle	Si-Ir-H Angle
(Cy-PSiP)Ir(H)Cl[20b] (**1-1**)	2.4143(12)	166.07(4)	130.64(5)	160.6(18)	68.7(18)
(Cy-PSiP)Ir(H)(NHPh)[52k]	2.056(2)	158.06(3)	137.35(8)	154.4	67.5
(Cy-PSiP)Ir(H)($SiHPh_2$) (**4-1**)	2.3829(7)	158.86(2)	141.34(3)	66.5(16)	151.8(16)
(Cy-PSiP)Ir(H)(PHMes) (**2-3c**)	2.2672(16)	156.65(5)	127.13(6)	150.0(14)	82.5(14)

The ^{29}Si NMR spectrum for complex **4-2**, displays two distinct resonances associated with the –SiMe fragment (11.8 ppm) and the –$SiHMes_2$ fragment (–16.9 ppm) respectively. The ^{29}Si NMR resonances for the analogous chlorosilyl complex **4-3** maintains a similar shift to that of **4-2** for the -SiMe fragment (12.4 ppm), while the chlorosilyl resonance is markedly more downfield to (45.0 ppm). This downfield shift is as expected due to the chlorine substituent on Si. These ^{29}Si resonances act as important indicators for this chemistry, as any modifications to the –$SiRMes_2$ group will affect the ^{29}Si shift.

These newly synthesized iridium silyl hydride complexes prompted an interest in attempting further transformations towards the isolation or observation of silylene complexes. Work produced by Bergman, Tilley and co-workers has shown that they were able to synthesize and isolate $[Cp^*(PMe_3)Ir(SiMes_2)]^+ {}^-[OTf]$, which features an extremely downfield shifted ^{29}Si NMR resonance corresponding to the silylene (=$SiMes_2$) fragment. This resonance appears at +301 ppm downfield of $SiMe_4$ as a reference and is indicative of a three-coordinate silylene ligand.[132] This prompted investigation into the ability of complexes **4-1** and **4-2**, both of which contain a –$SiHR_2$ moiety, to undergo transformations that would lead to similar silylene complexes. Thermal stability was initially targeted as a means to initiate potential 1,2-hydride migration from the silyl fragment (–$SiHR_2$, R = Ph

(**4-1**), Mes (**4-2**)) to the metal center. Work by Tilley and co-workers reports the first example of a silylene complex prepared by this α-migration method.[133] Such a transformation applied to complexes of the type (Cy-PSiP)Ir(H)($SiHR_2$) would result in the desired metal-silylene species (Scheme 4-6).

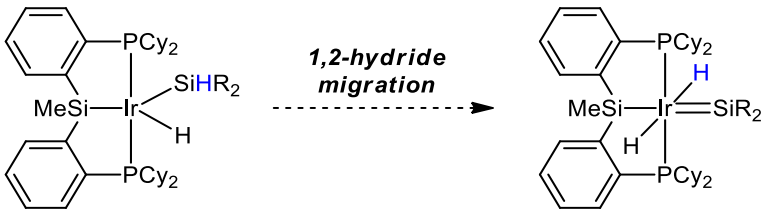

Scheme 4-6. Suggestion of a transformation leading to an iridium silylene complex.

Both **4-1** and **4-2** were heated in benzene-d_6 at 80 °C overnight in an attempt to facilitate hydride migration. The samples were monitored by $^{31}P\{^1H\}$ NMR and were found to be stable at 80 °C over several hours, with no evidence of Si-H reductive elimination or 1,2-hydride migration. In perspective, Bergman and co-workers were able to observe such migrations with various Cp*(PMe_3)Ir(SiR_3)$^+$ $^-$(OTf) complexes at room temperature within 25 min, generating Cp*(PMe_3)Ir(R)(SiR_2OTf) *via* a proposed silylene intermediate.[120a] Previous work in the Turculet group has shown an isolable (Cy-PSiP)Ir(H)($SiOTfPh_2$) complex with a geometry similar to **4-1** and a ^{29}Si shift at 58 ppm corresponding to the –$SiOTfPh_2$.[66] Based on observations made by Bergman and Tilley, silylenes typically have ^{29}Si NMR resonances in the range of δ 200-370 ppm, while (Cy-PSiP)Ir(H)($SiOTfPh_2$) is not showing such characteristics.[129b] It is then reasonable to rule out the possibility that this complex could be a silylene complex of the form (Cy-PSiP)Ir(H)(=$SiPh_2$)$^+$ $^-$(OTf) similar to Bergman and Tilley. It is likely that the triflate is too strongly bound to the silyl ligand, or not bulky enough to be forced into an outer-sphere position. A much larger, weakly coordinating anion such as $B(C_6F_5)_4^-$ or B{3,5-

$(CF_3)_2C_6H_3\}_4^-$ (shortened to BAr^{F-}) was thought to be better able to stabilize a silylene complex as it would satisfy the steric and electronic demands.

Employing these reagents, another method was envisioned according to precedented reactions leading to silylene species.[134] Through the use of trityl fluorinated borate such as trityl tetrakis [3,5-bis(trifluoromethyl)phenyl]borate (shortened to trityl-BAr^F) a hydride can be abstracted from a Si-H bond. The reaction of **4-2** in benzene with 1 equivalent of trityl-BAr^F at room temperature over the course an hour led to a multitude of products by $^{31}P\{^1H\}$ NMR, none of which appear to correspond to the desired silylene metal complex.

The challenge of isolating or identifying a silylene-containing species of the (Cy-PSiP) system relative to Bergman's or Tilley's Cp*[L] framework is likely due to electronic differences. An additional challenge associated with a (Cy-PSiP) silylene complex would be the generation of the silylene located *trans* to the –SiMe moiety in the ligand backbone. The added *trans*-labilizing effect from the (Cy-PSiP) ligand to the already elusive and unstable silylene fragment adds another layer of difficulty to the isolation of such a species. Future efforts will be directed towards synthesizing a cationic silyl hydride complex featuring a weakly coordinating counter anion, potentially promoting silylene formation. Alternatively, a strategy of base stabilizing[135] or silylene trapping[136] could be helping in observing, at least *in situ*, these type of silylene complexes.

4.2.2 Synthesis of (Cy-PSiP)IrCO

Previous work in the Turculet group as well as the work presented in this document, employs the use of the low coordinate, 14-electron (Cy-PSiP)Ir^{I} (**1-3**) fragment which demonstrates interesting results for C-H, N-H and P-H bond activation.[20b,52k,66] This complex has proven capable of aggressively cleaving these relatively strong bonds, but appears to be too reactive towards Si-H bond activation, leading to uncontrollable transformations for the smaller, more reactive secondary and primary silanes. These results have driven the efforts of this study away from the isolation of Ir^{III} silyl hydride species. Having observed that the reaction of *in situ* generated (Cy-PSiP)M^{I} (M = Ir (**1-3**), Rh (**1-4**)) with hydrosilanes did not lead to the formation of isolable metal silyl complexes (with the exception of complexes **4-1**, **4-2** and **4-3**), synthesis of stabilized M^{I} complexes was instead pursued in the hope that such complexes might exhibit favorable and controllable reactivity with Si-H bonds. In this context, carbonyl adducts of the type (Cy-PSiP)M(CO) (M = Ir, Rh) were initially targeted. The carbonyl ligand was chosen due to its low steric profile as well as its propensity to reduce the electron density at the metal center (*via* π-backbonding effects), potentially taming the reactivity of (Cy-PSiP)M^{I} such that further substrate transformations at the metal center may still be possible. The possibility of carbonyl insertion processes also opens up avenues for further substrate transformations once oxidative addition has occurred.

Several synthetic options for the preparation of (Cy-PSiP)Ir(CO) (**4-5**) are available (Scheme 4-7). The treatment of (Cy-PSiP)Ir^{I} (**1-3**) with CO was not prioritized as a synthetic route as the potential formation of a dicarbonyl complex would be difficult to avoid. Initial attempts to prepare **4-5** thus involved reacting Vaska's complex *trans*-

$IrCl(CO)(Ph_3P)_2$ with the tertiary silane (Cy-PSiP)H. After two hours of heating at 65 °C, 95% conversion of (Cy-PSiP)H to a mixture of two new compounds was observed by $^{31}P\{^1H\}$ NMR, as indicated by the appearance of two new resonances at 44.5 and 41.5 ppm (1:3 ratio, respectively; *cf*. (Cy-PSiP)Ir(H)Cl at 61.1 ppm). This mixture of products is assigned as a mixture of isomeric (Cy-PSiP)Ir(H)(Cl)(CO) (**4-4a,b**) species (Scheme 4-7). The reaction mixture contained an excess of Ph_3P that is liberated during the formation of **4-4a,b**, a drawback to using Vaska's complex. Attempts to isolate **4-4a,b** free of Ph_3P proved challenging due to the similar solubilities of both compounds. Multiple washes of the crude product with pentane dramatically decreased the yield of **4-4a,b** and did not result in sufficient purification of the crude material. As a result, a synthetic route that avoids Ph_3P was pursued. Treatment of **1-1** with CO (1 atm) in THF led to the quantitative formation (by ^{31}P NMR) of a mixture of **4-4a,b** isomers, (ca. 1:1 to 1:3 ratio, respectively). Complexes **4-4a,b** were readily isolated in 93% yield as a mixture of isomers when prepared by this route. The ^1H NMR spectrum of isolated **4-4a,b** complexes (benzene-d_6) contains two Ir-*H* resonances at -8.87 (t, $^2J_{HP}$ = 17 Hz) and -20.1 ppm (t, $^2J_{HP}$ = 14 Hz), consistent with the formulation of **4-4a,b** as a mixture of isomeric species in which the hydride ligand is coordinated *cis* to chemically equivalent PCy_2 groups.

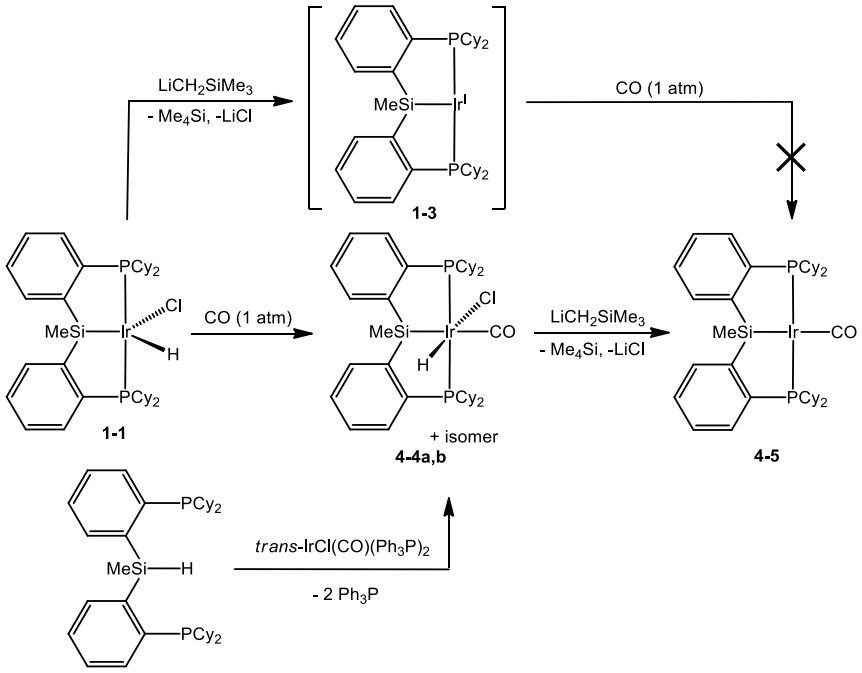

Scheme 4-7. Synthesis of (CyPSiP)IrCO (**4-5**) complex.

Treatment of isolated **4-4a,b** with $LiCH_2SiMe_3$ resulted in dehydrohalogenation to form the Ir^I carbonyl complex **4-5** (Scheme 4-7), which gives rise to a characteristic $^{31}P\{^1H\}$ NMR resonance at 71.7 ppm and an Ir*CO* stretch at 1927 cm^{-1} in the IR spectrum of the isolated complex. While complex **4-5** has been isolated in yields of up to 68% by this route, its formation appears to be extremely sensitive to the reaction parameters and the yield is highly variable. Product mixtures can often contain several additional unidentified (Cy-PSiP)Ir species (by ^{31}P NMR), as well as significant quantities of the dicarbonyl complex (Cy-PSiP)Ir$(CO)_2$ (**4-6**), which was independently prepared (*vide infra*). Complex **4-5** was partially characterized *in situ* due to the challenge associated with its isolation. The formation of **4-6** in these reactions in the absence of added CO suggests that free CO is generated during the course of the dehydrohalogenation process. As isolated **4-4a,b** itself appears to be immune to CO loss, it may be that (unobserved) intermediates of the type (Cy-PSiP)Ir(H)(CH_2SiMe_3)(CO) can undergo loss of a CO ligand, which is

subsequently trapped by **4-5**. The use of alternative reagents, including neopentyllithium, ^{n}BuLi, $CsCO_3$ or NEt_3, for the dehydrohalogenation of **4-4a,b** did not result in the clean formation of **4-5**.

Attempts to dehydrohalogenate **4-4a,b** *in situ* without the thorough removal of excess CO from the reaction mixture resulted in the quantitative formation (by ^{31}P NMR) of the dicarbonyl complex **4-6** (Scheme 4-8). Complex **4-6** was readily isolated in 77% yield and features a ^{31}P NMR resonance at 48.3 ppm. No metal hydride resonances were detected in the ^{1}H NMR spectrum of **4-6**. Crystals of **4-6** suitable for X-ray diffraction analysis were grown from a concentrated THF/pentane solution at room temperature.

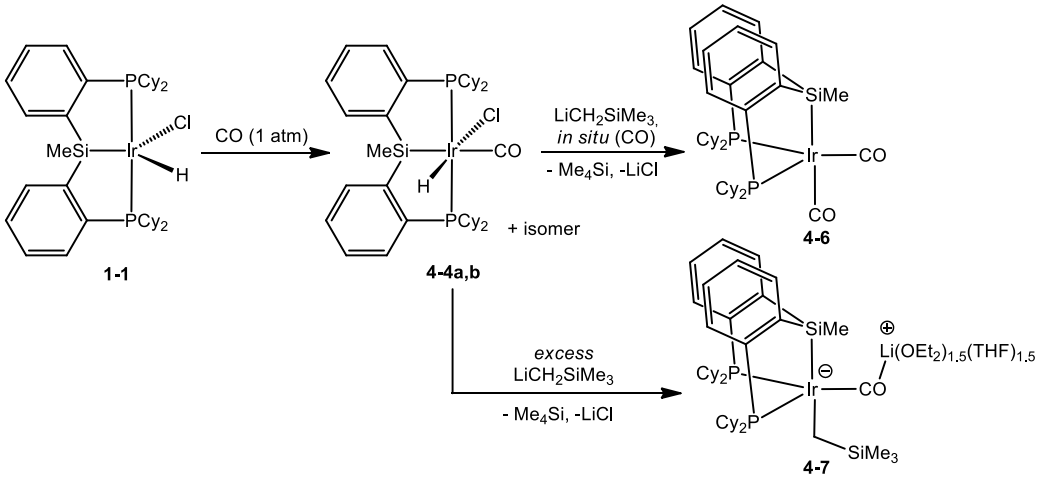

Scheme 4-8. Synthesis of **4-6** and **4-7** *via* dehydrohalogenation of **4-4a,b**.

The solid state structure of **4-6** (Figure 4-2) confirms the formulation of this complex as a five-coordinate dicarbonyl complex. The coordination geometry at the Ir center is approximately trigonal bipyramidal, with the PCy_2 donors occupying equatorial sites. One carbonyl ligand occupies an axial coordination site *trans* to Si, while the second CO is bound in the remaining equatorial site. While the majority of crystallographically characterized (Cy-PSiP)Ir complexes feature *trans*-disposed phosphino ligand arms,

examples of *fac*-κ^3-(Cy-PSiP) coordination to a metal center are known,[52k] and are commonly observed in the absence of a strong electronic preference for *mer*-κ^3-(Cy-PSiP) coordination (*e.g.* the requirement for square planar coordination geometry in four coordinate d^8 metal complexes enforces *mer*-κ^3 binding of PSiP ligands). In related five-coordinate complexes such as **1-1**, the observed *mer*-κ^3-(Cy-PSiP) coordination is possibly enforced by Si···H bonding interactions between the silyl donor and the Ir-*H*.[20b] In the absence of a hydride ligand, as in the case of **4-6**, *fac*-κ^3-(Cy-PSiP) coordination appears to correspond to the ground state structure.

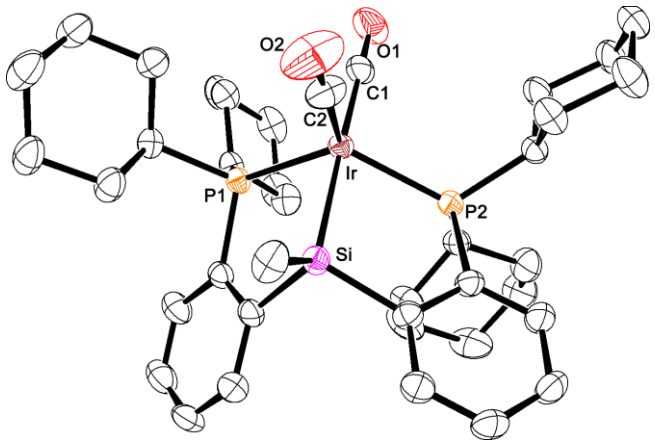

Figure 4-2. The crystallographically determined structure of **4-6** shown with 50% displacement ellipsoids. All H atoms have been omitted for clarity. Selected interatomic distances (Å) and angles (°): Ir-P1 2.332(1), Ir-P2 2.343(1), Ir-Si 2.410(1), Ir-C1 1.922(1), Ir-C2 1.879(1), P1-Ir-P2 123.08(1), Si-Ir-C1 172.84(1), P1-Ir-C2 114.23(1), P2-Ir-C2 118.64(1), C1-Ir-C2 99.59(10).

When an excess (5 equiv.) of $LiCH_2SiMe_3$ was used to dehydrohalogenate **4-4a,b**, $^{31}P\{^1H\}$ NMR analysis of the reaction mixture indicated the formation of a previously unobserved product (Scheme 4-8) as the major species with a resonance at 26.2 ppm. This complex, identified as (Cy-PSiP)Ir(CH_2SiMe_3)COLi (**4-7**) was isolated in 89% yield and crystals suitable for X-ray diffraction analysis were grown from a concentrated Et_2O/THF solution at low temperature (-35 °C). The crystallographically determined structure (Figure

4-3) revealed a five-coordinate zwitterionic Ir alkyl complex of the type (**4-7**•$(OEt_2)_{1.5}(THF)_{1.5}$). The formally anionic Ir center features trigonal bipyramidal coordination geometry with Si coordinated in an axial site, while the PCy_2 ligand arms occupy equatorial positions. The CH_2SiMe_3 group is coordinated *trans* to Si and a CO ligand occupies the final equatorial site. A tetrahedral solvated Li cation is coordinated to the oxygen atom of the carbonyl. As anticipated, the C1-O1 bond distance of 1.198(1) Å is elongated relative to that of free CO (1.128 Å) as well as relative to the C2-O2 bond distance of 1.149(1) Å observed for the equatorial CO ligand in **4-6**, which is consistent with increased π-backdonation from the formally anionic Ir center that can be envisioned to place a partial negative charge on O2. In accordance with this proposal, The Ir-C1 distance of 1.830(1) Å is slightly shorter than the Ir-C2 distance of 1.879(1) Å observed for **4-6**. The *fac*-like coordination of the κ^3-(Cy-PSiP) ligand in **4-7** is analogous to that observed for **4-6**, which once again highlights the structural variability of PSiP ligation.

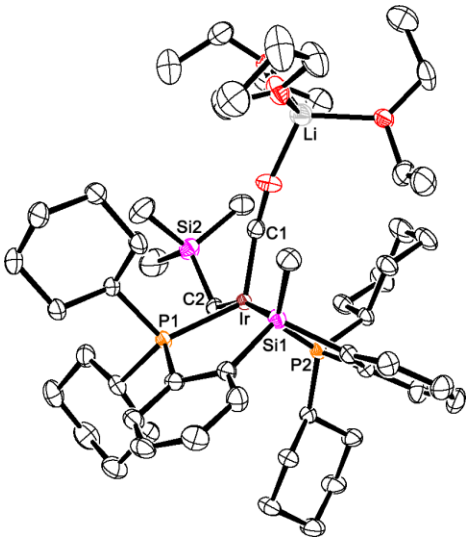

Figure 4-3. The crystallographically determined structure of **4-7**•$(OEt_2)_{1.5}(THF)_{1.5}$ shown with 50% displacement ellipsoids. All H atoms and selected carbon atoms have been omitted for clarity. Selected interatomic distances (Å) and angles (°): Ir-P1 2.334(1), Ir-P2 2.310(1), Ir-Si1 2.345(1), Ir-C1 1.830(1), Ir-C2 2.257(1), P1-Ir-P2 124.19(1), Si1-Ir-C1 90.03(1), Si1-Ir-C2 166.24(1), Ir-C1-O1 168.41(1).

The isolation of **4-7** was unexpected, and indicates that the dehydrohalogenation of **4-4a,b** is likely to be quite concentration dependent, and is likely part of the reason yields of **4-5** from this reaction are so variable. Examples of anionic late metal alkyl complexes are precedented in the literature.[137] It is possible to envision the abstraction of the alkyl ligand from **4-7** with a Lewis acid such as BPh_3 that may provide a more reliable route to the carbonyl complex **4-5** but this hypothesis has not been tested yet.

4.2.3 Synthesis and Reactivity of (Cy-PSiP)Rh(CO)

The synthesis of an analogous Rh complex was also pursued following a similar synthetic protocol to that developed for the synthesis of (Cy-PSiP)Ir(CO) (**4-5**). (Cy-PSiP)Rh(H)Cl (**1-2**) was first treated with CO (1 atm), leading to the quantitative (by ^{31}P NMR) consumption of the hydrido chloride starting material and the formation of two isomeric complexes (Cy-PSiP)Rh(H)(Cl)(CO) (**4-8a,b**) (Scheme 4-9). These two complexes give rise to $^{31}P\{^{1}H\}$ NMR resonances at 71.0 (d, $^{1}J_{RhP}$ = 106 Hz) and 69.5 ppm (d, $^{1}J_{RhP}$ = 106 Hz) in a ratio of 4:1, respectively. The ^{1}H NMR spectrum of **4-8a,b** features two hydride resonances at -8.92 (m) and -9.22 ppm (m), which is consistent with the formation of isomeric carbonyl complexes. Complexes **4-8a,b** were readily isolated in 82% overall yield as a mixture of isomers. Treatment of **4-8a,b** with one equiv. of $LiCH_2SiMe_3$ resulted in the quantitative (by ^{31}P NMR) formation of the desired Rh^{I} carbonyl complex (Cy-PSiP)Rh(CO) (**4-9**) (Scheme 4-9), which is characterized by a $^{31}P\ \{^{1}H\}$ NMR resonance at 76.6 ppm (d, $^{1}J_{RhP}$ = 155 Hz) and can be isolated in 88% yield. Unlike the Ir carbonyl analogue, the synthesis of **4-9** is readily reproducible and did not show any evidence for (Cy-PSiP)$Rh(CO)_2$ or instability of **4-9** leading to the latter. Crystals suitable

for X-ray diffraction analysis were obtained from a concentrated pentane solution of **4-9** at room temperature (Figure 4-4).

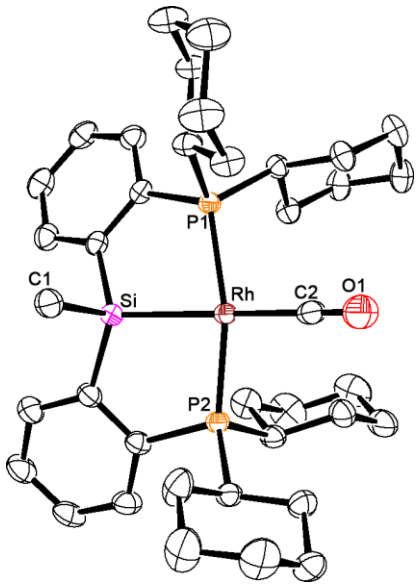

Figure 4-4. Crystallographically determined structures of **4-9** shown with thermal ellipsoids drawn at the 50% probability level. Hydrogen atoms have been omitted for clarity. Selected interatomic distances (Å) and angles (°): Rh-P1 2.2863(4), Rh-P2 2.2764(4), Rh-C2 1.8993(19), Rh-Si 2.3489(5), C2-O1 1.143(2), P1-Rh-P2 152.061(17), Si-Rh-C2 164.70(16), P1-Rh-C2 101.27(6), P2-Rh-C2 101.07(6), C1-Si-Rh 114.38(7).

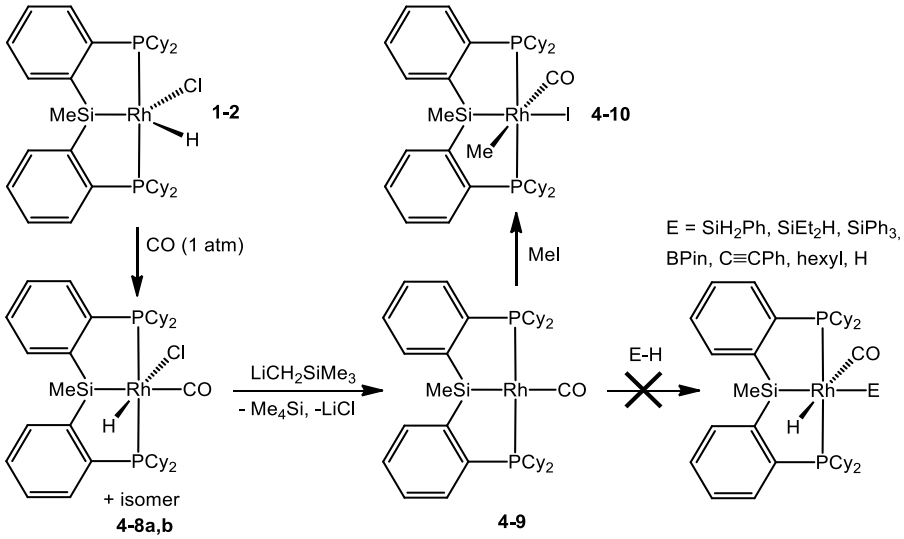

Scheme 4-9. Synthesis of **4-9** *via* dehydrohalogenation of **4-8a,b** and reactivity of **4-9** towards E-H bonds and MeI leading to **4-10**.

In an effort to determine if **4-9** undergoes oxidative addition reactions, the carbonyl complex was treated with one equiv. of MeI in a pentane solution. $^{31}P\{^{1}H\}$ NMR analysis of the reaction mixture indicated complete consumption of **4-9** over the course of an hour at room temperature along with clean formation of (Cy-PSiP)Rh(Me)(I)(CO) (**4-10**) (Scheme 4-9). This new complex gives rise to a single resonance at 56.9 ppm (d, $^{1}J_{PRh}$ = 103 Hz). The ^{1}H NMR spectrum of **4-10** features a well resolved doublet of triplets at 0.41 ppm (3 H, $^{1}J_{HRh}$ = 2 Hz, $^{2}J_{PH}$ = 7 Hz) that is assigned as the methyl bound to the rhodium center (Rh*Me*). Attempts to observe E-H bond activation with **4-9** were not successful as no reaction was observed upon treatment of **4-9** with $PhSiH_3$, Et_2SiH_2, Ph_3SiH, HBPin, phenylacetylene, 1-hexene or H_2, even after heating the reaction mixtures (up to 80 °C) for extended periods (ca. 8h) in benzene. Thus, while **4-9** can undergo oxidative addition of activated substrates such as MeI, it is unreactive towards less polar bonds.

4.2.4 Investigation of Other (Cy-PSiP)Ir-L Complexes

As the synthesis of the carbonyl complex (Cy-PSiP)Ir(CO) (**4-5**) demonstrates challenging and condition dependent behavior, as well as (Cy-PSiP)Rh(CO) (**4-9**) being unreactive towards E-H bond activation, an effort was made towards the development of different (Cy-PSiP)Ir-L complexes. Candidates for the L donor would ideally be labile and easy to ligate to the metal in a controlled fashion. Initial options include trialkylphosphines (such as PMe_3 or PCy_3) which may be able to dissociate from the metal center following E-H oxidative addition, to open up a coordination site on the metal center. No reaction between complex **1-1** and one equivalent of PCy_3 was observed. Although the reaction of **1-1** with one equivalent of $LiCH_2SiMe_3$ in C_6H_{12} to generate **1-3** *in situ* followed by the

addition of one equivalent of PCy_3 leads to a mixture of products by $^{31}P\{^1H\}$ NMR from which no clean product could be isolated. Among the observed products several broad resonances were observed, and it is reasonable to envision a dynamic process wherein PCy_3 is engaged in reversible coordination to the iridium center. As reliability and ease of monitoring is important for the future reactivity of (Cy-PSiP)Ir-L complexes, studies with this ligand were not pursued further.

A similar attempt was made with PMe_3, where **1-1** was reacted with 1 equivalent of PMe_3 in C_6H_6 at room temperature for 10 min. The initial bright yellow solution transitioned to a cloudy pale yellow. After removal of the solvent and volatile components, a $^{31}P\{^1H\}$ NMR spectrum was taken in C_6D_6 revealing the presence of two distinct species in a 1:4 ratio. These two complexes are identified to be (Cy-PSiP)Ir(H)(Cl)(PMe_3) and its structural isomer (**4-11a,b**). These two species have similar spectroscopic features, they both show a doublet and a triplet (32.3 (d), -53.7 (t) ppm for **4-11a**; and 34.0 (d), -56.5 (t) ppm for 4-11**b**), corresponding respectively to the two PCy_2 phosphines from the ligand, and the triplet being the coordinated PMe_3. The multiplicity suggests the ligand is in a *mer*-κ^3-(Cy-PSiP) coordination mode as the two PCy_2 phosphines give rise to a single resonance. The ^1H NMR spectrum shows a Ir–H hydride resonance at -23.46 ppm as a doublet of triplets ($^2J_{PMe3H}$ = 7 Hz, $^2J_{PCy2H}$ = 16 Hz, for **4-11b**) for the minor isomer, suggesting that the hydride is *cis* to all three phosphines. For the major isomer, another doublet of triplet at -13.0 ppm and ($^2J_{PMe3H}$ = 126 Hz, $^2J_{PCy2H}$ = 20 Hz, for **4-11a**) exhibits a larger coupling constant, suggesting that the hydride is *trans* to the –PMe3 fragment, while the smaller *cis* coupling indicates the two PCy_2 phosphines moieties are *cis* to the hydride. The six-coordinate complexes **4-11a,b** can then be treated with $LiCH_2SiMe_3$

resulting in the dehydrohalogenation of the two isomers. The resulting solution is dark red, and the powder isolated after purification bright red. $^{31}P\{^{1}H\}$ NMR analysis revealed a single set of two resonances as a doublet at 70.6 ppm and a triplet at −21.2 ppm. This compound is identified as (Cy-PSiP)Ir(PMe_3) (**4-12**), a compound previously synthesized in the Turculet group.[66] The spectroscopic data obtained in this experiment matches the previously reported data. Despite being a simple, scalable compound to synthesize, PMe_3 is a very strong L donor and tends to hinder reactivity due to its small size and lack of lability. This removes PMe_3 as an ideal candidate for effective stabilization of (Cy-PSiP)Ir-L complexes.

In an effort to design a (Cy-PSiP)Ir-L complex stabilized by a weaker L donor, (Cy-PSiP)Ir(C_2H_4) (**1-5b**) (first synthesized by a former member of the Turculet group) was revisited.[66] Minor modifications to the procedure allowed the reaction to be more easily reproduced and the product isolated in more consistent yields (~90%). An equivalent of $LiCH_2SiMe_3$ added to a solution of **1-1** in diethyl ether in a thick walled Teflon sealed reaction vessel under an atmosphere of ethylene shows an immediate color change from bright yellow to bright orange. After thorough filtration and removal of volatile components (Cy-PSiP)Ir(C_2H_4) (**1-5b**) can be isolated in 90% yield as a bright orange solid. $^{31}P\{^{1}H\}$ NMR analysis confirms the isolation of **1-5b**, as one resonance arises as a singlet at 65.4 ppm corresponding to the symmetry-equivalent phosphine donors of the (Cy-PSiP) ligand.[66]

With the purpose of synthesizing silyl hydride complexes in mind, the reactivity of **1-5b** was investigated with a variety of silanes such as Ph_3SiH, Me_2PhSiH, Et_2SiH_2, Ph_2SiH_2 and $PhSiH_3$. For the tertiary silanes Ph_3SiH and Me_2PhSiH the reaction was

carried in benzene from 1 up to 10 equiv. of silane, over the course of 24 h. No reaction between **1-5b** and the silane was observed by ^{31}P NMR. Reactions involving secondary and primary silanes such as Et_2SiH_2, Ph_2SiH_2 and $PhSiH_3$ all demonstrated complete consumption of **1-5b**, resulting in a complex mixture of multiple products, similar to the mixtures observed during the reaction of **1-3** with these substrates. Unfortunately, the addition of an ethylene neutral L ligand to the iridium metal center to form the 16-electron, 4-coordinate complex **1-5b** was not sufficient to tame the reactivity of (Cy-PSiP)Ir^I complexes.

4.2.5 Synthesis and Reactivity of (Cy-PSiP)Rh^{III} Cationic Species

Having noted that neither *in situ* generated (Cy-PSiP)Rh^I (**1-4**) nor (Cy-PSiP)Rh(CO) (**4-9**) undergo E-H bond activation chemistry in a reliable manner, the synthesis of cationic Rh^{III} species of the type (Cy-PSiP)RhH^+ was pursued in the hope that such complexes might show increased reactivity towards E-H bonds. Previous work from the Turculet group has demonstrated the synthesis of Ir^{III} cation-like species [(Cy-PSiP)IrH]X (X = OTf, BF_4, $B(C_6F_5)_4$) and the reactivity they exhibit with hydrosilanes that varied based on the nature of X (Scheme 4-10).[66] In light of these studies, Rh^{III} analogues were targeted.

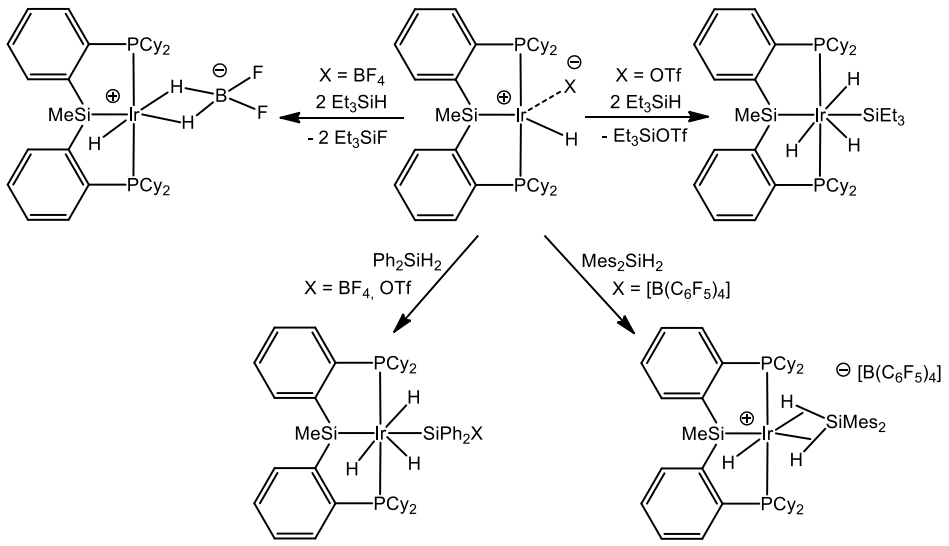

Scheme 4-10. Si-H activation chemistry previously observed for complexes of the type [(Cy-PSiP)IrH]X.

Treatment of (Cy-PSiP)Rh(H)Cl (**1-2**) with AgX (X = OTf, BF_4) in fluorobenzene led to the synthesis of the corresponding (Cy-PSiP)Rh(H)X (X = OTf, **4-13**; X = BF_4, **4-14**; Scheme 4-11) complexes. Both Rh complexes were isolated as pale-yellow solids in 97% (**4-13**) and 95% (**4-14**) yield. Complexes **4-13** and **4-14** each give rise to a single $^{31}P\{^1H\}$ NMR resonance at 59.3 ppm (d, $^1J_{PRh}$ = 119 Hz) and 59.6 ppm (d, $^1J_{PRh}$ = 119 Hz), respectively. The ^1H NMR spectra for these complexes each features an upfield-resonance hydride signal at -22.4 ppm (dt, $^1J_{HRh}$ = 31 Hz, $^2J_{HP}$ = 13 Hz) for **4-13** and -24.4 ppm (m, broad) for **4-14**. In the case of **4-14**, the ^{19}F NMR spectrum exhibits a broad resonance at -112.9 ppm, which may indicate exchange of the fluorine atoms of the BF_4^- anion due to a dynamic process such as coordination/decoordination of the fluorine atoms to Rh. X-ray quality crystals of both **4-13** and **4-14** were obtained from concentrated pentane solutions at low temperature (-35 °C) (Figure 4-4).

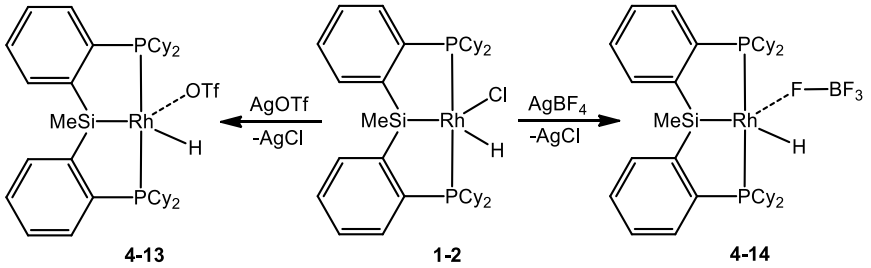

Scheme 4-11. Synthesis of (Cy-PSiP)Rh^{III} cation-like complexes (**4-13** and **4-14**).

The solid state structures of **4-13** and **4-14** both indicate inner sphere coordination of the OTf^- and BF_4^- anions (Figure 4-5; Table 4-2), analogous to observations made for the corresponding Ir species.[66] Complex **4-13** exhibits distorted square-based pyramidal geometry in the solid state, with the Si atom occupying the apical position. The Rh-O1 distance of 2.305(1) Å for **4-13** is longer than the Ir-O distance of 2.288(2) Å observed for (Cy-PSiP)Ir(H)OTf, and even longer than the Ir–O distance of 2.216(10) Å reported for Bergman's Cp*(PMe_3)Ir(Me)(OTf).[132] In the case of **4-14** the primary Rh-F interaction is *via* F1, exhibiting a Rh-F1 distance of 2.301(1) Å, once again, is longer than the Ir-F1 distance of 2.288(3) Å observed for (Cy-PSiPIr(H)BF_4. Like the Ir analogue, complex **4-14** also features a relatively short Rh···F2 distance of 2.506(1) Å, which is within the sum of the van der Waals radii for these two atoms. While κ^1-BF_4 coordination to a metal center is well known, examples of additional M–F interactions in mononuclear BF_4 complexes are rare, with only a handful of examples of Mo, Ag, and Zn complexes featuring such additional interactions having been crystallographically characterized.[138] The short Rh···F2 distance may simply be due to coincidental orientation of the BF_4^- anion. The observation of a Rh-bound BF_4^- anion in the solid state for **4-14** does not agree with the solution ^{19}F NMR data for this complex, which features a single (broad) resonance at room temperature rather than distinctly inequivalent F environments, as expected based on the

solid state structure. However, it is possible that the BF_4^- anion may undergo intramolecular fluorine exchange processes or exhibit fluxionality between inner and outer sphere coordination modes in solution, thus leading to the broad singlet observed by ^{19}F NMR spectroscopy.

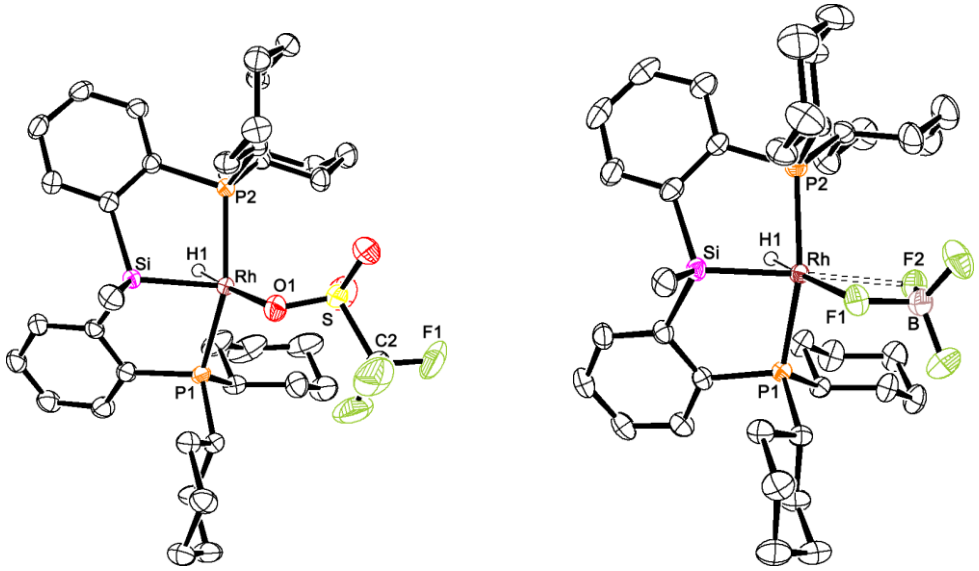

Figure 4-5. Crystallographically determined structures of **4-13** and **4-14** shown with 50% displacement ellipsoids. All non-hydrido H atoms have been omitted for clarity.

Table 4-2. Selected interatomic distances (Å**)** and angles (°) for **4-13** and **4-14**.

Bond Lengths (Å)				
4-13	Rh-P1	2.329(1)	Rh-H1	1.43(1)
	Rh-P2	2.310(1)	Rh-O1	2.305(1)
	Rh-Si	2.252(1)		
4-14	Rh-P1	2.305(1)	Rh-H1	1.515(1)
	Rh-P2	2.319(1)	Rh-F1	2.301(1)
	Rh-Si	2.250(1)	Rh-F2	2.506(1)
Bond Angles (°)				
4-13	P1-Rh-P2	155.59(1)	Si1-Rh-O1	105.65(1)
	Si1-Rh-H1	76.1(1)	H1-Rh-O1	176.57(1)
4-14	P1-Rh-P2	162.05(1)	Si1-Rh-F1	114.20(1)
	Si1-Rh-H1	72.36(1)	H1-Rh-F1	173.2(13)

The reactivity of **4-13** and **4-14** with Si-H bonds was evaluated through treatment of these complexes with hydrosilanes. Complex **4-13** was treated with a variety of tertiary silanes, including Ph_3SiH, Et_3SiH, and Me_2PhSiH. No reaction was observed even upon heating with up to 10 equiv. of the corresponding silane (THF solution, heating up to 65 °C for 5 days). The secondary and primary silanes Et_2SiH_2 and $PhSiH_3$ were also investigated, and in each case few (*ca.* 13% by ^{1}H NMR spectroscopy) evidence of the Si-H activation products was observed after two days at room temperature. The reaction mixtures were subsequently heated up to 65 °C for 4 days in THF but no significant conversion to the desired products was observed. However, significant side reactivity such as silane dehydrocoupling as well as substituent redistribution was observed as indicated by unusual resonances by ^{1}H NMR. Similar results were observed when the reactions were repeated with complex **4-14**. These results indicate that the synthesized Rh complexes do not appear to react with hydrosilanes in a productive manner, contrary to the observations made for [(Cy-PSiP)IrH]X (X = OTf, BF_4).

4.2.6 Attempted Synthesis of (Cy-PSiP)Ir(Me)OTf Complex

After numerous attempts at observing clean and reliable reactivity from (Cy-PSiP)Ir^{I} type complexes the interest of this study converged towards cationic (Cy-PSiP)Ir^{III} complexes. Cationic Ir^{III} complexes have shown remarkable reactivity towards Si-H bond activation and facile C-H(sp^3) bond cleavage.[120,132] In this context, Bergman and co-workers have shown the potential of Cp*(PMe_3)Ir(Me)OTf and its clean reactivity with various silanes (Me_3SiH, Ph_3SiH, $PhMe_2SiH$ and Ph_2SiH_2), leading to the isolation of complexes of the type Cp*(PMe_3)Ir(R')(SiR_2OTf) (R = Me, Ph; R' = H, Me, Ph). Such

reactivity may be accessible in the (Cy-PSiP) system through synthesis of complexes of the type [(Cy-PSiP)IrMe]X or [(Cy-PSiP)Ir(L)Me]X (L = neutral 2-electron donor).

The synthesis of (Cy-PSiP)Ir(Me)OTf was initially targeted as previous attempts in the Turculet group to isolate this complex has proven unreliable. This work revisited the synthesis where **1-3** generated *in situ* from the dehydrohalogenation of **1-1** by $LiCH_2SiMe_3$ was treated with 1 equiv. of MeOTf in C_6H_{12} at room temperature showing a rapid color change from bright orange to bright yellow. This reaction shows a new product[(κ^2–$Me_2SiC_6H_4PCy_2$)(κ^2–$C_6H_4PCy_2$)Ir(OTf)] (**4-15**) by ^{31}P NMR, which gives rise to two doublets corresponding to magnetically inequivalent –PCy_2 moieties (Scheme 4-12). The two doublets (d, 52.6 ppm, $^2J_{PP\,trans}$ = 299 Hz; d, -24.4 ppm, $^2J_{PP\,trans}$ = 299 Hz) show unusually large coupling, with a value of 299 Hz, in the range of a *trans* $^2J_{PP}$ coupling. Additionally, the ^{31}P resonance at -24.4 ppm is significantly more upfield than most of the shifts observed amongst the complexes synthesized in the Turculet group. The loss of C_s symmetry, as well as the large *trans* coupling of the two phosphorus containing moieties is similar to a previously observed complex in the Turculet group. Indeed, the complex (Cy-PSiP)Pd(Me), when exposed to heat (65 °C, 7h in benzene) undergoes an unusual structural rearrangement that features a reversible Si-C(sp^3) and Si-C(sp^2) cleavage (Scheme 4-12).[20c] There are several notable differences between complex **4-15** and the previously reported Pd complex. The geometry about the metal center differs, as the palladium complex shows a distorted square-planar geometry whereas the iridium complex is consistent with a distorted square pyramidal geometry with the silicon atom occupying the apical position. Additionally, in [(κ^2–$Me_2SiC_6H_4PCy_2$)(κ^2–$C_6H_4PCy_2$)Pd], the PCy_2 donor fragments were found to be *cis* to each other (d, 68.3 ppm, $^2J_{PP\,cis}$ = 19 Hz; d, -39.2

ppm, $^{2}J_{PP cis}$ = 19 Hz) whereas in **4-15** they were found to be *trans*.

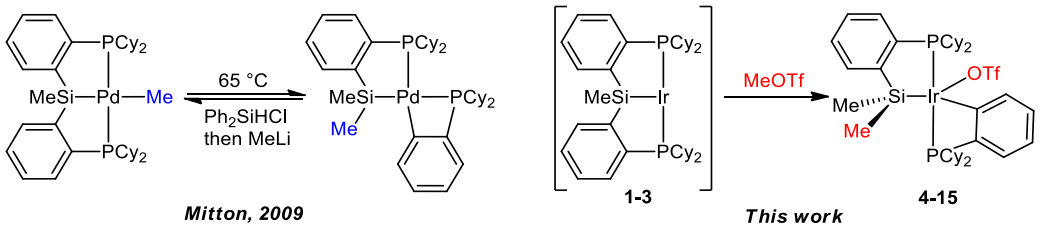

Scheme 4-12. Examples of (Cy-PSiP) complexes undergoing a structural rearrangement.

From a concentrated solution in Et_2O at low temperature (-35 °C), crystalline material of [(κ^2–$Me_2SiC_6H_4PCy_2$)(κ^2–$C_6H_4PCy_2$)Ir(OTf)] (**4-15**) suitable for single crystal X-ray diffraction analysis was obtained. The solid state structure of **4-15** reveals a distorted square pyramidal geometry about the iridium center. The C_1-symmetric structure also shows that the relative position of the phosphines is effectively *trans* to one another (P1-Ir-P2 angle is 163.42(2)°), and that the silicon atom occupies the apical position of the square based pyramid (Figure 4-6). The structure was also consistent with the formation of a 4-membered metallocycle.

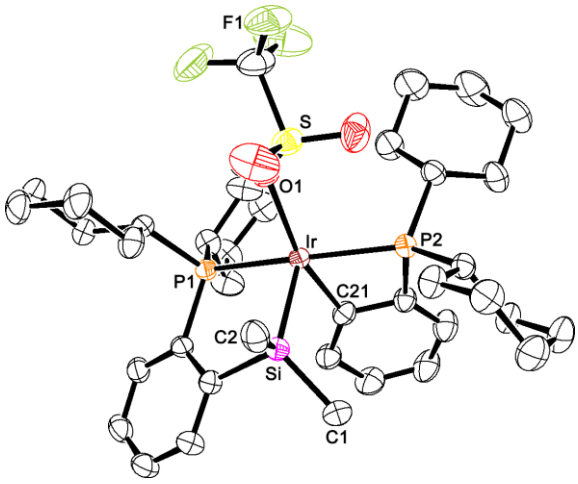

Figure 4-6. The crystallographically determined structure of **4-15** shown with 50% displacement ellipsoids. All H atoms have been omitted for clarity. Selected interatomic distances (Å) and angles (°): Ir-P1 2.3050(7), Ir-P2 2.3590(7), Ir-Si 2.3017(7), Ir-C21 2.023(3), Ir-O1 2.1956(1), P1-Ir-P2 163.42(2), Si-Ir-O1 114.19(6), Si-Ir-P1 84.82(2), Si-Ir-C21 82.61(8).

Despite several attempts at observing reversible Si-C(sp^3) cleavage leading to (Cy-PSiP)Ir(Me)OTf, no evidence of such complex or any related intermediates was able to be observed throughout these studies. Based on observations for [(κ^2–$Me_2SiC_6H_4PCy_2$)(κ^2–$C_6H_4PCy_2$)Pd], it is not unreasonable to envision a similar mechanism involving the formation of (Cy-PSiP)Ir(Me)OTf as a short lived intermediate that undergoes a Si-C reductive elimination to form a new Si-Me bond, resulting in a chelated κ^2–(Cy-PSiP)Ir^I(OTf) intermediate with no Si-Ir bond. This intermediate subsequently undergoes a Si-C oxidative addition of the Si-C_{aryl}(sp^2) bond resulting in the formation of the metallocycle observed in **4-15** (Scheme 4-13).

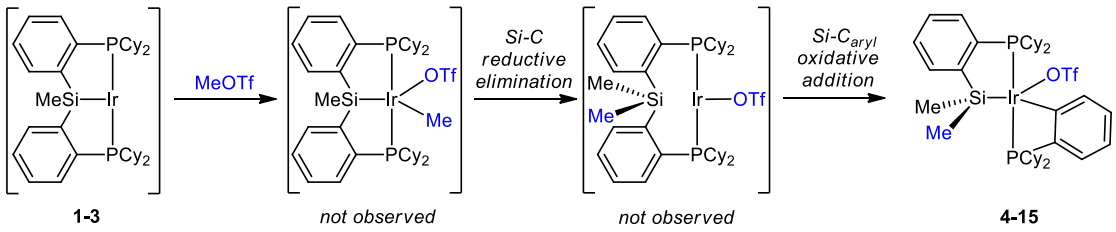

Scheme 4-13. Proposed mechanism for the formation of **4-15**.

4.2.7 Synthesis of (Cy-PSiP)Rh(Me)OTf Complex

Despite the surprising results observed during attempted syntheses of (Cy-PSiP)Ir(Me)OTf, similar reactions were targeted with Rh. In this context, (Cy-PSiP)RhHCl (**1-2**) was treated with 1 equiv. of $LiCH_2SiMe_3$ in C_6H_{12} over the course of 15 min to generate **1-4** *in situ*. Then 1 equiv. of MeOTf was added and rapid color change from dark orange to yellow was observed. The isolated compound was analyzed spectroscopically, with the $^{31}P\{^1H\}$ NMR spectrum revealing a single resonance (d, 54.6 ppm, $^1J_{RhP}$ = 120 Hz), indicating retention of C_s-symmetric geometry as well as *mer*-κ^3-Cy-PSiP coordination. This allows assignment of **4-16** as (Cy-PSiP)Rh(Me)OTf (Scheme 4-14). The

^{1}H NMR of **4-16** displays a resonance associated with the methyl bound to rhodium (Rh-*Me*), as the signal multiplicity reveals a doublet of triplets at 0.49 ppm consistent with coupling to the rhodium atom as well as the two magnetically equivalent phosphines (dt, 0.49 ppm, $^{2}J_{RhH}$ = 2 Hz, $^{3}J_{RhP}$ = 6 Hz).

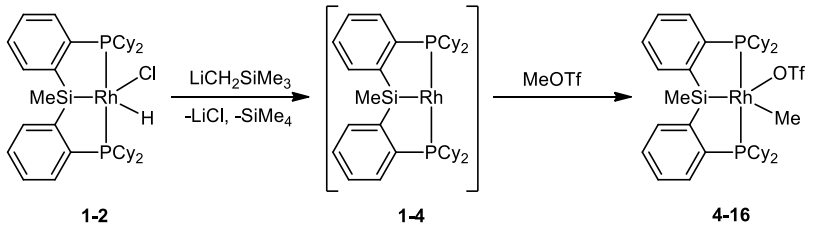

Scheme 4-14. Synthesis of (Cy-PSiP)Rh(Me)OTf (**4-16**).

No evidence of Si-C bond cleavage was observed, inconsistent with the iridium analogue. Complex **4-16** was heated in benzene at 70 °C over the course of 3 days in an attempt to observe further transformation, but no evidence of degradation or rearrangement was observed by ^{31}P NMR. This reaction was informative regarding potential C-H bond activation, as despite being in an abundance of available C-H(sp^2) bonds from the benzene solution, no (Cy-PSiP)Rh(Ph)OTf was observed. In the work of Bergman and co-workers, Cp*(PMe_3)Ir(CH_3)(OTf) was able to react readily with benzene to cleanly form Cp*(PMe_3)Ir(Ph)(OTf) as a result of a loss of methane and benzene C-H(sp^2) bond activation.[120a] Additional attempts at reactions with hydrosilanes lead to intractable mixtures from which no clean material could be isolated.

4.2.8 Synthesis of (Cy-PSiP)Ir(PMe$_3$)(Me)OTf Complex

Previous attempts to isolate (Cy-PSiP)Ir(Me)OTf, have revealed this complex to be elusive by the attempted synthetic route. The addition of a neutral L donor may lead to a stabilized (Cy-PSiP)Ir(L)(Me)OTf type complex, and to that end, a solution of (Cy-PSiP)Ir(PMe$_3$) (**4-12**) in benzene was reacted with 1 equiv. MeOTf at room temperature over the course of 30 min. As an immediate color change from dark red to pale yellow was observed, ^{31}P NMR monitoring showed the complete consumption of **4-12** as well as clean, quantitative formation of a new product which was isolated in >99% yield. The new complex (Cy-PSiP)Ir(PMe$_3$)(Me)OTf (**4-17**) gives rise to three distinct resonances by ^{31}P{^{1}H} NMR which suggests that **4-17** is a *fac*-κ^3-Cy-PSiP complex possessing three unique phosphorus environments (Scheme 4-15). The three resonances at 49.1 (dd), 35.6 (dd), -10.3 (dd) ppm respectively account for each phosphorus environment, with two resonances displaying large $^2J_{PP}$*trans* = 311 Hz coupling, consistent with the proposed structure in Scheme 4-15.

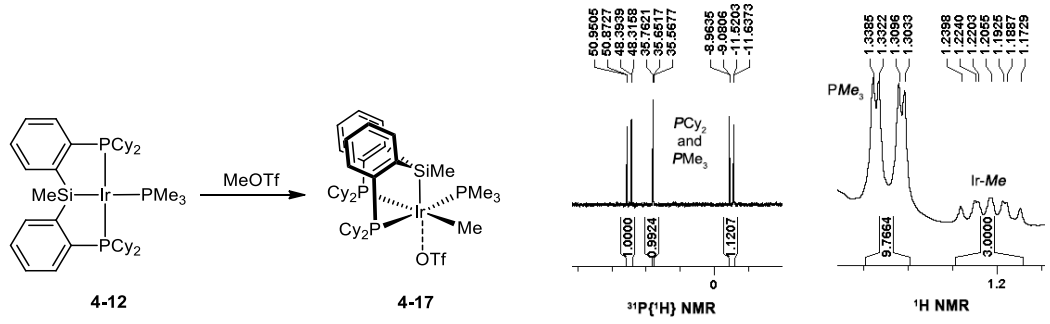

Scheme 4-15. Synthesis of (Cy-PSiP)Ir(PMe$_3$)(Me)OTf (**4-17**) and selected ^{31}P{^{1}H}; ^{1}H NMR spectroscopic features of **4-17**.

The ^{1}H NMR spectrum of **4-17** also desmonstrates an interesting multiplet at 1.20 ppm with $^3J_{PH}$ coupling to all three different phosphine environments. This resonance accounts for three protons and corresponds to the methyl bound to iridium. The –PMe$_3$

ligand gives rise to a doublet of doublets at 1.31 ppm which demonstrates a $^{2}J_{PH}$ coupling of 8 Hz as well as a weaker $^{4}J_{PH\textit{trans}}$ coupling of 2 Hz, as a result of the –PCy_2 phosphine being *trans* to the –PMe_3 ligand. In addition, the $^{4}J_{PH\textit{cis}}$ coupling to the other –PCy_2 moiety is not observable in this experiment. Overall, the addition of the neutral L donor PMe_3 enabled the stabilization of the desired (Cy-PSiP)Ir(PMe_3)(Me)OTf (**4-17**) at room temperature in a solution of CH_2Cl_2.

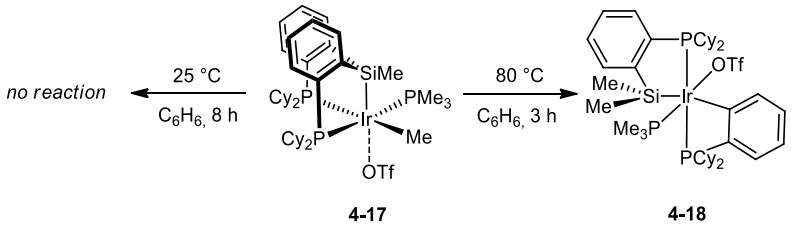

4-17 **4-18**

Scheme 4-16. Stability of **4-17** and attempt at C-H bond activation of benzene.

Stability and reactivity experiments were conducted in C_6H_6 despite the partial solubility of **4-17** in this solvent. A saturated solution of **4-17** in C_6H_6 at room temperature was monitored over a period of 8 h for potential evidence of benzene C-H(sp^2) bond activation. No evidence of such a reaction was observed unlike the complex Cp*(PMe_3)Ir(Me)OTf employed by Bergman and co-workers.[120a] The same solution was then heated to 80 °C for 3 h in C_6H_6 showing quantitative conversion to [(κ^2–$Me_2SiC_6H_4PCy_2$)(κ^2–$C_6H_4PCy_2$)Ir(PMe_3)(OTf)] (**4-18**) (observed *in situ* by $^{31}P\{^{1}H\}$ NMR). Complex **4-18** shows three distinct signals by $^{31}P\{^{1}H\}$ NMR (47.9 (dd), -25.4 (m), -45.5 (dd) ppm) corresponding to three unique phosphine environments. In this context, **4-18** shares similarities with **4-15** as one of the three phosphorus signals (-45.5 (dd) ppm) is observed to be unusually upfield, characteristic of a Si-C bond cleavage in the same fashion observed previously in section 4.2.5 of this chapter (Scheme 4-16). Unfortunately, no evidence of C-H(sp^2) bond activation of benzene was observed over the course of this

investigation.

4.2.9 Reactivity of (Cy-PSiP)Ir(PMe$_3$)(Me)OTf Complex

In an effort to understand the reactivity of **4-17**, reactions were attempted between **4-17** and a variety of substrates containing C-H and Si-H bonds. Additional efforts were also directed towards generating cationic species through use of an anion bulkier than triflate (*ie*. BF_{20}^- = $B(C_6F_5)_4^-$). Initial efforts were made to determine the coordination mode of the triflate anion in complex **4-17**. To do so, a solution of **4-17** in CD_2Cl_2 was prepared in a J-Young NMR tube. An atmosphere of CO was added to the solution, and an immediate lightening of the yellow solution was observed. ^{31}P NMR analysis revealed quantitative conversion of **4-17** to a new product (Cy-PSiP)Ir(Me)(CO)$(PMe_3)^+(OTf)^-$ (**4-19**) (Scheme 4-17). The Ir^{III} complex **4-19** shows only two resonances by $^{31}P\{^1H\}$ at 19.2 (d) and -66.6 (t) ppm respectively in a 2:1 ratio. This indicates that the –PCy_2 moieties in **4-19** are equivalent due to *mer*-κ^3-Cy-PSiP coordination. In the ^{1}H NMR spectrum, the signal associated with the methyl bound to iridium (Ir-*Me*) gives rise to a doublet of triplets at 0.16 ppm (dt, 3 H, $^3J_{PHtrans}$ = 15 Hz, $^3J_{PHcis}$ = 6 Hz), and shows coupling to two different phosphine environments with the associated $^3J_{PH}$ coupling. The resonance associated with the –PMe_3 methyls at 1.92 ppm (d, 9 H, $^2J_{PH}$ = 8 Hz) only displays coupling to the phosphorus atom of –PMe_3, likely due to the $^4J_{PHcis}$ of the ligand phosphine donors being too small to be observed in this experiment. An IR spectrum was obtained in CH_2Cl_2 as a thin film on NaCl plates, showing a CO stretch as an intense band at 2018 cm^{-1}.

This experiment was repeated with NH_3, and displayed similar reactivity as NH_3 neutral L ligand readily coordinates to the iridium center, forcing the triflate anion into outer-sphere coordination. Conversion to the *mer*-κ^3-Cy-PSiP complex (Cy-

PSiP)Ir(Me)(NH_3)(PMe_3)$^+$(OTf)$^-$ (**4-20**) is quantitative , as determined by NMR spectroscopy (Scheme 4-17). The $^{31}P\{^1H\}$ NMR spectrum of **4-20** shows two resonances at 28.1 (br) and -59.1 (t) ppm in a 2:1 ratio. The resonance in the ^1H NMR spectrum of **4-20** corresponding to (Ir*Me*) appears at -0.41 ppm as a not well resolved doublet of triplets, slightly more upfield than the analoguous **4-19**. The –PMe_3 fragment shows a resonance at 1.79 ppm as a doublet, and the –NH_3 protons are associated with a broad signal at 3.17 ppm, common for Ir-NH_3 complexes.[139]

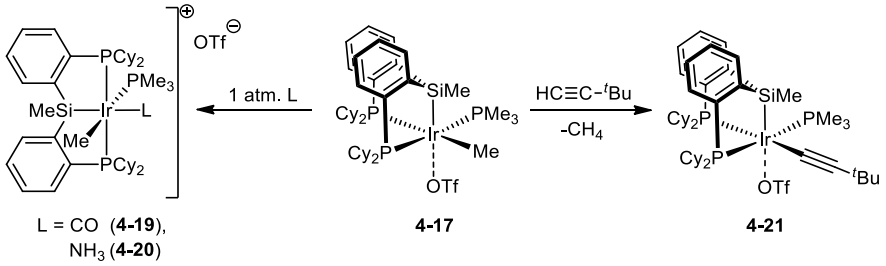

Scheme 4-17. Synthesis of (Cy-PSiP)Ir(Me)(CO)(PMe_3)$^+$(OTf)$^-$ (**4-19**), (Cy-PSiP)Ir(Me)(NH_3)(PMe_3)$^+$(OTf)$^-$ (**4-20**) and (Cy-PSiP)Ir(PMe_3)(CC^{t}Bu)(OTf) (**4-21**)

After successfully generating outer-sphere iridium cationic complexes through stabilization by neutral L donor ligands (CO and NH_3) and observing that benzene activation was not successful, a substrate featuring a more reactive C-H bond was tried. The treatment of **4-17** in benzene at room temperature over the course of 8 h with up to 10 equiv. of benzaldehyde surprisingly did not show any reaction and the starting material left unchanged. Subsequent heating of the reaction up to 80 °C displayed quantitative conversion of the starting material to **4-18** regardless of the presence of benzaldehyde, and this reaction was not pursued further.

A terminal alkyne was then chosen as a candidate for C-H oxidative addition. In this context, the reaction of **4-17** with 3,3-dimethyl-1-butyne in CH_2Cl_2 at room temperature over the course of 8 h led to complete consumption of **4-17** to cleanly form

the new complex (Cy-PSiP)Ir(PMe_3)(CC^{t}Bu)(OTf) (**4-21**), which was isolated as a bright yellow solid in 93% yield (Scheme 4-17). The $^{31}P\{^1H\}$ NMR spectrum of **4-21** revealed three distinct signals at 49.2 (dd), 31.6 (dd) and -11.5 (dd), quite similar to the spectroscopic features of starting material (**4-17**). The phosphorus signal distribution suggests a *fac*-κ^3-Cy-PSiP ligand geometry about the iridium metal centre. The absence of an Ir-*Me* signal is noticeable in the ^1H NMR spectrum of **4-21** and instead a new singlet at 1.35 ppm accounting for 9 protons is observed. This signal is associated to the *tert*-butyl group methyls of the –CC^{t}Bu ligand.

4.2.10 Attempts at the Synthesis of (Cy-PSiP)Ir(PMe_3)(Me)$^+$[$B(C_6F_5)_4$]$^-$ Complex

The abstraction of the triflate anion by a bulkier, more weakly coordinating anion such as $B(C_6F_5)_4^-$ is a known method to access a cationic species where the large counter anion is in an outer sphere coordination mode.[132] This method was investigated in order to isolate the (Cy-PSiP)Ir(Me)(PMe_3)$^+$ cationic species. To do so, a solution of complex **4-17** in CH_2Cl_2 was reacted with 1 equiv. of $LiBF_{20}$ or $AgBF_{20}$ at room temperature over the course of 1 h. In the $^{31}P\{^1H\}$ NMR spectrum of the newly synthesized complex (Cy-PSiP)Ir(Me)(PMe_3)$^+$($B(C_6F_5)_4$)$^-$ (**4-22**), three distinct resonances (49.6 (dd), 35.6 (m), -10.4 (dd) ppm) can be observed similar to those of **4-17** (Scheme 4-18). The ^1H NMR spectrum displays the characteristic Ir-*Me* multiplet at 1.20 ppm, also observed in **4-17**. While the ^{31}P and ^1H resonances are incredibly similar, a crucial difference was observed in the $^{19}F\{^1H\}$ NMR spectrum wherein the resonance at -78.8 (s) ppm associated with the triflate anion from compound **4-17** is no longer present. Instead, three distinct resonances can be observed at -133.1 (m), -163.6 (t) and -167.5 (brt) ppm, characteristic of the *ortho*, *para*

and *meta* fluorine resonances respectively, from the four perfluorinated aryl groups of the $B(C_6F_5)_4^-$ anion. This observation is consistent with the expected anion exchange.

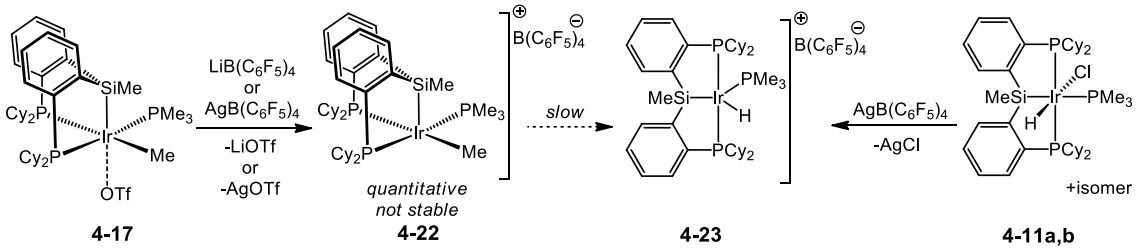

Scheme 4-18. Synthesis of iridium methyl (**4-22**) and hydride (**4-23**) cations.

Despite numerous efforts to isolate complex **4-22** for complete characterization, **4-22** was found to be unstable at room temperature in a solution as well as the solid state, and would start to convert to a new compound after only a few hours until complete conversion was observed over several days. To get a better understanding of the transformation, the compound resulting from the slow conversion of **4-22** was analysed by NMR spectroscopy. The new compound, (Cy-PSiP)Ir(H)$(PMe_3)^+B(C_6F_5)_4^-$ (**4-23**) shows only two resonances by $^{31}P\{^1H\}$ NMR as a doublet and a triplet (56.7 (d), -15.1 (t) ppm in a 2:1 ratio), suggesting that the ligand geometry had changed to *mer*-κ^3-Cy-PSiP about the iridium center (Scheme 4-18). The signal associated with the Ir-*Me* is no longer observable in the ^1H NMR spectrum, but rather a new signal upfield associated with a metal hydride (Ir-*H*) can be observed at -10.3 (dt) ppm as a doublet of triplets, and displays $^2J_{PH}$ = 95 Hz and $^2J_{PH}$ = 18 Hz coupling corresponding to the $–PMe_3$ and $–PCy_2$, respectively. The $^{19}F\{^1H\}$ spectrum shows the same resonances for both complexes, corresponding to the perfluorinated aryls in $B(C_6F_5)_4^-$. In order to confirm this claim, **4-23** was synthesized by an independent, alternative route. (Cy-PSiP)Ir(H)(Cl)(PMe_3) (**4-11a,b**) was prepared from the procedure described in section 4.2.4 of this chapter (*vide supra*), and was reacted with 1 equiv. of

$AgB(C_6F_5)_4$ in benzene, over the course of 1 h. Quantitative conversion was observed by ^{31}P NMR and **4-23** was isolated in 93% yield (Scheme 4-18). This reaction confirms that the cationic methyl complex **4-22** can be generated *in situ* but undergoes subsequent conversion to the cationic hydride complex **4-23**, even in the solid state.

The fact that this transformation occurs in the solid state calls the origin of the hydride (Ir-*H*) in to question. As the transformation occurs in the solid state, it is likely that the reaction is intramolecular, and may involve a metalation of a P-Cy cyclohexyl ring by complex **4-22** which subsequently undergoes *β*-H elimination leading to a complex similar to **4-23**, where a cyclohexyl ring contains a C-C(sp^2) unsaturation (Scheme 4-19).

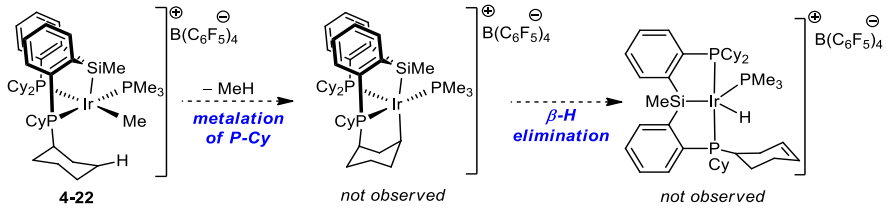

Scheme 4-19. Proposed mechanism for the slow transformation of **4-22** overtime.

Further investigation in order to improve the stability of cationic iridium methyl complexes is ongoing, as well as the exploration of the *in situ* reactivity of complex **4-22**.

4.3 Summary and Conclusions

The results presented throughout this chapter show the possibility of synthesizing and isolating coordinatively unsaturated Ir^{III} silyl hydride complexes *via* Si-H oxidative addition mediated by (Cy-PSiP)Ir^{I}. This study brings another complementary fragment to the previously studied N-H, P-H and O-H bond activation.

Complexes of the type (Cy-PSiP)Ir(H)($SiRR'_2$) (R = H, Cl; R' = Ph, Mes) are isolable and stable, although can vary geometrically when compared to amido, anilido and

phosphido hydride species encountered previously. The distorted trigonal bipyramidal or distorted square pyramidal configurations commonly is available to five coordinate complexes are observed, and are variable depending on the steric bulk of the silyl moieties. Although larger, bulky hydrosilanes were adequate candidates for silyl hydride complex generation, a noticeable synthetic challenge was encountered towards less bulky secondary and primary silanes, as no other silyl hydride species were isolated from these experiments. Interestingly, Rh analogues of the silyl hydride complexes were not isolable and remained elusive.

A significant amount of effort was also directed towards the observation of silylene complexes, but despite multiple attempts, terminal Ir silylene complexes were not observed.

In an attempt to stabilize and tame the uncontrollable reactivity of Ir^{I} towards smaller hydrosilanes, several (Cy-PSiP)IrL (L = CO, PMe_3, C_2H_4) complexes were synthesized and their reactivity was tested with reactive Si-H σ-bonds. The synthesis of (Cy-PSiP)IrL also provided challenges, especially towards the isolation of the Ir monocarbonyl complex, and led to the isolation of several unexpected complexes. (Cy-PSiP)IrL complexes were not capable of cleanly reacting with hydrosilanes.

The synthesis of cationic Ir^{III} and Rh^{III} was also explored and found to be successful. Special attention was directed to the synthesis of a cationic Ir methyl cation, and subsequent reactivity towards C-H was explored. Further challenges arose as attempts were made to synthesize cationic Ir methyl complexes with bulkier outer sphere anions, and investigations into a better method for isolation of such complexes are ongoing. These studies allow for better understanding of the reactivity and the stability of Ir silyl hydrides

as well as Ir^{III} and Rh^{III} cationic species.

4.4 Experimental

4.4.1 General Considerations

All experiments were conducted under nitrogen in an MBraun glovebox or using standard Schlenk techniques. Dry, oxygen-free solvents were used unless otherwise indicated. Tetrahydrofuran and diethyl ether were distilled from Na/benzophenone ketyl. Benzene, toluene, and pentane were sparged with nitrogen and dried by subsequent passage through a double-column solvent purification system (one activated alumina column and one column packed with activated Q-5). All purified solvents were stored over 4 Å molecular sieves. Benzene-d_6, cyclohexane-d_{12}, and dichloromethane-d_2 were degassed *via* three freeze-pump-thaw cycles and stored over 4 Å molecular sieves. The compounds (Cy-PSiP)Ir(H)Cl (**1-1**) and (Cy-PSiP)Rh(H)Cl (**1-2**),[20b] as well as $HClSiMes_2$[140] , H_2SiMes_2[140] , $Li(B(C_6F_5)_4)$, $Ag(B(C_6F_5)_4)$, and $(Ph_3C)(B(C_6F_5)_4)$ were prepared according to literature procedure. All other reagents were purchased from commercial suppliers and used without further purification. Unless otherwise stated, ^1H, ^{13}C, ^{31}P, and ^{29}Si NMR characterization data were collected at 300K on a Bruker AV-300 spectrometer operating at 300.1, 75.5, 121.5, and 59.6 MHz (respectively) with chemical shifts reported in parts per million downfield of $SiMe_4$ (for ^1H, ^{13}C, and ^{29}Si) or 85% H_3PO_4 in D_2O (for ^{31}P). ^1H and ^{13}C NMR chemical shift assignments are based on data obtained from ^{13}C-DEPTQ, ^1H-^1H COSY, ^1H-^{13}C HSQC, and ^1H-^{13}C HMBC NMR experiments. ^{29}Si NMR assignments are based on ^1H-^{29}Si HMQC and ^1H-^{29}Si HMBC experiments. In some cases, fewer than expected unique ^{13}C NMR resonances were observed, despite prolonged acquisition times. X-ray

data collection, solution, and refinement were carried out by Drs. Robert MacDonald, Michael J. Ferguson, and Yuqiao Zhou at the University of Alberta X-ray Crystallography Laboratory, Edmonton, Alberta.

4.4.2 Synthetic Details and Characterization Data

(CyPSiP)Ir(H)(SiHPh$_2$) (4-1). A solution of **3-3** (0.021 g, 0.025 mmol) in ca. 7 mL of benzene was treated with H_2SiPh_2 (0.009 g, 0.050 mmol). The resulting orange reaction mixture was allowed to stand at room temperature for 1 h, over the course of the course of which a color change to bright yellow was observed. ^{1}H and ^{31}P{^{1}H} NMR analysis of this reaction mixture indicated quantitative conversion **3-3** to **4-1**. ^{1}H NMR (benzene-d_6): δ 8.21 (d, 2 H, J = 7 Hz, H_{arom}), 8.07 (d, 4 H, J = 7 Hz, Si*Ph*$_2$, H_{arom}), 7.72 (m, 4 H, Si*Ph*$_2$, H_{arom}), 7.38 (m, 2 H, H_{arom}), 7.29 – 6.98 (overlapping resonances, 6 H, H_{arom}), 6.59 (brt, 1 H, J = 6.7 Hz, Si*H*Ph$_2$), 2.37 – 0.36 (overlapping resonances, 44 H, P*Cy* + Si*Me*; singlet resonances at 1.34 ppm was identified as corresponding to the Si*Me* group), -9.32 (br, 1 H, Ir*H*). ^{31}P{^{1}H} NMR (benzene-d_6): δ 42.0.

(CyPSiP)Ir(H)(SiHMes$_2$) (4-2). In a vial, a solution of **1-1** (0.020 g, 0.024 mmol) was dissolved in C_6H_{12}, then reacted with $LiCH_2SiMe_3$ (0.003 g, 0.029 mmol) to generate **1-3** *in situ*. Then, H_2SiMes_2 (0.007 g, 0.029 mmol) was added to the solution. Over the course of 1 h at room temperature, the solution color changed from dark orange to lighter orange. After a filtration through Celite, solvent and volatiles were removed *in vacuo*, affording **4-2** (0.021 g, 0.021 mmol) in 88 % yield, isolated as an orange solid. ^{1}H NMR (benzene-d_6): δ 7.98 (d, 1 H, J = 7.5 Hz, H_{arom}), 7.60 (m, 1 H, H_{arom}), 7.53 (m, 1 H, H_{arom}), 7.49 (m, 1 H, H_{arom}), 7.31 (m, 1 H, H_{arom}), 7.15 (overlapping resonances with benzene-d_6

residual, 1 H, H_{arom}), 7.00 – 6.93 (overlapping resonances, 3 H, ligand backbone + SiH*Mes₂*, H_{arom}), 6.91 (s, 1 H, SiH*Mes₂*, H_{arom}), 6.79 (s, 1 H, SiH*Mes₂*, H_{arom}), 6.69 (s, 1 H, SiH*Mes₂*, H_{arom}), 5.64 (m, 1 H, Si*H*Mes$_2$), 2.99 (m, 1 H, C*H*$_{Cy}$), 2.71 (m, 1 H, C*H*$_{Cy}$), 2.63 (s, 3 H, C*Me*$_{Mes}$), 2.44 (s, 3 H, C*Me*$_{Mes}$), 2.35 (s, 3 H, C*Me*$_{Mes}$), 2.23 (s, 3 H, C*Me*$_{Mes}$), 2.07 – 0.49 (overlapping resonances, 42 H, P*Cy*), 0.59 (s, 3 H, Si*Me*), -0.43 (m, 1 H, C*H*$_{2Cy}$), -6.81 (dd, 1 H, $^2J_{HP}$ = 106 Hz, $^2J_{HP}$ = 19 Hz, Ir*H*). $^{13}C\{^1H\}$ NMR (benzene-d_6): δ 158.6 (d, *J* = 51 Hz, C_{arom}), 155.5 (d, *J* = 43 Hz, C_{arom}), 147.1 (C_{arom}), 146.0 (C_{arom}), 144.4 (d, *J* = 44 Hz, C_{arom}), 144.3 (C_{arom}), 144.1 (C_{arom}), 142.9 (C_{arom}), 142.8 (d, *J* = 48 Hz, C_{arom}), 141.5 (C_{arom}), 137.2 (C_{arom}), 136.3 (C_{arom}), 132.4 (d, *J* = 19 Hz, *C*H$_{arom}$), 131.6 (d, *J* = 21 Hz, *C*H$_{arom}$), 130.8 (*C*H$_{arom}$), 129.9 (*C*H$_{arom}$), 129.0 (*C*H$_{arom}$), 128.9 (*C*H$_{arom}$), 128.4 (*C*H$_{arom}$), 127.5 (*C*H$_{arom}$), 127.1 (*C*H$_{arom}$), 126.8 (apparent d, *J* = 5 Hz, *C*H$_{arom}$), 41.1 (d, *J* = 15 Hz, *C*H$_{Cy}$), 39.9 (d, *J* = 20 Hz, *C*H$_{Cy}$), 39.7 (d, *J* = 10 Hz, *C*H$_{Cy}$), 38.9 (d, *J* = 28 Hz, *C*H$_{Cy}$), 38.1 (*C*H$_{2Cy}$), 38.0 (*C*H$_{2Cy}$), 31.6 (d, *J* = 6 Hz, *C*H$_{2Cy}$), 31.0 (d, *J* = 6 Hz, *C*H$_{2Cy}$), 30.9 (*C*H$_{2Cy}$), 29.7 (d, *J* = 6 Hz, *C*H$_{2Cy}$), 28.9 (d, *J* = 16 Hz, *C*H$_{2Cy}$), 28.7 (*C*H$_{2Cy}$), 28.5 (d, *J* = 6 Hz, *C*H$_{2Cy}$), 28.4 (*C*H$_{2Cy}$), 28.1 (d, *J* = 14 Hz, *C*H$_{2Cy}$), 27.7 (*C*H$_{2Cy}$), 27.7 – 27.5 (overlapping resonances, *C*H$_{2Cy}$), 27.1 (*C*H$_{2Cy}$), 26.9 (*C*H$_{2Cy}$), 26.6 (d, *J* = 12 Hz, *C*H$_{2Cy}$), 26.3 (d, *J* = 12 Hz, *C*H$_{2Cy}$), 25.7 (C*Me*), 23.3 (C*Me*), 21.2 (C*Me*), 21.0 (C*Me*), 14.3 (C*Me*), 12.0 (C*Me*), 1.6 (Si*Me*). ^{31}P NMR (benzene-d_6): δ 63.7 (d, 1 P, $^2J_{PP}$*cis* = 15 Hz, *P*Si*P*), 34.1 (d, 1 P, $^2J_{PP}$*cis* = 14 Hz, *P*Si*P*). ^{29}Si NMR (benzene-d_6): δ 11.5 (*Si*Me), -16.9 (*Si*HMes$_2$).

(CyPSiP)Ir(H)(SiClMes$_2$) (4-3). In a vial, a solution of **1-1** (0.031 g, 0.038 mmol) was dissolved in C_6H_{12}, then reacted with $LiCH_2SiMe_3$ (0.004 g, 0.038 mmol) to generate **1-3** *in situ*. Then, HClSiMes2 (0.011 g, 0.038 mmol) was added to the solution. Over the course of 1 h at room temperature, the solution color changed from dark orange to lighter

orange. After a filtration through Celite, solvent and volatiles were removed *in vacuo*, affording **4-3** (0.032 g, 0.030 mmol) in 78 % yield, isolated as an orange solid. ^{1}H NMR (dichloromethane-d_2): δ 7.84 (d, 1 H, J = 7 Hz, H_{arom}), 7.75 – 7.64 (overlapping resonances, 2 H, H_{arom}), 7.40 (m, 2 H, H_{arom}), 7.26 (m, 1 H, H_{arom}), 7.14 (m, 2 H, H_{arom}), 6.95 (s, 1 H, SiCl*Mes*$_2$, H_{arom}), 6.68 (s, 1 H, SiCl*Mes*$_2$, H_{arom}), 6.64 (s, 1 H, SiCl*Mes*$_2$, H_{arom}), 6.59 (s, 1 H, SiCl*Mes*$_2$, H_{arom}), 3.10 (m, 1 H, CH_{Cy}), 2.73 (m, 1 H, CH_{Cy}), 2.60 (m, 1 H, CH_{Cy}), 2.25 (s, 3 H, CMe_{Mes}), 2.20 (s, 3 H, CMe_{Mes}), 2.15 (s, 3 H, CMe_{Mes}), 2.03 (s, 3 H, CMe_{Mes}), 2.49 – 0.39 (overlapping resonances, 40 H, P*Cy*), 0.10 (s, 3 H, Si*Me*), -0.52 (m, 1 H, CH_{2Cy}), -8.42 (dd, 1 H, $^{2}J_{HP}$ = 99 Hz, $^{2}J_{HP}$ = 19 Hz, Ir*H*). ^{13}C{^{1}H} NMR (dichloromethane-d_2): δ 158.7 (C_{arom}), 153.4 (C_{arom}), 148.7 (C_{arom}), 147.2 (C_{arom}), 145.1 (C_{arom}), 144.1 (C_{arom}), 143.1 (C_{arom}), 142.6 (C_{arom}), 142.1 (C_{arom}), 139.6 (C_{arom}), 137.5 (C_{arom}), 136.8 (C_{arom}), 132.5 (CH$_{arom}$), 132.3 (d, J = 21 Hz, CH$_{arom}$), 131.6 (d, J = 21 Hz, CH$_{arom}$), 130.1 (CH$_{arom}$), 129.5 (CH$_{arom}$), 128.9 (d, J = 22 Hz, CH$_{arom}$), 128.8 (d, J = 5 Hz, CH$_{arom}$), 127.4 (CH$_{arom}$), 126.9 (CH$_{arom}$), 126.7 (apparent d, J = 6 Hz, CH$_{arom}$), 45.4 (d, J = 18 Hz, CH$_{Cy}$), 40.6 (d, J = 18 Hz, CH$_{Cy}$), 40.2 (d, J = 12 Hz, CH$_{Cy}$), 39.1 (d, J = 28 Hz, CH$_{Cy}$), 37.6 (CH$_{2Cy}$), 37.5 (CH$_{2Cy}$), 33.2 (d, J = 7 Hz, CH$_{2Cy}$), 31.3 – 31.1 (overlapping resonances, CH$_{2Cy}$), 30.6 (d, J = 6 Hz, CH$_{2Cy}$), 29.6 – 27.7 (overlapping resonances, CH$_{2Cy}$), 28.0 (C*Me*), 27.0 – 26.3 (overlapping resonances, CH$_{2Cy}$), 23.8 (C*Me*), 22.9 (C*Me*), 20.8 (C*Me*), 20.7 (C*Me*), 10.2 (C*Me*), 0.9 (Si*Me*). ^{31}P NMR (dichloromethane-d_2): δ 59.4 (d, 1 P, $^{2}J_{PP}$*$_{cis}$* = 12 Hz, *P*Si*P*), 42.5 (d, 1 P, $^{2}J_{PP}$*$_{cis}$* = 12 Hz, *P*Si*P*). ^{29}Si NMR (benzene-d_6): δ 44.3 (*Si*ClMes$_2$), 13.1 (*Si*Me).

(CyPSiP)Ir(H)(Cl)(CO) (4-4a, b). A thick-walled glass bomb adapted with a Teflon stopcock and containing a magnetic stirbar was charged with a solution of (Cy-PSiP)Ir(H)Cl (0.41 g, 0.50 mmol) in ca. 15 mL of THF. The solution was degassed *via*

three freeze-pump-thaw cycles and 1 atm. of CO was then introduced to the reaction vessel. The color of the solution immediately changed from bright yellow to pale yellow. The reaction mixture was vigorously stirred for an hour at room temperature. The volatile reaction components were subsequently removed *in vacuo* and the remaining residue was triturated with pentane (3 × 5 mL) to afford **(4-4a, b)** (0.39 g, 93% yield) as a pale yellow solid. NMR analysis of **(4-4a, b)** indicated that this compound exists as a mixture of two isomers **(4-4a, b)** - **a**,**b** formed in a ca. 1:1 up to 1:3 ratio. ^{1}H NMR (benzene-d_6): δ 8.12 (d, 2 H, J = 7 Hz, H_{arom}), 7.97 (d, 2 H, J = 7 Hz, H_{arom}), 7.53 (m, 2 H, H_{arom}), 7.52 (m, 2 H, H_{arom}), 7.38 (m, 2 H, H_{arom}), 7.25 (m, 2 H, H_{arom}), 7.23 (m, 2 H, H_{arom}), 7.11 (m, 2 H, H_{arom}), 1.88 – 0.82 (overlapping resonances, 88 H, P*Cy* for **a** + **b**), 0.91 (s, 3 H, Si*Me* for **a**), 0.85 (s, 3 H, Si*Me* for **b**), -8.87 (t, 1 H, $^{2}J_{HP}$ = 17 Hz, Ir-*H* for **a**), -20.15 (t, 1 H, $^{2}J_{HP}$ = 14 Hz, Ir-*H* for **b**). ^{31}P{^{1}H} NMR (benzene-d_6): δ 44.5 (s, **a**), 41.5 (s, **b**).

(CyPSiP)Ir(CO) (4-5). A thick-walled glass bomb adapted with a Teflon stopcock and containing a magnetic stirbar was charged with a solution of **(4-4a, b)** (0.39 g, 0.46 mmol) in ca. 15 mL of THF. The solution was degassed *via* three freeze-pump-thaw cycles and $LiCH_2SiMe_3$ (0.44 g, 0.46 mmol) was added. The color of the reaction mixture changed from pale yellow to dark orange. The reaction mixture was heated at 65 °C for 1 h, over the course of which the color changed to bright red. The volatile components of the reaction mixture were subsequently removed *in vacuo* and the remaining residue was triturated with pentane (3 × 5 mL) and recrystallized from pentane at -35 °C to afford **4-5** (0.26 g, 68% yield) as a bright red solid. ^{1}H NMR (benzene-d_6): δ 8.19 (d, 2 H, J = 4 Hz, H_{arom}), 7.51 (m, 2 H, H_{arom}), 7.31 (m, 2 H, H_{arom}), 7.21 (m, 2 H, H_{arom}), 1.88 – 0.82 (overlapping resonances, 44 H, P*Cy*), 0.80 (s, 3 H, Si*Me*). ^{31}P{^{1}H} NMR (benzene-d_6): δ 71.7. IR (thin

film, cm^{-1}): 1927 (IrCO).

(CyPSiP)Ir(CO)$_2$ (4-6). A thick-walled glass bomb adapted with a Teflon stopcock and containing a magnetic stirbar was charged with a solution of **1-1** (0.20 g, 0.24 mmol) in ca. 15 mL of THF. The solution was degassed *via* three freeze-pump-thaw cycles and 1 atm. of CO was then introduced to the reaction vessel. The reaction mixture was vigorously stirred for an hour at room temperature. An equivalent of $LiCH_2SiMe_3$ (0.022 g, 0.24 mmol) was added to the reaction mixture without exposure of the solution to vacuum. An immediate color change from yellow to orange was observed. The reaction mixture was subsequently heated at 65 °C for 2 h, over the course of which the color changed to dark orange. The volatile components of the reaction mixture were removed *in vacuo* and the remaining residue was triturated with pentane (3 × 5 mL) to afford **4-6** (0.15 g, 77% yield) as a bright orange solid. $^{31}P\{^1H\}$ NMR (121.5 MHz, benzene-d_6): δ 48.2. Crystals of **4-6** suitable for X-ray diffraction analysis were obtained from a concentrated THF/pentane solution at room temperature.

(Cy-PSiP)Ir(CH$_2$SiMe$_3$)COLi (4-7). A thick-walled glass bomb adapted with a Teflon stopcock and containing a magnetic stirbar was charged with a solution of (**4-4a,b**) (0.15 g, 0.18 mmol) in ca. 10 mL of THF. An excess of $LiCH_2SiMe_3$ (0.083 g, 0.89 mmol) was added to the solution. A color change from yellow to orange was observed. The reaction mixture was heated at 65 °C for 2 h, over the course of which a color change to bright yellow was observed. The volatile components of the reaction mixture were removed *in vacuo* and the remaining residue was triturated with pentane (3 × 5 mL) to afford **4-7** (0.142 g, 89% yield) as a bright yellow solid. $^{31}P\{^1H\}$ NMR (benzene-d_6): δ 26.2. ^1H NMR

(benzene-d_6): δ 7.73 (d, 2 H, J = 7 Hz, H_{arom}), 7.51 (m, 2 H, H_{arom}), 7.24 (m, 2 H, H_{arom}), 7.13 (overlapping resonances, 2 H, H_{arom}), 1.88 – 0.82 (overlapping resonances, 44 H, P*Cy*), 0.98 (s, 3 H, Si*Me*), 0.64 (s, 9 H, $CH_2Si\mathit{Me}_3$), -0.01 (s, 2 H, $Ir\mathit{CH}_2SiMe_3$). Crystals of **4-7** suitable for X-Ray diffraction analysis were obtained from a concentrated Et_2O/THF solution at -35 °C.

(CyPSiP)Rh(H)(Cl)(CO) (4-8a, b). A thick-walled glass bomb adapted with a Teflon stopcock and containing a magnetic stirbar was charged with a solution of **1-2** (0.25 g, 0.34 mmol) in ca. 15 mL of THF. The solution was degassed *via* three freeze-pump-thaw cycles and 1 atm. of CO was then introduced to the reaction vessel. The color of the solution immediately changed from A color change from bright orange to pale yellow was observed. The reaction mixture was allowed to stir vigorously at room temperature for an hour. The volatile components of the reaction mixture were subsequently removed under vacuum and the remaining residue was triturated with pentane (3 × 5 mL) to afford (**4-8a, b**) (0.21 g, 82% yield) as a pale orange solid. NMR analysis of (**4-8a, b**) indicated that this compound exists as a mixture of two isomers (**4-8a, b**) - **a**,**b** formed in a ca. 5:1 ratio ^{1}H NMR (benzene-d_6): δ 7.91 (d, J = 7 Hz, H_{arom}), 7.53 (m, H_{arom}), 7.25 (m, H_{arom}), 7.20 - 7.14 (overlapping resonances, H_{arom}), 2.00 – 0.80 (overlapping resonances, P*Cy*), 0.59 (s, Si*Me*), -8.92 (m, Rh-*H*, **a**), -9.22 (m, Rh-*H*, **b**). $^{13}C\{^1H\}$ NMR (benzene-d_6): δ 196.5 (d, J = 113 Hz, *C*O), 156.4 (apparent t, J = 22 Hz, Quat. C_{arom}), 142.4 (apparent dt, J = 23, 4 Hz, Quat. C_{arom}), 132.5 (apparent t, J = 9.0, CH_{arom}), 129.5 (d, J = 11 Hz, CH_{arom}), 128.1 - 127.4 (overlapping resonances, CH_{arom}), 36.1 (m, CH_{Cy}), 34.4 (apparent t, J = 14 Hz, CH_{Cy}), 29.5 – 25.4 (overlapping resonances, CH_{2Cy}), 9.12 (Si*Me*). $^{31}P\{^1H\}$ NMR (benzene-d_6): δ 71.0 (d, $^1J_{RhP}$ = 106 Hz, **a**), 69.5 (d, $^1J_{RhP}$ = 106 Hz, **b**). ^{29}Si NMR (benzene-d_6): δ 50.0.

(CyPSiP)Rh(CO) (4-9). A thick-walled glass bomb adapted with a Teflon stopcock and containing a magnetic stirbar was charged with a solution of (**4-8a, b**) (0.47 g, 0.62 mmol) in ca. 15 mL of THF. An equivalent of $LiCH_2SiMe_3$(0.061 g, 0.65 mmol) was added to the reaction mixture. The resulting solution was heated at 60 °C for 1 h. The volatile components of the reaction mixture were removed under vacuum and the remaining residue was extracted with pentane (ca. 25 mL). The pentane extracts were filtered through a glass fiber filter and the filtrate solution was concentrated in vacuo to afford **4-9** (0.40 g, 89% yield) as an orange crystalline solid. ^{1}H NMR (benzene-d_6): δ 8.19 (d, 2 H, J = 7 Hz, H_{arom}), 7.52 (m, 2 H, H_{arom}), 7.35 (m, 2 H, H_{arom}), 7.23 (m, 2 H, H_{arom}), 1.88 – 0.82 (overlapping resonances, 44 H, P*Cy*), 0.79 (s, 3 H, Si*Me*). ^{13}C{^{1}H} NMR (benzene-d_6): δ 203.3 (d, $^2J_{CRh}$ = 188 Hz, Rh*C*O), 159.1 (apparent t, J = 26.5 Hz, Quat C_{arom}), 144.90 (apparent dt, J = 22, 5 Hz, Quat C_{arom}), 133.5 (apparent t, J = 11, CH_{arom}), 130.4 (CH_{arom}), 129.9 (CH_{arom}), 127.9 (CH_{arom}), 40.4 (apparent t, J = 10 Hz, CH_{Cy}), 39.4 (apparent t, J = 12 Hz, CH_{Cy}), 31.7 (CH_{2Cy}), 30.4 (CH_{2Cy}), 30.3 (CH_{2Cy}), 27.7 – 27.2 (overlapping resonances, CH_{2Cy}), 27.0 (CH_{2Cy}), 26.4 (CH_{2Cy}), 8.9 (Si*Me*). ^{31}P{^{1}H} NMR (benzene-d_6): δ 76.6 (d, $^1J_{RhP}$ = 155 Hz). ^{29}Si NMR (benzene-d_6): δ 69.1.

(CyPSiP)Rh(CO)(Me)(I) (4-10). A solution of **4-9** (0.020 g, 0.028 mmol) in ca. 5 mL of pentane was treated with MeI (1 M solution in pentane, 0.028 mmol). The reaction mixture was allowed to stand at room temperature for 2 h, over the course of which a color change from bright orange color to yellow was observed. The volatile components of the reaction mixture were removed under vacuum to afford **4-10** (0.022 g, 93% yield) as a pale yellow solid. ^{1}H NMR (benzene-d_6): δ 7.92 (d, 2 H, J = 6.9 Hz, H_{arom}), 7.54 (m, 2 H, H_{arom}), 7.20 (m, 2 H, H_{arom}), 7.17 (m, 2 H, H_{arom}), 1.88 – 0.82 (overlapping resonances, 44 H, P*Cy*),

0.83 (s, 3 H, Si*Me*), 0.41 (dt, 3 H, $^{1}J_{HRh}$ = 2 Hz, $^{2}J_{PH}$ = 7 Hz, Rh*Me*). $^{31}P\{^{1}H\}$ NMR (benzene-d_6): δ 56.9 (d, $^{1}J_{PRh}$ = 103 Hz).

(CyPSiP)Ir(H)(Cl)(PMe$_3$) (4-11a, b). A solution of **1-1** (0.025 g, 0.030 mmol) in ca. 5 mL of benzene was prepared in a vial treated with 1.1 equiv. of PMe_3 (0.033 mL, 0.033 mmol, from a 1 M stock solution of PMe_3 in benzene). The reaction mixture was allowed to stand at room temperature for 15 min to ensure reaction completion, over the course of which a color change from bright yellow to pale yellow was observed. The volatile components of the reaction mixture were removed *in vacuo* to afford (**4-11a,b**) (0.028 g, 93% yield) as a pale yellow solid. NMR analysis of (**4-11a, b**) indicated that this compound exists as a mixture of two isomers (**4-11a, b**) - **a**,**b** formed in a ca. 3.5 : 1 ratio. ^{1}H NMR (benzene-d_6): δ 8.29 (d, 2 H, *J* = 7 Hz, H_{arom}, **4-11b**), 8.12 (d, 2 H, *J* = 7 Hz, H_{arom}, **4-11a**), 7.64 (m, 2 H, H_{arom}, **4-11b**), 7.41 (m, 2 H, H_{arom}, **4-11a**), 7.27 (m, 2 H, H_{arom}, **4-11b**), 7.19 (m, 2 H, H_{arom}, **4-11a**), 7.06 (overlapping resonance **a** and **b**, 2 H, H_{arom}), 3.62 (m, 2 H, CH_{Cy}, **4-11a**), 3.16 (m, 2 H, CH_{Cy}, **4-11a**), 2.77 – 0.32 (overlapping resonances, 40 H, P*Cy*, **4-11a**; overlapping resonances, 44 H, P*Cy*, **4-11b**), 1.66 (d, 9 H, *J* = 7.5 Hz, PMe_3, **4-11a**), 1.64 (d, 9 H, *J* = 6.6 Hz, PMe_3, **4-11b**), 0.96 (d, 3 H, *J* = 2 Hz, Si*Me*, **4-11b**) 0.92 (s, 3 H, Si*Me*, **4-11a**), -13.02 (dt, 3 H, $^{2}J_{HP\,trans}$ = 126 Hz, $^{2}J_{HP\,cis}$ = 20 Hz, Ir*H*, **4-11a**), -23.45 (dt, 3 H, $^{2}J_{HP}$ = 7 Hz, $^{2}J_{HP}$ = 16 Hz, Ir*H*, **4-11b**). $^{31}P\{^{1}H\}$ NMR (benzene-d_6): δ 34.0 (d, 2 P, $^{2}J_{PP}$ = 17 Hz, *P*Si*P*, **4-11b**), 32.3 (d, 2 P, $^{2}J_{PP}$ = 17 Hz, *P*Si*P*, **4-11a**), -53.7 (m, 1 P, Ir-*P*Me$_3$, **4-11a**), -56.5 (t, 1 P, $^{2}J_{PP}$ = 17 Hz, Ir-*P*Me$_3$, **4-11b**).

(CyPSiP)Ir(PMe$_3$) (4-12). A solution of **4-11a,b** (0.066 g, 0.073 mmol) in benzene was treated with $LiCH_2SiMe_3$ (0.008 g, 0.081 mmol) at room temperature over the course of 20 min. An immediate color change was observed from pale yellow to deep red. The

solution was filtered through Celite, then solvent and volatiles were removed *in vacuo*, affording **4-12** in quantitative yield (0.063 g, 0.073 mmol) as a dark red solid. NMR data was consistent with previously reported data.[66]

(CyPSiP)Rh(H)(OTf) (4-13). A solution of **1-2** (0.25 g, 0.34 mmol) in ca. 10 mL of C_6H_5F was treated with AgOTf (0.088 mg, 0.34 mmol). After standing at room temperature for 1 h, the volatile components of the reaction mixture were removed under vacuum and the remaining residue was extracted with THF (ca. 25 mL). The THF extracts were filtered through a glass fiber filter. The volatile components of the filtrate solution were removed under vacuum to afford **4-13** (0.28 g, 97% yield) as a pale yellow solid. ^{1}H NMR (benzene-d_6): δ 7.85 (d, 2 H, J = 7 Hz, H_{arom}), 7.31 (m, 2 H, H_{arom}), 7.21 (m, 2 H, H_{arom}), 7.11 (m, 2 H, H_{arom}), 1.88 – 0.82 (overlapping resonances, 44 H, P*Cy*), 0.90 (s, 3 H, Si*Me*), -22.45 (dt, $^1J_{RhH}$ = 35 Hz, $^2J_{PH}$ = 12 Hz). ^{13}C{^{1}H} NMR (benzene-d_6): δ 155.8 (C_{arom}), 139.5 (C_{arom}), 132.0 (apparent t, J = 8 Hz, CH_{arom}), 130.8 (CH_{arom}), 129.7 (CH_{arom}), 127.7 (CH_{arom}), 34.5 (CH_{Cy}), 34.0 (CH_{Cy}), 30.5 (CH_{2Cy}), 29.7 (CH_{2Cy}), 29.2 (CH_{2Cy}), 27.3 (CH_{2Cy}), 27.0 – 26.4 (overlapping resonances, CH_{2Cy}), 26.0 (CH_{2Cy}), 6.8 (Si*Me*). ^{31}P{^{1}H} NMR (benzene-d_6): δ 59.4 (d, 2 P, J_{Rh-P} = 119 Hz). ^{29}Si NMR (benzene-d_6): δ 69.06. ^{19}F{^{1}H} NMR (benzene-d_6): δ -76.4 (br, OSO_2CF_3) X-ray quality crystals of **4-13** were obtained from a concentrated pentane solution at low temperature (-35 °C).

(CyPSiP)Rh(H)(BF_4) (4-14). A solution of **1-2** (0.25 g, 0.34 mmol) in ca. 10 mL of C_6H_5F was treated with $AgBF_4$ (0.067 g, 0.34 mmol). After standing at room temperature for 1 h, the volatile components of the reaction mixture were removed under vacuum and the remaining residue was extracted with THF (ca. 15 mL). The THF extracts were filtered through a glass fiber filter. The volatile components of the filtrate solution

were removed under vacuum to afford **4-14** (0.25 g, 95% yield) as a pale yellow solid. ^{1}H NMR (500 MHz, benzene-d_6): δ 7.85 (d, 2 H, J = 6 Hz, H_{arom}), 7.32 (m, 2 H, H_{arom}), 7.21 (m, 2 H, H_{arom}), 7.15 (m, 2 H, H_{arom}), 1.88 – 0.82 (overlapping resonances, 44 H, P*Cy*), 0.85 (s, 3 H, Si*Me*), -24.4 (m, 1 H, Rh-H). ^{31}P{^{1}H} NMR (300 K, 202.47 MHz, benzene-d_6): δ 59.1 (d, 2 P, J_{Rh-P} = 121 Hz). ^{19}F NMR (470.59 MHz, benzene-d_6): δ -112.9 (m, BF_4). X-ray quality crystals of **4-14** were obtained from a concentrated pentane solution at low temperature (-35 °C).

[(κ^2–$Me_2SiC_6H_4PCy_2$)(κ^2–$C_6H_4PCy_2$)Ir(OTf)] (4-15). A solution of **1-1** (0.030 g, 0.037 mmol) in ca. 10 mL of Et_2O was treated with $LiCH_2SiMe_3$ (0.004 g, 0.040 mmol), an immediate color change from bright yellow to dark orange was observed, forming **1-3**. Then, MeOTf (0.007 g, 0.040 mmol) was added *via* syringe to the mixture. The resulting bright orange reaction mixture was allowed to stand at room temperature for 1 h, at which point the volatile components of the reaction mixture were removed *in vacuo*. The remaining residue was extracted with ca. 5 mL of benzene, and the benzene extracts were filtered through Celite. The filtrate solution was collected and dried under vacuum. The remaining residue was triturated with 3 × 5 mL pentane and subsequently dried under vacuum to afford **4-15** (84% conversion by ^{31}P NMR) as a yellow-orange solid. ^{31}P{^{1}H} NMR (benzene-d_6): δ 52.6 (d, 1 P, $^{2}J_{PP}$ = 300 Hz, *P*Si*P*), -24.6 (d, 1 P, $^{2}J_{PP}$ = 300 Hz, *P*Si*P*). Crystals suitable for X-ray diffraction analysis were obtained from a concentrated benzene solution of **4-15** at room temperature.

(CyPSiP)Rh(Me)(OTf) (4-16). A solution of **1-2** (0.035 g, 0.048 mmol) in ca. 10 mL of C_6H_5F was treated with $LiCH_2SiMe_3$ (0.005 g, 0.053 mmol), an immediate color change from yellow to dark orange was observed, forming **1-4**. Then, MeOTf (0.009 g,

0.053 mmol) was added *via* syringe to the mixture. The resulting bright orange reaction mixture was allowed to stand at room temperature for 1 h, at which point the volatile components of the reaction mixture were removed *in vacuo*. The remaining residue was extracted with ca. 5 mL of benzene, and the benzene extracts were filtered through Celite. The filtrate solution was collected and dried under vacuum. The remaining residue was triturated with 3 × 5 mL pentane and subsequently dried under vacuum to afford **4-16** (0.031 g, 75% yield) as a pale yellow solid. ^{1}H NMR (benzene-d_6): δ 7.91 (d, 2 H, J = 7 Hz, H_{arom}), 7.35 (m, 2 H, H_{arom}), 7.23 (m, 2 H, H_{arom}), 7.13 (m, 2 H, H_{arom}), 3.00 (apparent t, 2 H, J = 11 Hz, CH_{Cy}), 2.63 (m, 2 H, CH_{Cy}), 2.48 (m, 4 H, CH_{2Cy}), 2.27 – 0.68 (overlapping resonances, 36 H, P*Cy*), 1.00 (s, 3 H, Si*Me*), 0.49 (dt, 3 H, $^{2}J_{RhH}$ = 1.7 Hz, $^{3}J_{PH}$ = 6 Hz, Rh*Me*). ^{13}C{^{1}H} NMR (benzene-d_6): δ 157.9 (C_{arom}), 136.7 (C_{arom}), 133.0 (CH$_{arom}$), 132.6 (apparent t, J = 9, CH$_{arom}$), 129.7 (CH$_{arom}$), 127.8 (CH$_{arom}$), 35.7 (apparent t, J = 10 Hz, CH$_{Cy}$), 34.9 (apparent t, J = 11 Hz, CH$_{Cy}$), 31.5 (CH$_{2Cy}$), 29.6 (m, CH$_{2Cy}$), 28.3 (m, CH$_{2Cy}$), 28.0 – 27.0 (overlapping resonances, CH$_{2Cy}$), 26.4 (CH$_{2Cy}$), 9.8 (Si*Me*), 2.1 (Rh*Me*). ^{31}P{^{1}H} NMR (benzene-d_6): δ 54.6 (d, 2 P, $^{1}J_{PRh}$ = 120 Hz, *P*Si*P*). ^{29}Si NMR (benzene-d_6): δ 50.1. ^{19}F{^{1}H} NMR (benzene-d_6): δ -75.8.

(CyPSiP)Ir(PMe$_3$)(Me)(OTf) (4-17). A solution of **4-12** (0.046 g, 0.054 mmol) in ca. 10 mL of pentane was treated with MeOTf (0.010 g, 0.069 mmol), which was added *via* syringe to the mixture. An immediate color change from dark red to yellow was observed, forming **4-17**. The resulting bright yellow reaction mixture was allowed to stand at room temperature for 1 h, at which point the volatile components of the reaction mixture were removed *in vacuo*. The remaining residue was extracted with ca. 5 mL of benzene, and the benzene extracts were filtered through Celite. The filtrate solution was collected

and dried under vacuum. The remaining residue was triturated with 3 × 5 mL pentane and subsequently dried under vacuum to afford **4-17** (0.055 g, >99% yield) as a yellow solid. ^{1}H NMR (dichloromethane-d_2): δ 7.86 (m, 1 H, H_{arom}), 7.78 (d, 1 H, J = 7 Hz, H_{arom}), 7.63 (m, 1 H, H_{arom}), 7.50 (m, 1 H, H_{arom}), 7.43 – 7.30 (overlapping resonances, 4 H, H_{arom}), 2.87 (m, 1 H, CH_{Cy}), 2.74 (m, 1 H, CH_{Cy}), 2.58 (m, 1 H, CH_{Cy}), 2.49 (m, 1 H, CH_{Cy}), 2.48 (m, 4 H, CH_{2Cy}), 2.29 – 0.79 (overlapping resonances, 36 H, P*Cy*), 1.28 (dd, 9 H, $^{2}J_{PH}$ = 8 Hz, $^{4}J_{PH\textit{trans}}$ = 1.8 Hz, P*Me*$_3$), 1.17 (m, 3 H, Ir*Me*), 0.77 (s, 3 H, Si*Me*), 0.43 (m, 2 H, CH_{2Cy}), 0.00 (m, 2 H, CH_{2Cy}). ^{13}C{^{1}H} NMR (dichloromethane-d_2): δ 153.0 (C_{arom}), 145.5 (C_{arom}), 142.1 (C_{arom}), 147.4 (C_{arom}), 132.9 (d, J = 19 Hz, CH_{arom}), 132.4 (CH_{arom}), 132.1 (CH_{arom}), 131.1 (d, J = 14 Hz, CH_{arom}), 130.7 (CH_{arom}), 129.9 (d, J = 6 Hz, CH_{arom}), 128.8 (CH_{arom}), 128.7 (CH_{arom}), 43.4 (d, J = 26 Hz, CH_{Cy}), 42.3 (d, J = 19 Hz, CH_{Cy}), 37.8 (d, J = 17 Hz, CH_{Cy}), 33.2 (d, J = 5 Hz, CH_{2Cy}), 32.4 (d, J = 29 Hz, CH_{Cy}), 32.3 (d, J = 3 Hz, CH_{2Cy}), 31.9 (m, CH_{2Cy}), 30.9 (d, J = 5 Hz, CH_{2Cy}), 30.0 (CH_{2Cy}), 29.6 (CH_{2Cy}), 28.8 (m, CH_{2Cy}), 28.5 – 27.8 (overlapping resonances, CH_{2Cy}), 27.6 (d, J = 8.5 Hz, CH_{2Cy}), 27.1 (d, J = 13 Hz, CH_{2Cy}), 26.2 (CH_{2Cy}), 26.0 (d, J = 15.5 Hz, CH_{2Cy}), 16.4 (d, J = 36.5 Hz, P(CH_3)$_3$), 11.8 (br, Ir-*Me*), 1.3 (Si*Me*). ^{31}P{^{1}H} NMR (dichloromethane-d_2): δ 49.7 (dd, 1 P, $^{2}J_{PP\textit{trans}}$ = 310 Hz, $^{2}J_{PP\textit{cis}}$ = 10 Hz, *P*Cy$_2$), 35.7 (dd, 1 P, $^{2}J_{PP\textit{cis}}$ = 13 Hz, $^{2}J_{PP\textit{cis}}$ = 13 Hz, *P*Cy$_2$), -10.2 (dd, 1 P, $^{2}J_{PP\textit{trans}}$ = 310 Hz, $^{2}J_{PP\textit{cis}}$ = 15 Hz, *P*Me$_3$). ^{29}Si NMR (benzene-d_6): δ 18.6. ^{19}F{^{1}H} NMR (dichloromethane-d_2): δ -78.9.

[(κ^2–Me$_2$SiC$_6$H$_4$PCy$_2$)(κ^2–C$_6$H$_4$PCy$_2$)Ir(PMe$_3$)(OTf)] (4-18). ***NMR-Scale*** In a NMR tube, **4-17** (0.025 g, 0.024 mmol) was dissolved in C_6D_6, generating a yellow solution. The NMR tube was sealed and heated at 80 °C for 3 h. The color is slightly darker yellow, quantitative conversion was observed by ^{31}P{^{1}H} NMR. ^{31}P{^{1}H} NMR (benzene-

d$_6$): δ 47.9 (dd, 1 P, $^2J_{PP}$*trans* = 260 Hz, $^2J_{PP}$*cis* = 14 Hz, *P*Cy$_2$), -25.4 (dd, 1 P, $^2J_{PP}$*cis* = 15 Hz, $^2J_{PP}$*cis* = 15 Hz, *P*Cy$_2$), -45.8 (dd, 1 P, $^2J_{PP}$*trans* = 260 Hz, $^2J_{PP}$*cis* = 20 Hz, *P*Me$_3$).

(CyPSiP)Ir(PMe$_3$)(Me)(CO)$^+$(OTf)$^-$ (4-19). ***NMR-Scale*** In a J-Young NMR tube with a teflon stopcock, **4-17** (0.010 g, 0.010 mmol) was dissolved in CD_2Cl_2, generating a yellow solution. The NMR tube was freeze-pump-thawed 2 times and 1 atm. of CO was added at room temperature. An immediate color change to pale yellow was observed. Conversion from **4-17** to **4-19** was achieved in 94% (NMR yield). ^{1}H NMR (dichloromethane-*d*$_2$): δ 8.21 (d, 2 H, *J* = 7 Hz, *H*$_{arom}$), 7.84 (m, 2 H, *H*$_{arom}$), 7.57 (m, 2 H, *H*$_{arom}$), 7.47 (m, 2 H, *H*$_{arom}$), 2.79 (m, 2 H, C*H*$_{Cy}$), 2.33 (m, 2 H, C*H*$_{Cy}$), 2.79 (C*H*$_{Cy}$), 2.20 – 0.84 (overlapping resonances, 40 H, P*Cy*), 1.90 (d, 9 H, $^2J_{PH}$ = 8 Hz, P*Me*$_3$), 0.57 (s, 3 H, Si*Me*), 0.13 (dt, 3 H, $^3J_{PH}$*trans* = 15 Hz, $^3J_{PH}$*cis* = 6 Hz, Ir*Me*). ^{31}P{^{1}H} NMR (dichloromethane-*d*$_2$): δ 19.3 (d, 2 P, $^2J_{PP}$ = 14 Hz, *P*Cy$_2$), -66.6 (t, 1 P, $^2J_{PP}$ = 14 Hz, *P*Me$_3$). IR (Thin film, NaCl plates, cm^{-1}): 2012 (Ir*CO*).

(CyPSiP)Ir(PMe$_3$)(Me)(NH$_3$)$^+$(OTf)$^-$ (4-20). ***NMR-Scale*** In a J-Young NMR tube with a teflon stopcock, **4-17** (0.010 g, 0.010 mmol) was dissolved in CD_2Cl_2, generating a yellow solution. The NMR tube was freeze-pump-thawed 2 times and 1 atm. of NH_3 was added at room temperature. An immediate color change to pale yellow was observed. Conversion from **4-17** to **4-20** was achieved in quantitative yield (NMR yield). ^{1}H NMR (dichloromethane-*d*$_2$): δ 8.08 (d, 2 H, *J* = 7 Hz, *H*$_{arom}$), 7.84 (m, 2 H, *H*$_{arom}$), 7.47 – 7.27 (overlapping resonances, 6 H, *H*$_{arom}$), 3.18 (br, 3 H, IrN*H*$_3$), 2.18 – 0.81 (overlapping resonances, 40 H, P*Cy*), 1.76 (d, 9 H, $^2J_{PH}$ = 7 Hz, P*Me*$_3$), 0.66 (s, 3 H, Si*Me*), 0.19 (d, 2 H, C*H*$_{2Cy}$), -0.45 (dt, 3 H, $^3J_{PH}$ = 4 Hz, $^3J_{PH}$ = 7 Hz, Ir*Me*). ^{31}P{^{1}H} NMR (dichloromethane-*d*$_2$): δ 28.1 (br, 2 P, *P*Cy$_2$), -59.1 (t, 1 P, $^2J_{PP}$ = 16 Hz, *P*Me$_3$).

(CyPSiP)Ir(PMe$_3$)(CC^{t}Bu)(OTf) (4-21). A solution of **4-17** (0.035 g, 0.034 mmol) in ca. 10 mL of CH_2Cl_2 was treated with 3,3-dimethyl-1-butyne (0.003 g, 0.034 mmol), which was added *via* syringe (from a stock solution in CH_2Cl_2) to the mixture. Upon addition of the 3,3-dimethyl-1-butyne, no noticeable color change was observed. The formation of **4-21** was quantitative by ^{31}P NMR. The resulting orange reaction mixture was allowed to stand at room temperature for 1 h, at which point the volatile components of the reaction mixture were removed *in vacuo*. The remaining residue was extracted with ca. 5 mL of CH_2Cl_2, and the CH_2Cl_2 extracts were filtered through Celite. The filtrate solution was collected and dried under vacuum. The remaining residue was triturated with 3 × 5 mL pentane and subsequently dried under vacuum to afford **4-21** (0.034 g, 93% yield) as a bright yellow solid. ^{1}H NMR (dichloromethane-d_2): δ 7.85 (apparent t, 1 H, J = 7 Hz H_{arom}), 7.80 (d, 1 H, J = 7 Hz, H_{arom}), 7.62 (apparent t, 1 H, J = 7 Hz, H_{arom}), 7.51 (m, 1 H, H_{arom}), 7.44 – 7.35 (overlapping resonances, 4 H, H_{arom}), 3.30 (m, 1 H, CH_{Cy}), 2.93 (m, 1 H, CH_{Cy}), 2.60 – 2.45 (overlapping resonances, 4 H, CH_{Cy} + CH_{2Cy}), 2.29 (d, 1 H, J = 11 Hz, CH_{Cy}), 2.18 – 0.72 (overlapping resonances, 33 H, P*Cy*), 1.42 (dd, 9 H, $^2J_{PH}$ = 9.6 Hz, $^4J_{PH\textit{trans}}$ = 2 Hz, P*Me$_3$*), 1.31 (s, 9 H, CC^t*Bu*), 0.87 (s, 3 H, Si*Me*), 0.50 (m, 1 H, CH_{2Cy}), 0.23 (m, 1 H, CH_{2Cy}), 0.07 (m, 1 H, CH_{2Cy}), -0.02 (m, 1 H, CH_{2Cy}). ^{13}C{^{1}H} NMR (dichloromethane-d_2): δ 155.4 (Ir*C*C^{t}Bu), 152.6 (C_{arom}), 142.0 (C_{arom}), 141.1 (C_{arom}), 136.8 (C_{arom}), 135.3 (Ir*C*C^{t}Bu), 133.0 (*C*H$_{arom}$), 132.9 (d, J = 9 Hz, *C*H$_{arom}$), 132.7 (*C*H$_{arom}$), 131.6 (*C*H$_{arom}$), 131.0 (*C*H$_{arom}$), 130.1 (d, J = 6 Hz, *C*H$_{arom}$), 128.9 (d, J = 6 Hz, *C*H$_{arom}$), 43.0 (m, *C*H$_{Cy}$), 37.7 (d, J = 21 Hz, *C*H$_{Cy}$), 34.7 (d, J = 33 Hz, *C*H$_{Cy}$), 33.1 (d, J = 4 Hz, *C*H$_{2Cy}$), 32.9 (*C*H$_{2Cy}$), 32.4 (d, J = 4 Hz, *C*H$_{2Cy}$), 31.8 (CC(C(*C*H$_3$)$_3$)), 30.9 (d, J = 3 Hz, *C*H$_{2Cy}$), 29.4 (*C*H$_{2Cy}$), 29.0 (*C*H$_{2Cy}$), 28.4 – 27.8 (overlapping resonances, *C*H$_{2Cy}$), 27.4 (d, J = 9 Hz,

*C*H$_{2Cy}$), 26.6 (d, *J* = 14 Hz, *C*H$_{2Cy}$), 26.2 (d, *J* = 6 Hz, *C*H$_{2Cy}$), 26.0 (*C*H$_{2Cy}$), 25.8 (*C*H$_{2Cy}$), 17.7 (d, *J* = 38 Hz, P(*C*H$_3$)$_3$), 1.5 (Si*Me*). ^{31}P{^{1}H} NMR (dichloromethane-d_2): δ 49.7 (dd, 1 P, $^2J_{PP\,trans}$ = 299 Hz, $^2J_{PP\,cis}$ = 12 Hz, *P*Cy$_2$), 31.6 (dd, 1 P, $^2J_{PP\,cis}$ = 13 Hz, $^2J_{PP\,cis}$ = 13 Hz, *P*Cy$_2$), -12.6 (dd, 1 P, $^2J_{PP\,trans}$ = 297 Hz, $^2J_{PP\,cis}$ = 17 Hz, *P*Me$_3$). ^{29}Si NMR (benzene-d_6): δ 23.7. ^{19}F{^{1}H} NMR (dichloromethane-d_2): δ -78.9.

(CyPSiP)Ir(PMe$_3$)(Me)$^+$(B(C$_6$F$_5$)$_4$)$^-$ (4-22). In a vial, **4-17** (0.072 g, 0.071 mmol) was dissolved in C$_6$H$_5$F, generating a yellow solution. Then AgB(C$_6$F$_5$)$_4$ (0.072 g, 0.092 mmol) was added at room temperature. An immediate precipitate was observed and a change to paler yellow was observed. Conversion from **4-17** to **4-22** was achieved in quantitative yield (NMR yield). ^{1}H NMR (dichloromethane-d_2): δ 7.86 (m, 1 H, *H*$_{arom}$), 7.77 (d, 1 H, *J* = 7 Hz, *H*$_{arom}$), 7.63 (m, 1 H, *H*$_{arom}$), 7.48 (m, 1 H, *H*$_{arom}$), 7.51 – 7.30 (overlapping resonances, 4 H, *H*$_{arom}$), 2.88 (br, 1 H, C*H*$_{Cy}$), 2.74 (br, 1 H, C*H*$_{Cy}$), 2.58 – 2.42 (overlapping resonances, 2 H, C*H*$_{Cy}$), 2.28 – 0.79 (overlapping resonances, 36 H, P*Cy*), 1.27 (dd, 9 H, $^2J_{PH}$ = 8 Hz, $^2J_{PH}$ = 2 Hz, P*Me$_3$*), 1.17 (m, 3 H, Ir*Me*), 0.77 (s, 3 H, Si*Me*), 0.45 (m, 2 H, C*H*$_{2Cy}$), 0.00 (m, 2 H, C*H*$_{2Cy}$). ^{31}P{^{1}H} NMR (dichloromethane-d_2): δ 49.7 (dd, 1 P, $^2J_{PP\,trans}$ = 311 Hz, $^2J_{PP\,cis}$ = 9 Hz, *P*Cy$_2$), 35.7 (m, 1 P, *P*Cy$_2$), -10.5 (dd, 1 P, $^2J_{PP\,trans}$ = 311 Hz, $^2J_{PP\,cis}$ = 14 Hz, *P*Cy$_2$). ^{19}F{^{1}H} NMR (dichloromethane-d_2): δ -133.1 (m, *o*-C*F*), -163.6 (t, *p*-C*F*), -167.5 (brt, *m*-C*F*).

4.4.3 Crystallographic Solution and Refinement Details

Crystallographic data for each of **4-1**, **4-6**, **4-7**, **4-9**, **4-13**, **4-14** and **4-15** were obtained at 173(±2)K on a Bruker D8/APEX II CCD diffractometer using either graphite-monochromated Mo Kα (λ = 0.71073 Å) radiation (for **4-6**, **4-7**, **4-9** and **4-14**) or CuKα (λ

=1.54178 Å, microfocus source) radiation (for **4-1**, **4-13** and **4-15**), employing a sample that was mounted in inert oil and transferred to a cold gas stream on the diffractometer. Programs for diffractometer operation, data collection, and data reduction (including SAINT) were supplied by Bruker. Gaussian integration (face-indexed) was employed as the absorption correction method for **4-1**, **4-6**, **4-7**, **4-9**, **4-13**, **4-14**, and **4-15**. The structure of **4-6**, **4-7**, **4-9** and **4-15** were solved by use of the Patterson search/structure expansion, and **4-1**, **4-13**, **4-14**, was solved by use of intrinsic phasing methods. All structures were refined by use of full-matrix least-squares procedures (on F^2) with R_1 based on $F_o^2 \geq 2\sigma(F_o^2)$ and wR_2 based on $F_o^2 \geq -3\sigma(F_o^2)$.

For **4-1**, disorder involving the $SiHPh_2$ group was observed. The constituent atoms were modelled over two positions (A and B), such that C71A, C72A, C73A, C74A, C75A, C76A, C81A, C82A, C83A, C84A, C85A and C86A were refined with an occupancy factor of 0.816(3), while C71B, C72B, C73B, C74B, C75B, C76B, C81B, C82B, C83B, C84B, C85B and C86B were refined with an occupancy factor of 0.184(3). Anisotropic displacement parameters were employed for all the non-hydrogen atoms in **4-1**. The distances of the C71B to C86B atoms and adjacent carbons, as well as the according angles were constrained during refinement.

For **4-7**, disorder involving ethereal solvents bound to a Li atom (Et_2O and THF) were refined with an occupancy factor of 0.5 (involving atoms O4A, O4B, C91A, C92A, C93A, C94A, C91B, C92B, C93B, C94B. Anisotropic displacement parameters were employed for all the non-hydrogen atoms in **4-7**.

For **4-14**, disorder involving a fluorobenzene solvent unit was refined with an occupancy factor of 0.5 (involving atoms F1S and F3S). Anisotropic displacement

parameters were employed for all the non-hydrogen atoms in **4-14**. The distances between C1S and C2S, C1S and C6S, C2S and C3S, C3S and C4S, C4S and C5S, C5S and C6S, as well as the relevant angles were constrained during refinement with a value of 1.3900 Å and 120.0°.

Anisotropic displacement parameters were employed throughout for the non-hydrogen atoms. In the case of compounds containing metal-hydride bonds (M-*H*) such as **4-1, 4-13** and **4-14**: Ir-*H* (H1), Rh-*H* (H1) and Rh-*H* (H1) respectively, were located in the difference Fourier map and refined isotropically. All remaining hydrogen atoms were added at calculated positions and refined by use of a riding model employing isotropic displacement parameters based on the isotropic displacement parameter of the attached atom. Additional crystallographic information is provided in Appendix A.

Chapter 5: Conclusions and Future Work

5.1 Summary and Conclusions

As outlined in Chapter 1, pincer-type complexes are an important area of research leading to useful and reliable catalytic applications. Remarkable examples of catalysis featuring C-H and N-H bond activation have been reported, involving precious metals, notably Group 9 metals. Throughout the decades, ligand design, protocols and methods improved greatly to yield performant, efficient and well-thought frameworks that constitute robust systems for an ever-growing amount of catalytic applications. As a part of this quest for improvement and better design, the Turculet group focused on a modular and different ligand design: PSiP silyl pincer type complexes. Successful examples of C-H and N-H bond activation were reported with this new system, and the reactivity of these complexes towards other E-H bond activation (ie. P-H, O-H and Si-H) was remaining unexplored. This document contributes to a better understanding of said reactivity, and also details several methods, challenges and successful preparations in the context of further exploring bond activation.

In Chapter 2, efforts were directed at preparing and isolating rare, monomeric phosphido-hydride species. As the investigation progressed, a trend involving the steric bulk of reacted phosphides started to be visible: bulkier phosphides would tend to readily reductively eliminate forming phosphine complexes (**2-2a-c**) while less bulky ones, including primary phosphides, would lead to stable phosphido-hydride complexes (**2-1, 2-3a-d**). These species were successfully synthesized *via* P-H oxidative addition. Unfortunately, efforts at isolating Rh phosphido-hydride species were unsuccessful as only Rh phosphine complexes were isolated (**2-4a-d**), due to the fast P-H reductive elimination

of any phosphido-hydride intermediate.

The reactivity of Ir phosphido-hydride complexes was explored and has shown that migratory insertion of unsaturated substrates in the Ir-P bond that was initially targeted was not an accessible reaction. Yet, these complexes showed interesting reactivities with hydrosilanes, terminal alkynes and H_2, undergoing a P-H reductive elimination and a subsequent E-H oxidative addition (**2-8**, **2-9** and **2-10**). These encouraging elements of research are providing interesting opportunities for new late transition metal terminal phosphido hydride species applications, including in P-C and P-P bond formation reactions.

In Chapter 3, investigation of O-H bond oxidative addition was probed. First, the initially targeted alkoxo, aryloxo and hydroxo Ir hydride complexes were synthesized *via* protonolysis reactions. These mononuclear, coordinatively unsaturated complexes are relatively rare and did not exhibit reductive elimination in standard conditions. They were readily isolable, although sensitivity towards alkali metal halide impurities was observed. A reccurent issue of (Cy-PSiP)Ir(H)X (X = halide) competing with the formation of (Cy-PSiP)Ir(H)OR type species was observed.

Once the synthetic accessibility of (Cy-PSiP)Ir(H)OR complexes was demonstrated, attempts to prepare said complexes by an oxidative addition route proved significantly more challenging than anticipated with respect to analogous N-H oxidative addition. Mitigated success was observed as reactions between (Cy-PSiP)Ir^{I} and alcohols have shown that aryloxy-hydride complexes are more easily accessible than alkoxy-hydride complexes. Efforts were made towards achieving water activation to generate an Ir hydroxy-hydride complex. Unfortunately, this reaction was found to be challenging, and

despite utilizing harsh conditions and a large excess of water, no product of water activation was observed. However (Cy-PSiP)Ir(H)(OH) was synthesized by an alternative route and a crystallographic structure of this complex was solved and refined. These studies provide new insights with respect to bond activation chemistry in general, and better understanding of coordinatively unsaturated late transition metal aryloxo/alkoxo/hydroxo species.

Lastly, in Chapter 4, particular attention was given to Si-H bond activation, mediated by both Ir and Rh complexes. Stable, isolable silyl hydride iridium complexes were discussed (**4-1, 4-2** and **4-3**) and successfully prepared. A particular challenge concerning uncontrollable reactivity with smaller hydrosilanes towards Ir^{I} and Rh^{I} complexes was exposed and methods to circumvent it were proposed.

In this context, routes to synthesize Ir^{I} complexes stabilized with a neutral, L donor ligand were explored. The isolation of carbonyl complexes (**4-5** and **4-9**) was discussed, although their synthesis is sensitive to conditions thus hardly reproducible and the reactivity of related complexes did not demonstrate a significant improvement towards Si-H bond activation.

Yet, the exploration of such complexes prompted the idea of focusing on cationic species (methyl and hydride metal cations), to complement the study with a different type of complex (Ir^{I} vs Ir^{III} cationic). An interesting parallel was demonstrated with respect to the possibility of isolating a Rh methyl triflate complex (**4-16**), yet its Ir counterpart lead to a structure rearrangement when the synthesis was attempted (**4-15**). Subsequently, the stabilization by a neutral L donor (L = PMe_3) lead to successful isolation of various methyl cations (**4-17**, **4-19** and **4-20**). Further reactivity was explored including example of C-H(sp) bond activation, leading to a terminal alkynyl complex (**4-21**). Lastly, an attempt at

forcing the triflate moieties of these complexes outer-sphere was investigated by substituting triflate by a large, weakly coordinating anion such as $B(C_6F_5)_4^-$, successfully leading to **4-22**. Despite some stability issues, this complex is promising for further development involving the isolation of metal methyl cations.

5.2 Future Work

During the investigation of (Cy-PSiP)Ir(H)($SiRMes_2$) (R = H, Cl) reactivity, an effort has been made to synthesize products of the type $[(Cy\text{-}PSiP)Ir(H)(SiMes_2)]^+X^-$ (X = OTf, $B(C_6F_5)_4$ and $B(3,5\text{-}(CF_3)_2C_6H_3)_4$) and were targeted, while not isolated yet. The interest in these complexes is justified by the fact they can be viewed as Lewis base stabilized silylenes, where X = OTf^- can coordinate to the silicon atom. Preliminary research reveals that a solution of (Cy-PSiP)Ir(H)($SiClMes_2$) with AgOTf in a C_6H_5F solution led to quantitative formation of a new product (by ^{31}P NMR) featuring a triflate resonance in the $^{19}\{^1H\}$ NMR spectrum at -78.3 ppm. Reactions with weakly coordinating anion sources such as $AgB(C_6F_5)_4$ and $AgB(3,5\text{-}(CF_3)_2C_6H_3)_4$ could be envisioned, potentially leading to cationic (Cy-PSiP)Ir(H)(=$SiMes_2$) species (Scheme 5-1).

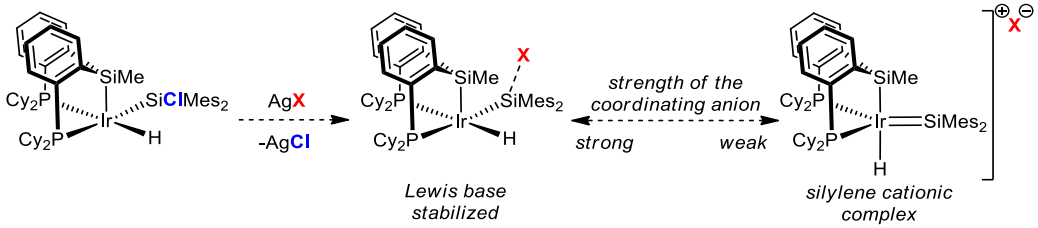

Scheme 5-1. Proposed synthetic strategy for (Cy-PSiP)Ir(H)(=SiR_2) species.

Alternatively, some further investigation can be made on the (PSiP) silyl ligand itself. It was presented as highly tunable with a modular design, thus, some additional

exploration can be done on this part. For example, it could be beneficial and synthetically relevant to study the difference in electronic and steric effects on the overall behavior and reactivity of (PSiP) silyl pincer complexes by changing the design features of the ligand. Such as having a different aromatic ring in the backbone (*eg.* bicyclic, heterocyclic, tethered, …) or even attempting a synthesis involving one aromatic arm, and one shorter aromatic arm (Scheme 5-2A).

A typical feature of the (PSiP) ligand is its two flanking donor groups. These two phosphines can be tuned at will during the first synthetic step of the ligand. These moieties could be tuned strategically to be less bulky (Scheme 5-2C), more donating, and even using two different phosphines on the same ligand framework (Scheme 5-2B). Despite the synthesis of all the different combinations involving phosphine variations would be tedious, some intuition and synthetically convenient phosphines can be chosen and investigated in a ligand synthesis. Once the various metal hydrido-chloride complexes would be prepared, they could be compared by observing differences in their spectroscopic features (typically hydrides in ^{1}H NMR and IR, phosphines in ^{31}P NMR, silyl donor in ^{29}Si NMR) and draw out a trend, informing about the electronic profile of said new complexes in comparison with the ones already known and investigated.

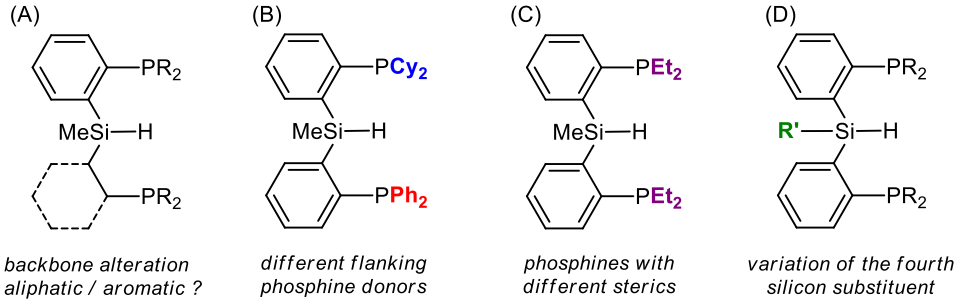

Scheme 5-2. Proposal of different ligand variations in backbone, flanking phosphines design and silicon-bound substituents.

Lastly, the ligand architecture of the (PSiP) framework revolves around a central, Si atom. This portion of the ligand is also tunable, less readily than the phosphine moieties, yet accomplishable. The fourth substituent on the Si atom is a methyl group in a large portion of this chemistry. Although, some examples of Si*H*, Si*OH*, Si*Cl*, Si*OTf*, Si*F*, Si*Ph*, and Si*Et* containing ligand precursors were reported.[21a,65e,h,141] For the purposes targeted in the Turculet lab, a synthetic choice would have to be made due to the numerous possible synthesis combinations. Although such ligand modifications may offer interesting insights with respect to the behavior of the resulting metal complexes this study would offer (Scheme 5-1D).

References

(1) Hartwig, J. F. *Organotransition Metal Chemistry: From Bonding to Catalysis*; Sausalito, 2010.

(2) (a) Knowles, W. S. *Angew. Chem. Int. Ed.* **2002**, *41*, 1998-2007; (b) Noyori, R. *Angew. Chem. Int. Ed.* **2002**, *41*, 2008-2022; (c) Sharpless, K. B. *Angew. Chem. Int. Ed.* **2002**, *41*, 2024-2032.

(3) (a) Chauvin, Y. *Angew. Chem. Int. Ed.* **2006**, *45*, 3741-3747; (b) Grubbs, R. H. *Angew. Chem. Int. Ed.* **2006**, *45*, 3760-3765; (c) Schrock, R. R. *Angew. Chem. Int. Ed.* **2006**, *45*, 3748-3759.

(4) Wu, X.-F.; Anbarasan, P.; Neumann, H.; Beller, M. *Angew. Chem. Int. Ed.* **2010**, *49*, 9047-9050.

(5) Morales-Morales, D.; Jensen, C. M. *The Chemistry of Pincer Compounds*; Elsevier B. V., Oxford, 2007.

(6) Morales-Morales, D. *Mini-Rev. Org. Chem.* **2008**, *5*.

(7) (a) Lu, Q.-N.; Chaloupka, S.; Venanzi, L. M. *Wuji Huaxue Xuebao* **2001**, *17*, 227; (b) Eberhard, M. R.; Matsukawa, S.; Yamamoto, Y.; Jensen, C. M. *J. Organomet. Chem.* **2003**, *687*, 185-189; (c) Wang, Z.; Eberhard, M. R.; Jensen, C. M.; Matsukawa, S.; Yamamoto, Y. *J. Organomet. Chem.* **2003**, *681*, 189-195.

(8) Jensen, C. M. *Chem. Commun.* **1999**, 2443-2449.

(9) Liu, F.; Goldman, A. S. *Chem. Commun.* **1999**, 655-656.

(10) Albrecht, M.; Lindner, M. M. *Dalton Trans.* **2011**, *40*, 8733-8744.

(11) Slagt, M. Q.; van Zwieten, D. A. P.; Moerkerk, A. J. C. M.; Gebbink, R. J. M. K.; van Koten, G. *Coord. Chem. Rev.* **2004**, *248*, 2275-2282.

(12) Fischer, J.; Schuermann, M.; Mehring, M.; Zachwieja, U.; Jurkschat, K. *Organometallics* **2006**, *25*, 2886-2893.

(13) (a) Espinet, P.; Garcia-Orodea, E.; Miguel, J. A. *Chem. Mater.* **2004**, *16*, 551-558; (b) Zim, D.; Gruber, A. S.; Ebeling, G.; Dupont, J.; Monteiro, A. L. *Org. Lett.* **2000**, *2*, 2881-2884.

(14) (a) Sebelius, S.; Olsson, V. J.; Wallner, O. A.; Szabo, K. J. *J. Am. Chem. Soc.* **2006**, *128*, 8150-8151; (b) Yao, Q.; Sheets, M. *J. Org. Chem.* **2006**, *71*, 5384-5387.

(15) (a) Lee, C.-I.; Zhou, J.; Ozerov, O. V. *J. Am. Chem. Soc.* **2013**, *135*, 3560-3566; (b) Wang, W.; Inoue, S.; Irran, E.; Driess, M. *Angew. Chem. Int. Ed.* **2012**, *51*, 3691-3694, S3691/3691-S3691/3624.

(16) Brueck, A.; Gallego, D.; Wang, W.; Irran, E.; Driess, M.; Hartwig, J. F. *Angew. Chem. Int. Ed.* **2012**, *51*, 11478-11482.

(17) Pugh, D.; Danopoulos, A. A. *Coord. Chem. Rev.* **2007**, *251*, 610-641.

(18) (a) Albrecht, M.; van Koten, G. *Angew. Chem. Int. Ed.* **2001**, *40*, 3750-3781; (b) Elschenbroich, C. In *Organometallics, Third Completely Revised and Extended Edition*; Wiley, Weinheim: 2006, p chapter 18; (c) van der Boom, M. E.; Milstein, D. *Chem. Rev.* **2003**, *103*, 1759-1792.

(19) (a) Fryzuk, M. D. *Can. J. Chem.* **1992**, *70*, 2839-2845; (b) Watson, L. A.; Ozerov, O. V.; Pink, M.; Caulton, K. G. *J. Am. Chem. Soc.* **2003**, *125*, 8426-8427; (c) Ozerov, O. V.; Guo, C.; Papkov, V. A.; Foxman, B. M. *J. Am. Chem. Soc.* **2004**, *126*, 4792-4793; (d) Liang, L.-C. *Coord. Chem. Rev.* **2006**, *250*, 1152-1177; (e) Mindiola, D. J. *Acc. Chem. Res.* **2006**, *39*, 813-821; (f) Csok, Z.; Vechorkin, O.; Harkins, S. B.; Scopelliti, R.; Hu, X. *J. Am. Chem. Soc.* **2008**, *130*, 8156-8157; (g) Wei, W.; Qin, Y.; Luo, M.; Xia, P.; Wong, M. S. *Organometallics* **2008**, *27*, 2268-2272.

(20) (a) MacInnis, M. C.; MacLean, D. F.; Lundgren, R. J.; McDonald, R.; Turculet, L. *Organometallics* **2007**, *26*, 6522-6525; (b) MacLean, D. F.; McDonald, R.; Ferguson, M. J.; Caddell, A. J.; Turculet, L. *Chem. Commun.* **2008**, 5146-5148; (c) Mitton, S. J.; McDonald, R.; Turculet, L. *Angew. Chem. Int. Ed.* **2009**, *48*, 8568-8571; (d) Mitton, S. J.; McDonald, R.; Turculet, L. *Organometallics* **2009**, *28*, 5122-5136; (e) MacInnis, M. C.; McDonald, R.; Ferguson, M. J.; Tobisch, S.; Turculet, L. *J. Am. Chem. Soc.* **2011**, *133*, 13622-13633; (f) Mitton, S. J.; Turculet, L. *Chem. Eur. J.* **2012**, *18*, 15258-15262.

(21) (a) Korshin, E. E.; Leitus, G.; Shimon, L. J. W.; Konstantinovski, L.; Milstein, D. *Inorg. Chem.* **2008**, *47*, 7177-7189; (b) Takaya, J.; Iwasawa, N. *J. Am. Chem. Soc.* **2008**, *130*, 15254-15255; (c) Takaya, J.; Iwasawa, N. *Organometallics* **2009**, *28*, 6636-6638; (d) Fang, H.; Choe, Y.-K.; Li, Y.; Shimada, S. *Chem. Asian J.* **2011**, *6*, 2512-2521; (e) Takaya, J.; Iwasawa, N. *Dalton Trans.* **2011**, *40*, 8814-8821; (f) Takaya, J.; Kirai, N.; Iwasawa, N. *J. Am. Chem. Soc.* **2011**, *133*, 12980-12983; (g) Takaya, J.; Sasano, K.; Iwasawa, N. *Org. Lett.* **2011**, *13*, 1698-1701; (h) Joost, M.; Mallet-Ladeira, S.; Miqueu, K.; Amgoune, A.; Bourissou, D. *Organometallics* **2013**, *32*, 898-902; (i) Kirai, N.; Takaya, J.; Iwasawa, N. *J. Am. Chem. Soc.* **2013**, *135*, 2493-2496.

(22) (a) Mankad, N. P.; Rivard, E.; Harkins, S. B.; Peters, J. C. *J. Am. Chem. Soc.* **2005**, *127*, 16032-16033; (b) Mazzeo, M.; Lamberti, M.; Massa, A.; Scettri, A.; Pellecchia, C.; Peters, J. C. *Organometallics* **2008**, *27*, 5741-5743; (c) Bauer, R. C.; Gloaguen, Y.; Lutz, M.; Reek, J. N. H.; de Bruin, B.; van der Vlugt, J. I. *Dalton Trans.* **2011**, *40*, 8822; (d) Mazzeo, M.; Strianese, M.; Kühl, O.; Peters, J. C. *Dalton Trans.* **2011**, *40*, 9026; (e) Pan, B.; Bezpalko, M. W.; Foxman, B. M.; Thomas, C. M. *Organometallics* **2011**, *30*, 5560-5563; (f) D'Auria, I.; Lamberti, M.; Mazzeo, M.; Milione, S.; Roviello, G.; Pellecchia, C. *Chem. Eur. J.* **2012**, *18*, 2349-2360; (g) Gloaguen, Y.; Jacobs, W.; de Bruin, B.; Lutz, M.; van der Vlugt, J. I. *Inorg. Chem.* **2013**, *52*, 1682-1684.

(23) (a) Segawa, Y.; Yamashita, M.; Nozaki, K. *J. Am. Chem. Soc.* **2009**, *131*, 9201-9203; (b) Segawa, Y.; Yamashita, M.; Nozaki, K. *Organometallics* **2009**, *28*, 6234-6242; (c) Hasegawa, M.; Segawa, Y.; Yamashita, M.; Nozaki, K. *Angew. Chem. Int. Ed.* **2012**, *51*, 6956-6960; (d) Ogawa, H.; Yamashita, M. *Dalton Trans.* **2013**, *42*, 625-629.

(24) (a) Kameo, H.; Ishii, S.; Nakazawa, H. *Dalton Trans.* **2012**, *41*, 11386; (b) Takaya, J.; Nakamura, S.; Iwasawa, N. *Chem. Lett.* **2012**, *41*, 967-969.

(25) Leis, W.; Mayer, H.; Kaska, W. *Coord. Chem. Rev.* **2008**, *252*, 1787-1797.

(26) Morales-Morales, D. *Rev. Soc. Quím. Méx.* **2004**, *48*, 338-346.

(27) (a) Moulton, C. J.; Shaw, B. L. *J. Chem. Soc., Dalton Trans.* **1976**, 1020; (b) Empsall, H. D.; Hyde, E. M.; Markham, R.; McDonald, W. S.; Norton, M. C.; Shaw, B. L.; Weeks, B. *J. Chem. Soc., Chem. Commun.* **1977**, 589; (c) Crocker, C.; Errington, R. J.; McDonald, W. S.; Odell, K. J.; Shaw, B. L.; Goodfellow, R. J. *J. Chem. Soc., Chem. Commun.* **1979**, 498; (d) Crocker, C.; Errington, R. J.; Markham, R.; Moulton, C. J.; Odell, K. J.; Shaw, B. L. *J. Am. Chem. Soc.* **1980**, *102*, 4373-4379.

(28) (a) van der Boom, M. E.; Gozin, M.; Ben-David, Y.; Shimon, L. J. W.; Frolow, F.; Kraatz, H.-B.; Milstein, D. *Inorg. Chem.* **1996**, *35*, 7068-7073; (b) Steenwinkel, P.; Kolmschot, S.; Gossage, R. A.; Dani, P.; Veldman, N.; Spek, A. L.; van Koten, G. *Eur. J. Inorg. Chem.* **1998**, *1998*, 477-483.

(29) (a) Gozin, M.; Weisman, A.; Ben-David, Y.; Milstein, D. *Nature* **1993**, *364*, 699-701; (b) Rybtchinski, B.; Milstein, D. *Angew. Chem. Int. Ed.* **1999**, *38*, 870-883.

(30) Gozin, M.; Aizenberg, M.; Liou, S.-Y.; Weisman, A.; Ben-David, Y.; Milstein, D. *Nature* **1994**, *370*, 42-44.

(31) (a) Arndtsen, B. A.; Bergman, R. G.; Mobley, T. A.; Peterson, T. H. *Acc. Chem. Res.* **1995**, *28*, 154-162; (b) Labinger, J. A.; Bercaw, J. E. *Nature* **2002**, *417*, 507-514.

(32) (a) Hoyano, J. K.; Graham, W. A. G. *J. Am. Chem. Soc.* **1982**, *104*, 3722-3723; (b) Janowicz, A. H.; Bergman, R. G. *J. Am. Chem. Soc.* **1982**, *104*, 352-354.

(33) Shilov, A. E.; Shul'pin, G. B. *Activation and Catalytic Reactions of Saturated Hydrocarbons in the Presence of Metal Complexes* Dordrecht, 2000.

(34) (a) Baudry, D.; Ephritikhine, M.; Felkin, H.; Holmes-Smith, R. *J. Chem. Soc., Chem. Commun.* **1983**, 788; (b) Burk, M. J.; Crabtree, R. H.; McGrath, D. V. *J. Chem. Soc., Chem. Commun.* **1985**, 1829.

(35) (a) Felkin, H.; Fillebeen-Khan, T.; Gault, Y.; Holmes-Smith, R.; Zakrzewski, J. *Tetrahedron Lett.* **1984**, *25*, 1279-1282; (b) Felkin, H.; Fillebeen-khan, T.; Holmes-Smith, R.; Yingrui, L. *Tetrahedron Lett.* **1985**, *26*, 1999-2000.

(36) (a) Burk, M. J.; Crabtree, R. H.; Parnell, C. P.; Uriarte, R. J. *Organometallics* **1984**, *3*, 816-817; (b) Burk, M. J.; Crabtree, R. H. *J. Am. Chem. Soc.* **1987**, *109*, 8025-8032.

(37) Aoki, T.; Crabtree, R. H. *Organometallics* **1993**, *12*, 294-298.

(38) Crabtree, R. H.; Parnell, C. P.; Uriarte, R. J. *Organometallics* **1987**, *6*, 696-699.

(39) Maguire, J. A.; Boese, W. T.; Goldman, A. S. *J. Am. Chem. Soc.* **1989**, *111*, 7088-7093.

(40) (a) Maguire, J. A.; Goldman, A. S. *J. Am. Chem. Soc.* **1991**, *113*, 6706-6708; (b) Maguire, J. A.; Petrillo, A.; Goldman, A. S. *J. Am. Chem. Soc.* **1992**, *114*, 9492-9498.

(41) (a) Gupta, M.; Hagen, C.; Flesher, R. J.; Kaska, W. C.; Jensen, C. M. *Chem. Commun.* **1996**, 2083; (b) Gupta, M.; Hagen, C.; Kaska, W. C.; Cramer, R. E.; Jensen, C. M. *J. Am. Chem. Soc.* **1997**, *119*, 840-841.

(42) (a) Wang, K.; Goldman, M. E.; Emge, T. J.; Goldman, A. S. *J. Organomet. Chem.* **1996**, *518*, 55-68; (b) Xu, W.-w.; Rosini, G. P.; Krogh-Jespersen, K.; Goldman, A. S.; Gupta, M.; Jensen, C. M.; Kaska, W. C. *Chem. Commun.* **1997**, 2273-2274.

(43) Renkema, K. B.; Kissin, Y. V.; Goldman, A. S. *J. Am. Chem. Soc.* **2003**, *125*, 7770-7771.

(44) Kanzelberger, M.; Singh, B.; Czerw, M.; Krogh-Jespersen, K.; Goldman, A. S. *J. Am. Chem. Soc.* **2000**, *122*, 11017-11018.

(45) (a) Krogh-Jespersen, K.; Czerw, M.; Summa, N.; Renkema, K. B.; Achord, P. D.; Goldman, A. S. *J. Am. Chem. Soc.* **2002**, *124*, 11404-11416; (b) Krogh-Jespersen, K.; Czerw, M.; Goldman, A. S. In *ACS Symp. Ser.*; American Chemical Society (ACS): 2004, p 216-233.

(46) (a) Haenel, M. W.; Oevers, S.; Angermund, K.; Kaska, W. C.; Fan, H.-J.; Hall, M. B. *Angew. Chem. Int. Ed.* **2001**, *40*, 3596; (b) Zhu, K.; Achord, P. D.; Zhang, X.; Krogh-Jespersen, K.; Goldman, A. S. *J. Am. Chem. Soc.* **2004**, *126*, 13044-13053; (c) Kuklin, S. A.; Sheloumov, A. M.; Dolgushin, F. M.; Ezernitskaya, M. G.; Peregudov, A. S.; Petrovskii, P. V.; Koridze, A. A. *Organometallics* **2006**, *25*, 5466-5476; (d) Punji, B.; Emge, T. J.; Goldman, A. S. *Organometallics* **2010**, *29*, 2702-2709.

(47) Morales-Morales, D.; Redón, R. o.; Yung, C.; Jensen, C. M. *Inorg. Chim. Acta* **2004**, *357*, 2953-2956.

(48) (a) Göttker-Schnetmann, I.; Brookhart, M. *J. Am. Chem. Soc.* **2004**, *126*, 9330-9338; (b) Göttker-Schnetmann, I.; White, P.; Brookhart, M. *J. Am. Chem. Soc.* **2004**, *126*, 1804-1811.

(49) Choi, J.; MacArthur, A. H. R.; Brookhart, M.; Goldman, A. S. *Chem. Rev.* **2011**, *111*, 1761-1779.

(50) (a) Müller, T. E.; Beller, M. *Chem. Rev.* **1998**, *98*, 675-704; (b) Hartwig, J. F. *Pure Appl. Chem.* **2004**, *76*; (c) Hartwig, J. F. *Nature* **2008**, *455*, 314-322; (d) Müller, T. E.; Hultzsch, K. C.; Yus, M.; Foubelo, F.; Tada, M. *Chem. Rev.* **2008**, *108*, 3795-3892; (e) Surry, D. S.; Buchwald, S. L. *Angew. Chem. Int. Ed.* **2008**, *47*, 6338-6361; (f) Aubin, Y.; Fischmeister, C.; Thomas, C. M.; Renaud, J.-L. *Chem. Soc. Rev.* **2010**, *39*, 4130; (g) van der Vlugt, J. I. *Chem. Soc. Rev.* **2010**, *39*, 2302.

(51) Crabtree, R. H. *The Organometallic Chemistry of the Transition Metals*; John Wiley & Sons, Inc.: NJ, 2005.

(52) For examples of related tetradentate tris(phosphino) silyl ligation, see: (a) Hillhouse, G. L.; Bercaw, J. E. *J. Am. Chem. Soc.* **1984**, *106*, 5472-5478; (b) Casalnuovo, A. L.; Calabrese, J. C.; Milstein, D. *Inorg. Chem.* **1987**, *26*, 971-973; (c) Park, S.; Roundhill, D. M.; Rheingold, A. L. *Inorg. Chem.* **1987**, *26*, 3972-3974; (d) Glueck, D. S.; Winslow, L. J. N.; Bergman, R. G. *Organometallics* **1991**, *10*, 1462-1479; (e) Hartwig, J. F.; Andersen, R. A.; Bergman, R. G. *Organometallics* **1991**, *10*, 1875-1887; (f) Beller, M.; Trauthwein, H.; Eichberger, M.; Breindl, C.; Herwig, J.; Müller, T. E.; Thiel, O. R. *Chem. Eur. J.* **1999**, *5*, 1306-1319; (g) Kanzelberger, M.; Zhang, X.; Emge, T. J.; Goldman, A. S.; Zhao, J.; Incarvito, C.; Hartwig, J. F. *J. Am. Chem. Soc.* **2003**, *125*, 13644-13645; (h) Utsunomiya, M.; Kuwano, R.; Kawatsura, M.; Hartwig, J. F. *J. Am. Chem. Soc.* **2003**, *125*, 5608-5609; (i) Zhao, J. *Science* **2005**, *307*, 1080-1082; (j) Sykes, A. C.; White, P.; Brookhart, M. *Organometallics* **2006**, *25*, 1664-1675; (k) Morgan, E.; MacLean, D. F.; McDonald, R.; Turculet, L. *J. Am. Chem. Soc.* **2009**, *131*, 14234-14236.

(53) Kauffman, G. B. *ACS Symp. Ser.* **1994**, *565*, 2.

(54) For a related example of pincer-Ir mediated N-H bond activation involving reversible aromatization/dearomatization of a pyridine based PNP ligand, see: Khaskin, E.; Iron, M. A.; Shimon, L. J. W.; Zhang, J.; Milstein, D. *J. Am. Chem. Soc.* **2010**, *132*, 8542-8543.

(55) Huang, Z.; Zhou, J.; Hartwig, J. F. *J. Am. Chem. Soc.* **2010**, *132*, 11458-11460.

(56) (a) Issleib, K.; Kümmel, R. *J. Organomet. Chem.* **1965**, *3*, 84-91; (b) Bordwell, F. G. *Acc. Chem. Res.* **1988**, *21*, 456-463; (c) Nam, P. C.; Nguyen, M. T.; Chandra, A. K. *J. Phys. Chem. A* **2004**, *108*, 11362-11368; (d) Li, J. N.; Liu, L.; Fu, Y.; Guo, Q. X. *Tetrahedron* **2006**, *62*, 4453-4462; (e) Luo, Y. R. *Comprehensive Handbook of Chemical Bond Energies*; CRC Press: Boca Raton, FL, 2007.

(57) Aizenberg, M.; Milstein, D. *J. Am. Chem. Soc.* **1995**, *117*, 6456-6464.

(58) (a) Auburn, M. J.; Stobart, S. R. *Inorg. Chem.* **1985**, *24*, 318-323; (b) Joslin, F. L.; Stobart, S. R. *J. Chem. Soc., Chem. Commun.* **1989**, 504; (c) Auburn, M. J.; Holmes-Smith, R. D.; Stobart, S. R.; Bakshi, P. K.; Cameron, T. S. *Organometallics* **1996**, *15*, 3032-3036; (d) Gossage, R. A.; McLennan, G. D.; Stobart, S. R. *Inorg. Chem.* **1996**, *35*, 1729-1732; (e) Brost, R. D.; Bruce, G. C.; Joslin, F. L.; Stobart, S. R. *Organometallics* **1997**, *16*, 5669-5680; (f) Bushnell, G. W.; Casado, M. A.; Stobart, S. R. *Organometallics* **2001**, *20*, 601-603.

(59) (a) Stradiotto, M.; Fujdala, K. L.; Tilley, T. D. *Chem. Commun.* **2001**, 1200-1201; (b) Sangtrirutnugul, P.; Stradiotto, M.; Tilley, T. D. *Organometallics* **2006**, *25*, 1607-1617; (c) Sangtrirutnugul, P.; Tilley, T. D. *Organometallics* **2007**, *26*, 5557-5568; (d) Sangtrirutnugul, P.; Tilley, T. D. *Organometallics* **2008**, *27*, 2223-2230; (e)Related NSiN ligation featuring pyridyl donors has also been reported: Fernández-Alvarez, F. J.; Lalrempuia, R.; Oro, L. A. *Coord. Chem. Rev.* **2017**, *350*, 49-60.

(60) Turculet, L. In *Pincer and Pincer-Type Complexes: Applications in Organic Synthesis and Catalysis*; Szabó, K. J., Wendt, O. F., Eds.; Wiley-VCH: Weinheim, 2014, p 149-188.

(61) Ruddy, A. J.; Mitton, S. J.; McDonald, R.; Turculet, L. *Chem. Commun.* **2012**, *48*, 1159-1161.

(62) (a) Mankad, N. P.; Whited, M. T.; Peters, J. C. *Angew. Chem. Int. Ed.* **2007**, *46*, 5768-5771; (b) Takaoka, A.; Mendiratta, A.; Peters, J. C. *Organometallics* **2009**, *28*, 3744-3753; (c) Whited, M. T.; Mankad, N. P.; Lee, Y.; Oblad, P. F.; Peters, J. C. *Inorg. Chem.* **2009**, *48*, 2507-2517; (d) Lee, Y.; Mankad, N. P.; Peters, J. C. *Nat. Chem.* **2010**, *2*, 558-565; (e) Mankad, N. P.; Müller, P.; Peters, J. C. *J. Am. Chem. Soc.* **2010**, *132*, 4083-4085; (f) Takaoka, A.; Gerber, L. C. H.; Peters, J. C. *Angew. Chem. Int. Ed.* **2010**, *49*, 4088-4091; (g) Tsay, C.; Mankad, N. P.; Peters, J. C. *J. Am. Chem. Soc.* **2010**, *132*, 13975-13977; (h) Takaoka, A.; Peters, J. C. *Inorg. Chem.* **2011**, *51*, 16-18; (i) Suess, D. L. M.; Tsay, C.; Peters, J. C. *J. Am. Chem. Soc.* **2012**, *134*, 14158-14164; (j) Takaoka, A.; Moret, M.-E.; Peters, J. C. *J. Am. Chem. Soc.* **2012**, *134*, 6695-6706; (k) Tsay, C.; Peters, J. C. *Chem. Sci.* **2012**, *3*, 1313; (l) Fong, H.; Peters, J. C. *Inorg. Chem.* **2014**, *54*, 5124-5135.

(63) Murphy, L. J.; Hollenhorst, H.; McDonald, R.; Ferguson, M.; Lumsden, M. D.; Turculet, L. *Organometallics* **2017**, *36*, 3709-3720.

(64) (a) MacInnis, M. C.; Ruddy, A. J.; McDonald, R.; Ferguson, M. J.; Turculet, L. *Dalton Trans.* **2016**, *45*, 15850-15858; (b) Murphy, L. J.; Ferguson, M. J.; McDonald, R.; Lumsden, M. D.; Turculet, L. *Organometallics* **2018**, *37*, 4814-4826; (c) Murphy, L. J.; Ruddy, A. J.; McDonald, R.; Ferguson, M. J.; Turculet, L. *Eur. J. Inorg. Chem.* **2018**, *2018*, 4481-4493.

(65) For other recent studies involving PSiP ligation, see: (a) Bernal, M. J.; Torres, O.; Martín, M.; Sola, E. *J. Am. Chem. Soc.* **2013**, *135*, 19008-19015; (b) Suh, H.-W.; Guard, L. M.; Hazari, N. *Chem. Sci.* **2014**, *5*, 3859; (c) Takaya, J.; Iwasawa, N. In *Pincer and Pincer-Type Complexes: Applications in Organic Synthesis and Catalysis*; Szabó, K. J., Wendt, O. F., Eds.; Wiley-VCH: Weinheim, 2014, p 229-248; (d) Takaya, J.; Iwasawa, N. *Chem. Eur. J.* **2014**, *20*, 11812-11819; (e) Whited, M. T.; Deetz, A. M.; Boerma, J. W.; DeRosha, D. E.; Janzen, D. E. *Organometallics* **2014**, *33*, 5070-5073; (f) Bernal, M. J.; Martín, M.; Sola, E. *Organometallics* **2015**, *34*, 800-803; (g) Charboneau, D. J.; Balcells, D.; Hazari, N.; Lant, H. M. C.; Mayer, J. M.; Melvin, P. R.; Mercado, B. Q.; Morris, W. D.; Repisky, M.; Suh, H.-W. *Organometallics* **2016**, *35*, 3154-3162; (h) Kameo, H.; Kawamoto, T.; Sakaki, S.; Bourissou, D.; Nakazawa, H. *Chem. Eur. J.* **2016**, *22*, 2370-2375; (i) Kim, J.; Kim, Y.; Sinha, I.; Park, K.; Kim, S. H.; Lee, Y. *Chem. Commun.* **2016**, *52*, 9367-9370; (j) Whited, M. T.; Deetz, A. M.; Donnell, T. M.; Janzen, D. E. *Dalton Trans.* **2016**, *45*, 9758-9761.

(66) Morgan, E. Rhodium and Iridium Pincer Complexes Supported by Bis(phosphino)silyl Ligation: Applications in Bond Cleavage Chemistry. PhD Thesis, Dalhousie University, 2013.

(67) (a) Obligacion, J. V.; Chirik, P. J. *J. Am. Chem. Soc.* **2013**, *135*, 19107-19110; (b) Zhang, L.; Zuo, Z.; Leng, X.; Huang, Z. *Angew. Chem. Int. Ed.* **2014**, *53*, 2696-2700.

(68) (a) Bart, S. C.; Lobkovsky, E.; Chirik, P. J. *J. Am. Chem. Soc.* **2004**, *126*, 13794-13807; (b) Yu, R. P.; Darmon, J. M.; Hoyt, J. M.; Margulieux, G. W.; Turner, Z. R.; Chirik, P. J. *ACS Catal.* **2012**, *2*, 1760-1764; (c) Scheuermann, M. L.; Semproni, S. P.; Pappas, I.; Chirik, P. J. *Inorg. Chem.* **2014**, *53*, 9463-9465; (d) Ríos, P.; Curado, N.; López-Serrano, J.; Rodríguez, A. *Chem. Commun.* **2016**, *52*, 2114-2117.

(69) (a) Roundhill, D. M. *Chem. Rev.* **1992**, *92*, 1-27; (b) Ahmed, M.; Jackstell, R.; Seayad, A. M.; Klein, H.; Beller, M. *ChemInform* **2004**, *35*; (c) Surry, D. S.; Buchwald, S. L. *J. Am. Chem. Soc.* **2007**, *129*, 10354-10355; (d) Lavallo, V.; Frey, G. D.; Donnadieu, B.; Soleilhavoup, M.; Bertrand, G. *Angew. Chem. Int. Ed.* **2008**, *47*, 5224-5228; (e) Pouy, M. J.; Stanley, L. M.; Hartwig, J. F. *J. Am. Chem. Soc.* **2009**, *131*, 11312-11313; (f) Vo, G. D.; Hartwig, J. F. *J. Am. Chem. Soc.* **2009**, *131*, 11049-11061; (g) Lundgren, R. J.; Sappong-Kumankumah, A.; Stradiotto, M. *Chem. Eur. J.* **2010**, *16*, 1983-1991; (h) Lundgren, R. J.; Stradiotto, M. *Angew. Chem. Int. Ed.* **2010**, *49*, 9322-9324.

(70) (a) Yoshida, T.; Okano, T.; Otsuka, S. *J. Am. Chem. Soc.* **1980**, *102*, 5966-5967; (b) Lewis, N. S.; Nocera, D. G. *Proceedings of the National Academy of Sciences* **2006**, *103*, 15729-15735; (c) Burford, R. J.; Piers, W. E.; Ess, D. H.; Parvez, M. *J. Am. Chem. Soc.* **2014**, *136*, 3256-3263.

(71) (a) Rosenberg, L. *ACS Catal.* **2013**, *3*, 2845-2855; (b) Glueck, D. S. *Top. Organomet. Chem.* **2010**, *31*, 65-100; (c) Waterman, R. *Dalton Trans* **2009**, 18-26; (d) Greenberg, S.; Stephan, D. W. *Chem Soc Rev* **2008**, *37*, 1482-1489; (e) Waterman, R. *Chem. Soc. Rev.* **2013**, *42*, 5629-5641; (f) Koshti, V.; Gaikwad, S.; Chikkali, S. H. *Coord. Chem. Rev.* **2014**, *265*, 52-73.

(72) Kovacik, I.; Wicht, D. K.; Grewal, N. S.; Glueck, D. S.; Incarvito, C. D.; Guzei, I. A.; Rheingold, A. L. *Organometallics* **2000**, *19*, 950-953.

(73) Jaska, C. A.; Lough, A. J.; Manners, I. *Dalton Trans.* **2005**, 326-331.

(74) (a) Latypov, S. K.; Polyancev, F. M.; Ganushevich, Y. S.; Miluykov, V. A.; Sinyashin, O. G. *Dalton Trans* **2016**, *45*, 2053-2059; (b) Ganushevich, Y. S.; Miluykov, V. A.; Polyancev, F. M.; Latypov, S. K.; Lonnecke, P.; Hey-Hawkins, E.; Yakhvarov, D. G.; Sinyashin, O. G. *Organometallics* **2013**, *32*, 3914-3919.

(75) Schunn, R. A. *Inorg. Chem.* **1973**, *12*, 1573-1579.

(76) (a) Ebsworth, E. A. V.; Mayo, R. A. *J. Chem. Soc., Dalton Trans.* **1988**, 477-484; (b) Ebsworth, E. A. V.; Gould, R. O.; Mayo, R. A.; Walkinshaw, M. *J. Chem. Soc., Dalton Trans.* **1987**, 2831-2838; (c) Ebsworth, E. A. V.; Mayo, R. *Angew. Chem. Int. Ed.* **1985**, *24*, 68-70.

(77) NOTE: The long Ir-PPh_2 distance observed by Tejel and co-workers is likely due, in part, to the strong trans influence of the phosphino group coordinated trans to the PPh2 ligand in this complex. (a) Serrano, A. L.; Casado, M. A.; Ciriano, M. A.; de Bruin, B.; López, J. A.; Tejel, C. *Inorg Chem* **2016**, *55*, 828-839; (b) Geer, A. M.; Serrano, A. L.; de Bruin, B.; Ciriano, M. A.; Tejel, C. *Angew. Chem. Int. Ed.* **2015**, *54*, 472-475.

(78) Rosenberg, L. *Coord. Chem. Rev.* **2012**, *256*, 606-626.

(79) (a) Fryzuk, M. D.; Joshi, K.; Chadha, R. K.; Rettig, S. J. *J. Am. Chem. Soc.* **1991**, *113*, 8724-8736; (b) Fryzuk, M. D.; Joshi, K. *Organometallics* **1989**, *8*, 722-726; (c) Fryzuk, M. D.; Bhangu, K. *J. Am. Chem. Soc.* **1988**, *110*, 961-963.

(80) Riehl, J. F.; Jean, Y.; Eisenstein, O.; Pélissier, M. *Organometallics* **1992**, *11*, 729-737.

(81) Zhuravel, M. A.; Glueck, D. S.; Zakharov, L. N.; Rheingold, A. L. *Organometallics* **2002**, *21*, 3208-3214.

(82) *Proceedings of the Royal Society of London. Series A - Mathematical and Physical Sciences* **1937**, *161*, 220-235.

(83) Derrah, E. J.; Pantazis, D. A.; McDonald, R.; Rosenberg, L. *Organometallics* **2007**, *26*, 1473-1482.

(84) Borowski, A. F.; Sabo-Etienne, S.; Christ, M. L.; Donnadieu, B.; Chaudret, B. *Organometallics* **1996**, *15*, 1427-1434.

(85) (a) Wauters, I.; Debrouwer, W.; Stevens, C. V. *Beilstein J Org Chem* **2014**, *10*, 1064-1096; (b) Tappe, F. M. J.; Trepohl, V. T.; Oestreich, M. *Synthesis* **2010**, 3037-3062; (c) Schwan, A. L. *Chem. Soc. Rev.* **2004**, *33*, 218-224.

(86) Hartwig, J. F. *Inorg. Chem.* **2007**, *46*, 1936-1947.

(87) Böhm, V. P. W.; Brookhart, M. *Angew. Chem. Int. Ed.* **2001**, *40*, 4694-4696.

(88) (a) Han, L. B.; Tilley, T. D. *J. Am. Chem. Soc.* **2006**, *128*, 13698-13699; (b) Stradiotto, M.; Fujdala, K. L.; Tilley, T. D. *Helv. Chim. Acta* **2001**, *84*, 2958-2970.

(89) (a) Scriban, C.; Glueck, D. S.; Zakharov, L. N.; Kassel, W. S.; DiPasquale, A. G.; Golen, J. A.; Rheingold, A. L. *Organometallics* **2006**, *25*, 5757-5767; (b) Scriban, C.; Kovacik, I.; Glueck, D. S. *Organometallics* **2005**, *24*, 4871-4874; (c) Belli, R. G.; Burton, K. M. E.; Rufh, S. A.; McDonald, R.; Rosenberg, L. *Organometallics* **2015**, *34*, 5637-5646.

(90) (a) Shulyupin, M. O.; Kazankova, M. A.; Beletskaya, I. P. *Org. Lett.* **2002**, *4*, 761-763; (b) Kazankova, M. A.; Efimova, I. V.; Kochetkov, A. N.; Afanas'ev, V. V.; Beletskaya, I. P.; Dixneuf, P. H. *Synlett* **2001**, 497-500; (c) Ananikov, V. P.; Makarov, A. V.; Beletskaya, I. P. *Chem-Eur J* **2011**, *17*, 12623-12630; (d) Ananikov, V. P.; Beletskaya, I. P. *Chem-Asian J* **2011**, *6*, 1423-1430; (e) Rajpurohit, J.; Kumar, P.; Shukla, P.; Shanmugam, M.; Shanmugam, M. *Organometallics* **2018**, *37*, 2297-2304.

(91) (a) Derrah, E. J.; Giesbrecht, K. E.; McDonald, R.; Rosenberg, L. *Organometallics* **2008**, *27*, 5025-5032; (b) Sues, P. E.; Lough, A. J.; Morris, R. H. *J. Am. Chem. Soc.* **2014**, *136*, 4746-4760.

(92) Derrah, E. J.; McDonald, R.; Rosenberg, L. *Chem. Commun.* **2010**, *46*, 4592-4594.

(93) (a) Itazaki, M.; Katsube, S.; Kamitani, M.; Nakazawa, H. *Chem. Commun.* **2016**, *52*, 3163-3166; (b) Giuseppe, A. D.; Luca, R. D.; Castarlenas, R.; Pérez-Torrente, J. J.; Crucianelli, M.; Oro, L. A. *Chem. Commun.* **2016**, *52*, 5554-5557.

(94) (a) Bartlett, R. A.; Olmstead, M. M.; Power, P. P.; Sigel, G. A. *Inorg. Chem.* **1987**, *26*, 1941-1946; (b) Bartlett, R. A.; Olmstead, M. M.; Power, P. P. *Inorg. Chem.* **1986**, *25*, 1243-1247; (c) Heutz, F. J. L.; Samuels, M. C.; Kamer, P. C. J. *Catal Sci Technol* **2015**, *5*, 3296-3301; (d) Bhadbhade, M. M.; Field, L. D.; Gilbert-Wilson, R.; Guest, R. W.; Jensen, P. *Inorg. Chem.* **2011**, *50*, 6220-6228; (e) Heyhawkins, E.; Kurz, S.; Sieler, J.; Baum, G. *J. Organomet. Chem.* **1995**, *486*, 229-235.

(95) Greenhalgh, M. D.; Frank, D. J.; Thomas, S. P. *Adv. Synth. Catal.* **2014**, *356*, 584-590.

(96) (a) Bryndza, H. E.; Tam, W. *Chem. Rev.* **1988**, *88*, 1163-1188; (b) Nelson, D. J.; Nolan, S. P. *Coord. Chem. Rev.* **2017**, *353*, 278-294; (c) Fulton, J. R.; Holland, A. W.; Fox, D. J.; Bergman, R. G. *Acc. Chem. Res.* **2002**, *35*, 44-56; (d) Gunnoe, T. B. *Eur. J. Inorg. Chem.* **2007**, 1185-1203; (e) Lippert, B.; Miguel, P. J. S. *Coord. Chem. Rev.* **2016**, *327*, 333-348.

(97) Togni, A.; Grützmacher, H. *Catalytic Heterofunctionalization*; Wiley-VCH: Weinheim, Germany, 2001.

(98) Keith, J. A.; Henry, P. M. *Angew. Chem. Int. Ed.* **2009**, *48*, 9038-9049.

(99) (a) Wang, D.; Astruc, D. *Chem. Rev.* **2015**, *115*, 6621-6686; (b) Pàmies, O.; Bäckvall, J.-E. *Chem. Eur. J.* **2001**, *7*, 5052-5058.

(100) (a) Gunanathan, C.; Milstein, D. *Acc. Chem. Res.* **2011**, *44*, 588-602; (b) Gunanathan, C.; Milstein, D. *Top. Organomet. Chem.* **2011**, *37*, 55-84; (c) Milstein, D. *Top. Catal.* **2010**, *53*, 915-923; (d) Alberico, E.; Sponholz, P.; Cordes, C.; Nielsen, M.; Drexler, H. J.; Baumann, W.; Junge, H.; Beller, M. *Angew. Chem. Int. Ed.* **2013**, *52*, 14162-14166; (e) Nielsen, M.; Alberico, E.; Baumann, W.; Drexler, H. J.; Junge, H.; Gladiali, S.; Beller, M. *Nature* **2013**, *495*, 85-89; (f) Rodriguez-Lugo, R. E.; Trincado, M.; Vogt, M.; Tewes, F.; Santiso-Quinones, G.; Grützmacher, H. *Nat. Chem.* **2013**, *5*, 342-347; (g) Dobereiner, G. E.; Crabtree, R. H. *Chem. Rev.* **2010**, *110*, 681-703; (h) Gunanathan, C.; Milstein, D. *Chem. Rev.* **2014**, *114*, 12024-12087; (i) Zhao, J.; Hartwig, J. F. *Organometallics* **2005**, *24*, 2441-2446; (j) Fujita, K.; Tanino, N.; Yamaguchi, R. *Org. Lett.* **2007**, *9*, 109-111.

(101) (a) Hashiguchi, B. G.; Bischof, S. M.; Konnick, M. M.; Periana, R. A. *Acc. Chem. Res.* **2012**, *45*, 885-898; (b) Webb, J. R.; Burgess, S. A.; Cundari, T. R.; Gunnoe, T. B. *Dalton Trans.* **2013**, *42*, 16646-16665; (c) Ess, D. H.; Gunnoe, T. B.; Cundari, T. R.; Goddard, W. A., III; Periana, R. A. *Organometallics* **2010**, *29*, 6801-6815; (d) Cundari, T. R.; Grimes, T. V.; Gunnoe, T. B. *J. Am. Chem. Soc.* **2007**, *129*, 13172-13182; (e) Feng, Y.; Lail, M.; Foley, N. A.; Gunnoe, T. B.; Barakat, K. A.; Cundari, T. R.; Petersen, J. L. *J. Am. Chem. Soc.* **2006**, *128*, 7982-7994; (f) Truscott, B. J.; Nelson, D. J.; Lujan, C.; Slawin, A. M. Z.; Nolan, S. P. *Chem-Eur J* **2013**, *19*, 7904-7916; (g) Bercaw, J. E.; Hazari, N.; Labinger, J. A. *Organometallics* **2009**, *28*, 5489-5492; (h) Bercaw, J. E.; Hazari, N.; Labinger, J. A.; Oblad, P. F. *Angew. Chem. Int. Ed.* **2008**, *47*, 9941-9943; (i) Williams, T. J.; Caffyn, A. J. M.; Hazari, N.; Oblad, P. F.; Labinger, J. A.; Bercaw, J. E. *J. Am. Chem. Soc.* **2008**, *130*, 2418-2419; (j) Hanson, S. K.; Heinekey, D. M.; Goldberg, K. I. *Organometallics* **2008**, *27*, 1454-1463; (k) Kloek, S. M.; Heinekey, D. M.; Goldberg, K. L. *Angew. Chem. Int. Ed.* **2007**, *46*, 4736-4738; (l) Lohr, T. L.; Piers, W. E.; Parvez, M. *Chem. Sci.* **2013**, *4*, 770-775.

(102) (a) Gowrisankar, S.; Sergeev, A. G.; Anbarasan, P.; Spannenberg, A.; Neumann, H.; Beller, M. *J. Am. Chem. Soc.* **2010**, *132*, 11592-11598; (b) Zhang, H.; Ruiz-Castillo, P.; Buchwald, S. L. *Org. Lett.* **2018**, *20*, 1580-1583; (c) Carrow, B. P.; Hartwig, J. F. *J. Am. Chem. Soc.* **2011**, *133*, 2116-2119; (d) Miyaura, N. *J. Organomet. Chem.* **2002**, *653*, 54-57; (e) Christian, A. H.; Muller, P.; Monfette, S. *Organometallics* **2014**, *33*, 2134-2137; (f) Enthaler, S.; Company, A. *Chem. Soc. Rev.* **2011**, *40*, 4912-4924.

(103) (a) Piers, W. E. *Organometallics* **2011**, *30*, 13-16; (b) Hetterscheid, D. G. H.; Reek, J. N. H. *Angew. Chem. Int. Ed.* **2012**, *51*, 9740-9747; (c) Blakemore, J. D.; Schley, N. D.; Balcells, D.; Hull, J. F.; Olack, G. W.; Incarvito, C. D.; Eisenstein, O.; Brudvig, G. W.; Crabtree, R. H. *J. Am. Chem. Soc.* **2010**, *132*, 16017-16029; (d) Savini, A.; Bellachioma, G.; Ciancaleoni, G.; Zuccaccia, C.; Zuccaccia, D.; Macchioni, A. *Chem. Commun.* **2010**, *46*, 9218-9219; (e) Codola, Z.; Cardoso, J. M. S.; Royo, B.; Costas, M.; Lloret-Fillol, J. *Chem-Eur J* **2013**, *19*, 7203-7213; (f) Lalrempuia, R.; McDaniel, N. D.; Muller-Bunz, H.; Bernhard, S.; Albrecht, M. *Angew. Chem. Int. Ed.* **2010**, *49*, 9765-9768; (g) Hull, J. F.; Balcells, D.; Blakemore, J. D.; Incarvito, C. D.; Eisenstein, O.; Brudvig, G. W.; Crabtree, R. H. *J. Am. Chem. Soc.* **2009**, *131*, 8730-8731; (h) Hintermair, U.; Sheehan, S. W.; Parent, A. R.; Ess, D. H.; Richens, D. T.; Vaccaro, P. H.; Brudvig, G. W.; Crabtree, R. H. *J. Am. Chem. Soc.* **2013**, *135*, 10837-10851; (i) Kohl, S. W.; Weiner, L.; Schwartsburd, L.; Konstantinovski, L.; Shimon, L. J. W.; Ben-David, Y.; Iron, M. A.; Milstein, D. *Science* **2009**, *324*, 74-77.

(104) Bradley, D. C.; Mehrota, R. C.; Rothwell, I. P.; Singh, A. *Alkoxo and Aryloxo Derivatives of Metals*; Academic Press: San Diego, 2001.

(105) (a) Caulton, K. G. *New J. Chem.* **1994**, *18*, 25-41; (b) Mayer, J. M. *Comments Inorg. Chem.* **1988**, *8*, 125-135.

(106) (a) Holland, P. L.; Andersen, R. A.; Bergman, R. G. *Comments Inorg. Chem.* **1999**, *21*, 115-129; (b) Bryndza, H. E.; Fong, L. K.; Paciello, R. A.; Tam, W.; Bercaw, J. E. *J. Am. Chem. Soc.* **1987**, *109*, 1444-1456; (c) Bryndza, H. E.; Domaille, P. J.; Tam, W.; Fong, L. K.; Paciello, R. A.; Bercaw, J. E. *Polyhedron* **1988**, *7*, 1441-1452; (d) Bulls, A. R.; Bercaw, J. E.; Manriquez, J. M.; Thompson, M. E. *Polyhedron* **1988**, *7*, 1409-1428; (e) Stoutland, P. O.; Bergman, R. G.; Nolan, S. P.; Hoff, C. D. *Polyhedron* **1988**, *7*, 1429-1440; (f) Holland, P. L.; Andersen, R. A.; Bergman, R. G.; Huang, J. K.; Nolan, S. P. *J. Am. Chem. Soc.* **1997**, *119*, 12800-12814; (g) Devarajan, D.; Gunnoe, T. B.; Ess, D. H. *Inorg. Chem.* **2012**, *51*, 6710-6718.

(107) Johnson, T. J.; Folting, K.; Streib, W. E.; Martin, J. D.; Huffman, J. C.; Jackson, S. A.; Eisenstein, O.; Caulton, K. G. *Inorg. Chem.* **1995**, *34*, 488-499.

(108) Montag, M.; Zhang, J.; Milstein, D. *J. Am. Chem. Soc.* **2012**, *134*, 10325-10328.

(109) (a) Comanescu, C. C.; Iluc, V. M. *Polyhedron* **2018**, *143*, 176-183; (b) Comanescu, C. C.; Iluc, V. M. *Organometallics* **2014**, *33*, 6059-6064.

(110) (a) Ozerov, O. V. *Chem. Soc. Rev.* **2009**, *38*, 83-88; (b) Gillard, R. D.; Heaton, B. T.; Vaughan, D. H. *J Chem Soc A* **1970**, 3126-3130; (c) Milstein, D.; Calabrese, J. C.; Williams, I. D. *J. Am. Chem. Soc.* **1986**, *108*, 6387-6389; (d) Stevens, R. C.; Bau, R.; Milstein, D.; Blum, O.; Koetzle, T. F. *J. Chem. Soc., Dalton Trans.* **1990**, 1429-1432; (e) Blum, O.; Milstein, D. *J. Am. Chem. Soc.* **2002**, *124*, 11456-11467; (f) Burn, M. J.; Fickes, M. G.; Hartwig, J. F.; Hollander, F. J.; Bergman, R. G. *J. Am. Chem. Soc.* **1993**, *115*, 5875-5876; (g) Sponsler, M. B.; Weiller, B. H.; Stoutland, P. O.; Bergman, R. G. *J. Am. Chem. Soc.* **1989**, *111*, 6841-6843; (h) Darensbourg, M. Y.; Ludwig, M.; Riordan, C. G. *Inorg. Chem.* **1989**, *28*, 1630-1634; (i) Dibugno, C.; Pasquali, M.; Leoni, P.; Sabatino, P.; Braga, D. *Inorg. Chem.* **1989**, *28*, 1390-1394; (j) Seligson, A. L.; Cowan, R. L.; Trogler, W. C. *Inorg. Chem.* **1991**, *30*, 3371-3381; (k) Ladipo, F. T.; Kooti, M.; Merola, J. S. *Inorg. Chem.* **1993**, *32*, 1681-1688; (l) Morales-Morales, D.; Lee, D. W.; Wang, Z.; Jensen, C. M. *Organometallics* **2001**, *20*, 1144-1147; (m) Millard, M. D.; Moore, C. E.; Rheingold, A. L.; Figueroa, J. S. *J. Am. Chem. Soc.* **2010**, *132*, 8921-8923; (n) Kläring, P.; Pahl, S.; Braun, T.; Penner, A. *Dalton Trans.* **2011**, *40*, 6785; (o) Dorta, R.; Rozenberg, H.; Shimon, L. J. W.; Milstein, D. *Chem-Eur J* **2003**, *9*, 5237-5249; (p) Dorta, R.; Togni, A. *Organometallics* **1998**, *17*, 3423-3428; (q) Tani, K.; Iseki, A.; Yamagata, T. *Angew. Chem. Int. Ed.* **1998**, *37*, 3381-3383; (r) Yoshida, T.; Matsuda, T.; Okano, T.; Kitani, T.; Otsuka, S. *J. Am. Chem. Soc.* **1979**, *101*, 2027-2038.

(111) Olmstead, W. N.; Margolin, Z.; Bordwell, F. G. *J. Org. Chem.* **1980**, *45*, 3295-3299.

(112) Klein, D. P.; Hayes, J. C.; Bergman, R. G. *J. Am. Chem. Soc.* **1988**, *110*, 3704-3706.

(113) (a) Green, L. M.; Meek, D. W. *Organometallics* **1989**, *8*, 659-666; (b) Doyle, L. E.; Piers, W. E.; Borau-Garcia, J.; Sgro, M. J.; Spasyuk, D. M. *Chem. Sci.* **2016**, *7*, 921-931.

(114) Rees, W. M.; Churchill, M. R.; Fettinger, J. C.; Atwood, J. D. *Organometallics* **1985**, *4*, 2179-2185.

(115) Churchill, M. R.; Fettinger, J. C.; Rees, W. M.; Atwood, J. D. *J. Organomet. Chem.* **1986**, *308*, 361-371.

(116) Janik, T. S.; Bernard, K. A.; Churchill, M. R.; Atwood, J. D. *J. Organomet. Chem.* **1987**, *323*, 247-259.

(117) (a) Edwards, A. J.; Elipe, S.; Esteruelas, M. A.; Lahoz, F. J.; Oro, L. A.; Valero, C. *Organometallics* **1997**, *16*, 3828-3836; (b) Lee, D. W.; Jensen, C. M.; Morales-Morales, D. *Organometallics* **2003**, *22*, 4744-4749.

(118) Yoshida, T.; Thorn, D. L.; Okano, T.; Ibers, J. A.; Otsuka, S. *J. Am. Chem. Soc.* **1979**, *101*, 4212-4221.

(119) Arndtsen, B. A.; Bergman, R. G. *Science* **1995**, *270*, 1970-1973.

(120) (a) Burger, P.; Bergman, R. G. *J. Am. Chem. Soc.* **1993**, *115*, 10462-10463; (b) Klei, S. R.; Tilley, T. D.; Bergman, R. G. *J. Am. Chem. Soc.* **2000**, *122*, 1816-1817.

(121) Yang, J.; Brookhart, M. *J. Am. Chem. Soc.* **2007**, *129*, 12656-12657.

(122) Yang, J.; Brookhart, M. *Adv. Synth. Catal.* **2008**, *351*, 175-187.

(123) Yang, J.; White, P. S.; Schauer, C. K.; Brookhart, M. *Angew. Chem. Int. Ed.* **2008**, *47*, 4141-4143.

(124) Yang, J.; White, P. S.; Brookhart, M. *J. Am. Chem. Soc.* **2008**, *130*, 17509-17518.

(125) (a) Park, S.; Brookhart, M. *Organometallics* **2010**, *29*, 6057-6064; (b) Park, S.; Brookhart, M. *Chem. Commun.* **2011**, *47*, 3643.

(126) Park, S.; Bézier, D.; Brookhart, M. *J. Am. Chem. Soc.* **2012**, *134*, 11404-11407.

(127) (a) Calimano, E.; Tilley, T. D. *J. Am. Chem. Soc.* **2008**, *130*, 9226-9227; (b) Calimano, E.; Tilley, T. D. *J. Am. Chem. Soc.* **2009**, *131*, 11161-11173.

(128) Fan, L.; Parkin, S.; Ozerov, O. V. *J. Am. Chem. Soc.* **2005**, *127*, 16772-16773.

(129) (a) Glaser, P. B.; Tilley, T. D. *J. Am. Chem. Soc.* **2003**, *125*, 13640-13641; (b) Waterman, R.; Hayes, P. G.; Tilley, T. D. *Acc. Chem. Res.* **2007**, *40*, 712-719.

(130) (a) Böhme, E. *Die Naturwissenschaften* **1931**, *19*, 691-691; (b) Beddie, C.; Hall, M. B. *J. Am. Chem. Soc.* **2004**, *126*, 13564-13565.

(131) (a) Fryzuk, M. D.; MacNeil, P. A. *Organometallics* **1982**, *1*, 1540-1541; (b) Fryzuk, M. D.; Huang, L.; McManus, N. T.; Paglia, P.; Rettig, S. J.; White, G. S. *Organometallics* **1992**, *11*, 2979-2990; (c) Watson, L. A.; Coalter Iii, J. N.; Ozerov, O.; Pink, M.; Huffman, J. C.; Caulton, K. G. *New J. Chem.* **2002**, *27*, 263-273; (d) Walstrom, A. N.; Watson, L. A.; Pink, M.; Caulton, K. G. *Organometallics* **2004**, *23*, 4814-4816; (e) Clarke, Z. E.; Maragh, P. T.; Dasgupta, T. P.; Gusev, D. G.; Lough, A. J.; Abdur-Rashid, K. *Organometallics* **2006**, *25*, 4113-4117; (f) Whited, M. T.; Grubbs, R. H. *Organometallics* **2008**, *27*, 5737-5740.

(132) Klei, S. R.; Tilley, T. D.; Bergman, R. G. *Organometallics* **2002**, *21*, 3376-3387.

(133) Mitchell, G. P.; Tilley, T. D. *Angew. Chem. Int. Ed.* **1998**, *37*, 2524-2526.

(134) DeMott, J. C.; Gu, W.; McCulloch, B. J.; Herbert, D. E.; Goshert, M. D.; Walensky, J. R.; Zhou, J.; Ozerov, O. V. *Organometallics* **2015**, *34*, 3930-3933.

(135) (a) Straus, D. A.; Tilley, T. D.; Rheingold, A. L.; Geib, S. J. *J. Am. Chem. Soc.* **1987**, *109*, 5872-5873; (b) Zybill, C.; Müller, G. *Angewandte Chemie International Edition in English* **1987**, *26*, 669-670; (c) Ueno, K.; Tobita, H.; Shimoi, M.; Ogino, H. *J. Am. Chem. Soc.* **1988**, *110*, 4092-4093.

(136) (a) Straus, D. A.; Grumbine, S. D.; Tilley, T. D. *J. Am. Chem. Soc.* **1990**, *112*, 7801-7802; (b) Leis, C.; Zybill, C.; Lachmann, J.; Müller, G. *Polyhedron* **1991**, *10*, 1163-1171; (c) Woo, L. K.; Smith, D. A.; Young, V. G. *Organometallics* **1991**, *10*, 3977-3982.

(137) Wick, D. D.; Goldberg, K. I. *J. Am. Chem. Soc.* **1997**, *119*, 10235-10236.

(138) (a) Poorters, L.; Armspach, D.; Matt, D.; Toupet, L.; Jones, P. G. *Angew. Chem. Int. Ed.* **2007**, *46*, 2663-2665; (b) Varonka, M. S.; Warren, T. H. *Inorg. Chem.* **2009**, *48*, 5605-5607; (c) Fenton, H.; Tidmarsh, I. S.; Ward, M. D. *Dalton Trans.* **2010**, *39*, 3805; (d) Cimadevilla, F.; García, M. E.; García-Vivó, D.; Ruiz, M. A.; Rueda, M. T.; Halut, S. *J. Organomet. Chem.* **2012**, *699*, 67-74.

(139) (a) Salomon, M. A.; Jungton, A.-K.; Braun, T. *Dalton Trans.* **2009**, 7669; (b) Betoré, M. P.; Casado, M. A.; García-Orduña, P.; Lahoz, F. J.; Polo, V.; Oro, L. A. *Organometallics* **2016**, *35*, 720-731.

(140) Braddock-Wilking, J.; Schieser, M.; Brammer, L.; Huhmann, J.; Shaltout, R. *J. Organomet. Chem.* **1995**, *499*, 89-98.

(141) (a) Kameo, H.; Ikeda, K.; Sakaki, S.; Takemoto, S.; Nakazawa, H.; Matsuzaka, H. *Dalton Trans.* **2016**, *45*, 7570-7580; (b) Imayoshi, R.; Nakajima, K.; Takaya, J.; Iwasawa, N.; Nishibayashi, Y. *Eur. J. Inorg. Chem.* **2017**, *2017*, 3769-3778.

Appendix A: Crystallographic Experimental Details

Table A1. Crystallographic experimental details for **2-2c**.

A. Crystal Data	
formula	$C_{43}H_{70}IrP_3Si$
formula weight	900.19
crystal dimensions (mm)	0.30 × 0.29 × 0.08
crystal system	triclinic
space group	$P\bar{1}$ (No. 2)
unit cell parameters[a]	
a (Å)	10.1287 (19)
b (Å)	10.960 (2)
c (Å)	21.081 (4)
α (deg)	102.048 (3)
β (deg)	94.584 (3)
γ (deg)	111.596 (2)
V (Å^3)	2096.1 (7)
Z	2
ρ_{calcd} (g cm^{-3})	1.426
μ (mm^{-1})	3.356
B. Data Collection and Refinement Conditions	
diffractometer	Bruker D8/APEX II CCD[b]
radiation (λ [Å])	graphite-monochromated Mo Kα (0.71073)
temperature (°C)	–100
scan type	ω scans (0.3°) (20 s exposures)
data collection 2θ limit (deg)	51.60
total data collected	7791 (-12 ≤ h ≤ 12, -13 ≤ k ≤ 13, 0 ≤ l ≤ 25)
independent reflections	7791 (R_{int} = 0.0000)
number of observed reflections (*NO*)	7387 [$F_o^2 \geq 2\sigma(F_o^2)$]
structure solution method	direct methods (*SHELXS–97*[c])
refinement method	full-matrix least-squares on F^2 (*SHELXL–97*[c])
absorption correction method	multi-scan (*TWINABS*)
range of transmission factors	0.7658–0.4285
data/restraints/parameters	7791 / 0 / 438
goodness-of-fit (*S*)[d] [all data]	1.071
final R indices[e]	
R_1 [$F_o^2 \geq 2\sigma(F_o^2)$]	0.0434
wR_2 [all data]	0.0994
largest difference peak and hole	3.059 and –1.625 e Å^{-3}

(continued)

Table A1. Crystallographic experimental details for **2-2c** (continued).

[a]Obtained from least-squares refinement of 3320 reflections with $4.50° < 2\theta < 47.92°$.

[b]Programs for diffractometer operation, data collection, data reduction and absorption correction were those supplied by Bruker. The crystal used for data collection was found to display non-merohedral twinning. Both components of the twin were indexed with the program *CELL_NOW* (Bruker AXS Inc., Madison, WI, 2004). The second twin component can be related to the first component by 180º rotation about the [$^2/_5$ $^1/_2$ 1] axis in real space and about the [0 0 1] axis in reciprocal space. Integrated intensities for the reflections from the two components were written into a *SHELXL-97* HKLF 5 reflection file with the data integration program *SAINT* (version 7.68A), using all reflection data (exactly overlapped, partially overlapped and non-overlapped). The refined value of the twin fraction (*SHELXL-97* BASF parameter) was 0.4315(10).

[c]Sheldrick, G. M. *Acta Crystallogr.* **2008**, *A64*, 112–122.

[d]$S = [\Sigma w(F_o^2 - F_c^2)^2/(n-p)]^{1/2}$ (n = number of data; p = number of parameters varied; $w = [\sigma^2(F_o^2) + (0.0424P)^2 + 7.8454P]^{-1}$ where $P = [\mathrm{Max}(F_o^2, 0) + 2F_c^2]/3$).

[e]$R_1 = \Sigma||F_o| - |F_c||/\Sigma|F_o|$; $wR_2 = [\Sigma w(F_o^2 - F_c^2)^2/\Sigma w(F_o^4)]^{1/2}$.

Table A2. Crystallographic experimental details for **2-3c**.

A. Crystal Data	
formula	$C_{46}H_{68}IrP_3Si$
formula weight	934.20
crystal dimensions (mm)	0.15 × 0.13 × 0.12
crystal system	triclinic
space group	$P\bar{1}$ (No. 2)
unit cell parameters[a]	
a (Å)	11.8659 (2)
b (Å)	18.6585 (4)
c (Å)	20.9944 (4)
α (deg)	102.5370 (8)
β (deg)	98.5244 (7)
γ (deg)	95.7853 (8)
V (Å^3)	4444.43 (15)
Z	4
ρ_{calcd} (g cm^{-3})	1.396
μ (mm^{-1})	7.307
B. Data Collection and Refinement Conditions	
diffractometer	Bruker D8/APEX II CCD[b]
radiation (λ [Å])	Cu Kα (1.54178) (microfocus source)
temperature (°C)	–100
scan type	ω scans (0.8°) (5 s exposures)
data collection 2θ limit (deg)	140.24
total data collected	15931 (-14 ≤ h ≤ 14, -22 ≤ k ≤ 21, 0 ≤ l ≤ 25)
independent reflections	15931 (R_{int} = 0.0000)
number of observed reflections (*NO*)	14958 [$F_o^2 \geq 2\sigma(F_o^2)$]
structure solution method	Patterson/structure expansion (*DIRDIF–2008*[c])
refinement method	full-matrix least-squares on F^2 (*SHELXL–97*[d])
absorption correction method	multi-scan (*TWINABS*)
range of transmission factors	0.4619–0.4070
data/restraints/parameters	15931 / 6[e] / 942
goodness-of-fit (*S*)[f] [all data]	1.226
final R indices[g]	
R_1 [$F_o^2 \geq 2\sigma(F_o^2)$]	0.0343
wR_2 [all data]	0.0887
largest difference peak and hole	1.563 and –0.935 e Å^{-3}

(continued)

Table A2. Crystallographic experimental details for **2-3c** (continued).

[a]Obtained from least-squares refinement of 4803 reflections with $5.76° < 2\theta < 139.22°$.

[b]Programs for diffractometer operation, data collection, data reduction and absorption correction were those supplied by Bruker. The crystal used for data collection was found to display non-merohedral twinning. Both components of the twin were indexed with the program *CELL_NOW* (Bruker AXS Inc., Madison, WI, 2004). The second twin component can be related to the first component by 180º rotation about the [1 0 $^{-1}/_{4}$] axis in real space and about the [–1 1 0] axis in reciprocal space. Integrated intensities for the reflections from the two components were written into a *SHELXL-97* HKLF 5 reflection file with the data integration program *SAINT* (version 7.68A), using all reflection data (exactly overlapped, partially overlapped and non-overlapped). The refined value of the twin fraction (*SHELXL-97* BASF parameter) was 0.4605(7).

[c]Beurskens, P. T.; Beurskens, G.; de Gelder, R.; Smits, J. M. M.; Garcia-Granda, S.; Gould, R. O. (2008). The *DIRDIF-2008* program system. Crystallography Laboratory, Radboud University Nijmegen, The Netherlands.

[d]Sheldrick, G. M. *Acta Crystallogr.* **2008**, *A64*, 112–122.

[e](a) The Ir–H1 distances in both crystallographically-independent molecules were constrained to be 1.50(1) Å. (b) The P1···H1 and P2···H1 distances were constrained to be equal (within 0.003 Å) during refinement ($d(P1\cdots H1)_A = d(P2\cdots H1)_A$; $d(P1\cdots H1)_B = d(P2\cdots H1)_B$). (c) The Si–H1 distances in both molecules were constrained to be equal (within 0.003 Å) during refinement ($d(Si\cdots H1)_A = d(Si\cdots H1)_B$). (d) The P3–H3P distances in both molecules were constrained to be equal (within 0.003 Å) during refinement ($d(P3–H3P)_A = d(P3–H3P)_B$).

[f]$S = [\Sigma w(F_o^2 - F_c^2)^2/(n-p)]^{1/2}$ (n = number of data; p = number of parameters varied; $w = [\sigma^2(F_o^2) + 13.4335P]^{-1}$ where $P = [\mathrm{Max}(F_o^2, 0) + 2F_c^2]/3$).

[g]$R_1 = \Sigma||F_o| - |F_c||/\Sigma|F_o|$; $wR_2 = [\Sigma w(F_o^2 - F_c^2)^2/\Sigma w(F_o^4)]^{1/2}$.

Table A3. Crystallographic experimental details for **2-3d,d'**.

A. Crystal Data	
formula	$C_{41}H_{66}IrP_3Si$
formula weight	872.13
crystal dimensions (mm)	0.39× 0.28 × 0.23
crystal system	monoclinic
space group	$P2_1/n$ (an alternate setting of $P2_1/c$ [No. 14])
unit cell parameters[a]	
a (Å)	11.8070 (3)
b (Å)	17.5157 (4)
c (Å)	20.3215 (5)
β (deg)	91.2944 (9)
V (Å^3)	4201.57 (18)
Z	4
ρ_{calcd} (g cm^{-3})	1.379
μ (mm^{-1})	7.687
B. Data Collection and Refinement Conditions	
diffractometer	Bruker D8/APEX II CCD[b]
radiation (λ [Å])	Cu Kα (1.54178) (microfocus source)
temperature (°C)	–100
scan type	ω and ϕ scans (1.0°) (5 s exposures)
data collection 2θ limit (deg)	147.97
total data collected	29535 (-14 ≤h≤ 14, -21 ≤k≤ 21, -25 ≤l≤ 25)
independent reflections	8422 (R_{int} =0.0238)
number of observed reflections (*NO*)	8385 [$F_o^2 \geq 2\sigma(F_o^2)$]
structure solution method	Patterson/structure expansion (*DIRDIF–2008*[c])
refinement method	full-matrix least-squares on F^2 (*SHELXL–2014*[d])
absorption correction method	Gaussian integration (face-indexed)
range of transmission factors	0.3910–0.1437
data/restraints/parameters	8422 / 1[e] / 441
goodness-of-fit (*S*)[f] [all data]	1.187
final *R* indices[g]	
R_1 [$F_o^2 \geq 2\sigma(F_o^2)$]	0.0251
wR_2 [all data]	0.0582
largest difference peak and hole	1.623 and –1.073 e Å^{-3}

(continued)

Table A3. Crystallographic Experimental Details for **2-3d,d'** (continued).

[a]Obtained from least-squares refinement of 9920 reflections with $6.66° < 2\theta < 147.06°$.

[b]Programs for diffractometer operation, data collection, data reduction and absorption correction were those supplied by Bruker.

[c]Beurskens, P. T.; Beurskens, G.; de Gelder, R.; Smits, J. M. M.; Garcia-Granda, S.; Gould, R. O. (2008). The *DIRDIF-2008* program system. Crystallography Laboratory, RadboudUniversityNijmegen, The Netherlands.

[d]Sheldrick, G. M. *Acta Crystallogr.* **2015**, *C71*, 3–8.

[e]The P3B–C2B distance was constrained to be 1.85(1) Å during refinement.

[e]$S = [\Sigma w(F_o^2 - F_c^2)^2/(n-p)]^{1/2}$ (n = number of data; p = number of parameters varied; $w = [\sigma^2(F_o^2) + (0.0127P)^2 + 7.6284P]^{-1}$ where $P = [\mathrm{Max}(F_o^2, 0) + 2F_c^2]/3$).

[f]$R_1 = \Sigma||F_o| - |F_c||/\Sigma|F_o|$; $wR_2 = [\Sigma w(F_o^2 - F_c^2)^2/\Sigma w(F_o^4)]^{1/2}$.

Table A4. Crystallographic Experimental Details for **2-8**.

A. Crystal Data	
formula	$C_{52}H_{78}IrP_3Si$
formula weight	1016.34
crystal dimensions (mm)	0.10 × 0.10 × 0.06
crystal system	monoclinic
space group	$P2_1/c$ (No. 14)
unit cell parameters[a]	
a (Å)	14.7219(2)
b (Å)	16.1995(3)
c (Å)	21.8240(4)
β (deg)	106.2306(8)
V (Å^3)	4997.31(15)
Z	4
ρ_{calcd} (g cm^{-3})	1.351
μ (mm^{-1})	6.542
B. Data Collection and Refinement Conditions	
diffractometer	Bruker D8/APEX II CCD[b]
radiation (λ [Å])	Cu Kα (1.54178) (microfocus source)
temperature (°C)	–100
scan type	ω and ϕ scans (1.0°) (5 s exposures)
data collection 2θ limit (deg)	148.41
total data collected	169982 (-18 ≤ h ≤ 18, -20 ≤ k ≤ 20, -26 ≤ l ≤ 27)
independent reflections	10142 (R_{int} = 0.0519)
number of observed reflections (*NO*)	9375 [$F_o^2 \geq 2\sigma(F_o^2)$]
structure solution method	intrinsic phasing (*SHELXT-2014*[c])
refinement method	full-matrix least-squares on F^2 (*SHELXL–2017*[d])
absorption correction method	Gaussian integration (face-indexed)
range of transmission factors	0.7462–0.5779
data/restraints/parameters	10142 / 0 / 540
goodness-of-fit (*S*)[e] [all data]	1.026
final R indices[f]	
R_1 [$F_o^2 \geq 2\sigma(F_o^2)$]	0.0180
wR_2 [all data]	0.0449
largest difference peak and hole	0.584 and –0.732 e Å^{-3}

(continued)

Table A4. Crystallographic Experimental Details for **2-8** (continued).

[a]Obtained from least-squares refinement of 9645 reflections with $6.26° < 2\theta < 147.62°$.

[b]Programs for diffractometer operation, data collection, data reduction and absorption correction were those supplied by Bruker.

[c]Sheldrick, G. M. *Acta Crystallogr.* **2015**, *A71*, 3–8. (*SHELXT-2014*)

[d]Sheldrick, G. M. *Acta Crystallogr.* **2015**, *C71*, 3–8. (*SHELXL-2017*)

[e]$S = [\Sigma w(F_o^2 - F_c^2)^2/(n - p)]^{1/2}$ (n = number of data; p = number of parameters varied; $w = [\sigma^2(F_o^2) + (0.0237P)^2 + 2.20236P]^{-1}$ where $P = [\text{Max}(F_o^2, 0) + 2F_c^2]/3$).

[f]$R_1 = \Sigma||F_o| - |F_c||/\Sigma|F_o|$; $wR_2 = [\Sigma w(F_o^2 - F_c^2)^2/\Sigma w(F_o^4)]^{1/2}$.

Table A5. Crystallographic Experimental Details for **3-3**.

A. Crystal Data	
formula	$C_{72}H_{109}IrO_3P_2Si$
formula weight	1304.82
crystal dimensions (mm)	0.31×0.29×0.05
crystal system	monoclinic
space group	$P2_1/n$ (an alternate setting of $P2_1/c$ [No. 14])
unit cell parameters[a]	
a (Å)	15.5579(6)
b (Å)	16.5406(6)
c (Å)	27.9646(10)
β (deg)	105.2975(5)
V (Å^3)	6941.4(4)
Z	4
ρ_{calcd} (g cm^{-3})	1.249
μ (mm^{-1})	2.030
B. Data Collection and Refinement Conditions	
diffractometer	Bruker PLATFORM/APEX II CCD[b]
radiation (λ [Å])	graphite-monochromated Mo Kα (0.71073)
temperature (°C)	–80
scan type	ω scans (0.3°) (20 s exposures)
data collection 2θ limit (deg)	55.11
total data collected	58824 (-20≤h≤20, -21≤k≤21, -35≤l≤36)
independent reflections	16032 (R_{int} = 0.0301)
number of observed reflections (*NO*)	13727 [$F_o^2 \geq 2\sigma(F_o^2)$]
structure solution method	intrinsic phasing (*SHELXT-2014*[c])
refinement method	full-matrix least-squares on F^2 (*SHELXL–2016*[d])
absorption correction method	Gaussian integration (face-indexed)
range of transmission factors	0.8245–0.4195
data/restraints/parameters	16032 / 58[e] / 728
goodness-of-fit (*S*)[f] [all data]	1.026
final *R* indices[g]	
R_1 [$F_o^2 \geq 2\sigma(F_o^2)$]	0.0262
wR_2 [all data]	0.0679
largest difference peak and hole	1.531 and –0.539 e Å^{-3}

(continued)

Table A5. Crystallographic Experimental Details for **3-3** (continued).

[a]Obtained from least-squares refinement of 9987 reflections with $4.62° < 2\theta < 55.02°$.

[b]Programs for diffractometer operation, data collection, data reduction and absorption correction were those supplied by Bruker.

[c]Sheldrick, G. M. *ActaCrystallogr.***2015**, *A71*, 3–8. (*SHELXT-2014*)

[d]Sheldrick, G. M. *ActaCrystallogr.***2015**, *C71*, 3–8. (*SHELXL-2017*)

[e]The C–C distancesof the disordered *tert*-butyl group were restrained to be approximately the same by use of the *SHELXL***SADI** instruction. Likewise, the 1,2 and 1,3 C–C and C···C distances within the disordered solvent pentane molecule were similarly restrained.

[f]$S = [\Sigma w(F_o^2 - F_c^2)^2/(n-p)]^{1/2}$ (n = number of data; p = number of parameters varied; $w = [\sigma^2(F_o^2) + (0.0352P)^2 + 4.0190P]^{-1}$ where$P = [\mathrm{Max}(F_o^2, 0) + 2F_c^2]/3$).

[g]$R_1 = \Sigma||F_o| - |F_c||/\Sigma|F_o|$; $wR_2 = [\Sigma w(F_o^2 - F_c^2)^2/\Sigma w(F_o^4)]^{1/2}$.

Table A6. Crystallographic Experimental Details for **3-4**.

A. Crystal Data	
formula	$C_{45}H_{76.75}Cl_{0.25}IrO_{2.75}P_2Si$
formula weight	952.90
crystal dimensions (mm)	0.45 × 0.27 × 0.21
crystal system	orthorhombic
space group	*Pnma* (No. 62)
unit cell parameters[a]	
a (Å)	16.5941(5)
b (Å)	15.1029(4)
c (Å)	18.6764(6)
V (Å^3)	4680.7(2)
Z	4
ρ_{calcd} (g cm^{-3})	1.352
μ (mm^{-1})	6.804
B. Data Collection and Refinement Conditions	
diffractometer	Bruker D8/APEX II CCD[b]
radiation (λ [Å])	Cu Kα (1.54178) (microfocus source)
temperature (°C)	–100
scan type	ω and ϕ scans (1.0°) (5-10-10 s exposures)[c]
data collection 2θ limit (deg)	147.92
total data collected	96806 (-20 ≤ *h* ≤ 19, -18 ≤ *k* ≤ 18, -23 ≤ *l* ≤ 23)
independent reflections	4919 (R_{int} = 0.0377)
number of observed reflections (*NO*)	4897 [$F_o^2 \geq 2\sigma(F_o^2)$]
structure solution method	intrinsic phasing (*SHELXT-2014*[c])
refinement method	full-matrix least-squares on F^2 (*SHELXL–2016*[d])
absorption correction method	Gaussian integration (face-indexed)
range of transmission factors	0.3011–0.0816
data/restraints/parameters	4919 / 0 / 270
goodness-of-fit (*S*)[e] [all data]	1.089
final *R* indices[f]	
R_1 [$F_o^2 \geq 2\sigma(F_o^2)$]	0.0205
wR_2 [all data]	0.0562
largest difference peak and hole	1.634 and –1.156 e Å^{-3}

(continued)

Table A6. Crystallographic Experimental Details for **3-4** (continued).

[a]Obtained from least-squares refinement of 9740 reflections with $9.22° < 2\theta < 147.46°$.

[b]Programs for diffractometer operation, data collection, data reduction and absorption correction were those supplied by Bruker.

[c]Data were collected with the detector set at three different positions. Low-angle (detector $2\theta = -33^{o}$) data frames were collected using a scan time of 5 s, medium-angle (detector $2\theta = 75^{o}$) frames using a scan time of 10 s, and high-angle (detector $2\theta = 117^{o}$) frames using a scan time of 10 s.

[c]Sheldrick, G. M. *Acta Crystallogr.* **2015**, *A71*, 3–8. (*SHELXT-2014*)

[d]Sheldrick, G. M. *Acta Crystallogr.* **2015**, *C71*, 3–8. (*SHELXL-2016*)

[e]$S = [\Sigma w(F_o^2 - F_c^2)^2/(n - p)]^{1/2}$ (n = number of data; p = number of parameters varied; $w = [\sigma^2(F_o^2) + (0.0310P)^2 + 3.3834P]^{-1}$ where $P = [\mathrm{Max}(F_o^2, 0) + 2F_c^2]/3$).

[f]$R_1 = \Sigma||F_o| - |F_c||/\Sigma|F_o|$; $wR_2 = [\Sigma w(F_o^2 - F_c^2)^2/\Sigma w(F_o^4)]^{1/2}$.

Table A7. Crystallographic Experimental Details for **4-1**.

A. Crystal Data	
formula	$C_{49}H_{67}IrP_2Si_2$
formula weight	966.34
crystal dimensions (mm)	0.16 × 0.08 × 0.07
crystal system	triclinic
space group	$P\bar{1}$ (No. 2)
unit cell parameters[a]	
a (Å)	12.4101(8)
b (Å)	14.0625(9)
c (Å)	14.4805(9)
α (deg)	87.706(3)
β (deg)	76.083(4)
γ (deg)	71.167(3)
V (Å^3)	2319.6(3)
Z	2
ρ_{calcd} (g cm^{-3})	1.384
μ (mm^{-1})	6.945
B. Data Collection and Refinement Conditions	
diffractometer	Bruker D8/APEX II CCD[b]
radiation (λ [Å])	Cu Kα (1.54178) (microfocus source)
temperature (°C)	–100
scan type	ω and ϕ scans (1.0°) (5 s exposures)
data collection 2θ limit (deg)	148.45
total data collected	16839 (-15 ≤ h ≤ 15, -17 ≤ k ≤ 17, -18 ≤ l ≤ 18)
independent reflections	9049 (R_{int} = 0.0174)
number of observed reflections (*NO*)	8544 [$F_o^2 \geq 2\sigma(F_o^2)$]
structure solution method	intrinsic phasing (*SHELXT-2014*[c])
refinement method	full-matrix least-squares on F^2 (*SHELXL–2017*[d])
absorption correction method	Gaussian integration (face-indexed)
range of transmission factors	0.4212–0.2631
data/restraints/parameters	9049 / 0 / 519
goodness-of-fit (S)[e] [all data]	1.102
final R indices[f]	
R_1 [$F_o^2 \geq 2\sigma(F_o^2)$]	0.0233
wR_2 [all data]	0.0584
largest difference peak and hole	0.602 and –1.003 e Å^{-3}

(continued)

Table A7. Crystallographic Experimental Details for **4-1** (continued).

[a]Obtained from least-squares refinement of 9491 reflections with $6.30° < 2\theta < 147.30°$.

[b]Programs for diffractometer operation, data collection, data reduction and absorption correction were those supplied by Bruker

[c]Sheldrick, G. M. *Acta Crystallogr.* **2015**, *A71*, 3–8. (*SHELXT-2014*)

[d]Sheldrick, G. M. *Acta Crystallogr.* **2015**, *C71*, 3–8. (*SHELXL-2017*)

[e]$S = [\Sigma w(F_o^2 - F_c^2)^2/(n - p)]^{1/2}$ (n = number of data; p = number of parameters varied; $w = [\sigma^2(F_o^2) + (0.0183P)^2 + 3.1785P]^{-1}$ where $P = [\mathrm{Max}(F_o^2, 0) + 2F_c^2]/3$).

[f]$R_1 = \Sigma||F_o| - |F_c||/\Sigma|F_o|$; $wR_2 = [\Sigma w(F_o^2 - F_c^2)^2/\Sigma w(F_o^4)]^{1/2}$.

Table A8. Crystallographic Experimental Details for **4-6**.

A. Crystal Data	
formula	$C_{39}H_{55}IrO_2P_2Si$
formula weight	838.06
crystal dimensions (mm)	0.34×0.33 × 0.13
crystal system	monoclinic
space group	$P2_1/n$ (an alternate setting of $P2_1/c$ [No. 14])
unit cell parameters[a]	
a (Å)	10.5878 (4)
b (Å)	18.2888 (6)
c (Å)	19.2237 (7)
β (deg)	98.9625 (4)
V (Å^3)	3677.0 (2)
Z	4
ρ_{calcd} (g cm^{-3})	1.514
μ (mm^{-1})	3.783
B. Data Collection and Refinement Conditions	
diffractometer	Bruker PLATFORM/APEX II CCD[b]
radiation (λ [Å])	graphite-monochromated Mo Kα (0.71073)
temperature (°C)	–80
scan type	ω scans (0.3°) (15 s exposures)
data collection 2θ limit (deg)	56.60
total data collected	34011 (-14 ≤h≤ 14, -23 ≤k≤ 24, -25 ≤l≤ 25)
independent reflections	9063 (R_{int} = 0.0249)
number of observed reflections (*NO*)	7923 [$F_o^2 \geq 2\sigma(F_o^2)$]
structure solution method	Patterson/structure expansion (*DIRDIF–2008*[c])
refinement method	full-matrix least-squares on F^2 (*SHELXL–2014*[d])
absorption correction method	Gaussian integration (face-indexed)
range of transmission factors	0.7519–0.3953
data/restraints/parameters	9063 / 0 / 407
goodness-of-fit (*S*)[e] [all data]	1.048
final *R* indices[f]	
R_1 [$F_o^2 \geq 2\sigma(F_o^2)$]	0.0196
wR_2 [all data]	0.0493
largest difference peak and hole	1.102 and –0.482 e Å^{-3}

(continued)

Table A8. Crystallographic Experimental Details for **4-6** (continued).

[a]Obtained from least-squares refinement of 9869 reflections with $4.46° < 2\theta < 55.22°$.

[b]Programs for diffractometer operation, data collection, data reduction and absorption correction were those supplied by Bruker.

[c]Beurskens, P. T.; Beurskens, G.; de Gelder, R.; Smits, J. M. M.; Garcia-Granda, S.; Gould, R. O. (2008). The *DIRDIF-2008* program system. Crystallography Laboratory, RadboudUniversityNijmegen, The Netherlands.

[d]Sheldrick, G. M. *Acta Crystallogr.* **2015**, *C71*, 3–8.

[e]$S = [\Sigma w(F_o^2 - F_c^2)^2/(n - p)]^{1/2}$ (n = number of data; p = number of parameters varied; $w = [\sigma^2(F_o^2) + (0.0269P)^2 + 0.3828P]^{-1}$ where $P = [\text{Max}(F_o^2, 0) + 2F_c^2]/3$).

[f]$R_1 = \Sigma||F_o| - |F_c||/\Sigma|F_o|$; $wR_2 = [\Sigma w(F_o^2 - F_c^2)^2/\Sigma w(F_o^4)]^{1/2}$.

Table A9. Crystallographic Experimental Details for **4-7**.

A. Crystal Data	
formula	$C_{54}H_{93}IrLiO_4P_2Si_2$
formula weight	1123.54
crystal dimensions (mm)	0.37 × 0.16 × 0.09
crystal system	orthorhombic
space group	$P2_12_12_1$ (No. 19)
unit cell parameters[a]	
a (Å)	13.2167 (4)
b (Å)	20.4003 (7)
c (Å)	20.8827 (7)
V (Å^3)	5630.5 (3)
Z	4
ρ_{calcd} (g cm^{-3})	1.325
μ (mm^{-1})	2.511
B. Data Collection and Refinement Conditions	
diffractometer	Bruker D8/APEX II CCD[b]
radiation (λ [Å])	graphite-monochromated Mo Kα (0.71073)
temperature (°C)	–100
scan type	ω scans (0.3°) (20 s exposures)
data collection 2θ limit (deg)	56.72
total data collected	51998 (-17 ≤*h*≤ 17, -27 ≤*k*≤ 27, -27 ≤*l*≤ 27)
independent reflections	13874 (R_{int} = 0.0338)
number of observed reflections (*NO*)	12939 [$F_o^2 \geq 2\sigma(F_o^2)$]
structure solution method	Patterson/structure expansion (*DIRDIF–2008*[c])
refinement method	full-matrix least-squares on F^2 (*SHELXL–2013*[d])
absorption correction method	Gaussian integration (face-indexed)
range of transmission factors	0.8768–0.5335
data/restraints/parameters	13874 / 0 / 626
Flack absolute structure parameter[e]	0.0017(18)
goodness-of-fit (*S*)[f] [all data]	0.948
final *R* indices[g]	
R_1 [$F_o^2 \geq 2\sigma(F_o^2)$]	0.0195
wR_2 [all data]	0.0378
largest difference peak and hole	0.781 and –0.574 e Å^{-3}

(continued)

Table A9. Crystallographic Experimental Details for **4-7** (continued).

[a]Obtained from least-squares refinement of 9870 reflections with $4.44° < 2\theta < 44.90°$.

[b]Programs for diffractometer operation, data collection, data reduction and absorption correction were those supplied by Bruker.

[c]Beurskens, P. T.; Beurskens, G.; de Gelder, R.; Smits, J. M. M.; Garcia-Granda, S.; Gould, R. O. (2008). The *DIRDIF-2008* program system. Crystallography Laboratory, RadboudUniversityNijmegen, The Netherlands.

[d]Sheldrick, G. M. *Acta Crystallogr.***2008**, *A64*, 112–122.

[e]Flack, H. D. *Acta Crystallogr.***1983**, *A39*, 876–881; Flack, H. D.; Bernardinelli, G. *Acta Crystallogr.***1999**, *A55*, 908–915; Flack, H. D.; Bernardinelli, G. *J. Appl. Cryst.***2000**, *33*, 1143–1148. The Flack parameter will refine to a value near zero if the structure is in the correct configuration and will refine to a value near one for the inverted configuration.

[f]$S = [\Sigma w(F_o^2 - F_c^2)^2/(n-p)]^{1/2}$ (n = number of data; p = number of parameters varied; $w = [\sigma^2(F_o^2)]^{-1}$.

[g]$R_1 = \Sigma||F_o| - |F_c||/\Sigma|F_o|$; $wR_2 = [\Sigma w(F_o^2 - F_c^2)^2/\Sigma w(F_o^4)]^{1/2}$.

Table A10. Crystallographic Experimental Details for **4-9**.

A. Crystal Data	
formula	$C_{38}H_{55}OP_2RhSi$
formula weight	720.76
crystal dimensions (mm)	0.40 × 0.32 × 0.16
crystal system	orthorhombic
space group	*Pbca* (No. 61)
unit cell parameters[a]	
a (Å)	17.2533 (6)
b (Å)	17.1976 (6)
c (Å)	24.2899 (9)
V (Å^3)	7207.2 (4)
Z	8
ρ_{calcd} (g cm^{-3})	1.329
μ (mm^{-1})	0.624
B. Data Collection and Refinement Conditions	
diffractometer	Bruker PLATFORM/APEX II CCD[b]
radiation (λ [Å])	graphite-monochromated Mo Kα (0.71073)
temperature (°C)	–80
scan type	ω scans (0.3°) (15 s exposures)
data collection 2θ limit (deg)	56.65
total data collected	63202 (-22≤*h*≤22, -22≤*k*≤22, -32≤*l*≤32)
independent reflections	8944 (R_{int} = 0.0270)
number of observed reflections (*NO*)	7924 [$F_o^2 \geq 2\sigma(F_o^2)$]
structure solution method	Patterson/structure expansion (*DIRDIF–2008*[c])
refinement method	full-matrix least-squares on F^2 (*SHELXL–2014*[d])
absorption correction method	Gaussian integration (face-indexed)
range of transmission factors	0.9558–0.8021
data/restraints/parameters	8944 / 0 / 389
goodness-of-fit (*S*)[e] [all data]	1.040
final *R* indices[f]	
R_1 [$F_o^2 \geq 2\sigma(F_o^2)$]	0.0305
wR_2 [all data]	0.0829
largest difference peak and hole	1.048 and –0.580 e Å^{-3}

(continued)

Table A10. Crystallographic Experimental Details for **4-9** (continued).

[a]Obtained from least-squares refinement of 9654 reflections with $4.74° < 2\theta < 46.28°$.

[b]Programs for diffractometer operation, data collection, data reduction and absorption correction were those supplied by Bruker.

[c]Beurskens, P. T.; Beurskens, G.; de Gelder, R.; Smits, J. M. M.; Garcia-Granda, S.; Gould, R. O. (2008). The *DIRDIF-2008* program system. Crystallography Laboratory, RadboudUniversityNijmegen, The Netherlands.

[d]Sheldrick, G. M. *Acta Crystallogr.* **2015**, *C71*, 3–8.

[e]$S = [\Sigma w(F_o^2 - F_c^2)^2/(n - p)]^{1/2}$ (n = number of data; p = number of parameters varied; $w = [\sigma^2(F_o^2) + (0.0392P)^2 + 6.2076P]^{-1}$ where $P = [\text{Max}(F_o^2, 0) + 2F_c^2]/3$).

[f]$R_1 = \Sigma||F_o| - |F_c||/\Sigma|F_o|$; $wR_2 = [\Sigma w(F_o^2 - F_c^2)^2/\Sigma w(F_o^4)]^{1/2}$.

Table A11. Crystallographic Experimental Details for **4-13**.

A. Crystal Data	
formula	$C_{41}H_{59}F_3O_3P_2RhSSi$
formula weight	881.88
crystal dimensions (mm)	0.31×0.21×0.16
crystal system	monoclinic
space group	$P2_1/n$ (an alternate setting of $P2_1/c$ [No. 14])
unit cell parameters[a]	
a (Å)	11.6692 (3)
b (Å)	17.3924 (5)
c (Å)	20.1281 (6)
β (deg)	92.8208 (10)
V (Å^3)	4080.2 (2)
Z	4
ρ_{calcd} (g cm^{-3})	1.436
μ (mm^{-1})	5.307
B. Data Collection and Refinement Conditions	
diffractometer	Bruker D8/APEX II CCD[b]
radiation (λ [Å])	Cu Kα (1.54178) (microfocus source)
temperature (°C)	–100
scan type	$\omega$and ϕscans (1°) (5 s exposures)
data collection 2θ limit (deg)	145.73
total data collected	27976 (-14≤h≤14, -21≤k≤21, -24≤l≤24)
independent reflections	8120 (R_{int} = 0.0222)
number of observed reflections (*NO*)	8009 [$F_o^2 \geq 2\sigma(F_o^2)$]
structure solution method	intrinsic phasing (*SHELXT*[c])
refinement method	full-matrix least-squares on F^2 (*SHELXL–2013*[c])
absorption correction method	Gaussian integration (face-indexed)
range of transmission factors	0.6704–0.3673
data/restraints/parameters	8120 / 0 / 476
extinction coefficient (x)[d]	0.00018(2)
goodness-of-fit (S)[e] [all data]	1.056
final R indices[f]	
R_1 [$F_o^2 \geq 2\sigma(F_o^2)$]	0.0207
wR_2 [all data]	0.0537
largest difference peak and hole	0.340and –0.516 e Å^{-3}

(continued)

Table A11. Crystallographic Experimental Details for **4-13** (continued).

[a]Obtained from least-squares refinement of 9610 reflections with $6.72° < 2\theta < 144.54°$.

[b]Programs for diffractometer operation, data collection, data reduction and absorption correction were those supplied by Bruker.

[c]Sheldrick, G. M. *ActaCrystallogr.***2008**, *A64*, 112–122.

[d]$F_c^* = kF_c[1 + x\{0.001F_c^2\lambda^3/\sin(2\theta)\}]^{-1/4}$ where k is the overall scale factor.

[e]$S = [\Sigma w(F_o^2 - F_c^2)^2/(n - p)]^{1/2}$ (n = number of data; p = number of parameters varied; $w = [\sigma^2(F_o^2) + (0.0242P)^2 + 2.1919P]^{-1}$ where $P = [\text{Max}(F_o^2, 0) + 2F_c^2]/3$).

[f]$R_1 = \Sigma||F_o| - |F_c||/\Sigma|F_o|$; $wR_2 = [\Sigma w(F_o^2 - F_c^2)^2/\Sigma w(F_o^4)]^{1/2}$.

Table A12. Crystallographic Experimental Details for **4-14**.

A. Crystal Data	
formula	$C_{43}H_{61}BF_5P_2RhSi$
formula weight	876.66
crystal dimensions (mm)	0.29×0.18×0.17
crystal system	orthorhombic
space group	$Pca2_1$ (No. 29)
unit cell parameters[a]	
a (Å)	17.8144 (6)
b (Å)	13.4860 (4)
c (Å)	17.9713 (6)
V (Å^3)	4317.5 (2)
Z	4
ρ_{calcd} (g cm^{-3})	1.349
μ (mm^{-1})	0.548
B. Data Collection and Refinement Conditions	
diffractometer	Bruker D8/APEX II CCD[b]
radiation (λ [Å])	graphite-monochromated Mo Kα (0.71073)
temperature (°C)	–100
scan type	ω scans (0.3°) (20 s exposures)
data collection 2θ limit (deg)	56.76
total data collected	38171 (-23≤h≤23, -17≤k≤18, -23≤l≤24)
independent reflections	10538 (R_{int} = 0.0250)
number of observed reflections (*NO*)	9950 [$F_o^2 \geq 2\sigma(F_o^2)$]
structure solution method	intrinsic phasing (*SHELXT*[c])
refinement method	full-matrix least-squares on F^2 (*SHELXL–2013*[c])
absorption correction method	Gaussian integration (face-indexed)
range of transmission factors	0.9888–0.8816
data/restraints/parameters	10538 / 0 / 480480
Flack absolute structure parameter[d]	–0.004(6)
goodness-of-fit (*S*)[e] [all data]	1.029
final*R* indices[f]	
R_1 [$F_o^2 \geq 2\sigma(F_o^2)$]	0.0240
wR_2 [all data]	0.0627
largest difference peak and hole	0.508 and –0.344 e Å^{-3}

(continued)

Table A12. Crystallographic Experimental Details for **4-14** (continued).

[a]Obtained from least-squares refinement of 9796 reflections with $4.42° < 2\theta < 56.24°$.

[b]Programs for diffractometer operation, data collection, data reduction and absorption correction were those supplied by Bruker.

[c]Sheldrick, G. M. *ActaCrystallogr.***2008**, *A64*, 112–122.

[d]Flack, H. D. *ActaCrystallogr.***1983**, *A39*, 876–881; Flack, H. D.; Bernardinelli, G. *ActaCrystallogr.***1999**, *A55*, 908–915; Flack, H. D.; Bernardinelli, G. *J. Appl. Cryst.***2000**, *33*, 1143–1148. The Flack parameter will refine to a value near zero if the structure is in the correct configuration and will refine to a value near one for the inverted configuration.

[e]$S = [\Sigma w(F_o^2 - F_c^2)^2/(n-p)]^{1/2}$ (n = number of data; p = number of parameters varied; $w = [\sigma^2(F_o^2) + (0.0388P)^2 + 0.6268P]^{-1}$ where $P = [\mathrm{Max}(F_o^2, 0) + 2F_c^2]/3$).

[f]$R_1 = \Sigma||F_o| - |F_c||/\Sigma|F_o|$; $wR_2 = [\Sigma w(F_o^2 - F_c^2)^2/\Sigma w(F_o^4)]^{1/2}$.

Table A13. Crystallographic Experimental Details for **4-15**.

A. Crystal Data	
formula	$C_{39}H_{58}F_3IrO_3P_2SSi$
formula weight	946.14
crystal dimensions (mm)	0.26 × 0.20 × 0.03
crystal system	orthorhombic
space group	*Pbca* (No. 61)
unit cell parameters[a]	
a (Å)	17.2449 (3)
b (Å)	20.8720 (4)
c (Å)	22.4089 (4)
V (Å^3)	8065.8 (3)
Z	8
ρ_{calcd} (g cm^{-3})	1.558
μ (mm^{-1})	8.336
B. Data Collection and Refinement Conditions	
diffractometer	Bruker D8/APEX II CCD[b]
radiation (λ [Å])	Cu Kα (1.54178) (microfocus source)
temperature (°C)	–100
scan type	ω and ϕ scans (1.0°) (5 s exposures)
data collection 2θ limit (deg)	148.15
total data collected	55172 (-21≤*h*≤21, -20≤*k*≤23, -27≤*l*≤27)
independent reflections	7913 (R_{int} = 0.0284)
number of observed reflections (*NO*)	7022 [$F_o^2 \geq 2\sigma(F_o^2)$]
structure solution method	Patterson/structure expansion (*DIRDIF–2008*[c])
refinement method	full-matrix least-squares on F^2 (*SHELXL–2014*[d])
absorption correction method	Gaussian integration (face-indexed)
range of transmission factors	0.8212–0.3038
data/restraints/parameters	7913 / 0 / 453
goodness-of-fit (*S*)[e] [all data]	1.080
final *R* indices[f]	
R_1 [$F_o^2 \geq 2\sigma(F_o^2)$]	0.0222
wR_2 [all data]	0.0631
largest difference peak and hole	1.246 and –0.624 e Å^{-3}

(continued)

Table A13. Crystallographic Experimental Details for **4-15** (continued).

[a]Obtained from least-squares refinement of 9041 reflections with $7.74° < 2\theta < 147.70°$.

[b]Programs for diffractometer operation, data collection, data reduction and absorption correction were those supplied by Bruker.

[c]Beurskens, P. T.; Beurskens, G.; de Gelder, R.; Smits, J. M. M.; Garcia-Granda, S.; Gould, R. O. (2008). The *DIRDIF-2008* program system. Crystallography Laboratory, RadboudUniversityNijmegen, The Netherlands.

[d]Sheldrick, G. M. *Acta Crystallogr.* **2015**, *C71*, 3–8.

[e]$S = [\Sigma w(F_o^2 - F_c^2)^2/(n - p)]^{1/2}$ (n = number of data; p = number of parameters varied; $w = [\sigma^2(F_o^2) + (0.0289P)^2 + 10.3549P]^{-1}$ where $P = [\mathrm{Max}(F_o^2, 0) + 2F_c^2]/3$).

[f]$R_1 = \Sigma||F_o| - |F_c||/\Sigma|F_o|$; $wR_2 = [\Sigma w(F_o^2 - F_c^2)^2/\Sigma w(F_o^4)]^{1/2}$.

Appendix B: Selected NMR Spectra of Reported Compounds

Selected Spectra of Compounds Reported in Chapter 2

Figure B1. For **2-1** (a) $^{31}P\{^{1}H\}$ NMR spectrum (121.5 MHz, C_6D_6). (b) ^{1}H NMR spectrum (300 MHz, C_6D_6). * indicates pentane impurity. ¤ indicates cyclohexane impurity.

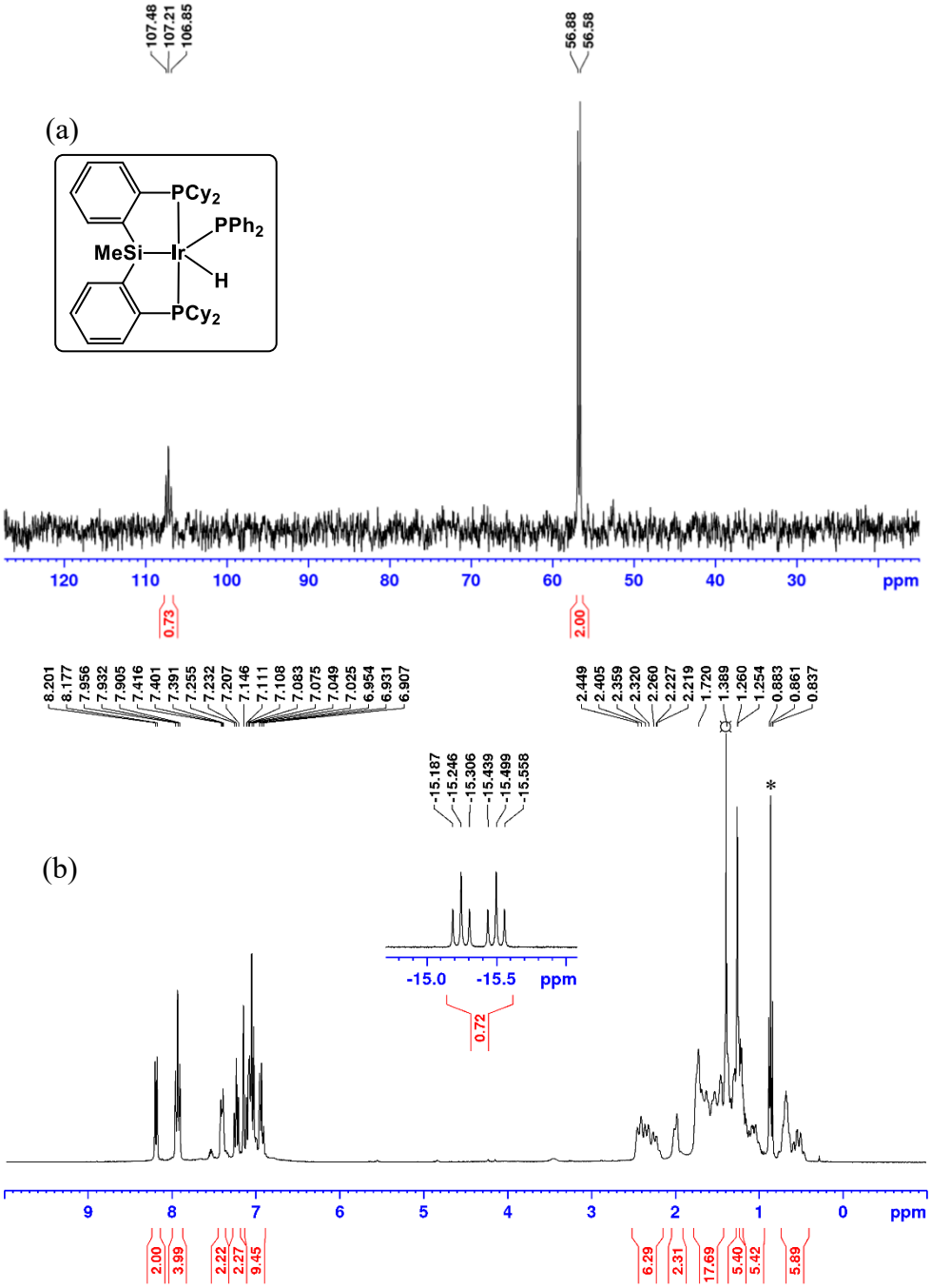

Figure B2. For **2-1** $^{13}C\{^{1}H\}$ NMR spectrum (75.5 MHz, C_6D_6).

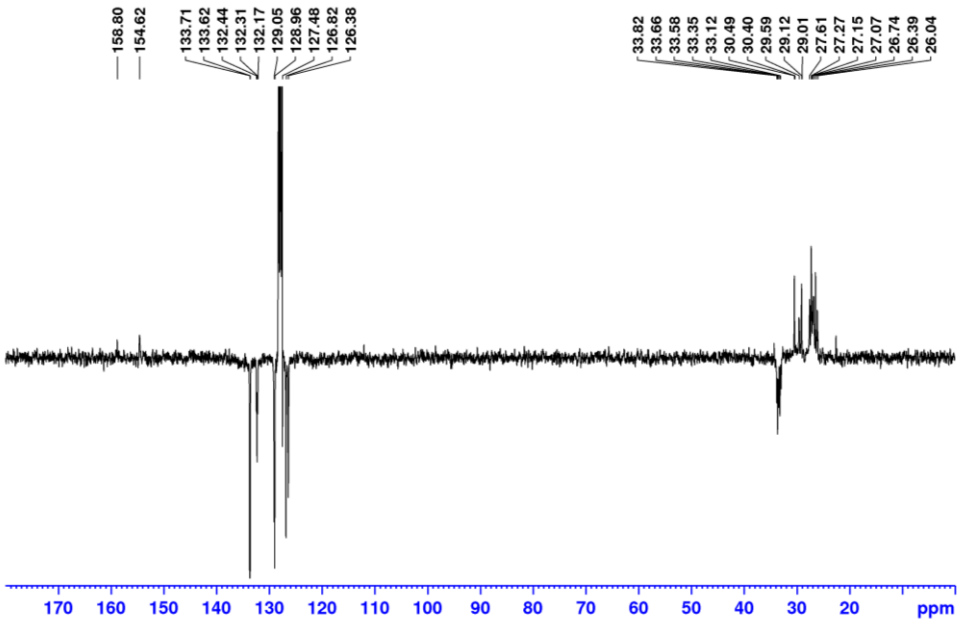

Figure B3. For **2-2a** (a) $^{31}P\{^{1}H\}$ NMR spectrum (121.5 MHz, C_6D_6). (b) ^{1}H NMR spectrum (300 MHz, C_6D_6). ▲, ◊ and ■ indicate resonances associated with each inequivalent phosphorus atom. * indicates pentane impurity.

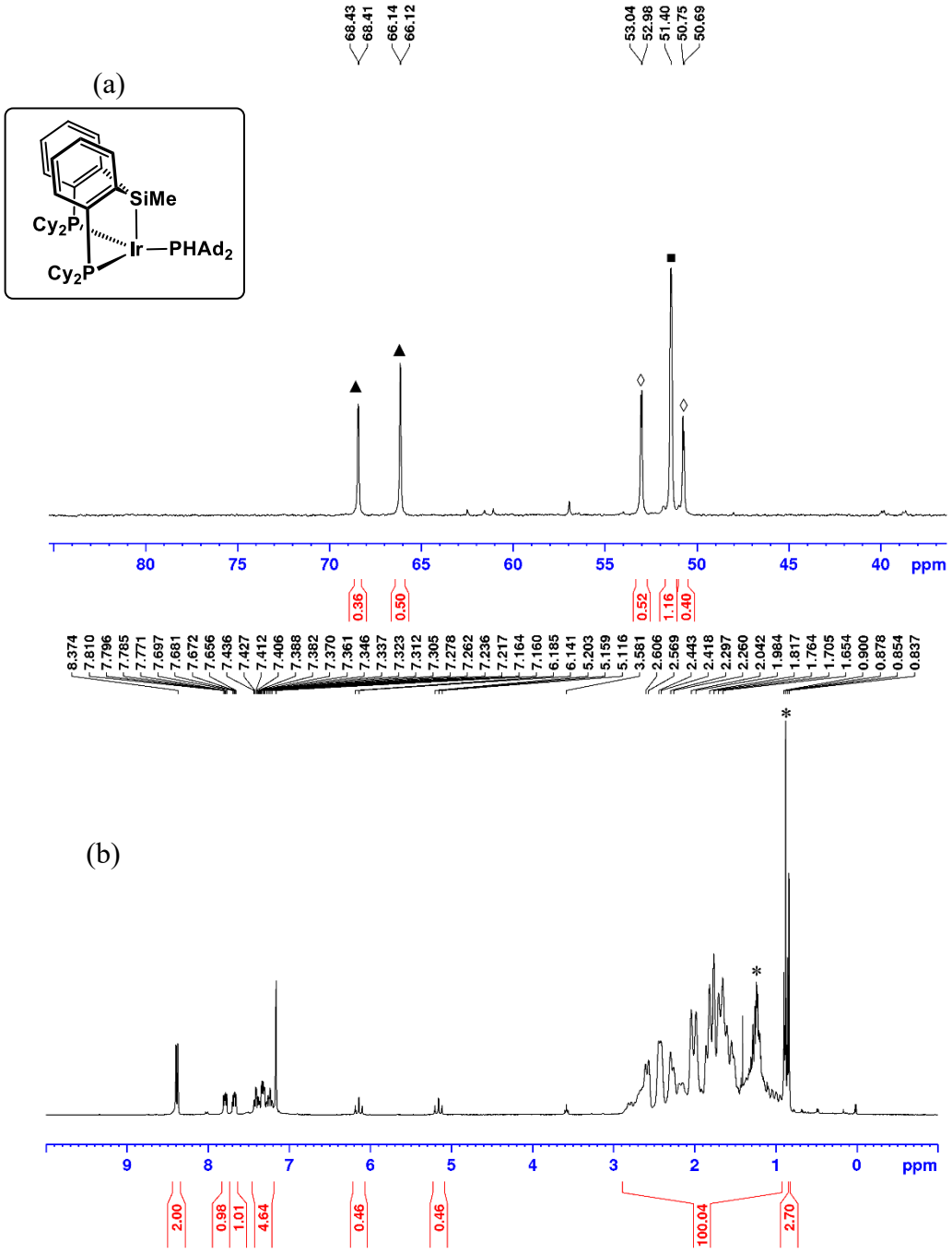

Figure B4. For **2-2a** $^{13}C\{^{1}H\}$ NMR spectrum (75.5 MHz, C_6D_6). * indicates pentane impurity.

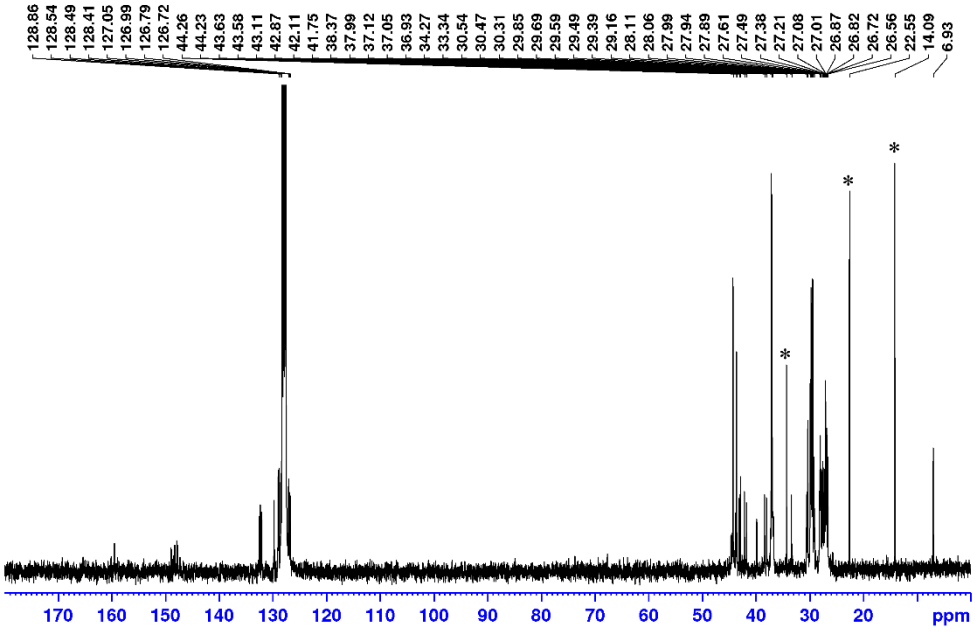

Figure B5. For **2-2b** (a) $^{31}P\{^{1}H\}$ NMR spectrum (121.5 MHz, C_6D_6). (b) ^{1}H NMR spectrum (300 MHz, C_6D_6). * indicates pentane impurity.

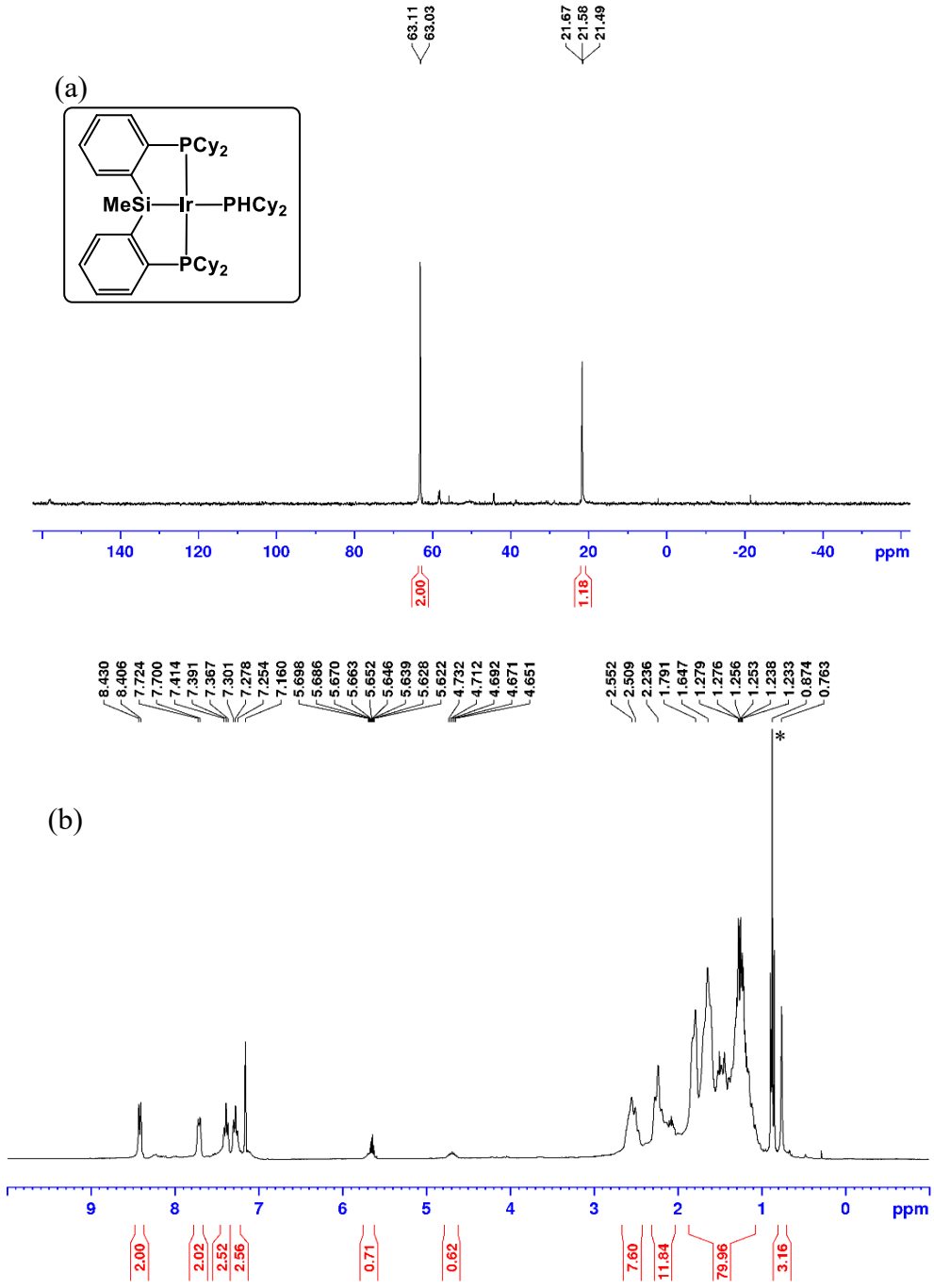

Figure B6. For **2-2b** $^{13}C\{^{1}H\}$ NMR spectrum (75.5 MHz, C_6D_6). * indicates pentane impurity.

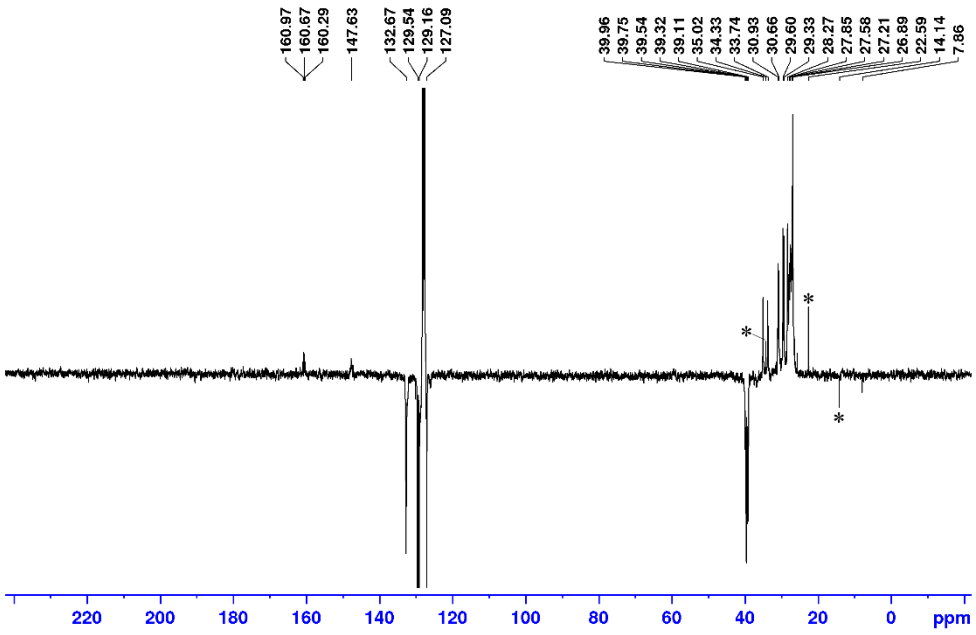

Figure B7. For **2-2c** (a) $^{31}P\{^{1}H\}$ NMR spectrum (121.5 MHz, C_6D_6). (b) ^{1}H NMR spectrum (300 MHz, C_6D_6). * indicates pentane impurity.

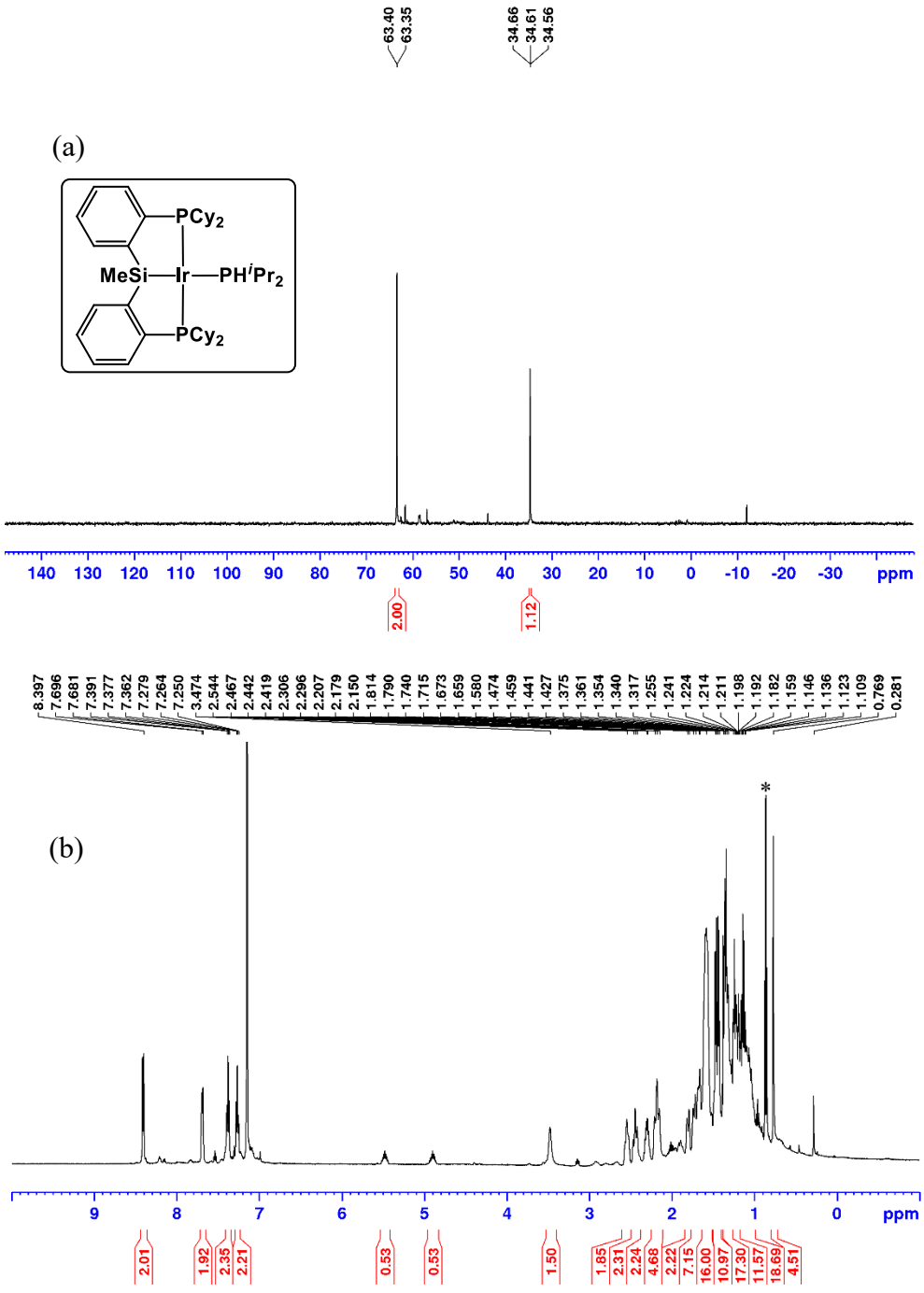

Figure B8. For **2-2c** $^{13}C\{^{1}H\}$ NMR spectrum (75.5 MHz, C_6D_6). * indicates pentane impurity.

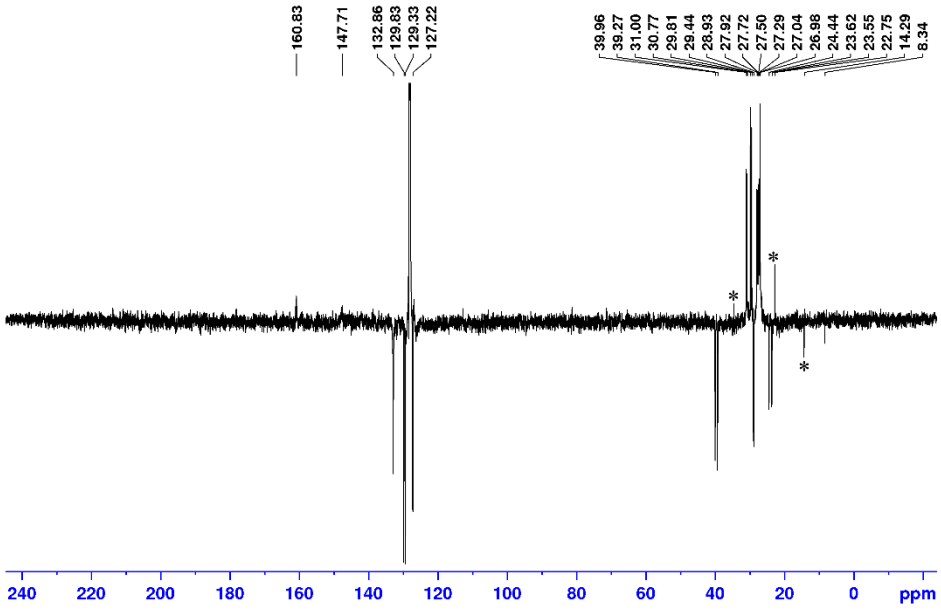

Figure B9. For **2-3a** (a) $^{31}P\{^{1}H\}$ NMR spectrum (121.5 MHz, C_6D_6). (b) ^{1}H NMR spectrum (300 MHz, C_6D_6).

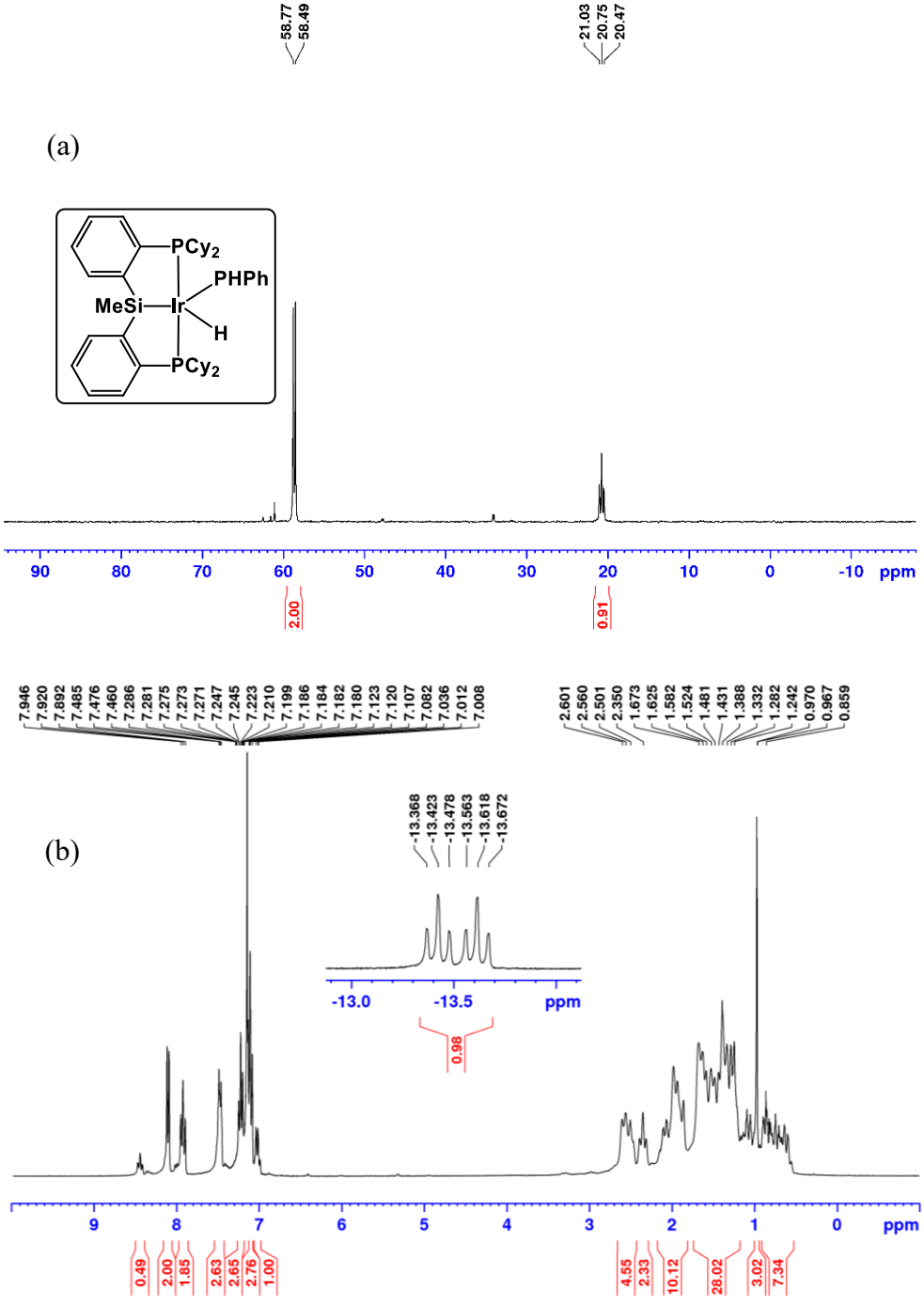

Figure B10. For **2-3a** $^{13}C\{^{1}H\}$ NMR spectrum (75.5 MHz, C_6D_6).

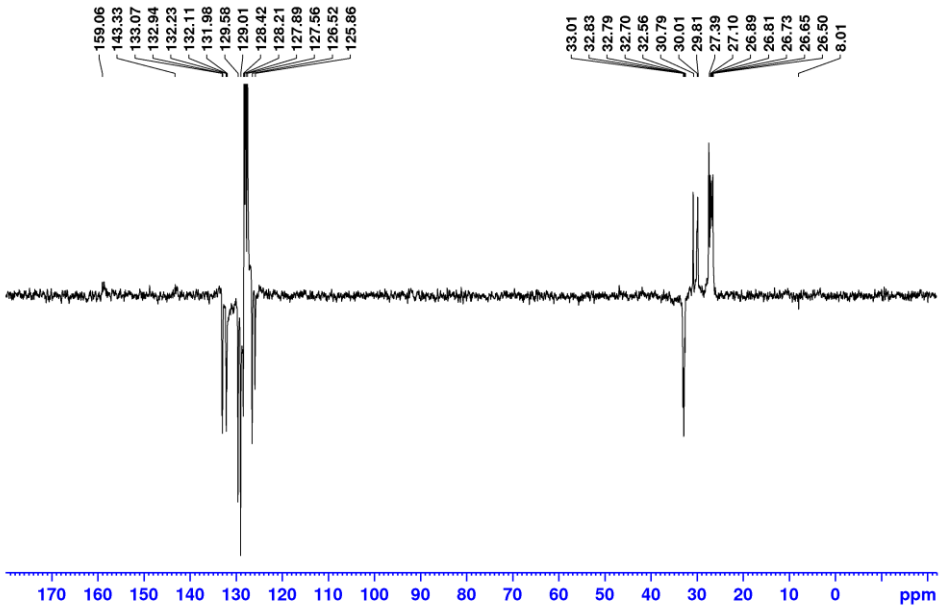

Figure B11. For **2-3b** (a) $^{31}P\{^{1}H\}$ NMR spectrum (121.5 MHz, C_6D_6). (b) ^{1}H NMR spectrum (300 MHz, C_6D_6). (c) $^{13}C\{^{1}H\}$ NMR spectrum (75.5 MHz, C_6D_6). * indicates pentane impurity. ¤ indicates cyclohexane impurity.

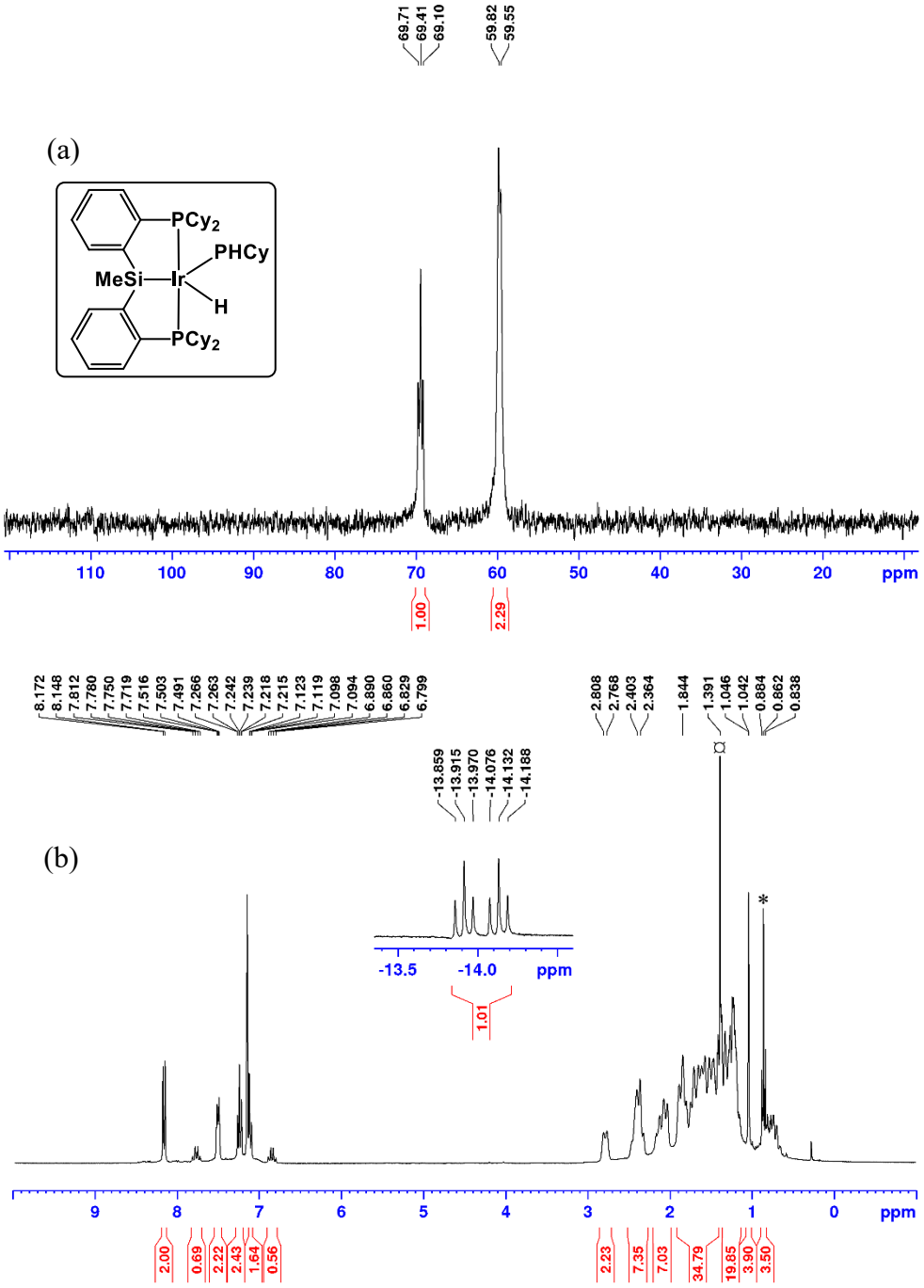

Figure B12. For **2-3b** $^{13}C\{^{1}H\}$ NMR spectrum (75.5 MHz, C_6D_6).

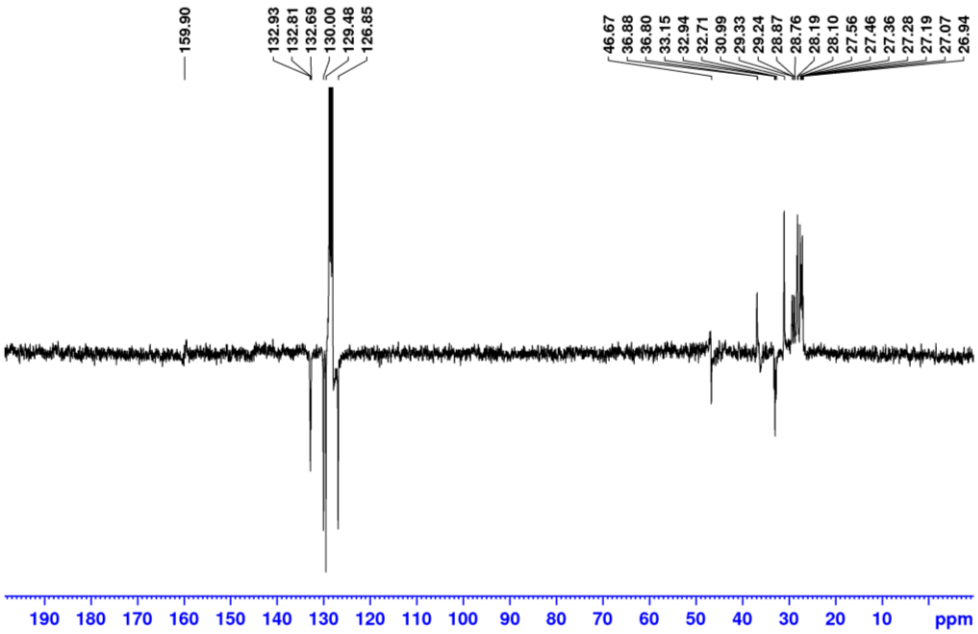

Figure B13. For **2-3c** (a) $^{31}P\{^{1}H\}$ NMR spectrum (121.5 MHz, C_6D_6). (b) ^{1}H NMR spectrum (300 MHz, C_6D_6).

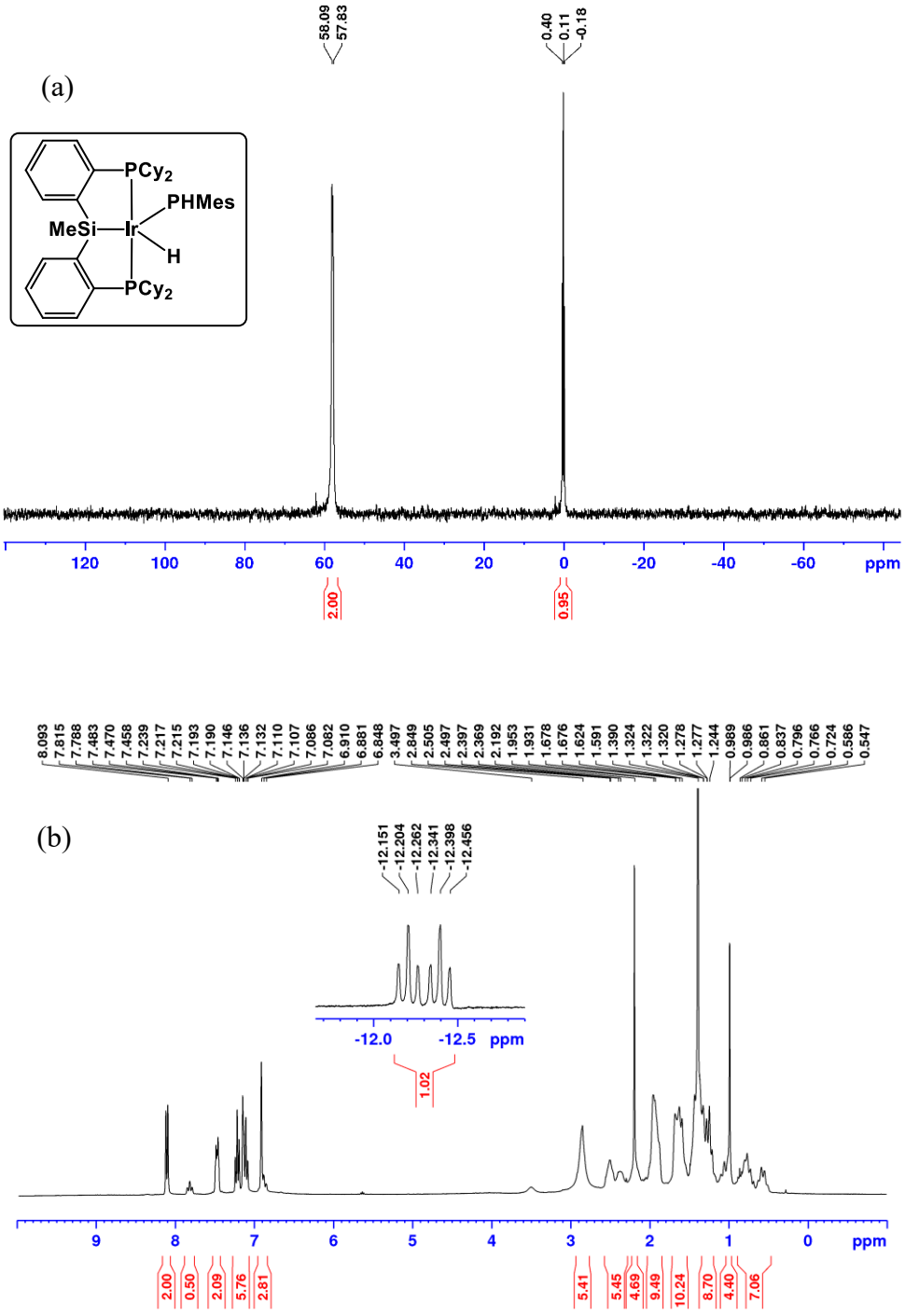

Figure B14. For **2-3c** $^{13}C\{^{1}H\}$ NMR spectrum (75.5 MHz, C_6D_6).

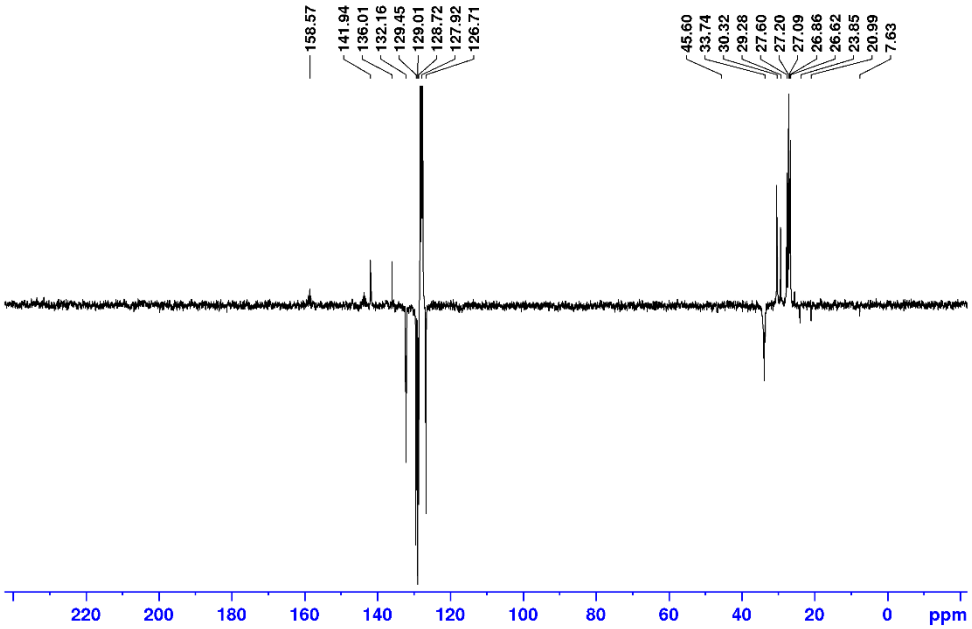

Figure B15. For **2-3d,d'** (a) $^{31}P\{^{1}H\}$ NMR spectrum (121.5 MHz, C_6D_6). (b) ^{1}H NMR spectrum (300 MHz, C_6D_6). ▲ indicates resonances corresponding to the *mer* isomer. ◊ indicates resonances corresponding to the *fac* isomer.

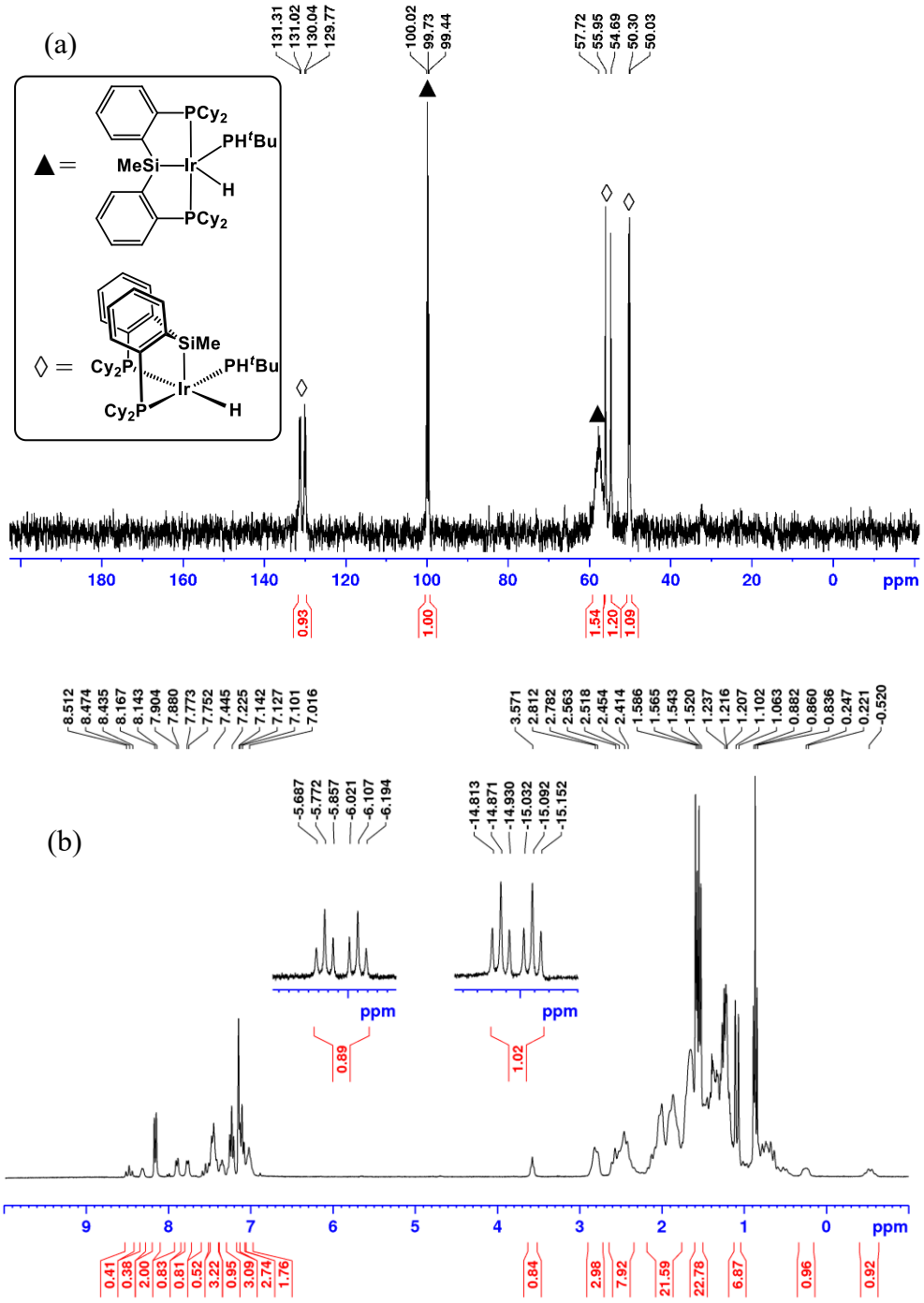

Figure B16. For **2-3d,d'** $^{13}C\{^{1}H\}$ NMR spectrum (75.5 MHz, C_6D_6).

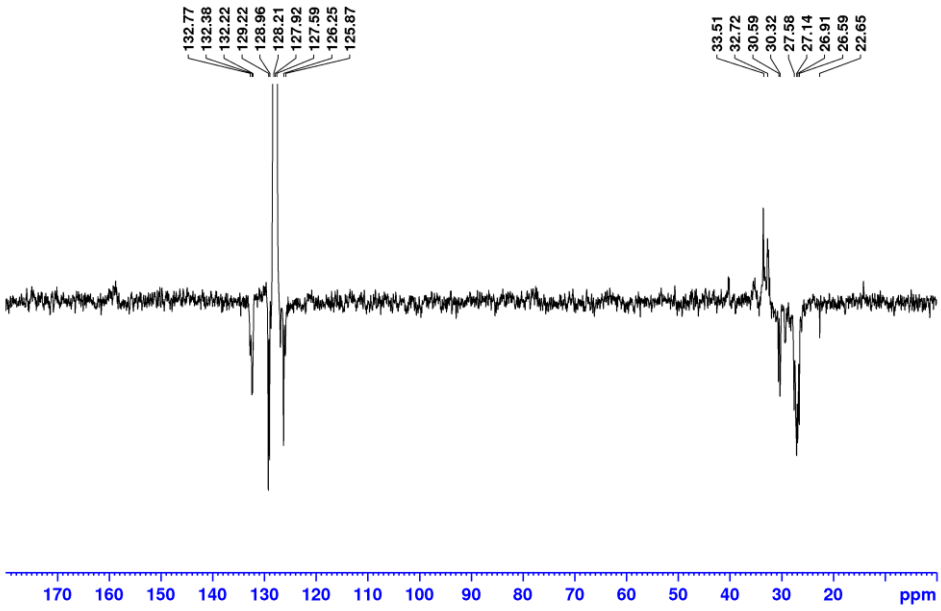

Figure B17. For **2-4a** (a) $^{31}P\{^{1}H\}$ NMR spectrum (121.5 MHz, C_6D_6). (b) ^{1}H NMR spectrum (300 MHz, C_6D_6). * indicates pentane impurity.

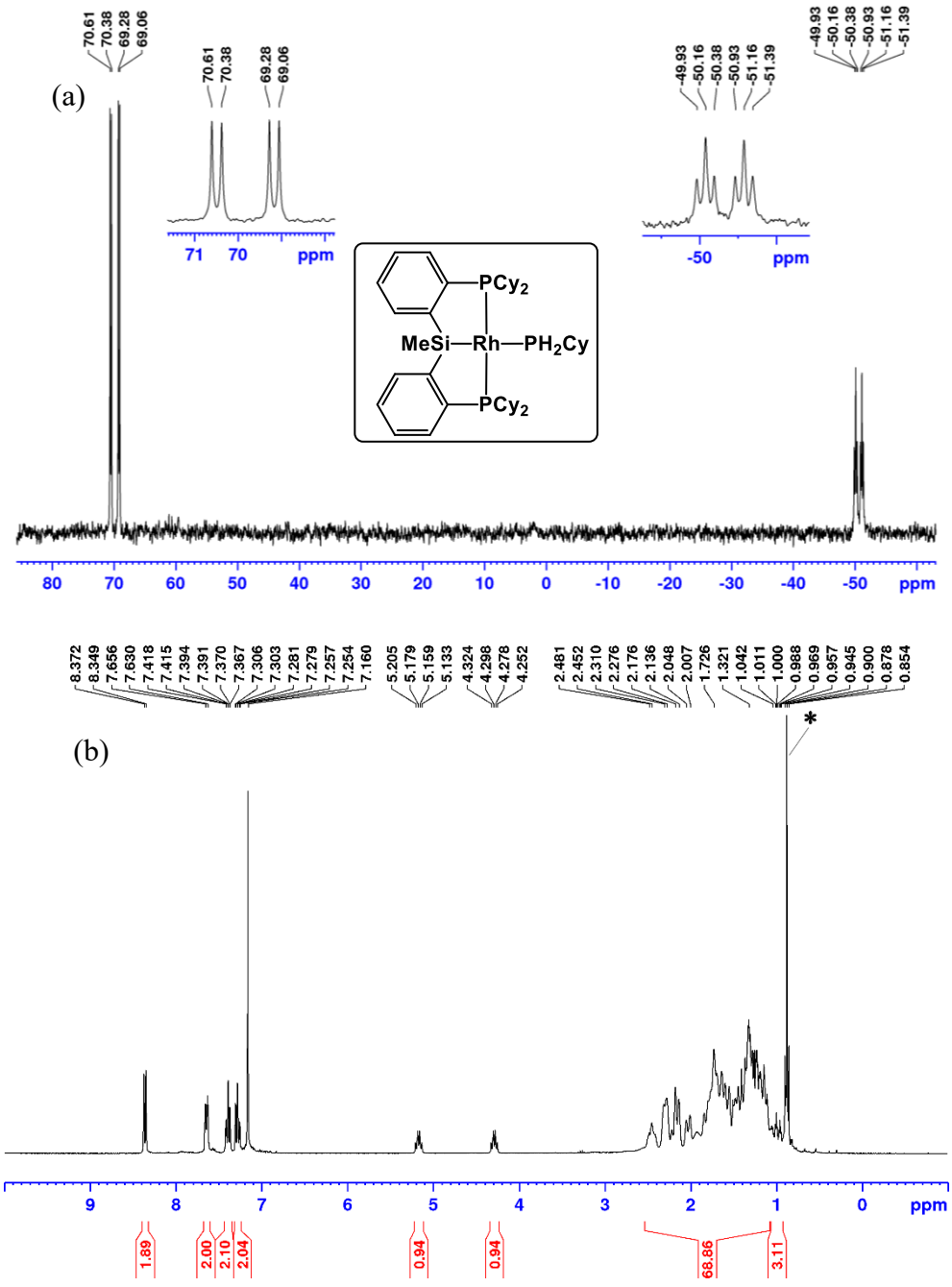

Figure B18. For **2-4a** $^{13}C\{^{1}H\}$ NMR spectrum (75.5 MHz, C_6D_6).

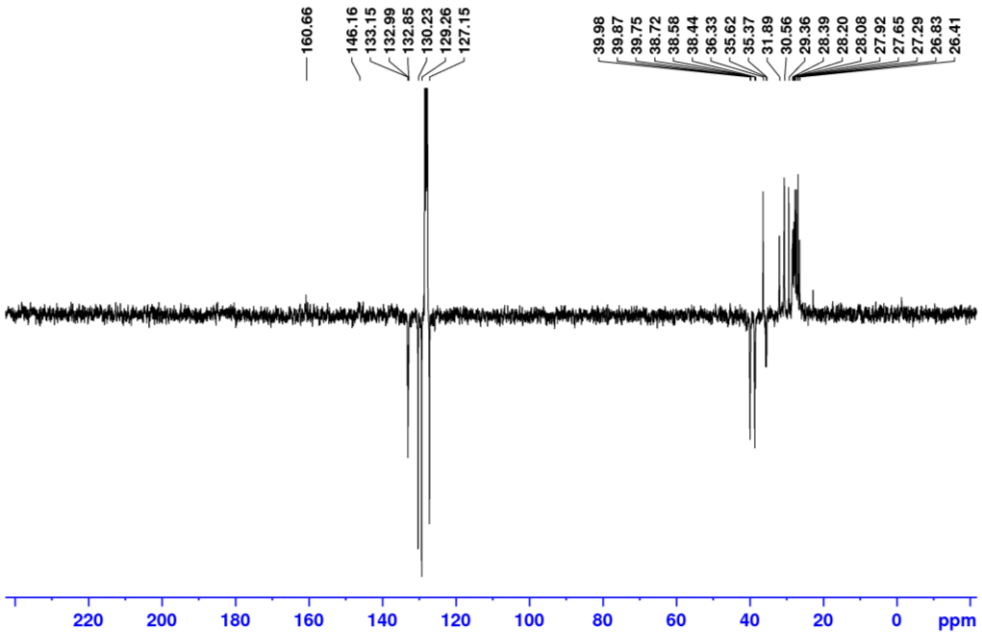

Figure B19. For **2-4b** (a) $^{31}P\{^{1}H\}$ NMR spectrum (121.5 MHz, C_6D_6). (b) ^{1}H NMR spectrum (300 MHz, C_6D_6). (c) $^{13}C\{^{1}H\}$ NMR spectrum (75.5 MHz, C_6D_6).

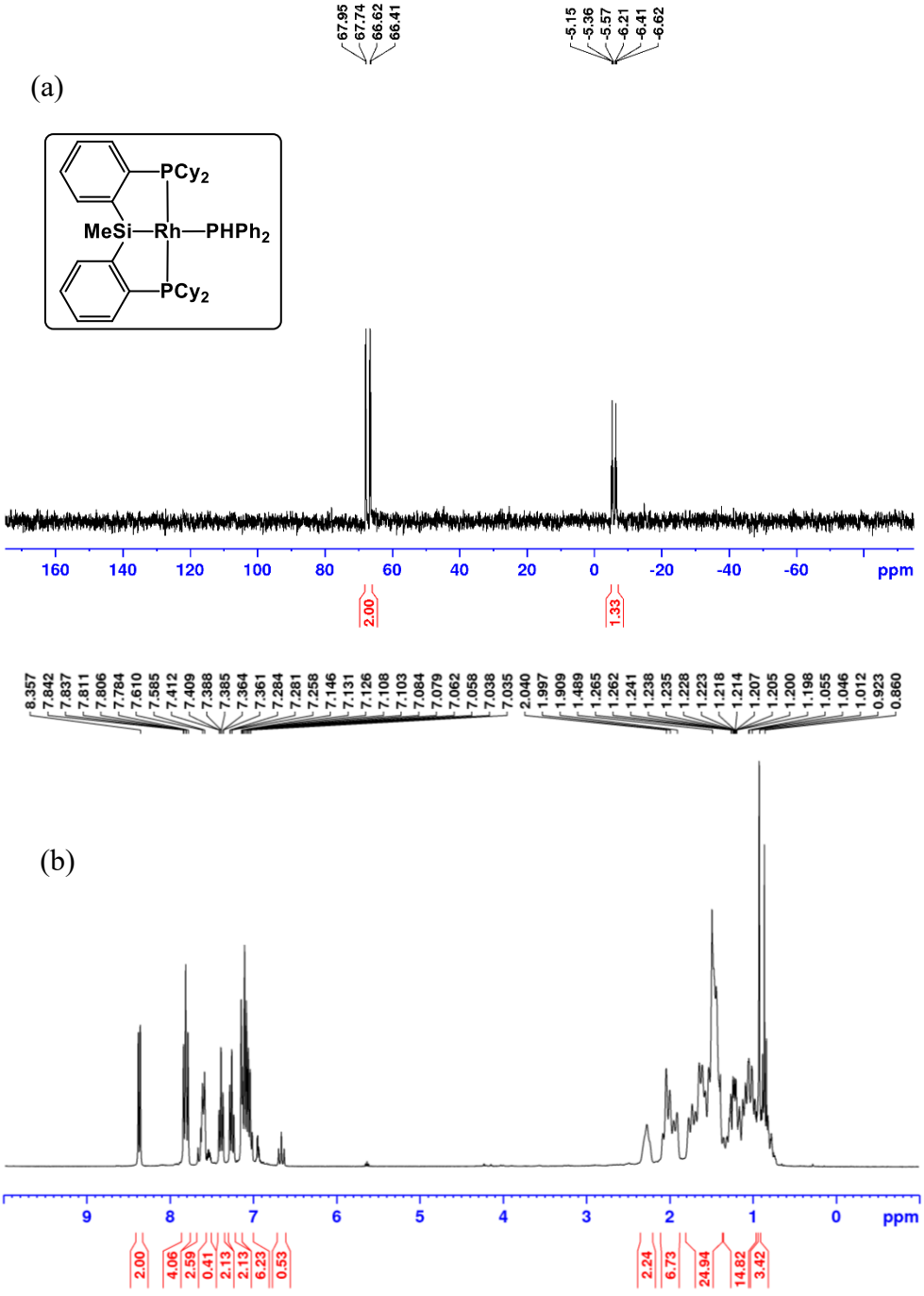

Figure B20. For **2-4b** $^{13}C\{^{1}H\}$ NMR spectrum (75.5 MHz, C_6D_6).

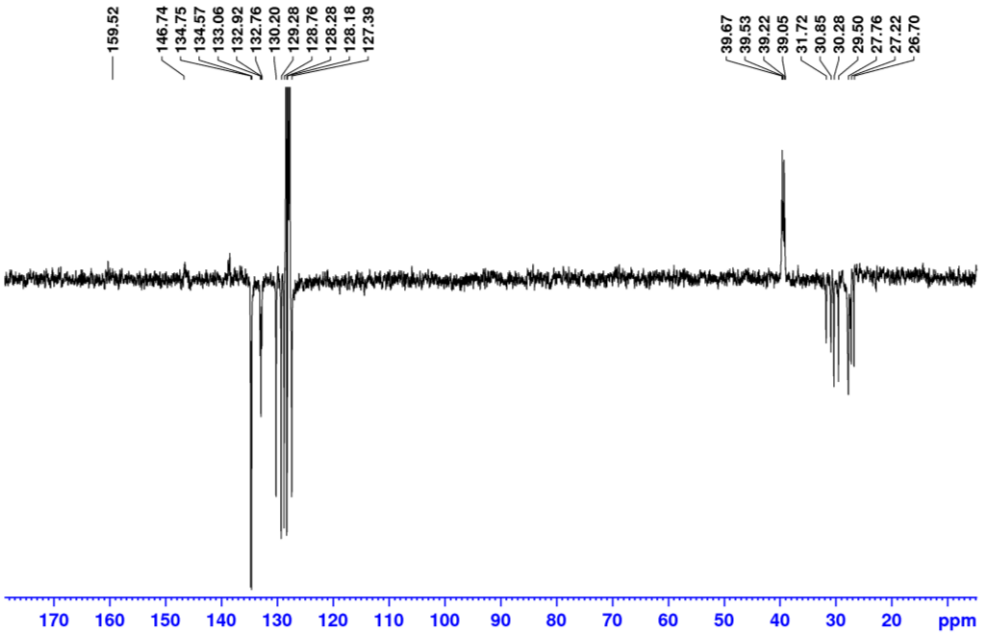

Figure B21. For **2-4c** (a) $^{31}P\{^{1}H\}$ NMR spectrum (121.5 MHz, C_6D_6). (b) ^{1}H NMR spectrum (300 MHz, C_6D_6). * indicates pentane impurity.

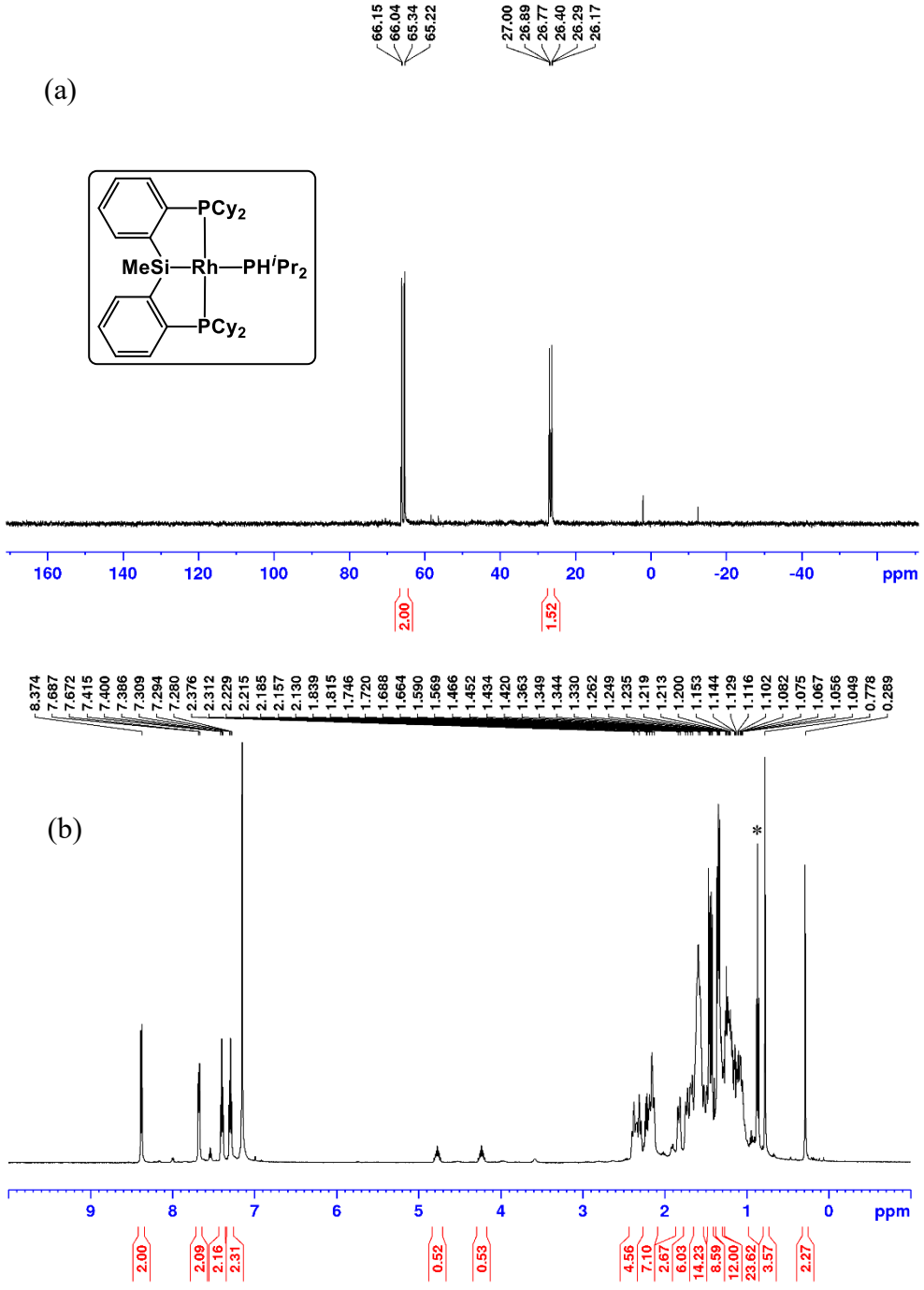

Figure B22. For **2-4c** $^{13}C\{^{1}H\}$ NMR spectrum (75.5 MHz, C_6D_6). * indicates pentane impurity.

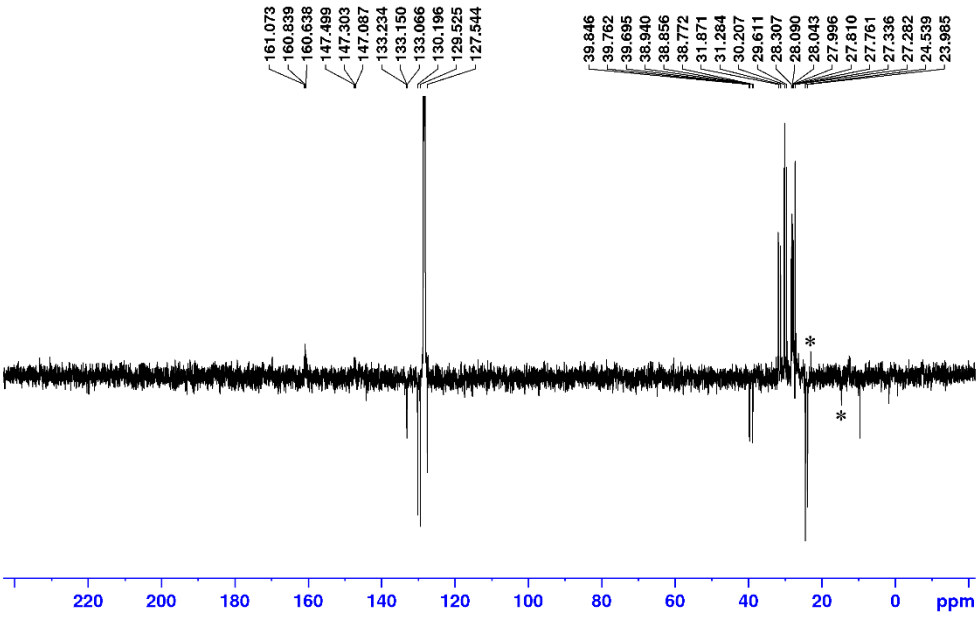

Figure B23. For **2-4d** (a) $^{31}P\{^{1}H\}$ NMR spectrum (121.5 MHz, C_6D_6). (b) ^{1}H NMR spectrum (300 MHz, C_6D_6). * indicates pentane impurity.

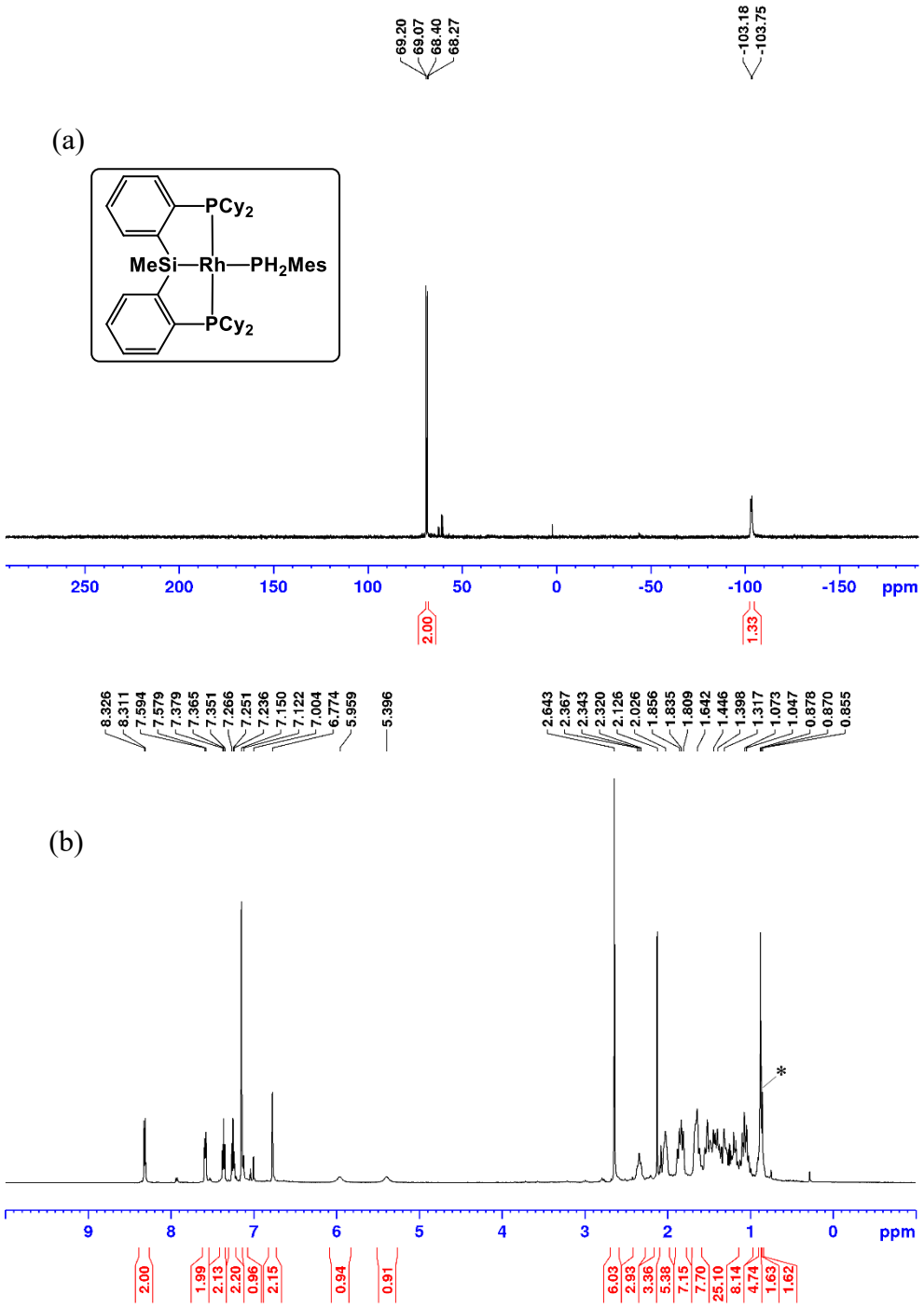

Figure B24. For **2-4d** $^{13}C\{^{1}H\}$ NMR spectrum (75.5 MHz, C_6D_6). * indicates pentane impurity.

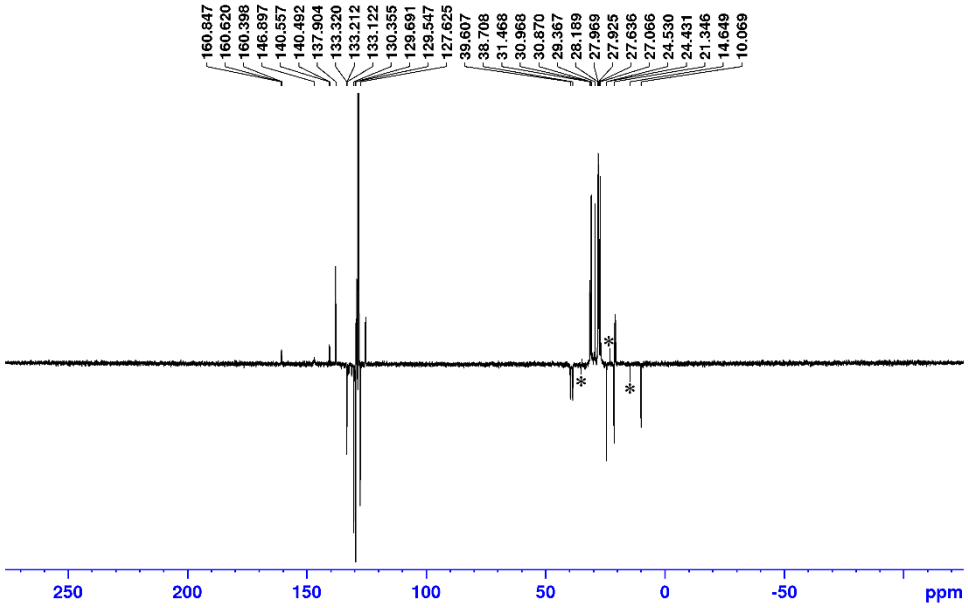

Figure B25. For **2-5** (a) $^{31}P\{^{1}H\}$ NMR spectrum (121.5 MHz, CD_2Cl_2). (b) ^{1}H NMR spectrum (300 MHz, CD_2Cl_2).

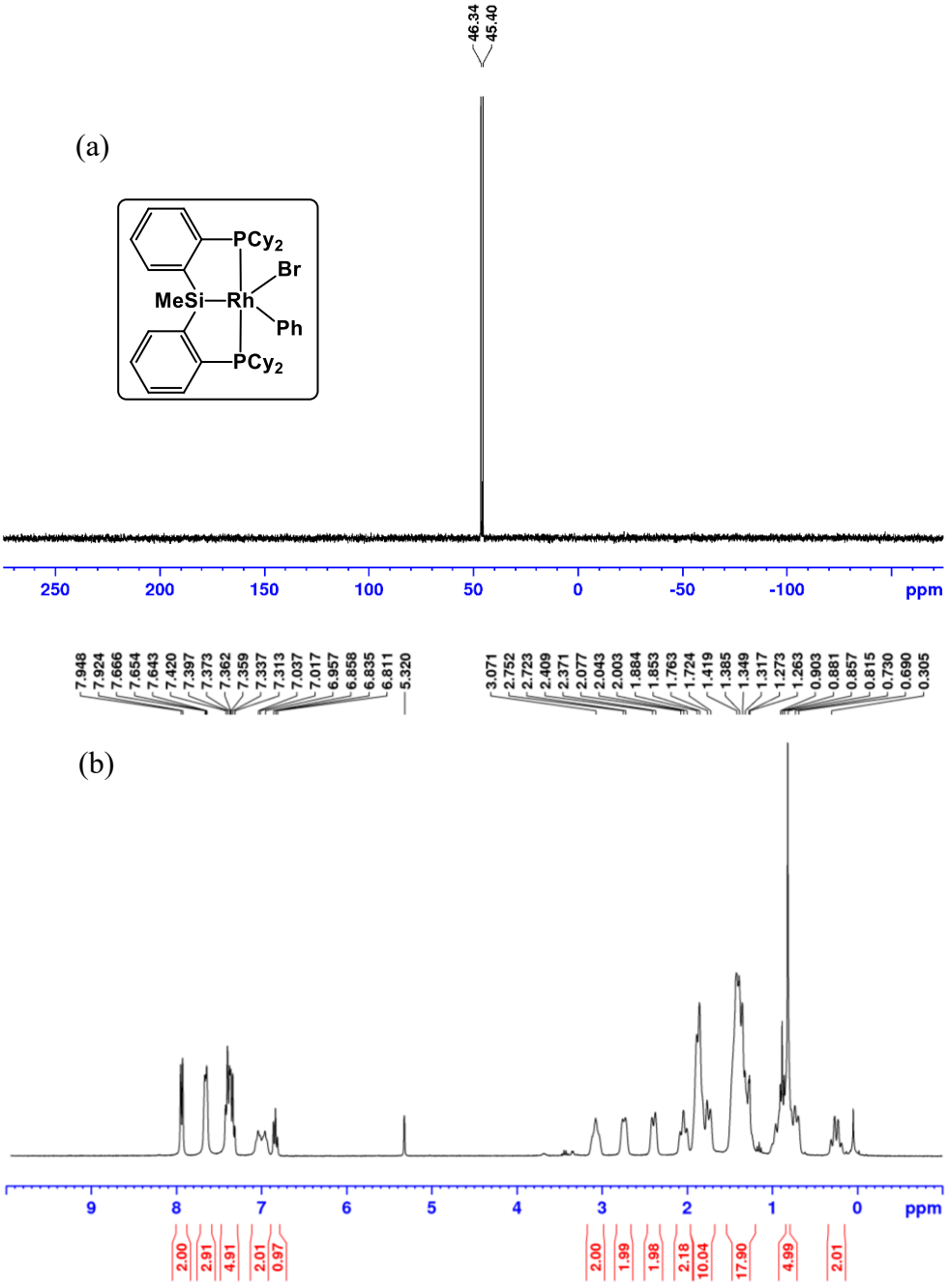

Figure B26. For **2-5** $^{13}C\{^{1}H\}$ NMR spectrum (75.5 MHz, CD_2Cl_2).

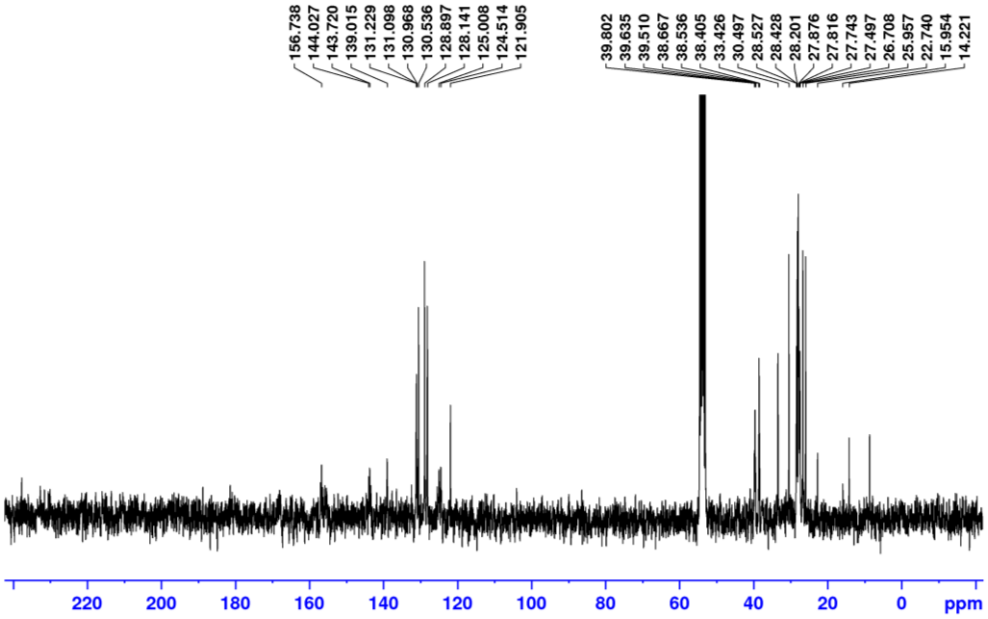

Figure B27. For **2-6** (a) $^{31}P\{^{1}H\}$ NMR spectrum (121.5 MHz, C_6D_6). (b) ^{1}H NMR spectrum (300 MHz, C_6D_6).

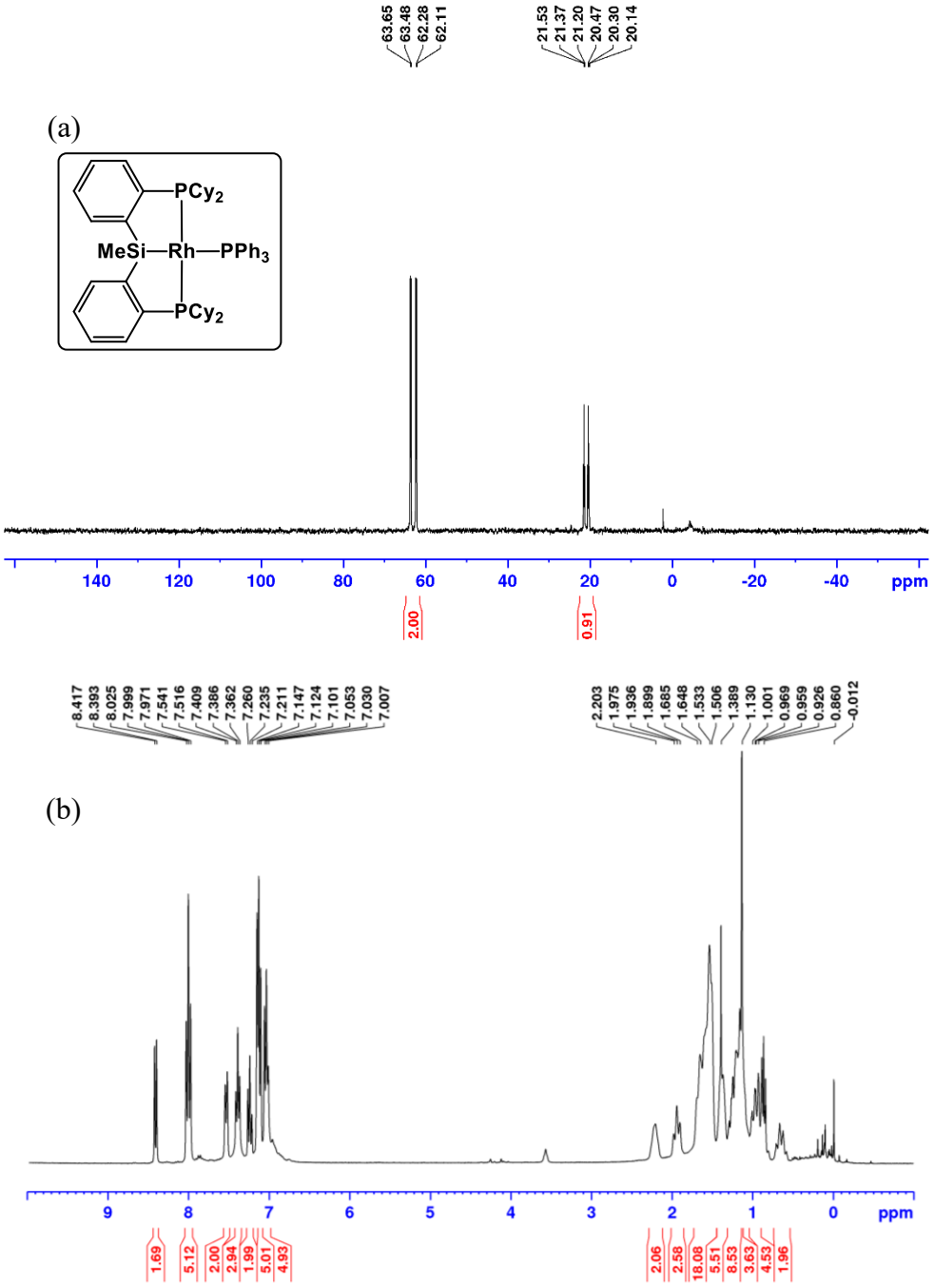

Figure B28. For **2-6** $^{13}C\{^{1}H\}$ NMR spectrum (75.5 MHz, C_6D_6).

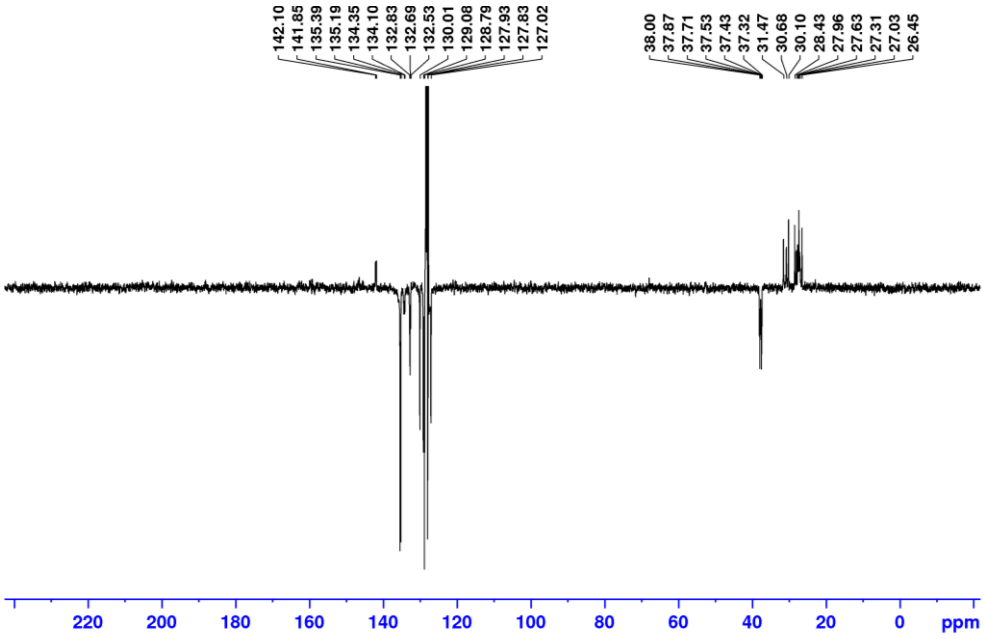

Figure B29. For **2-8a,b** (a) $^{31}P\{^{1}H\}$ NMR spectrum (121.5 MHz, C_6D_6). (b) ^{1}H NMR spectrum (300 MHz, C_6D_6). ▲**b** and ◊ **a** indicate resonances associated with each isomer.

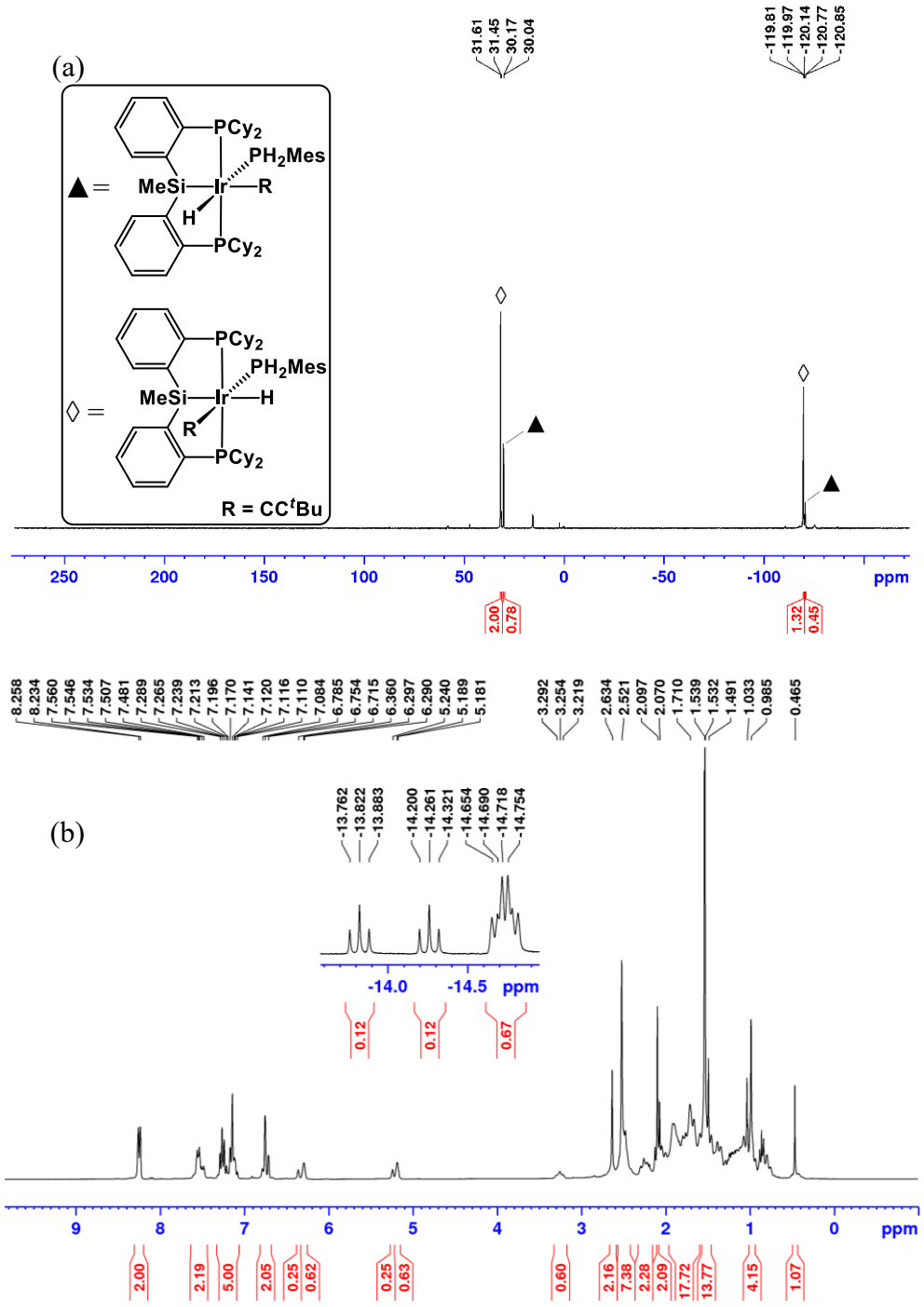

Figure B30. For **2-8a,b** (a) $^{13}C\{^{1}H\}$ NMR spectrum (75.5 MHz, C_6D_6).

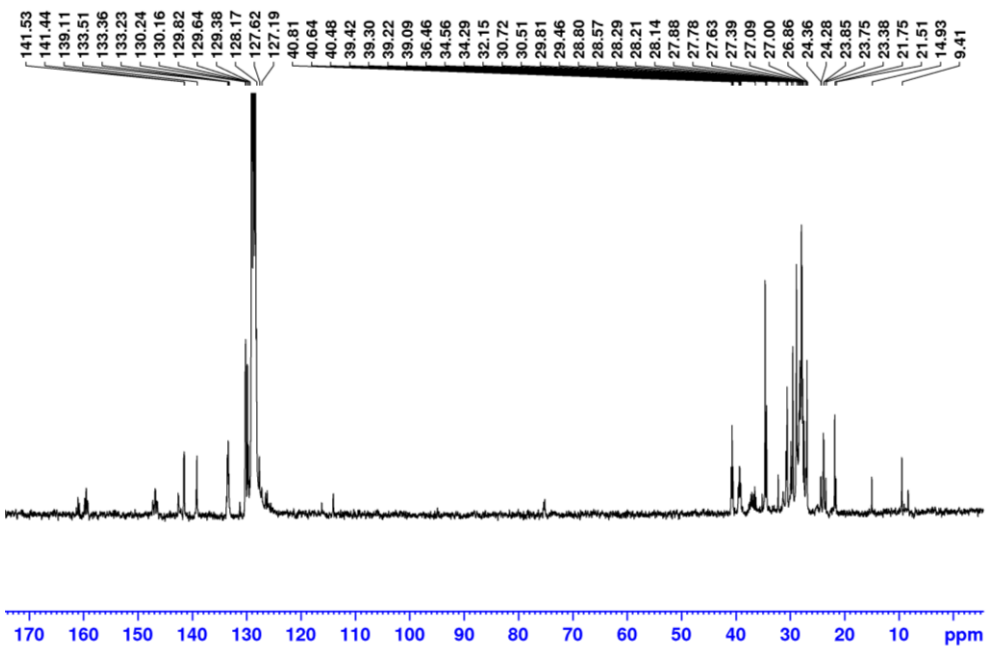

Figure B31. For **2-9** (a) $^{31}P\{^{1}H\}$ NMR spectrum (121.5 MHz, C_6D_6). (b) ^{1}H NMR spectrum (300 MHz, C_6D_6).

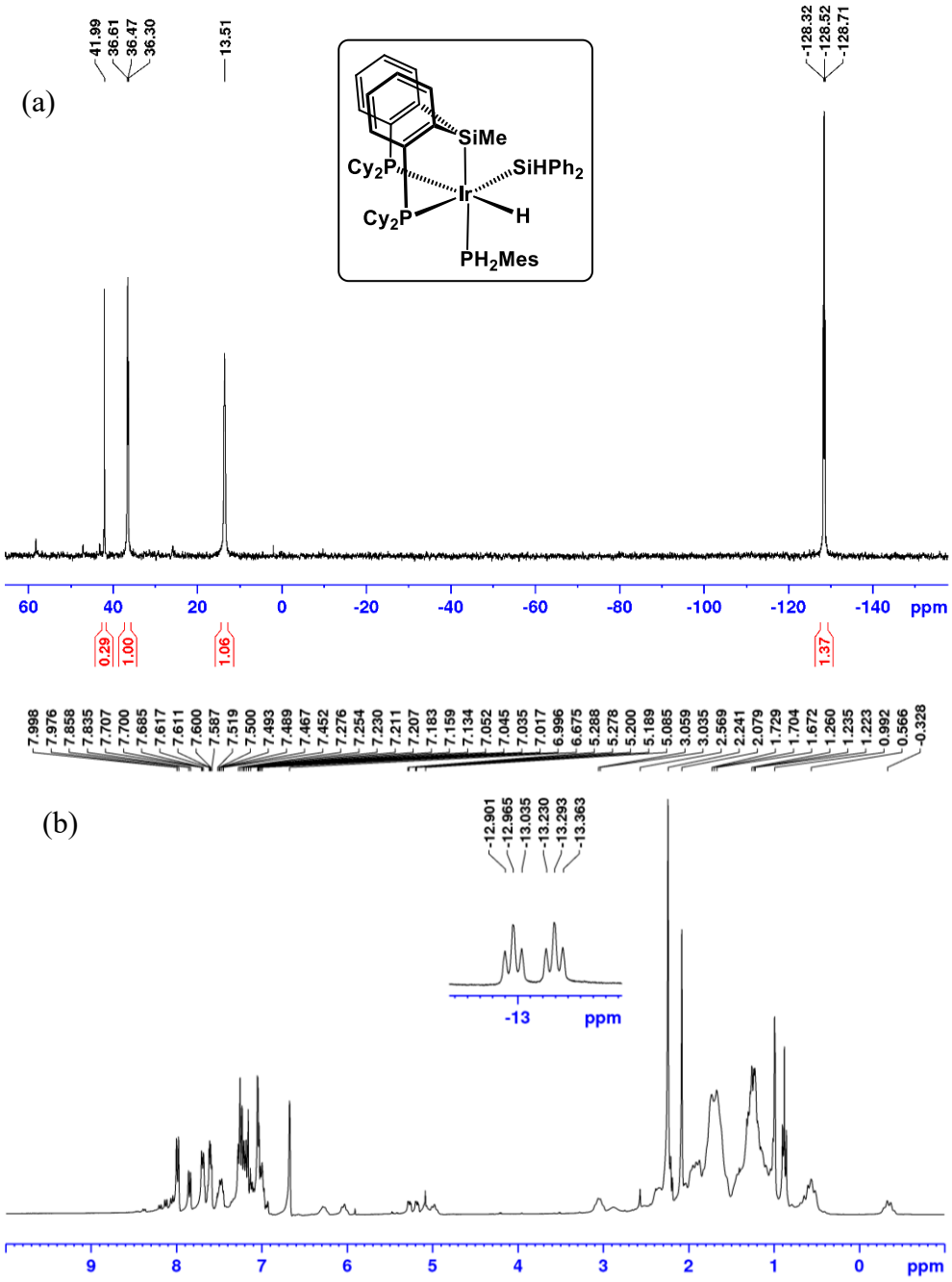

Figure B32. For **2-9** (a) $^{13}C\{^{1}H\}$ NMR spectrum (75.5 MHz, C_6D_6).

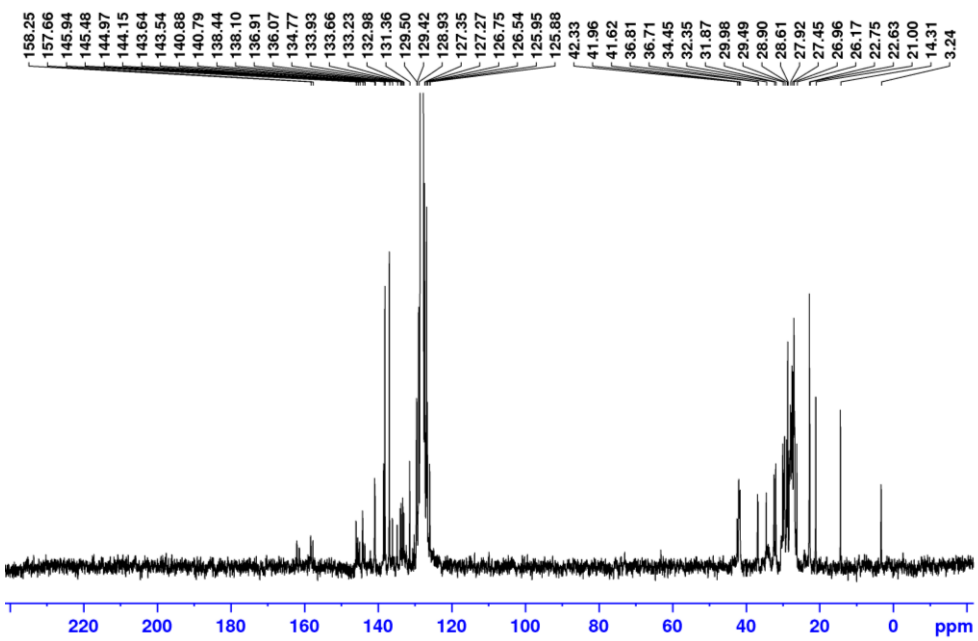

Figure B33. For **2-10** (a) $^{31}P\{^{1}H\}$ NMR spectrum (121.5 MHz, C_6D_6). (b) ^{31}P NMR spectrum (121.5 MHz, C_6D_6).

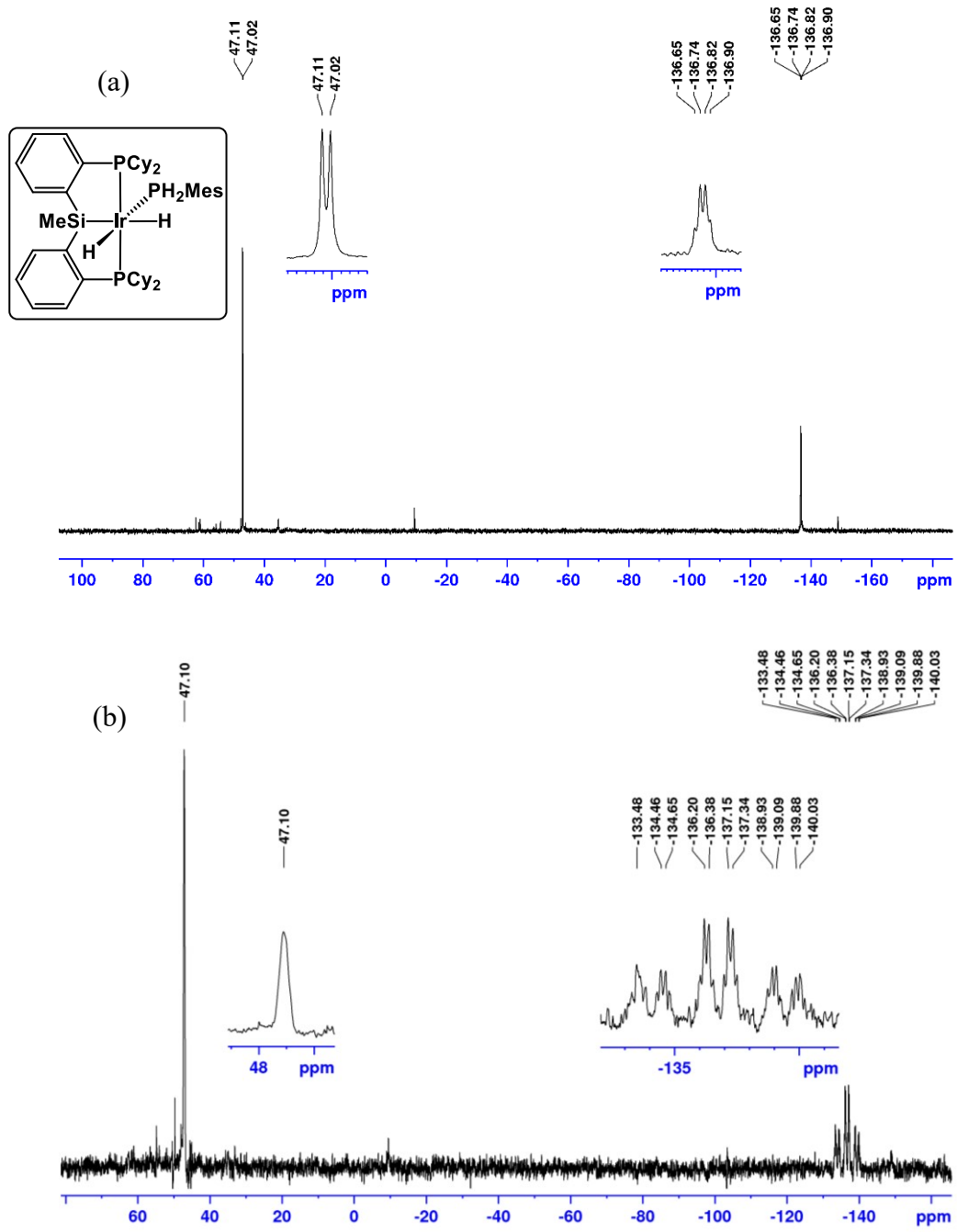

Figure B34. For **2-10** ^{1}H NMR spectrum (300 MHz, C_6D_6).

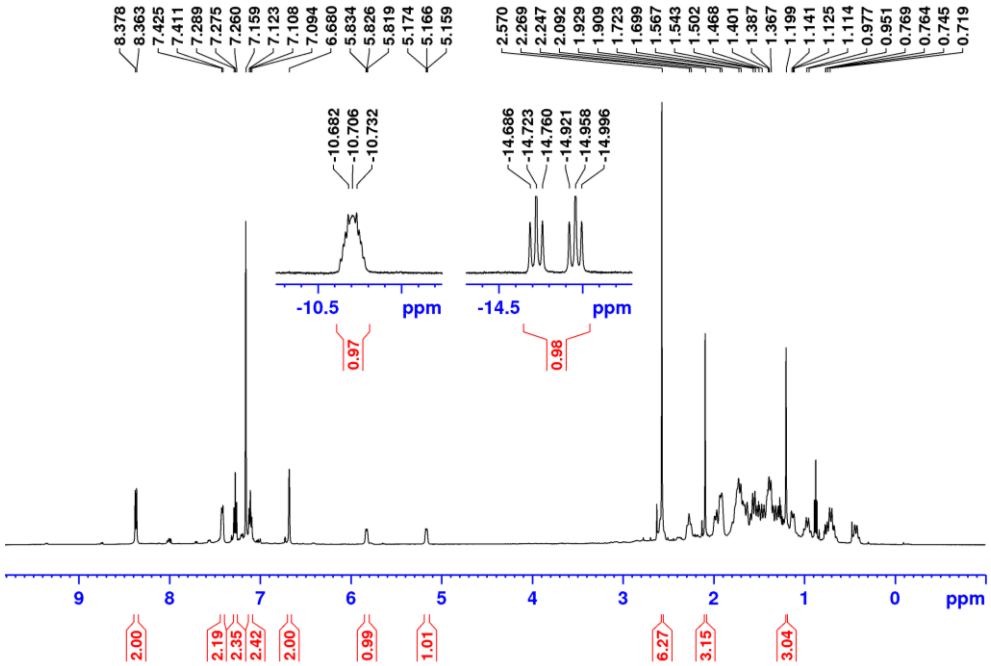

Selected Spectra of Compounds Reported in Chapter 3

Figure B35. For **3-1a** (a) $^{31}P\{^{1}H\}$ NMR spectrum (121.5 MHz, C_6D_6). (b) ^{1}H NMR spectrum (300 MHz, C_6D_6).

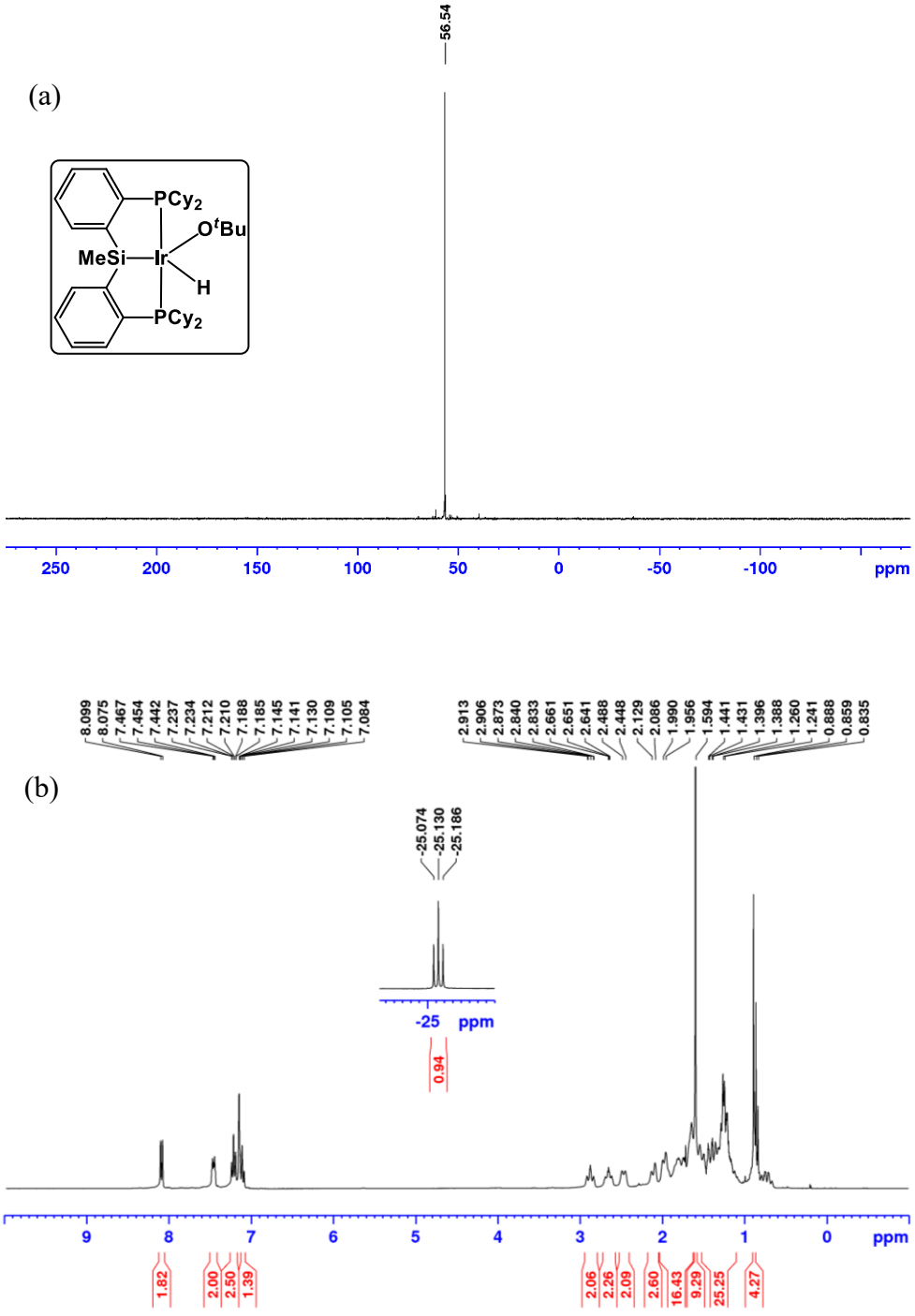

Figure B36. For **3-1a** $^{13}C\{^{1}H\}$ NMR spectrum (75.5 MHz, C_6D_6). * indicates pentane impurity.

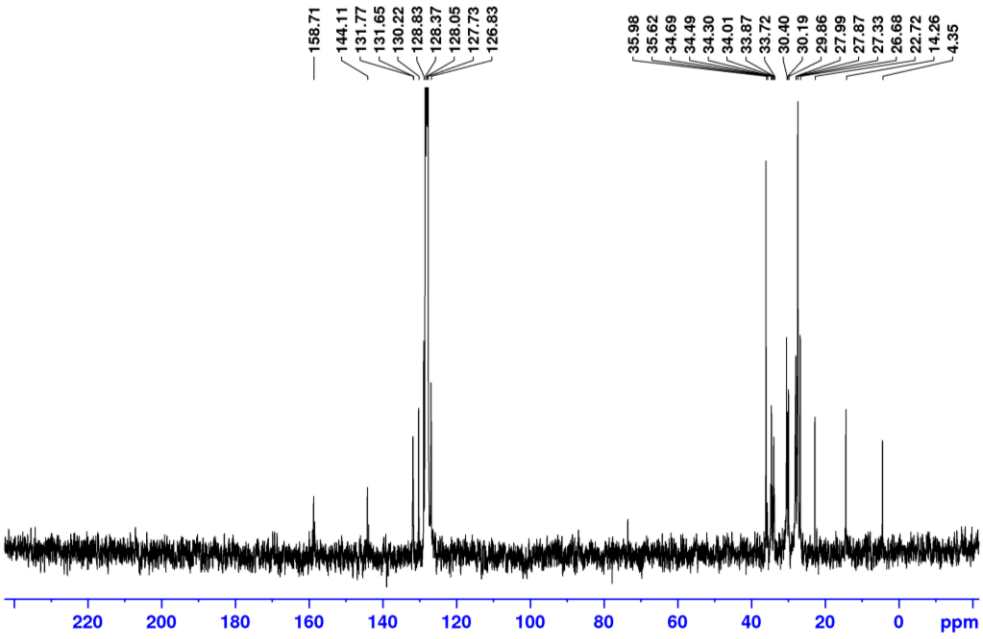

Figure B37. For **3-1b** (a) $^{31}P\{^{1}H\}$ NMR spectrum (121.5 MHz, C_6D_6). (b) ^{1}H NMR spectrum (300 MHz, C_6D_6).

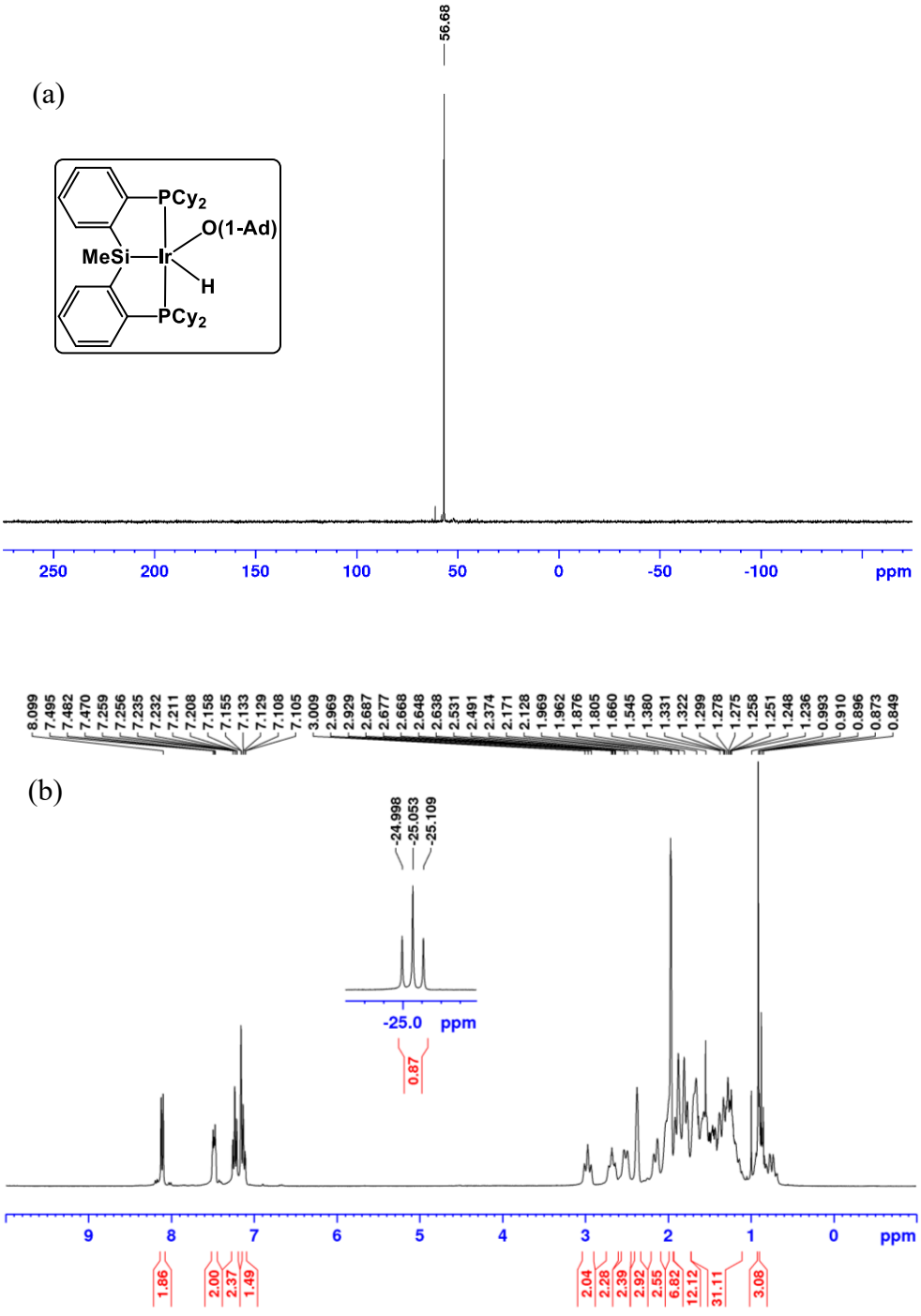

Figure B38. For **3-1b** $^{13}C\{^{1}H\}$ NMR spectrum (75.5 MHz, C_6D_6).

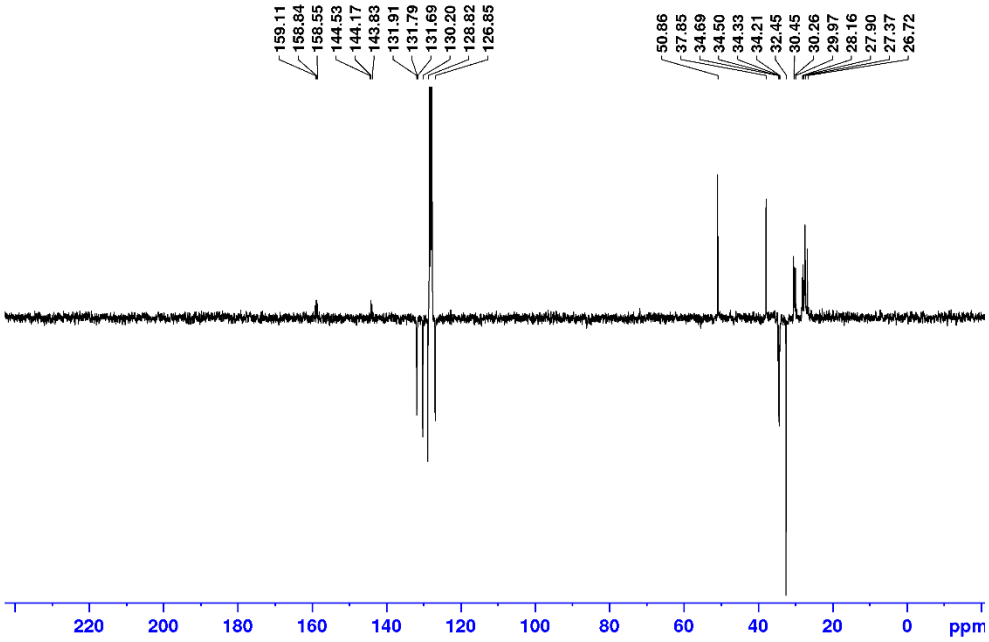

Figure B39. For **3-1c** (a) $^{31}P\{^{1}H\}$ NMR spectrum (121.5 MHz, C_6D_6). (b) ^{1}H NMR spectrum (300 MHz, C_6D_6).

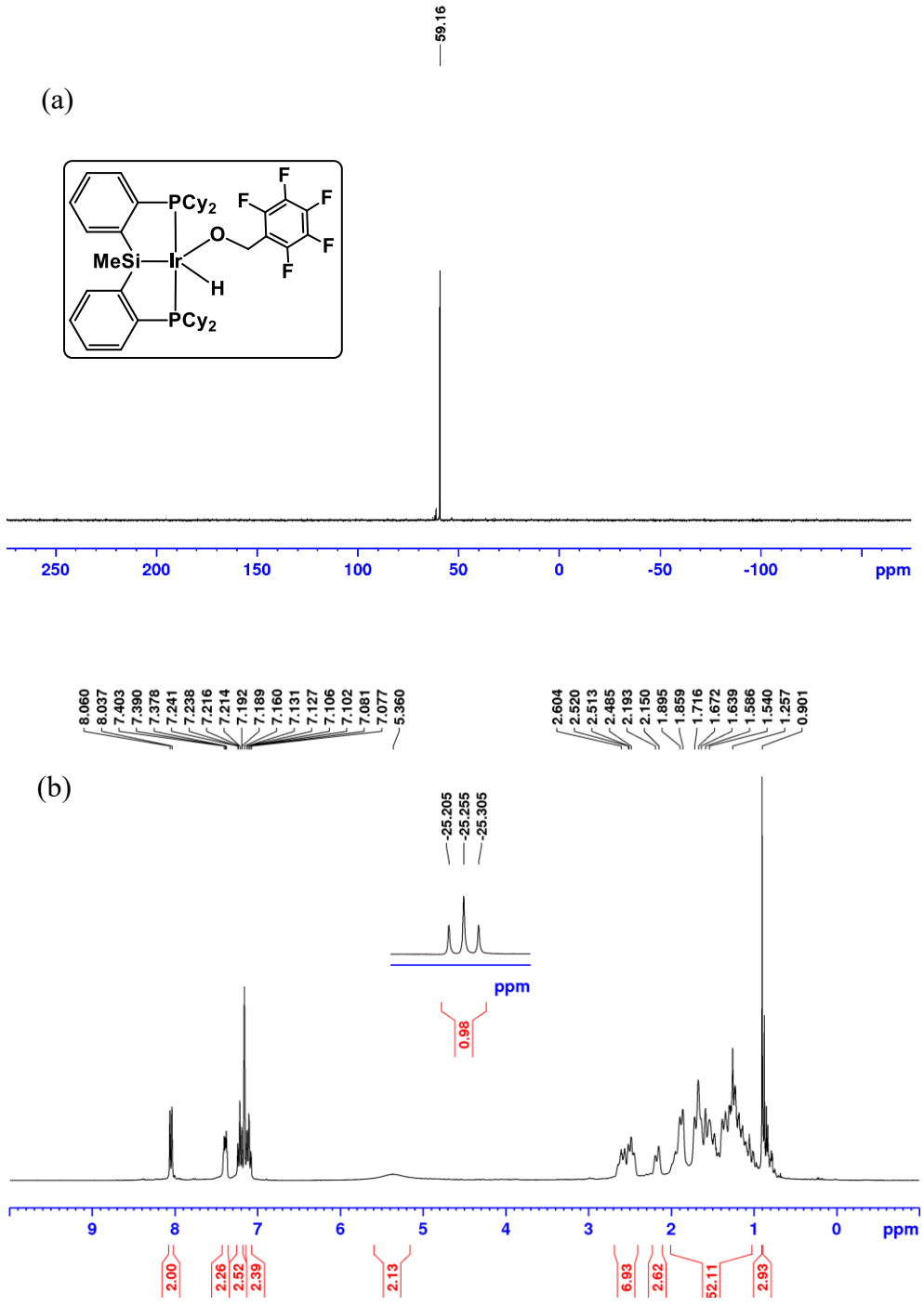

Figure B40. For **3-1c** $^{13}C\{^{1}H\}$ NMR spectrum (75.5 MHz, C_6D_6).

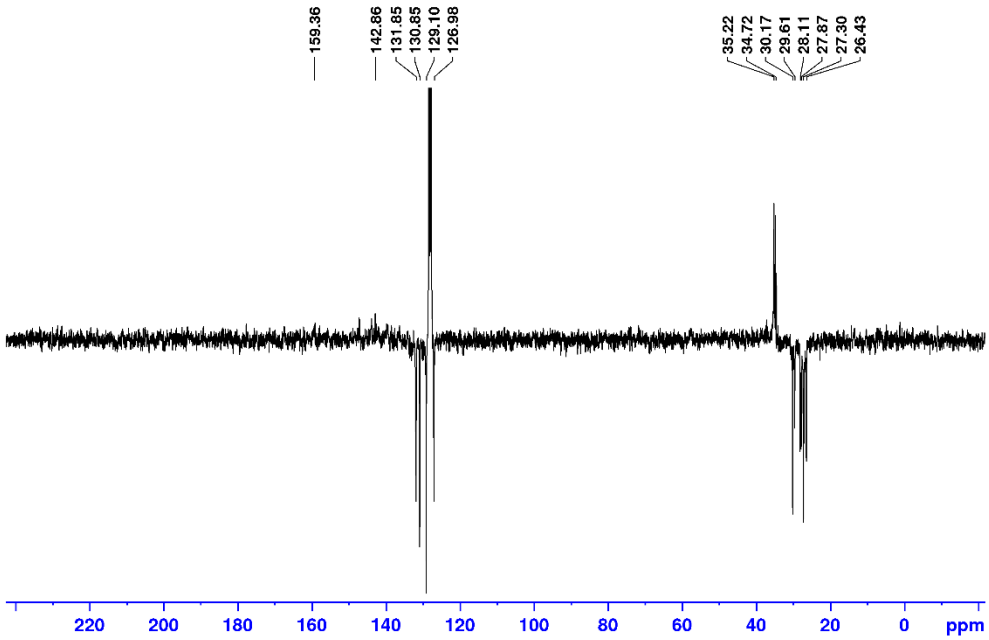

Figure B41. For **3-2a** (a) $^{31}P\{^{1}H\}$ NMR spectrum (121.5 MHz, C_6D_6). (b) ^{1}H NMR spectrum (300 MHz, C_6D_6).

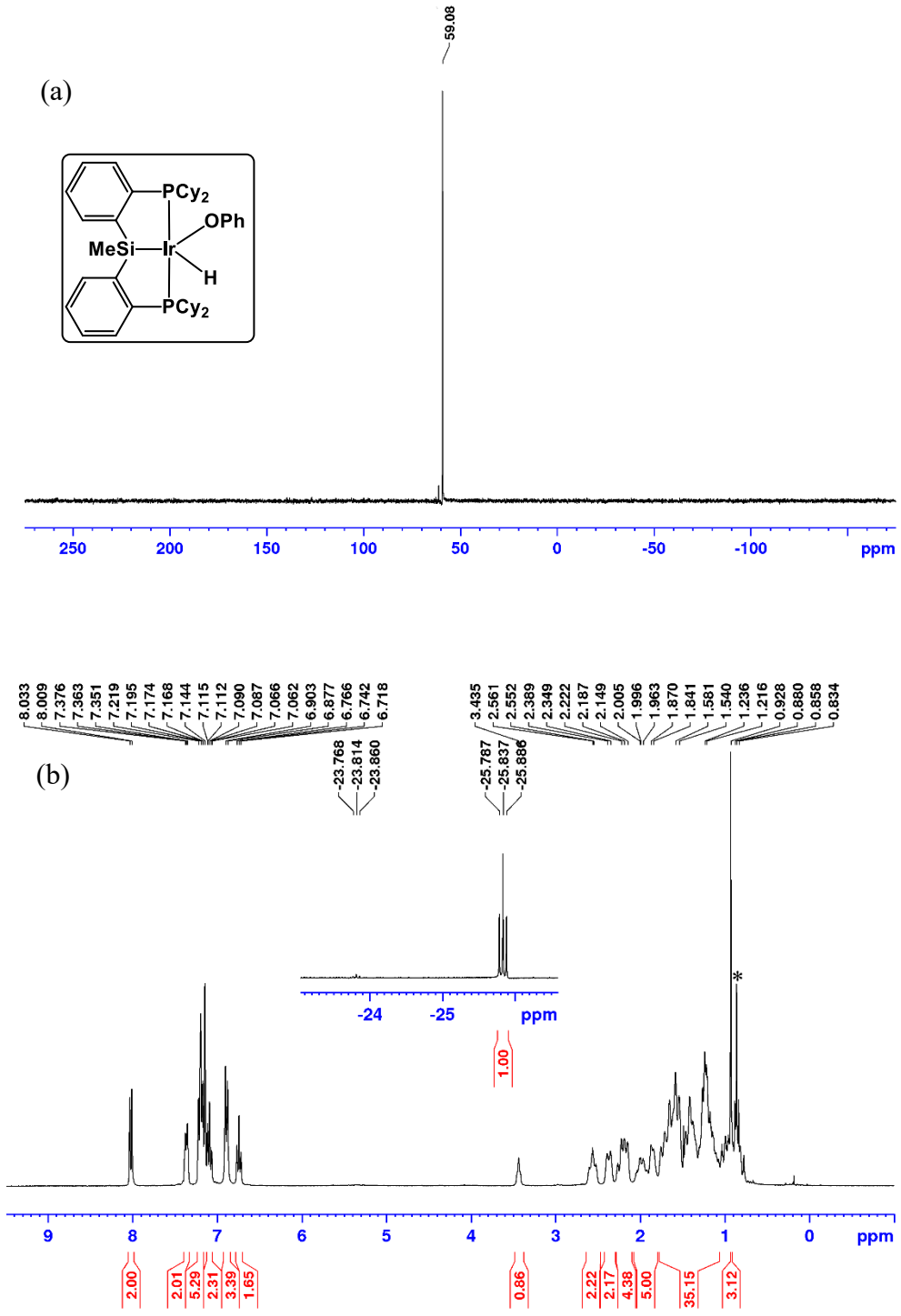

Figure B42. For **3-2a** $^{13}C\{^{1}H\}$ NMR spectrum (75.5 MHz, C_6D_6). * indicates pentane impurity.

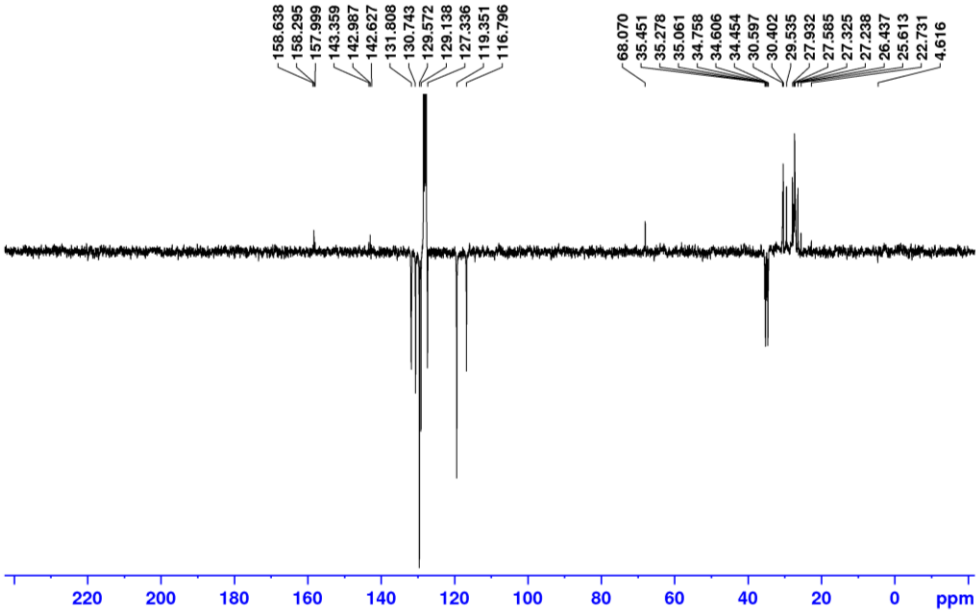

Figure B43. For **3-2b** (a) $^{31}P\{^{1}H\}$ NMR spectrum (121.5 MHz, C_6D_6). (b) ^{1}H NMR spectrum (300 MHz, C_6D_6). * indicates pentane impurity.

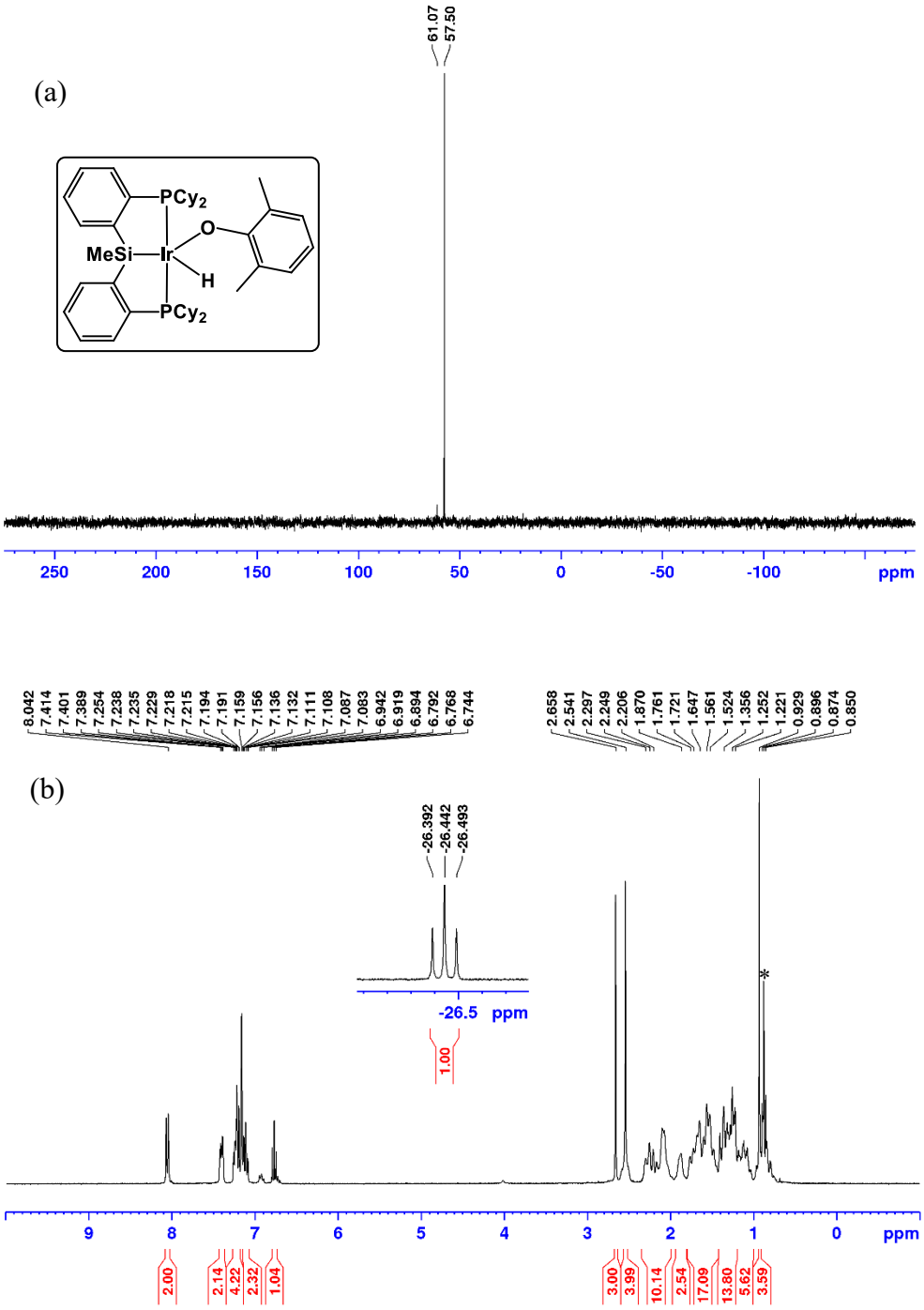

Figure B44. For **3-2b** $^{13}C\{^{1}H\}$ NMR spectrum (75.5 MHz, C_6D_6).

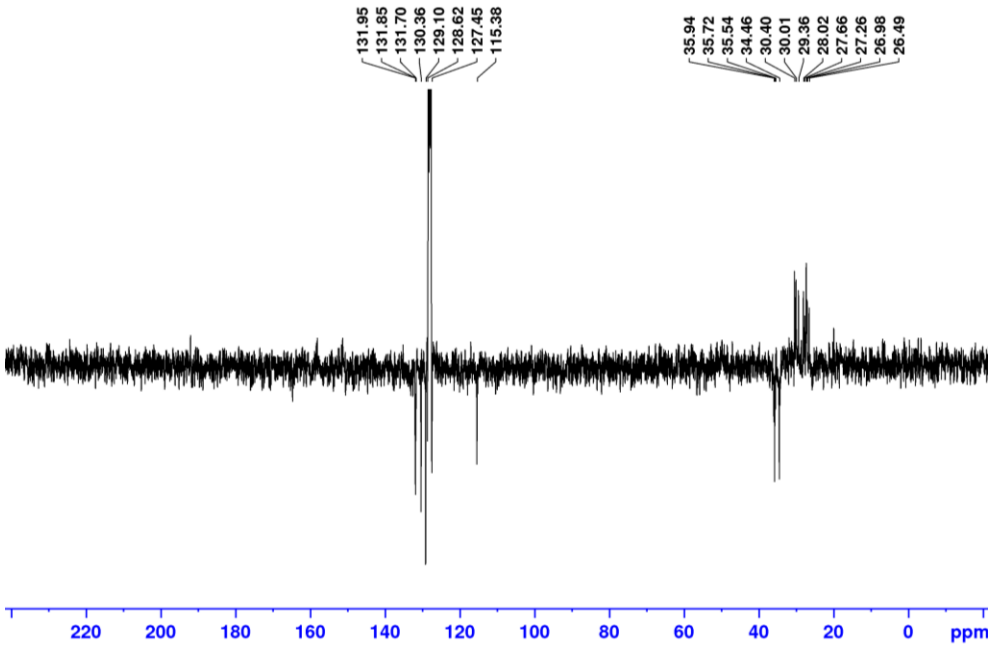

Figure B45. For **3-2c** (a) $^{31}P\{^{1}H\}$ NMR spectrum (202.5 MHz, C_6D_6). (b) ^{1}H NMR spectrum (500 MHz, C_6D_6).

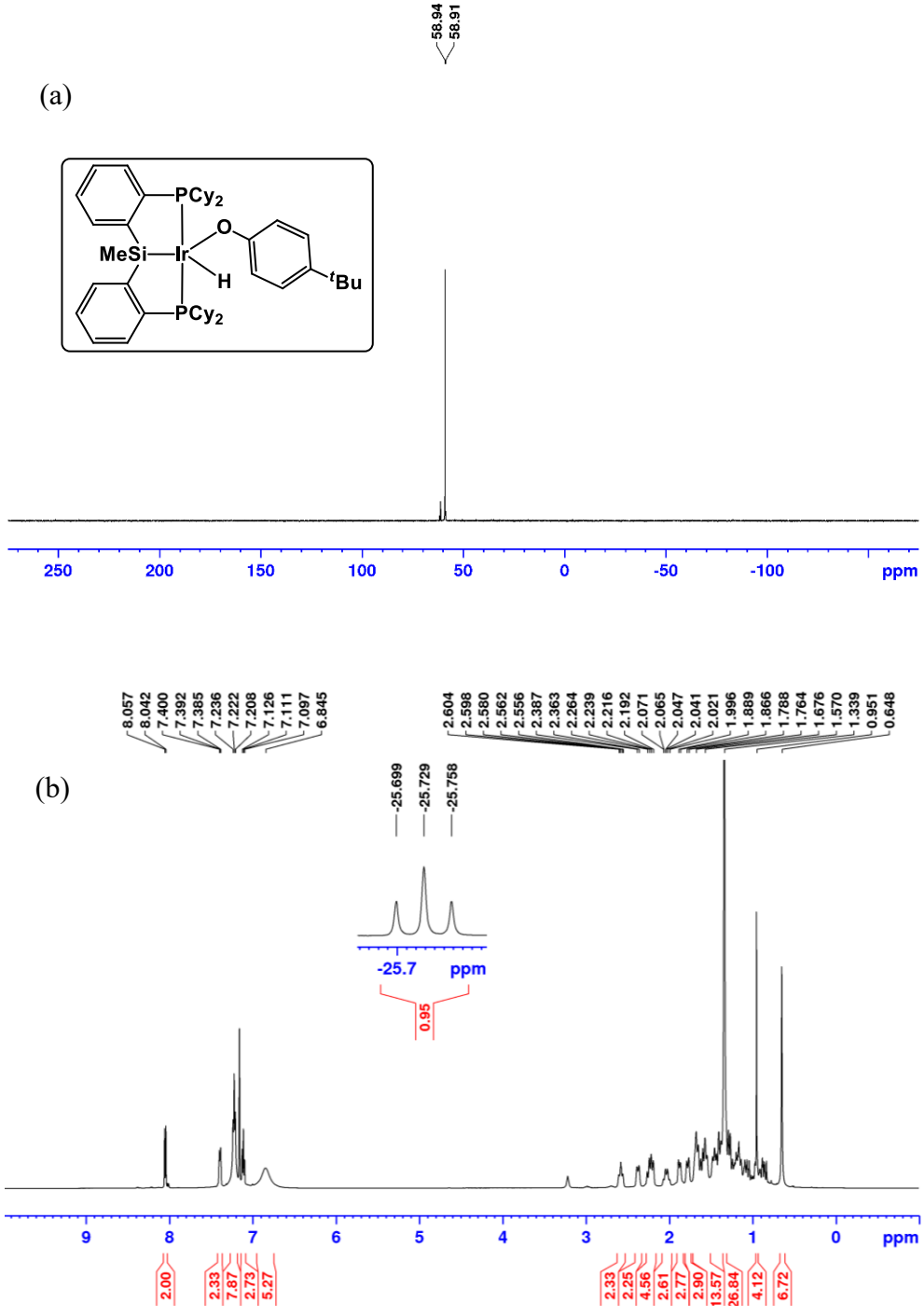

Figure B46. For **3-2c** $^{13}C\{^{1}H\}$ NMR spectrum (125.7 MHz, C_6D_6).

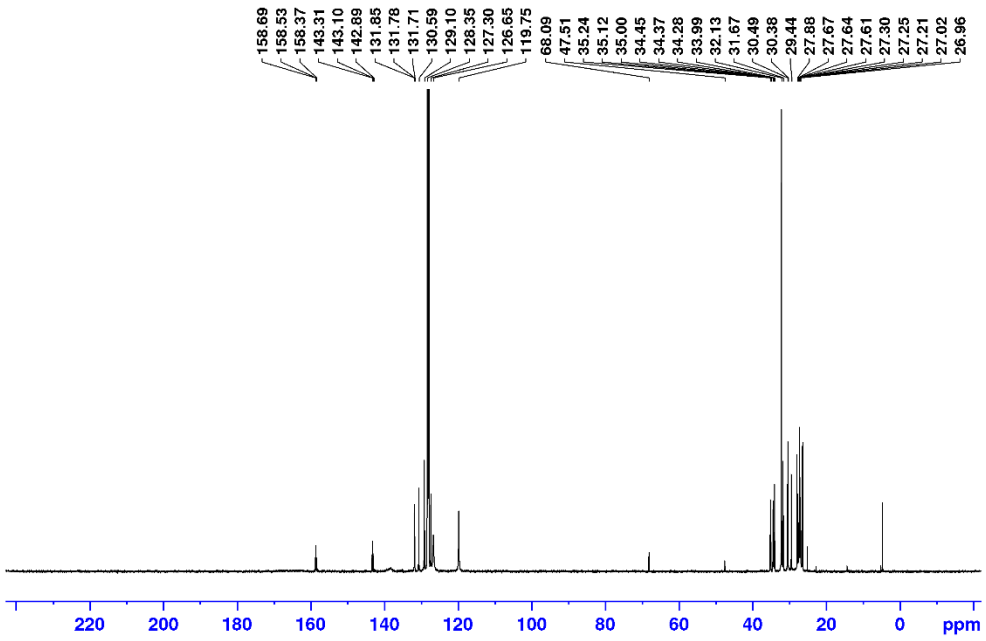

Figure B47. For **3-4** (a) $^{31}P\{^{1}H\}$ NMR spectrum (121.5 MHz, C_6D_6). (b) ^{1}H NMR spectrum (300 MHz, C_6D_6). ▲indicates resonances associated with **1.1** impurity.¤ indicates THF impurity. * indicates pentane impurity.

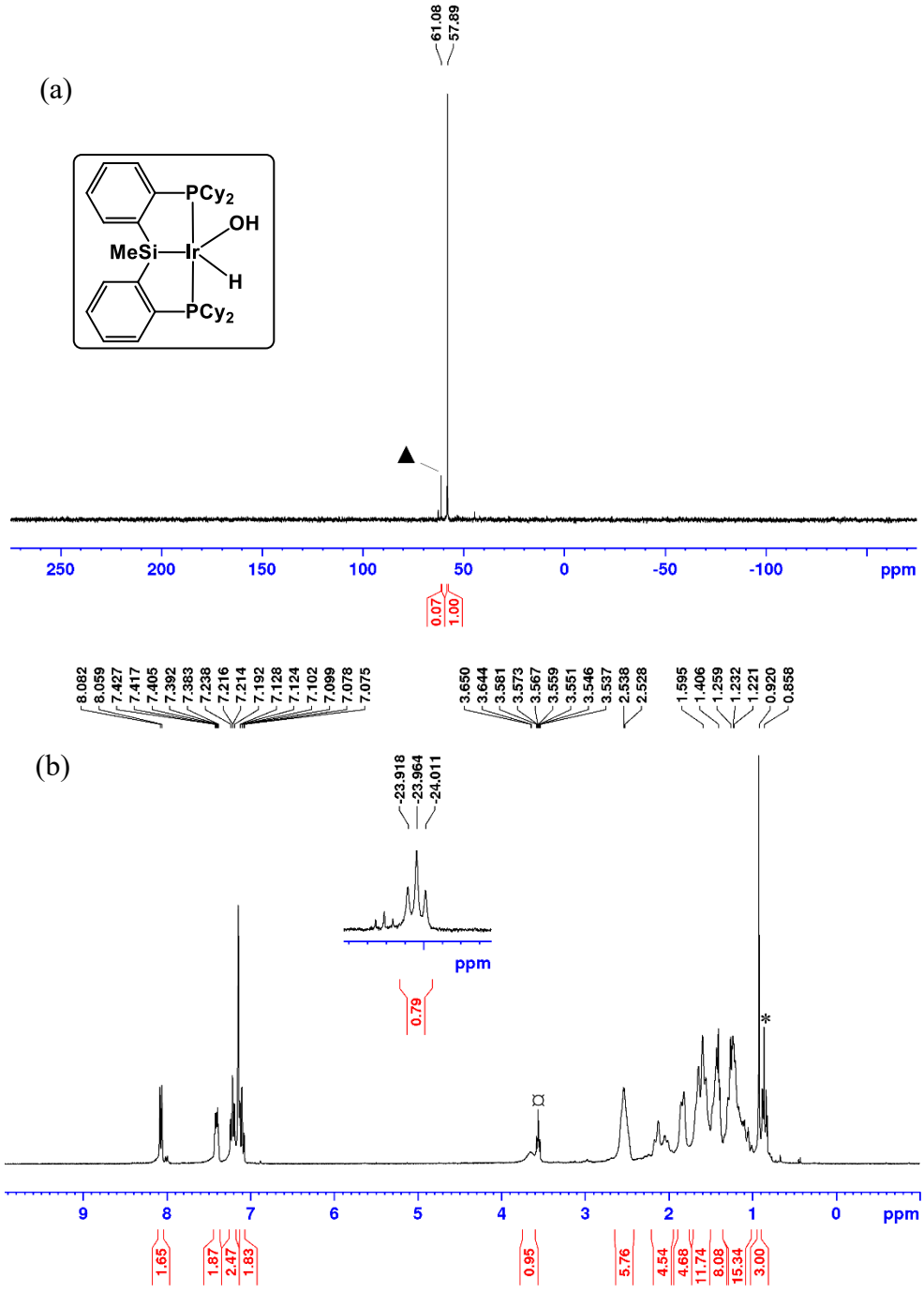

Figure B48. For **3-4d** (a) $^{31}P\{^{1}H\}$ NMR spectrum (121.5 MHz, C_6D_6). (b) ^{1}H NMR spectrum (300 MHz, C_6D_6). * indicates pentane impurity.

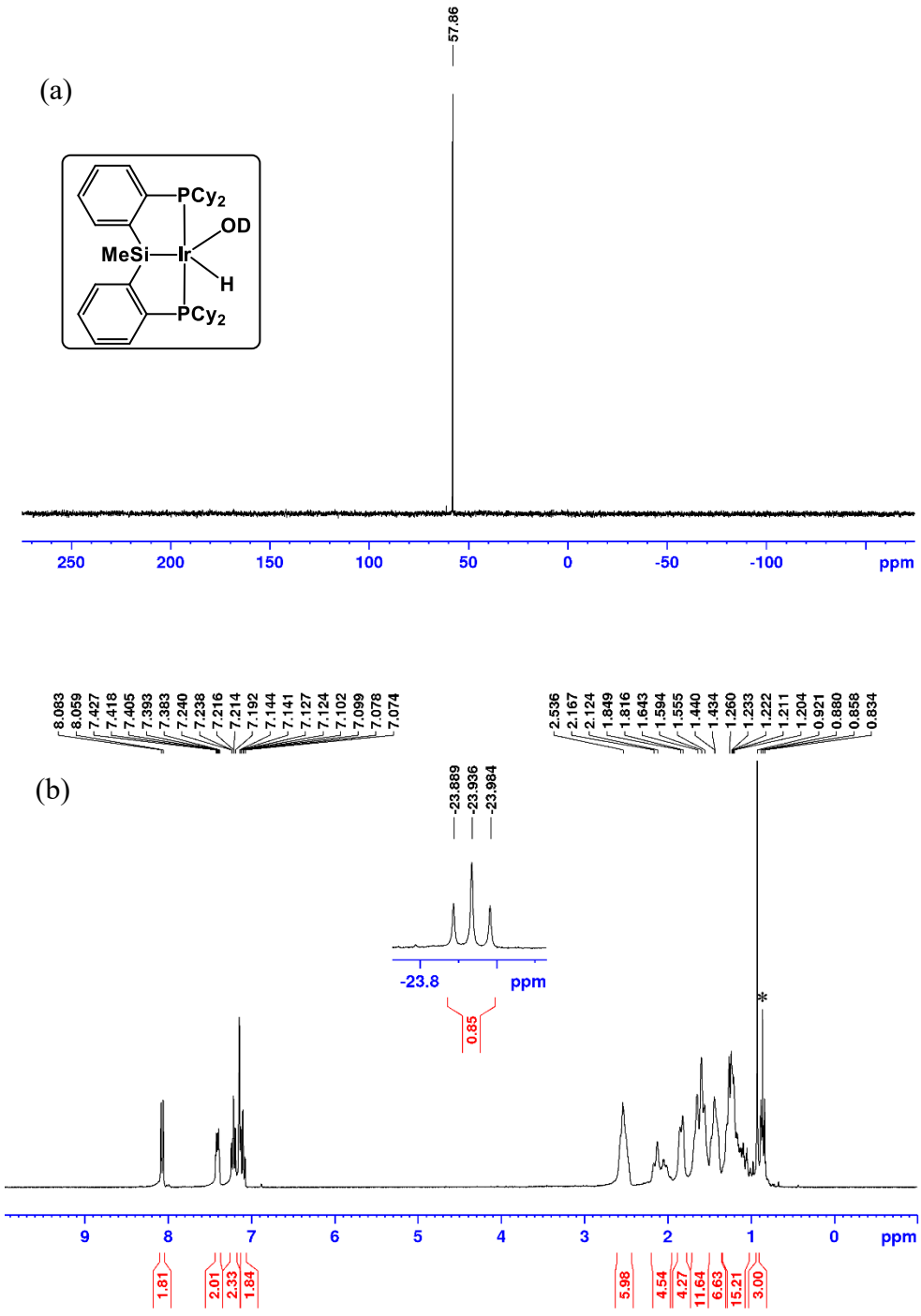

Figure B49. For **3-4d** $^{13}C\{^{1}H\}$ NMR spectrum (75.5 MHz, C_6D_6

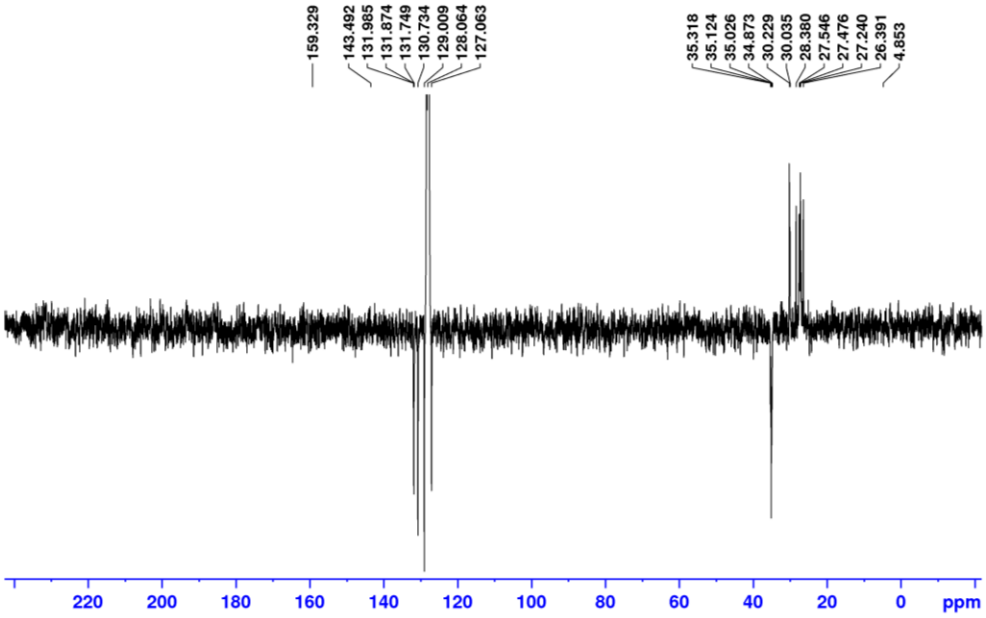

Figure B50. For **3-6** (a) $^{31}P\{^{1}H\}$ NMR spectrum (121.5 MHz, C_6D_6). (b) ^{1}H NMR spectrum (300 MHz, C_6D_6).

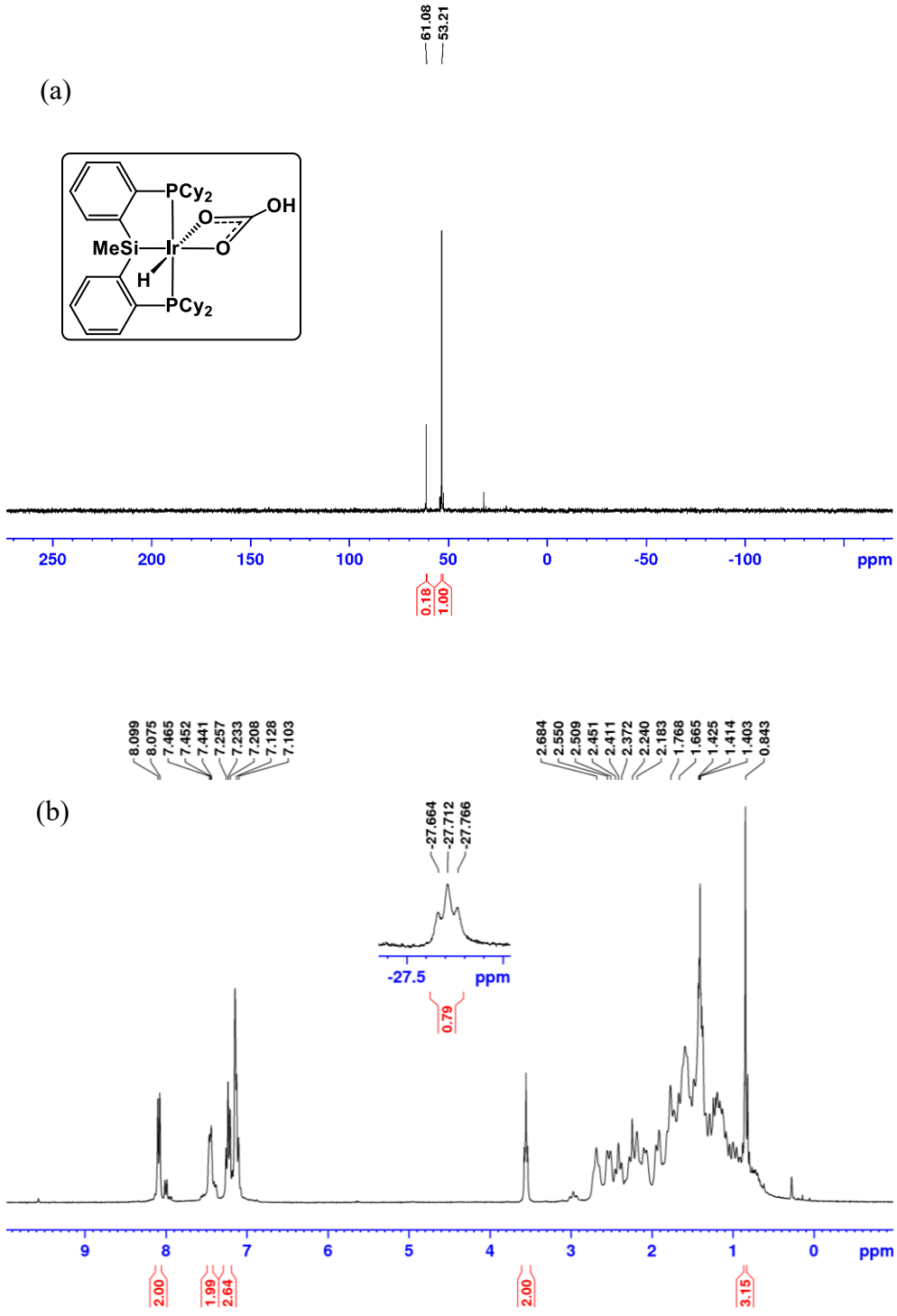

Figure B51. For **3-7** (a) $^{31}P\{^{1}H\}$ NMR spectrum (121.5 MHz, C_6D_6). (b) ^{1}H NMR spectrum (300 MHz, C_6D_6).

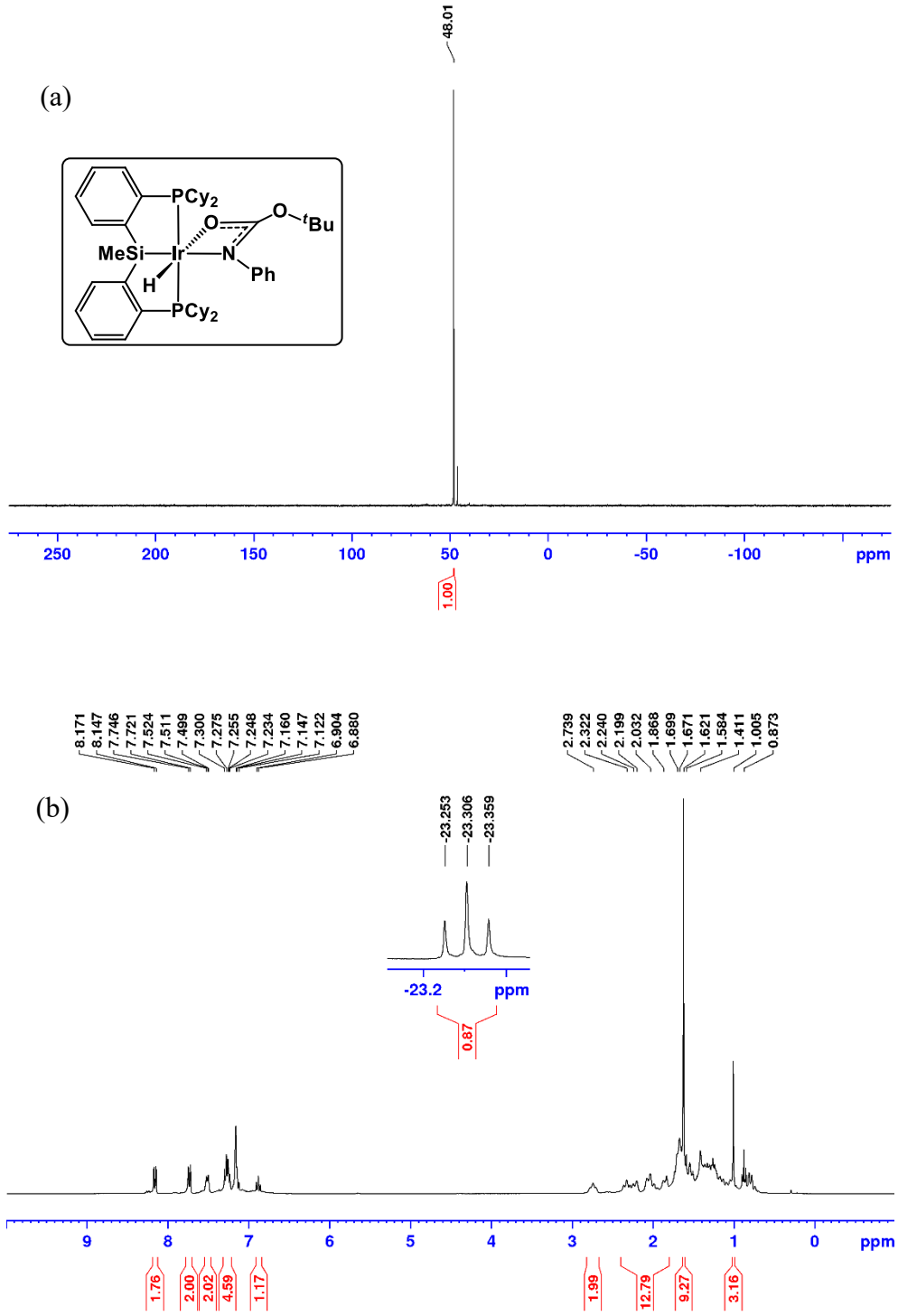

Figure B52. For **3-7** $^{13}C\{^{1}H\}$ NMR spectrum (75.5 MHz, C_6D_6).

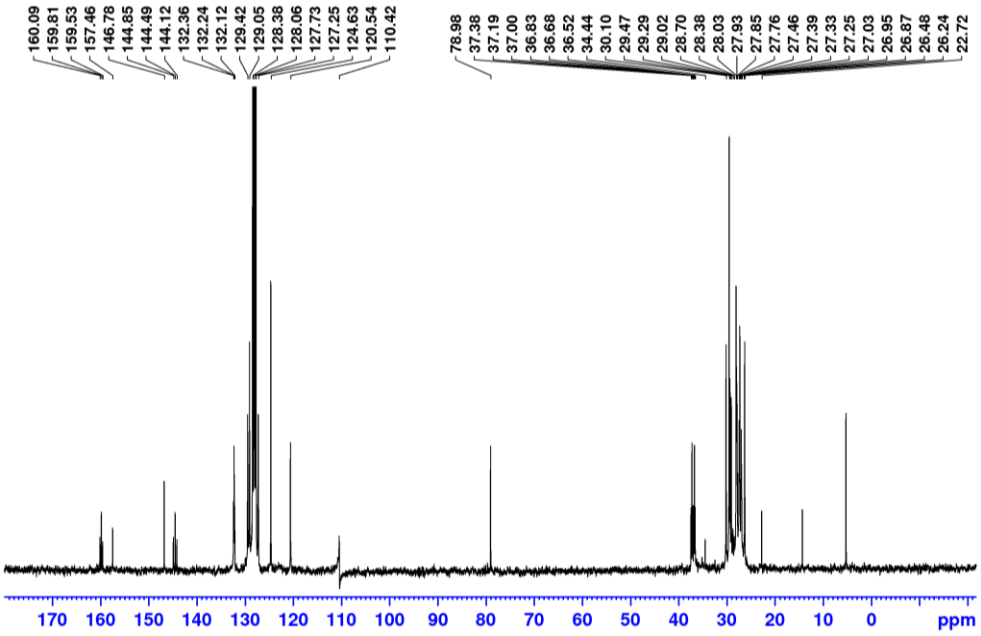

Selected Spectra of Compounds Reported in Chapter 4

Figure B53. For **4-1** (a) $^{31}P\{^{1}H\}$ NMR spectrum (121.5 MHz, C_6D_6). (b) ^{1}H NMR spectrum (300 MHz, C_6D_6). (Spectra are from a reaction crude, containing excess H_2SiPh_2).

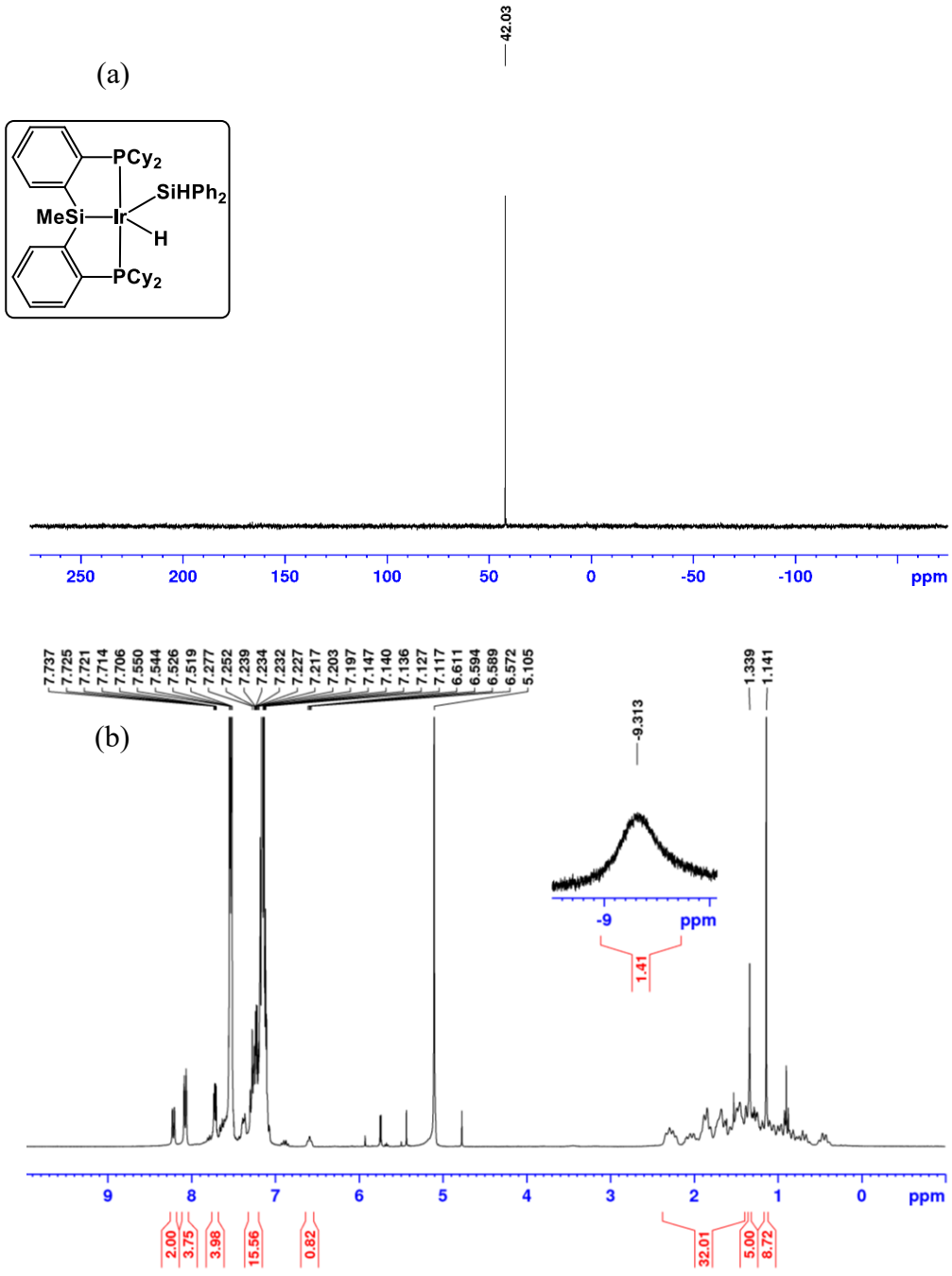

Figure B54. For **4-2** (a) $^{31}P\{^{1}H\}$ NMR spectrum (121.5 MHz, C_6D_6). (b) ^{1}H NMR spectrum (300 MHz, C_6D_6).

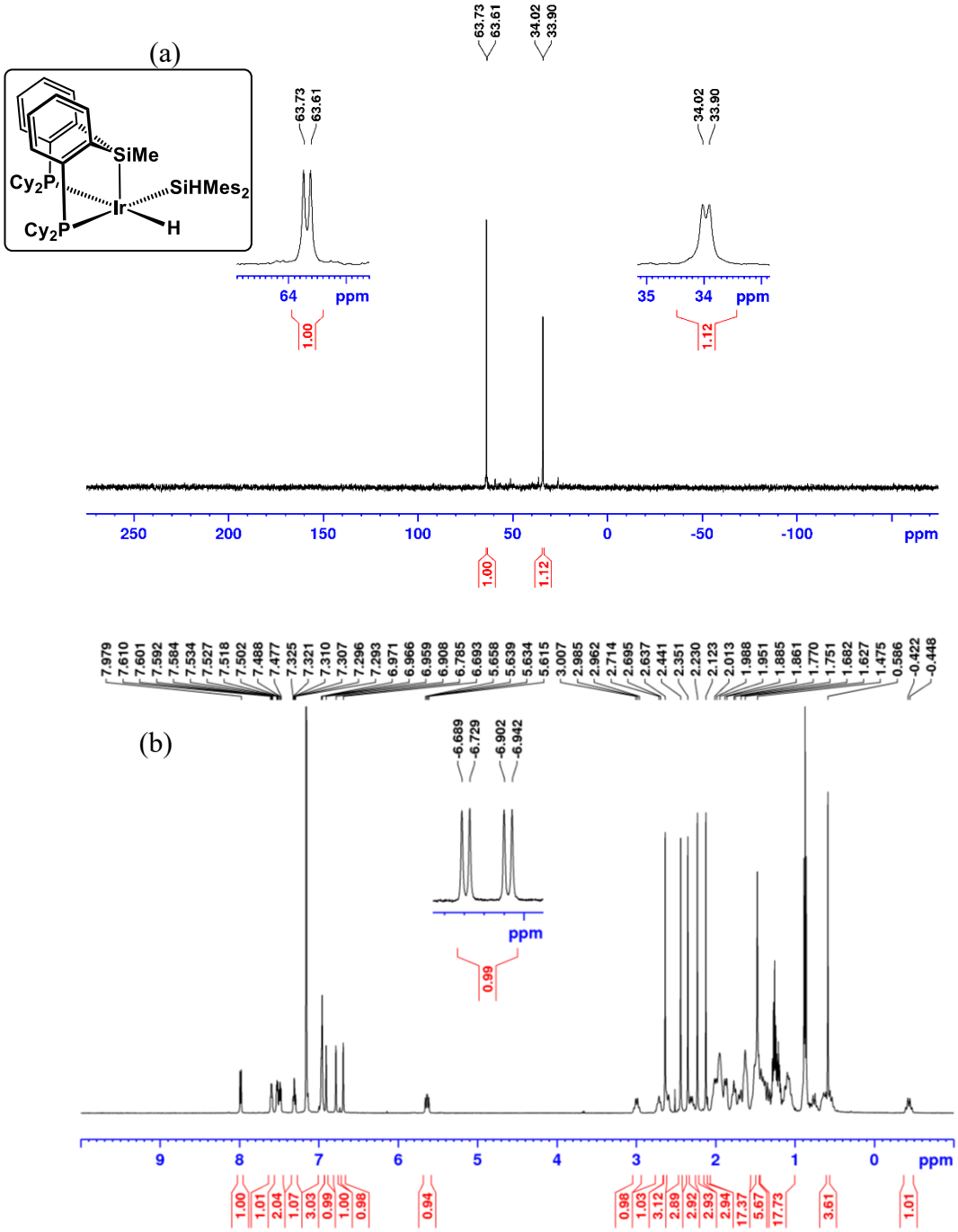

Figure B55. For **4-2** $^{13}C\{^{1}H\}$ NMR spectrum (75.5 MHz, C_6D_6).

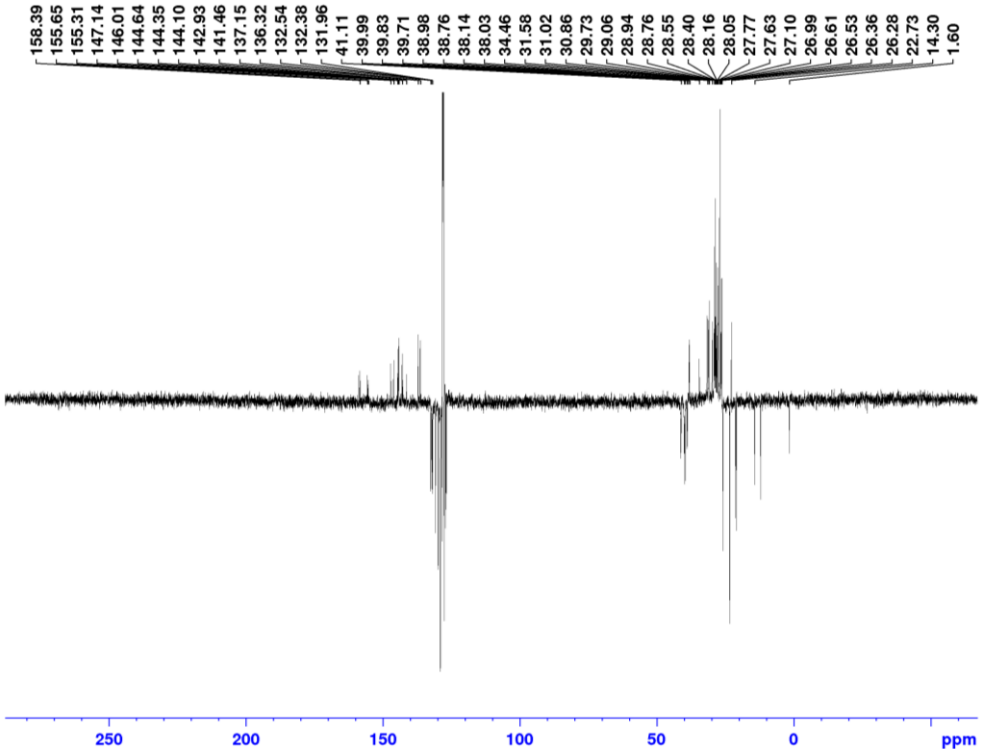

Figure B56. For **4-3** (a) $^{31}P\{^{1}H\}$ NMR spectrum (121.5 MHz, CD_2Cl_2). (b) ^{1}H NMR spectrum (300 MHz, CD_2Cl_2).

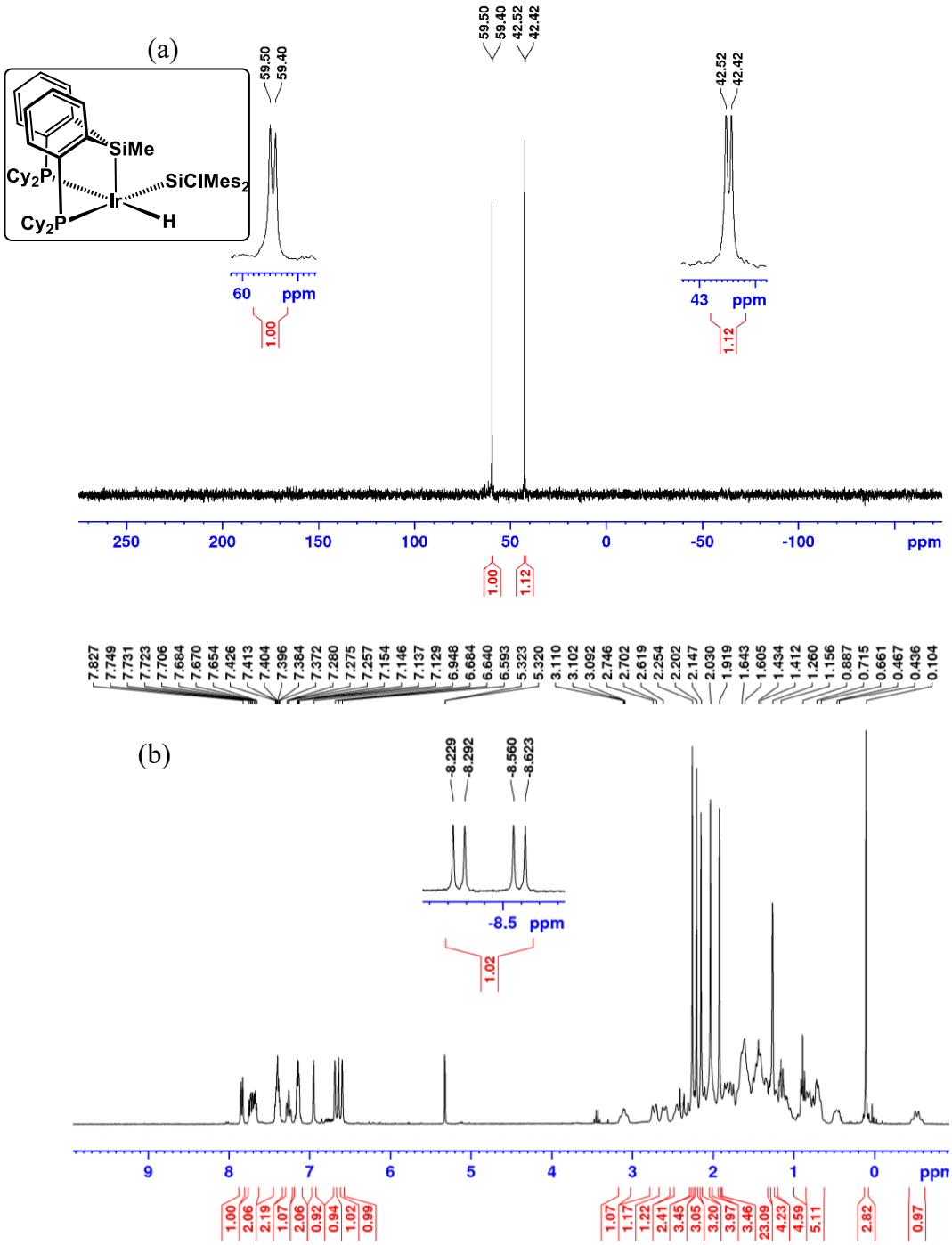

Figure B57. For **4-3** $^{13}C\{^{1}H\}$ NMR spectrum (75.5 MHz, CD_2Cl_2).

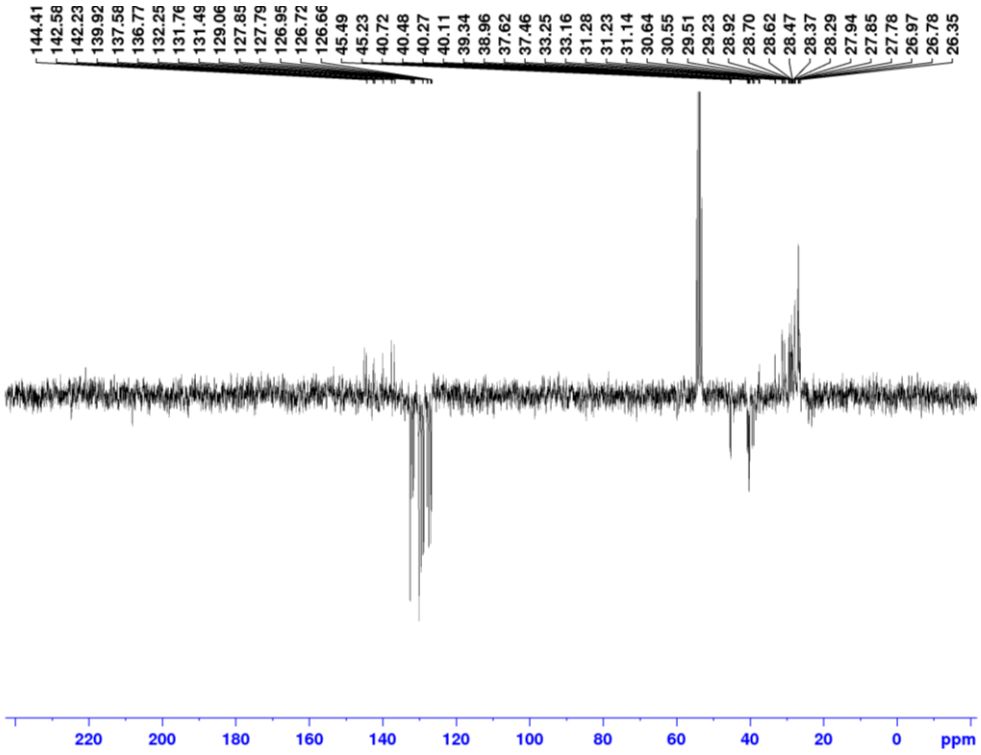

Figure B58. For **4-4a,b** (a) $^{31}P\{^{1}H\}$ NMR spectrum (121.5 MHz, C_6D_6). (b) ^{1}H NMR spectrum (300 MHz, C_6D_6).

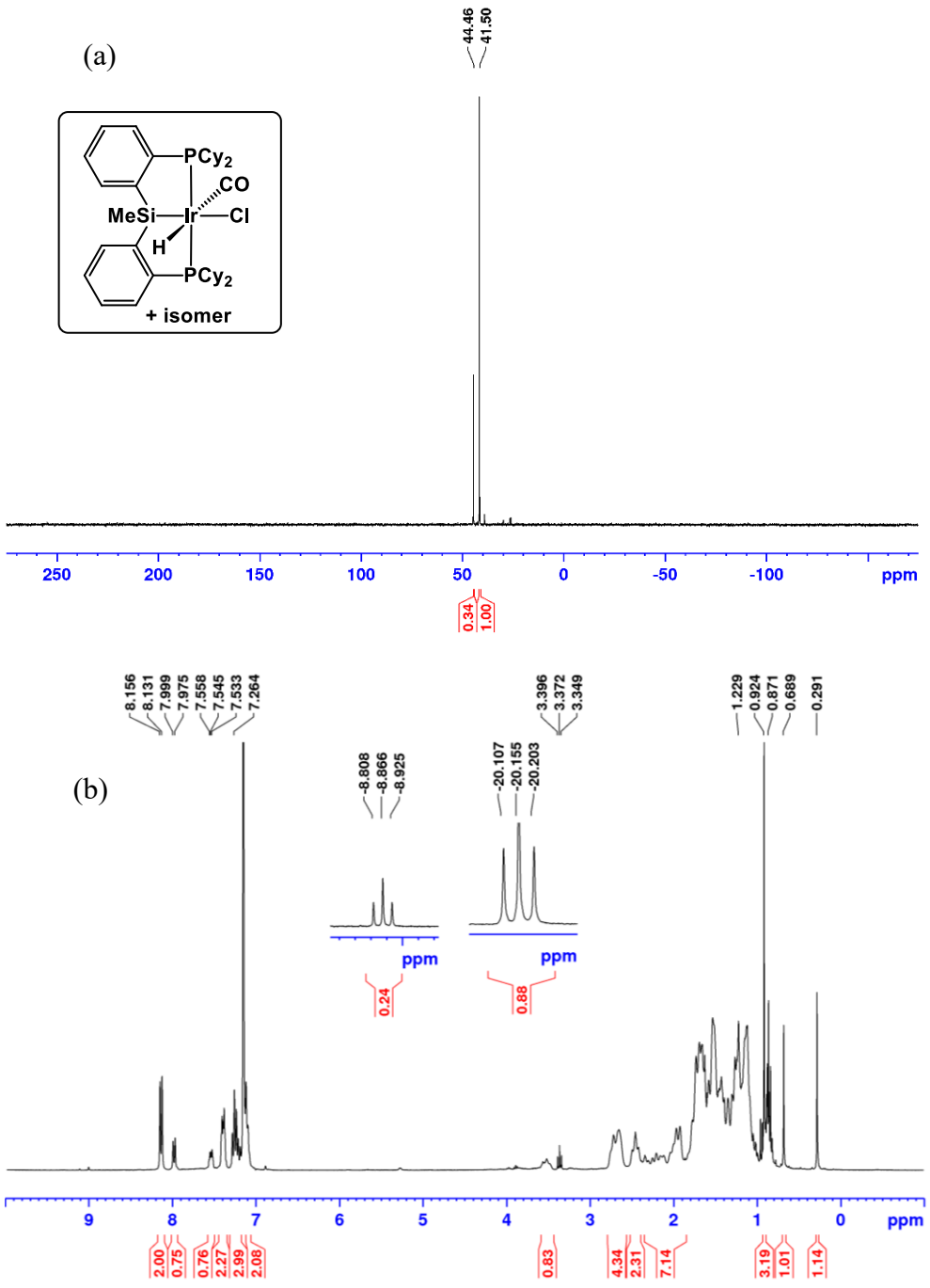

Figure B59. For **4-5** (a) $^{31}P\{^{1}H\}$ NMR spectrum (121.5 MHz, C_6D_6). (b) ^{1}H NMR spectrum (300 MHz, C_6D_6).

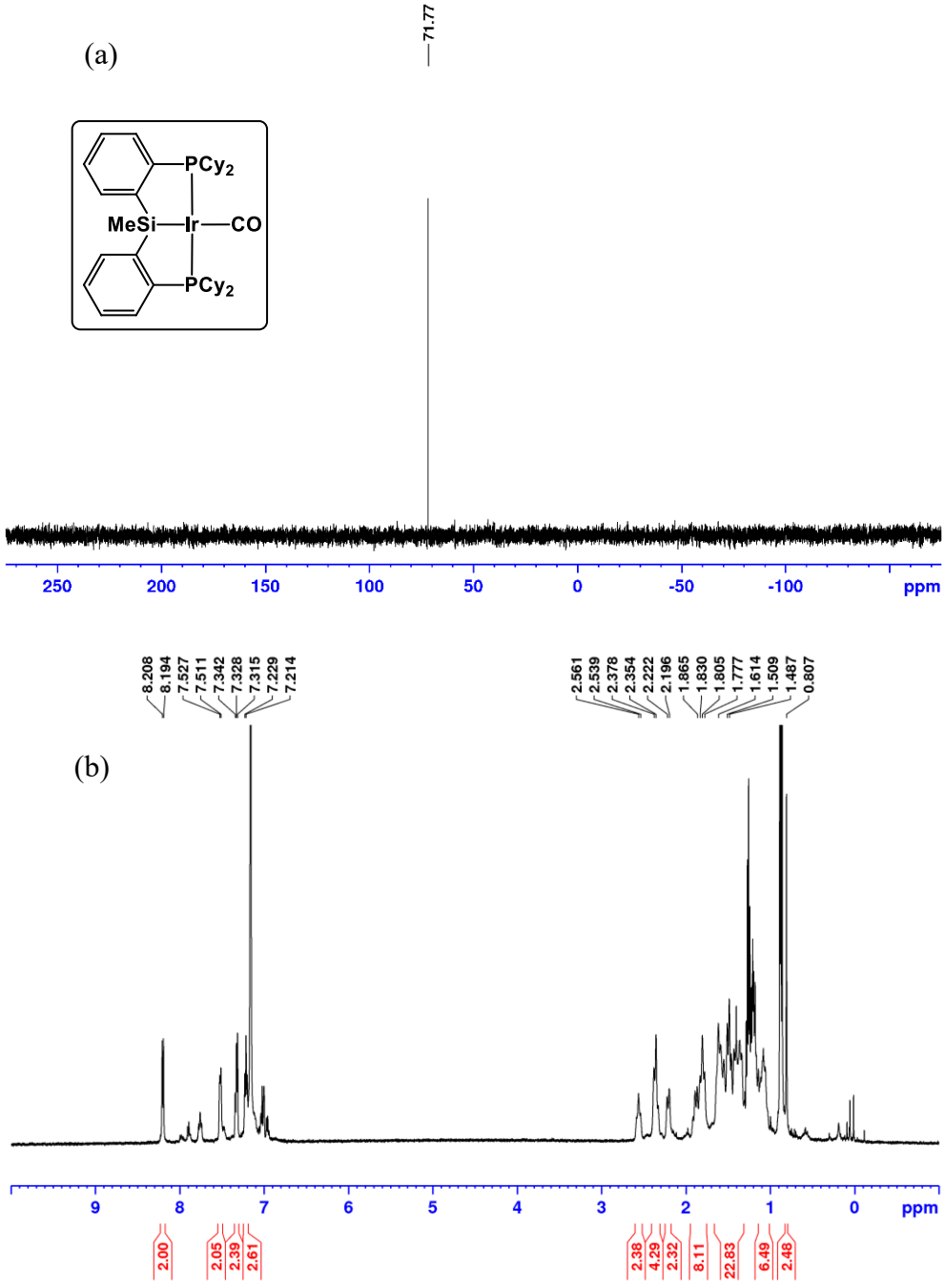

Figure B60. For **4-6** $^{31}P\{^{1}H\}$ NMR spectrum (121.5 MHz, C_6D_6).

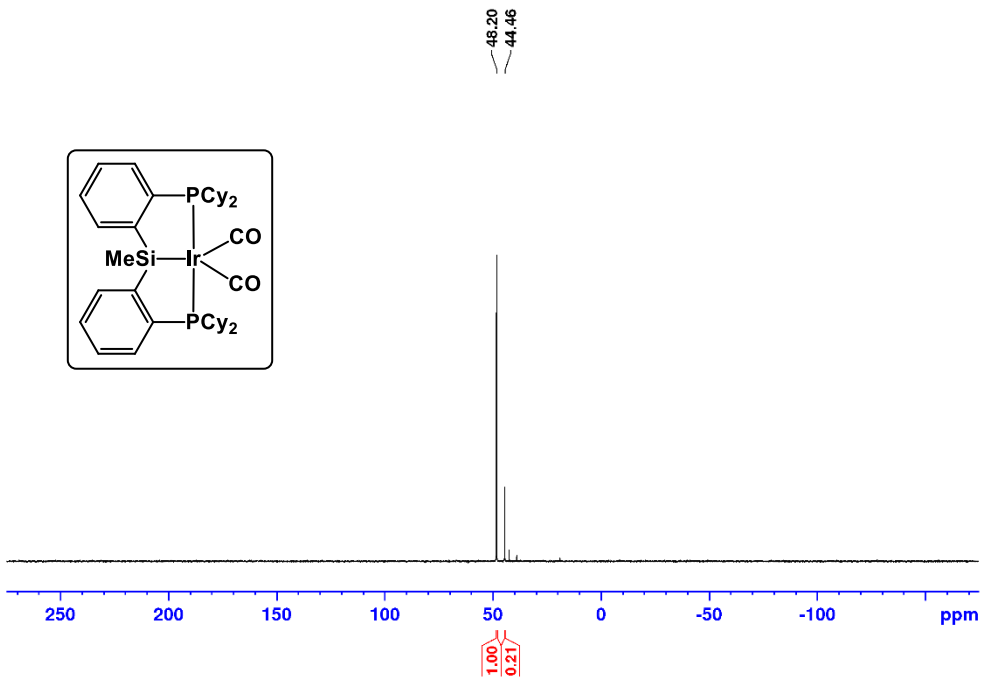

Figure B61. For **4-7** $^{31}P\{^{1}H\}$ NMR spectrum (121.5 MHz, C_6D_6).

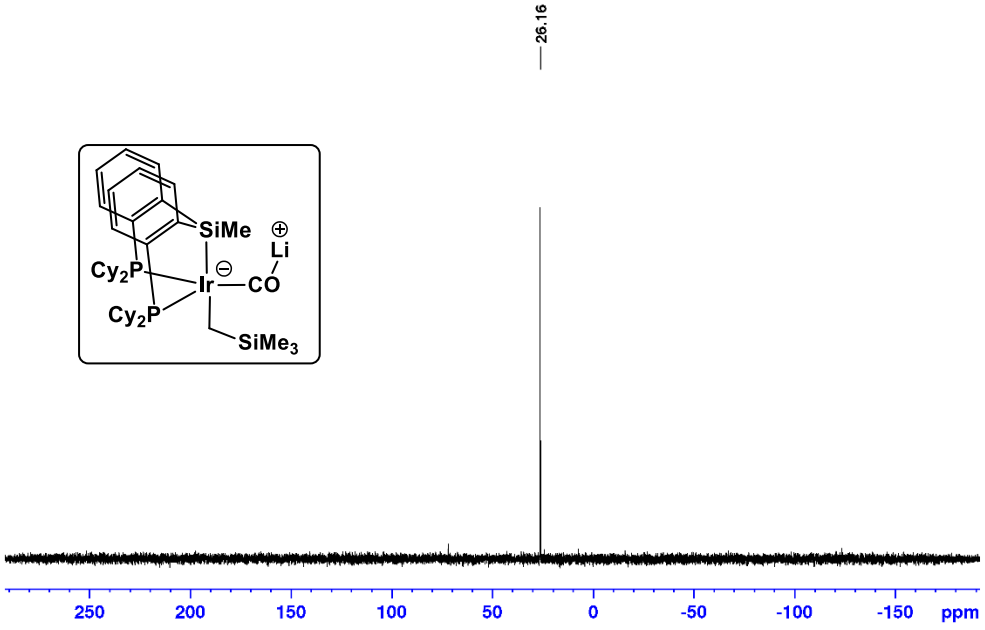

Figure B62. For **4-8a,b** (a) $^{31}P\{^{1}H\}$ NMR spectrum (121.5 MHz, C_6D_6). (b) ^{31}P NMR spectrum (121.5 MHz, C_6D_6).

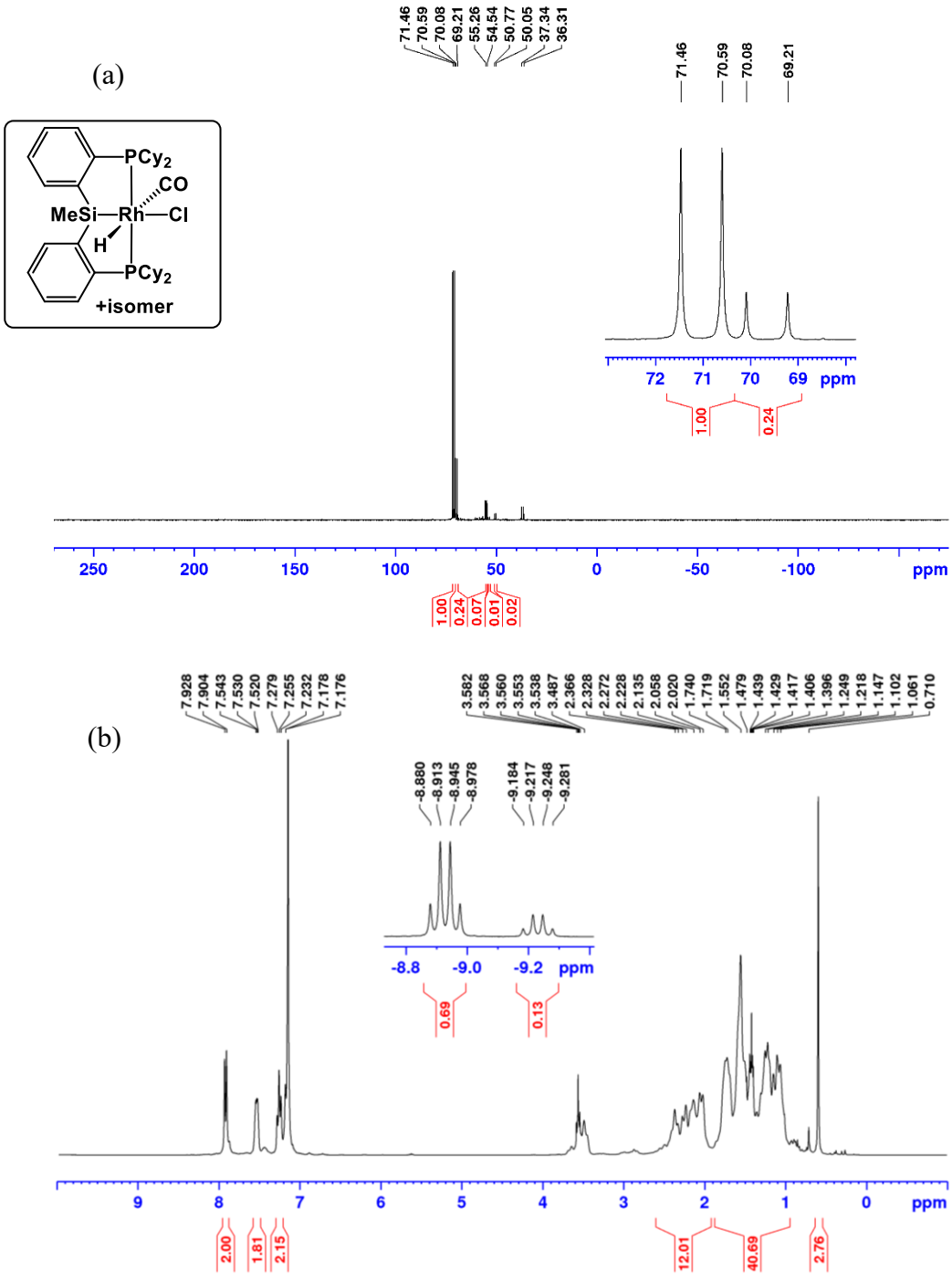

Figure B63. For **4-8a,b** $^{13}C\{^{1}H\}$ NMR spectrum (75.5 MHz, C_6D_6).

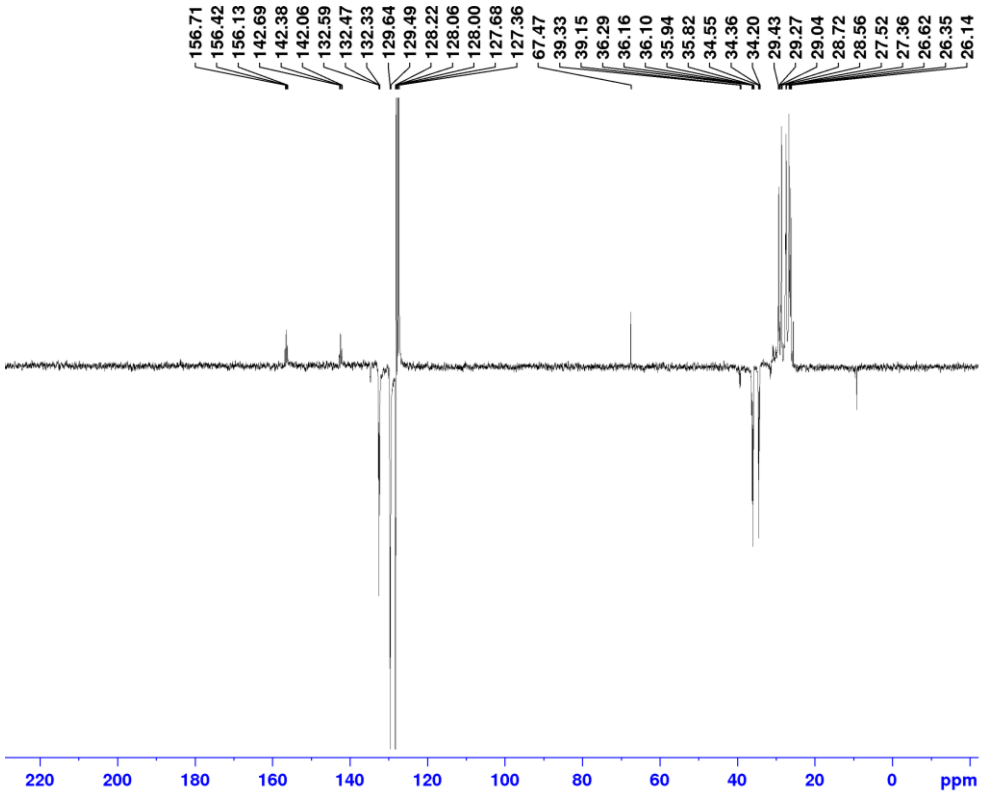

Figure B64. For **4-8a,b** (a) $^{31}P\{^{1}H\}$ NMR spectrum (121.5 MHz, C_6D_6). (b) ^{31}P NMR spectrum (121.5 MHz, C_6D_6).

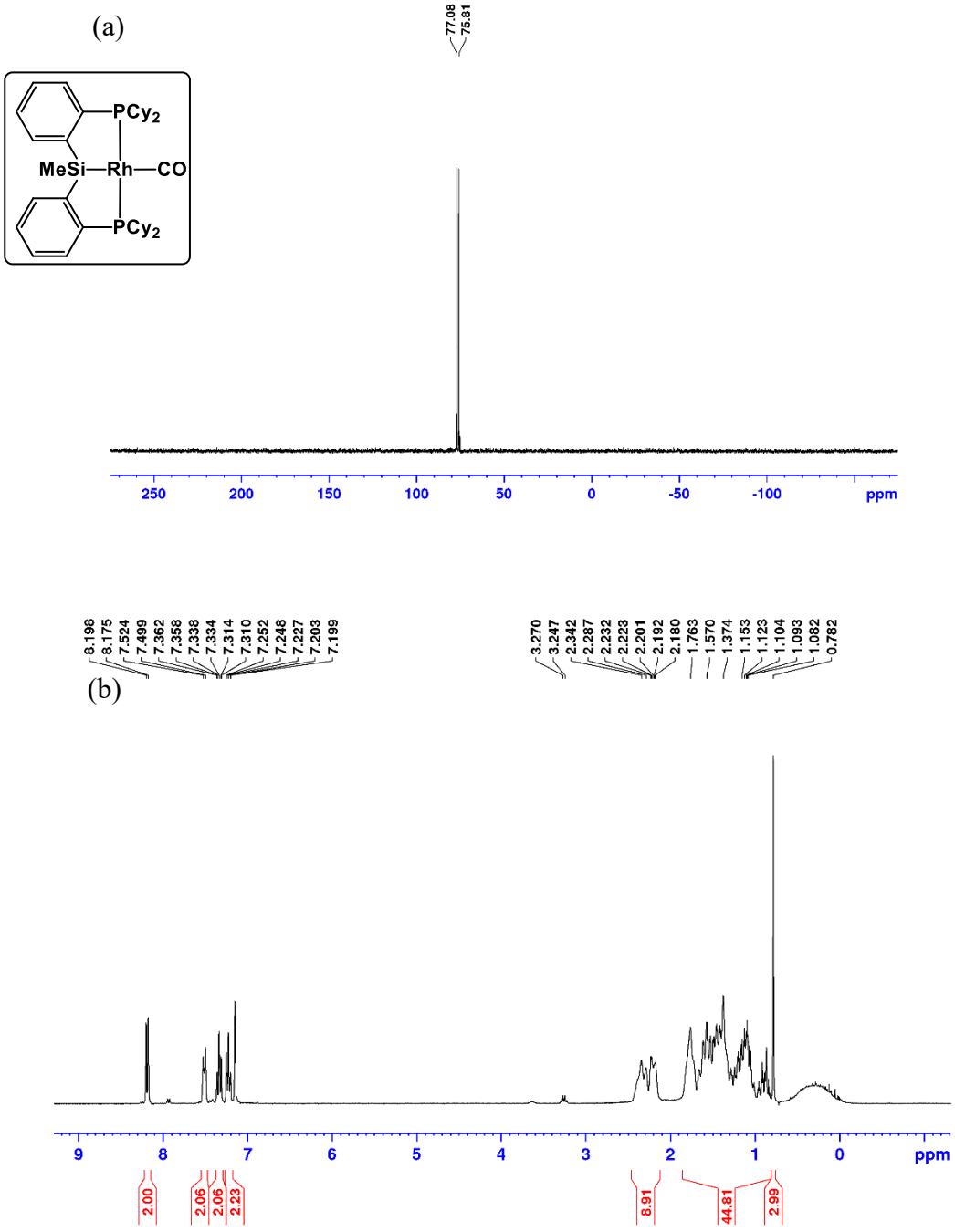

Figure B65. For **4-9** $^{13}C\{^{1}H\}$ NMR spectrum (125.7 MHz, C_6D_6).

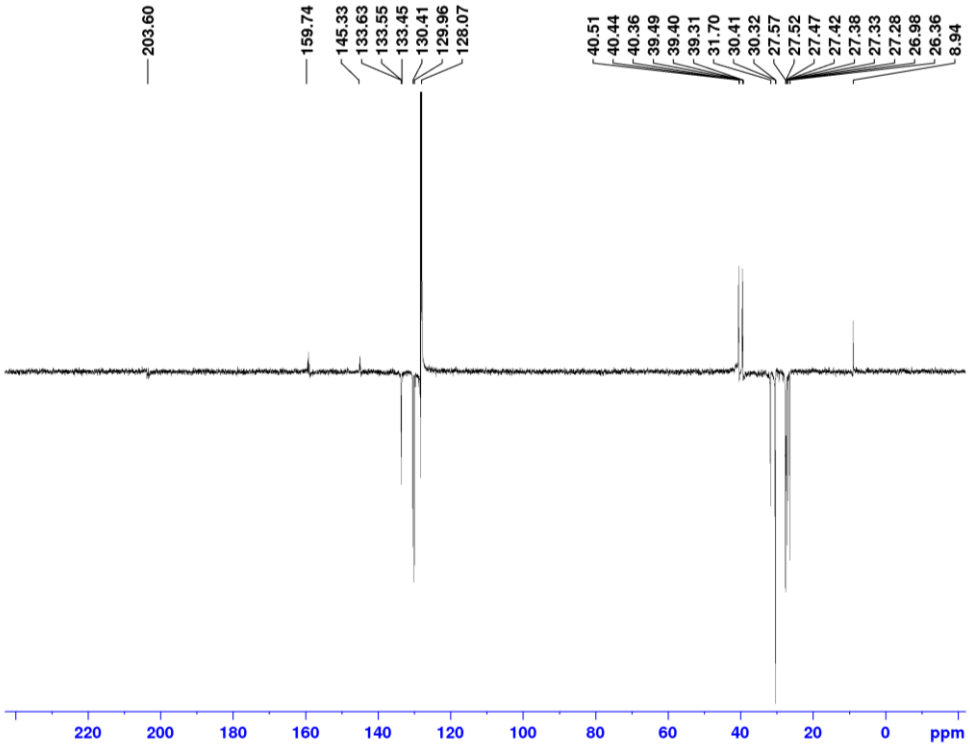

Figure B66. For **4-10** (a) $^{31}P\{^{1}H\}$ NMR spectrum (121.5 MHz, C_6D_6). (b) ^{31}P NMR spectrum (121.5 MHz, C_6D_6).

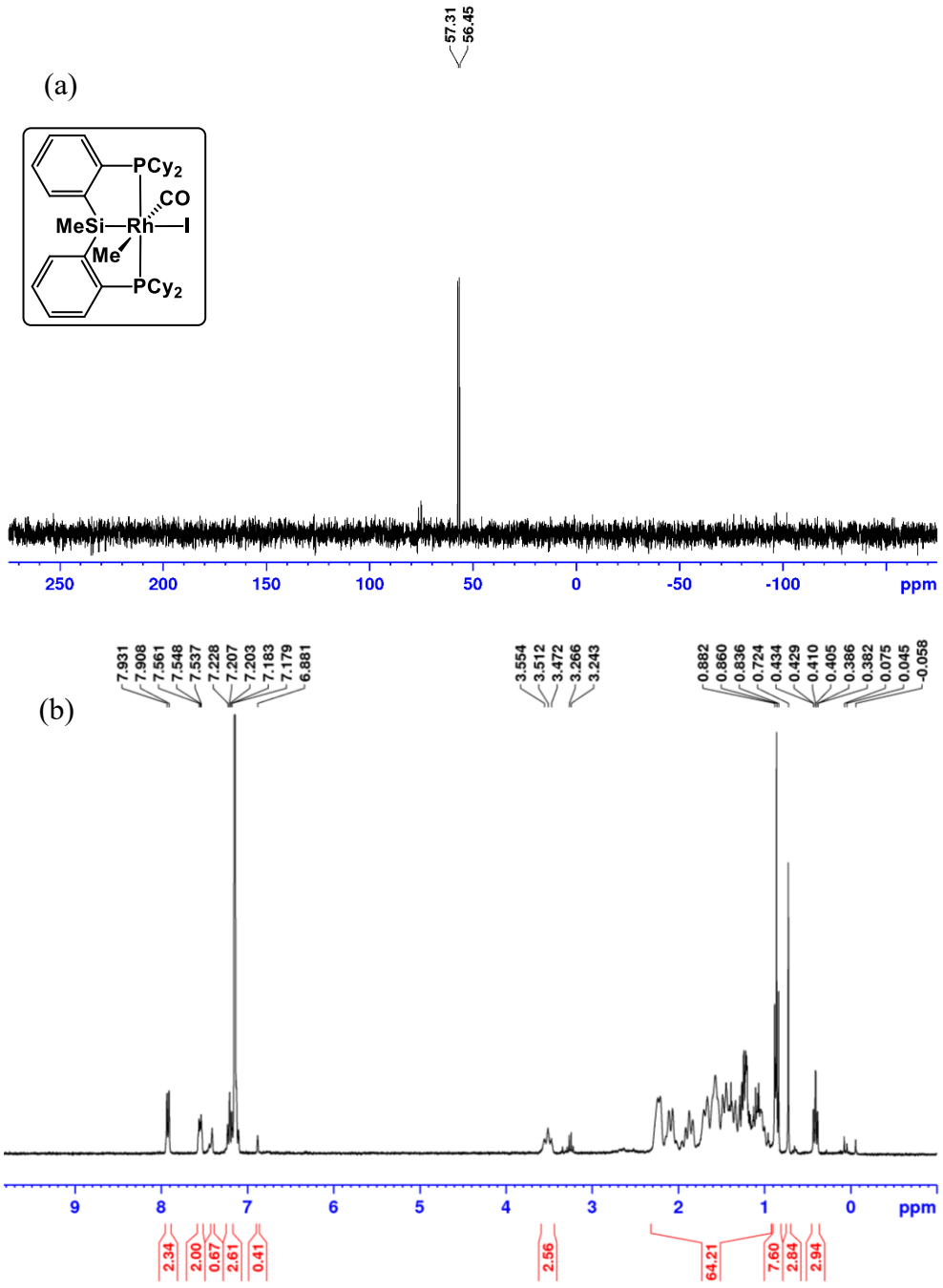

Figure B67. For **4-11a,b** (a) $^{31}P\{^{1}H\}$ NMR spectrum (121.5 MHz, C_6D_6). (b) ^{1}H NMR spectrum (300 MHz, C_6D_6). ▲ and ◊ indicate resonances associated with each isomer.

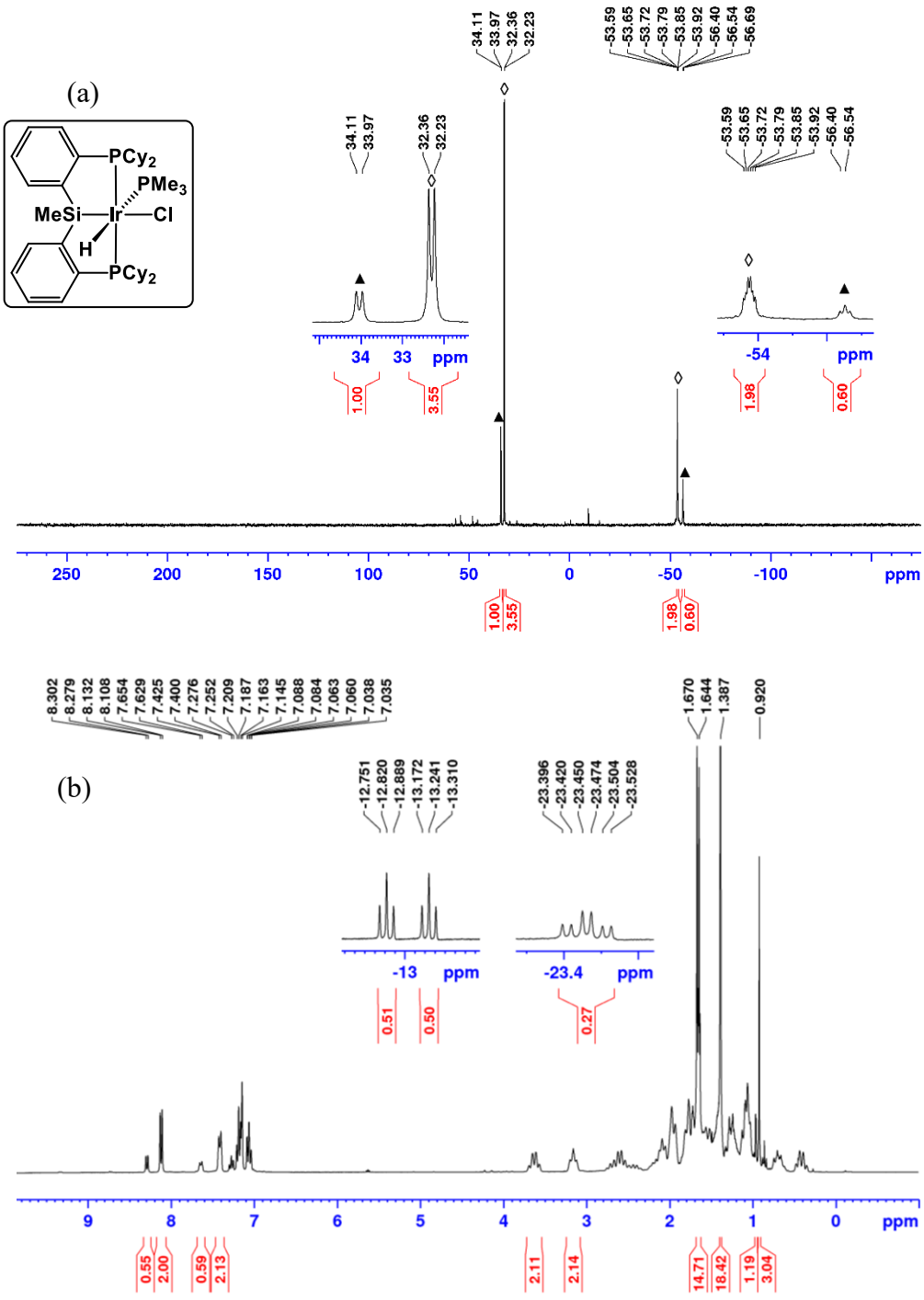

Figure B68. For **4-13** (a) $^{31}P\{^{1}H\}$ NMR spectrum (202.4 MHz, C_6D_6). (b) ^{1}H NMR spectrum (500 MHz, C_6D_6).

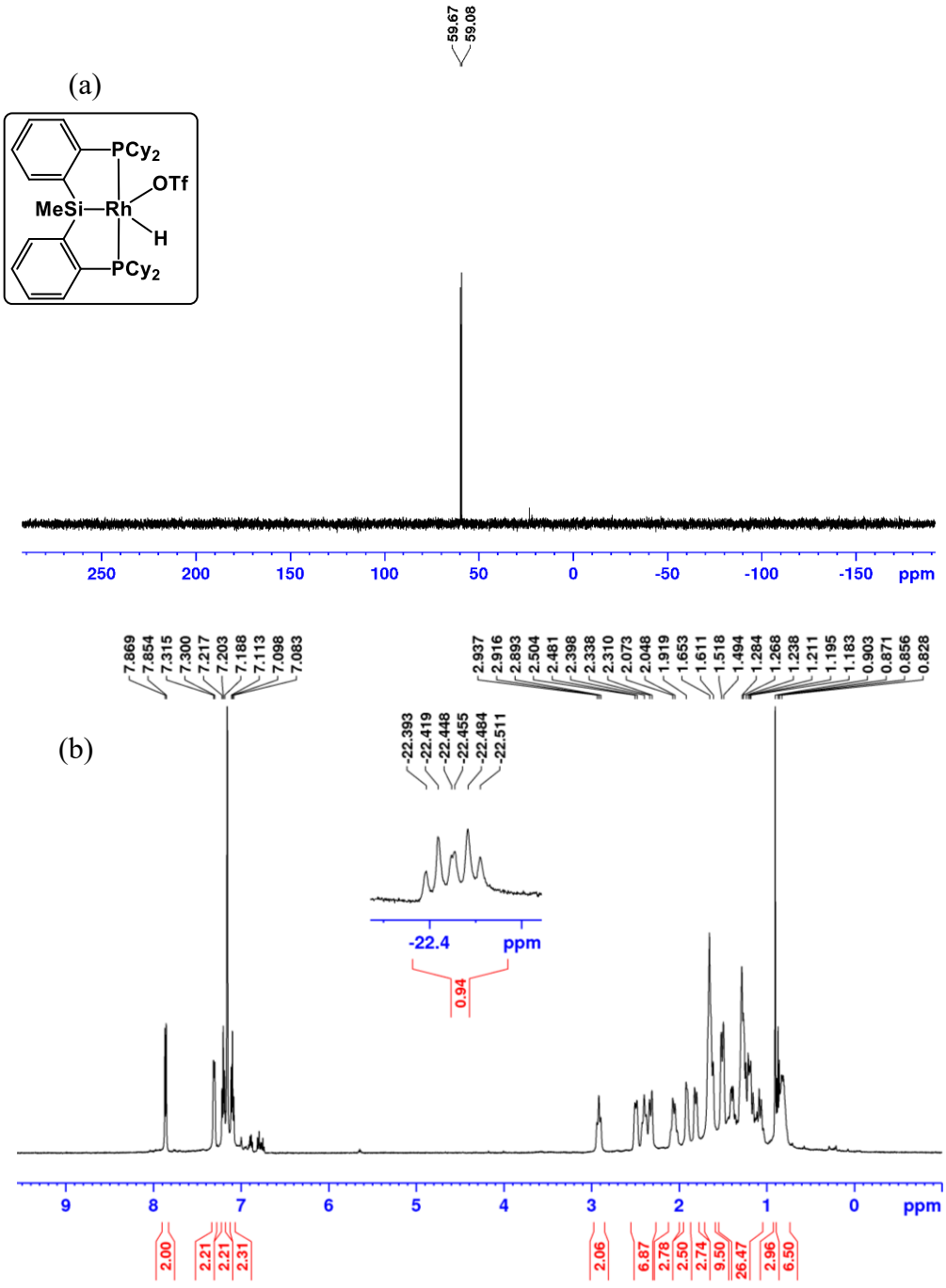

Figure B69. For **4-14** (a) $^{31}P\{^{1}H\}$ NMR spectrum (202.4 MHz, C_6D_6). (b) ^{1}H NMR spectrum (500 MHz, C_6D_6).

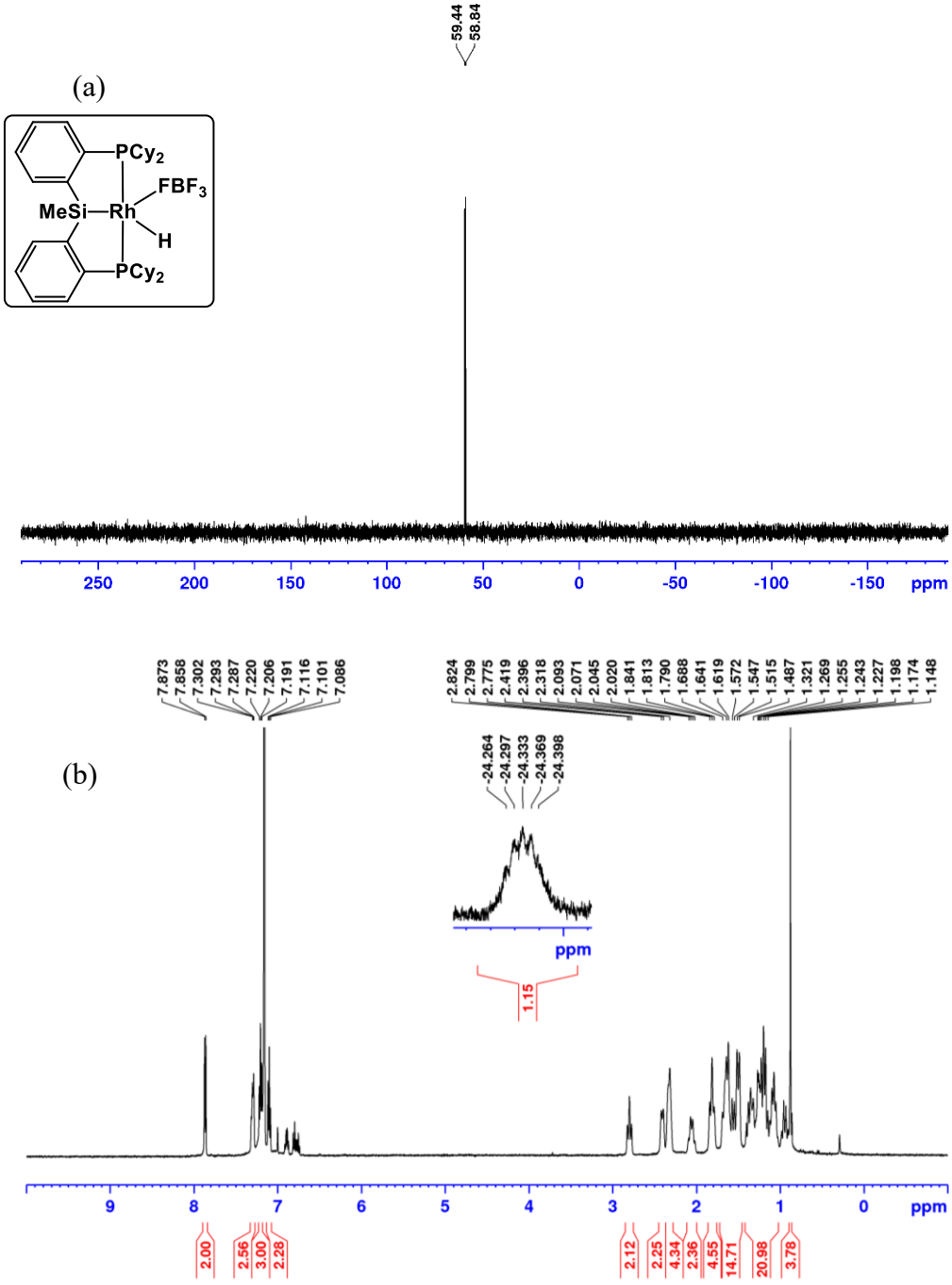

Figure B70. For **4-14** $^{19}F\{^{1}H\}$ NMR spectrum (470.6 MHz, C_6D_6).

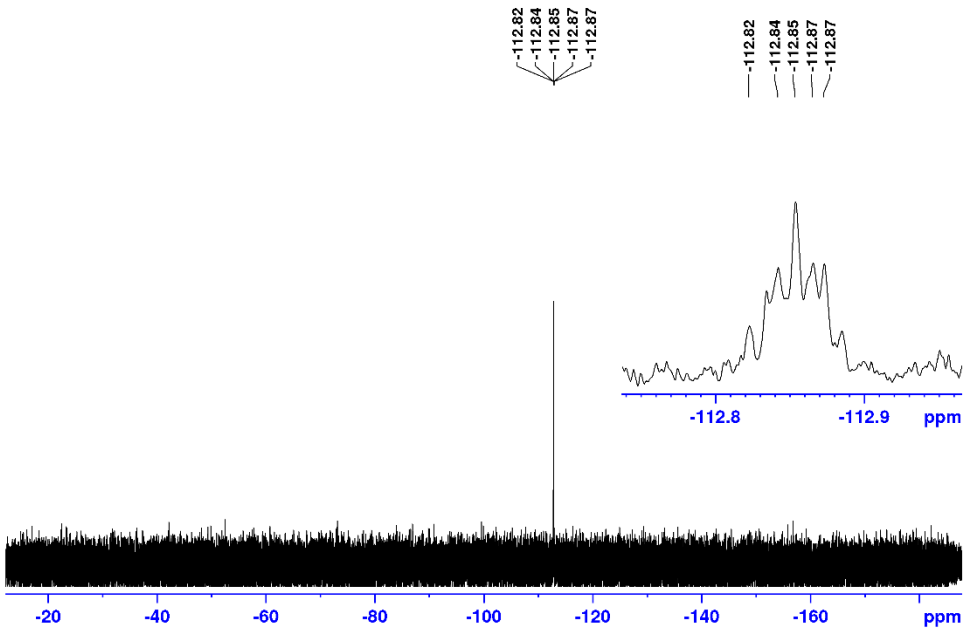

Figure B71. For **4-15** $^{31}P\{^{1}H\}$ NMR spectrum (121.5 MHz, C_6D_6).

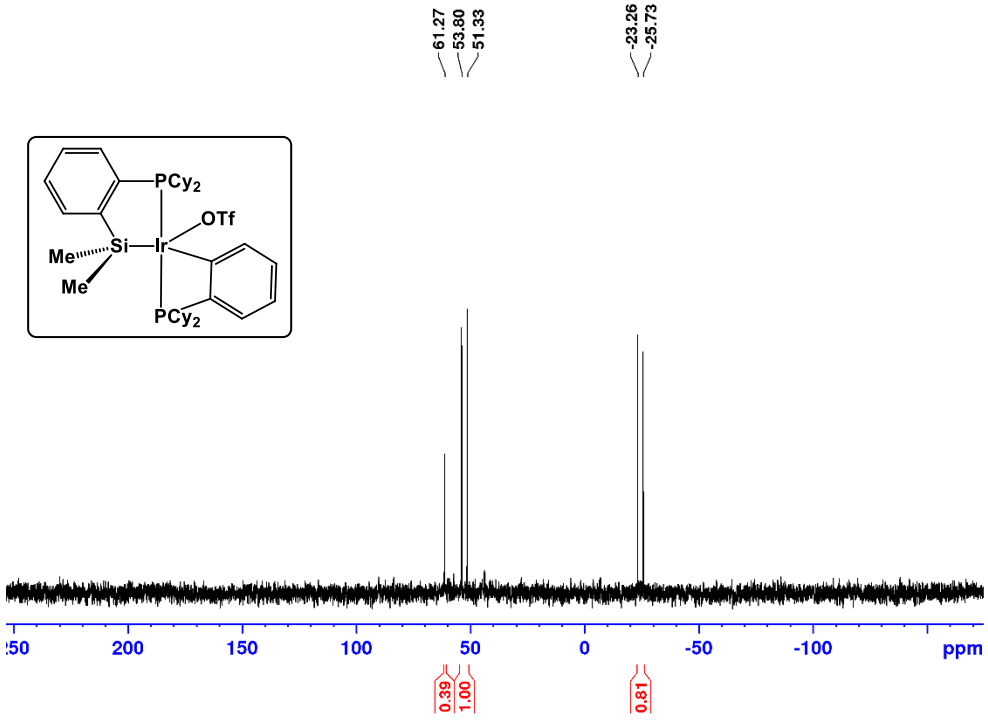

Figure B72. For **4-16** (a) $^{31}P\{^{1}H\}$ NMR spectrum (121.5 MHz, C_6D_6). (b) ^{1}H NMR spectrum (300 MHz, C_6D_6).

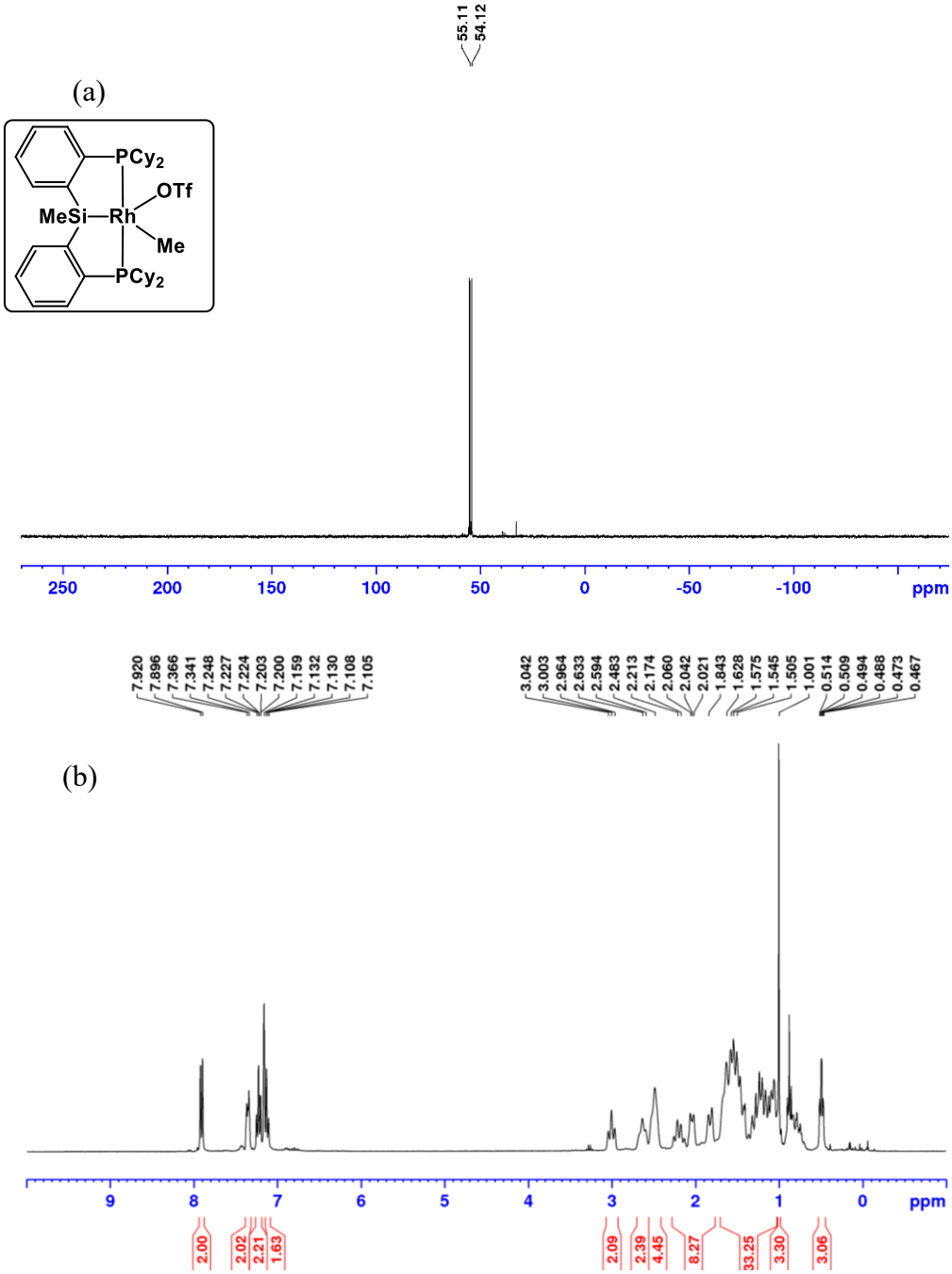

Figure B73. For **4-16** (a) ^{13}C NMR spectrum (121.5 MHz, C_6D_6). (b) $^{19}F\{^1H\}$ NMR spectrum (282.4 MHz, C_6D_6).

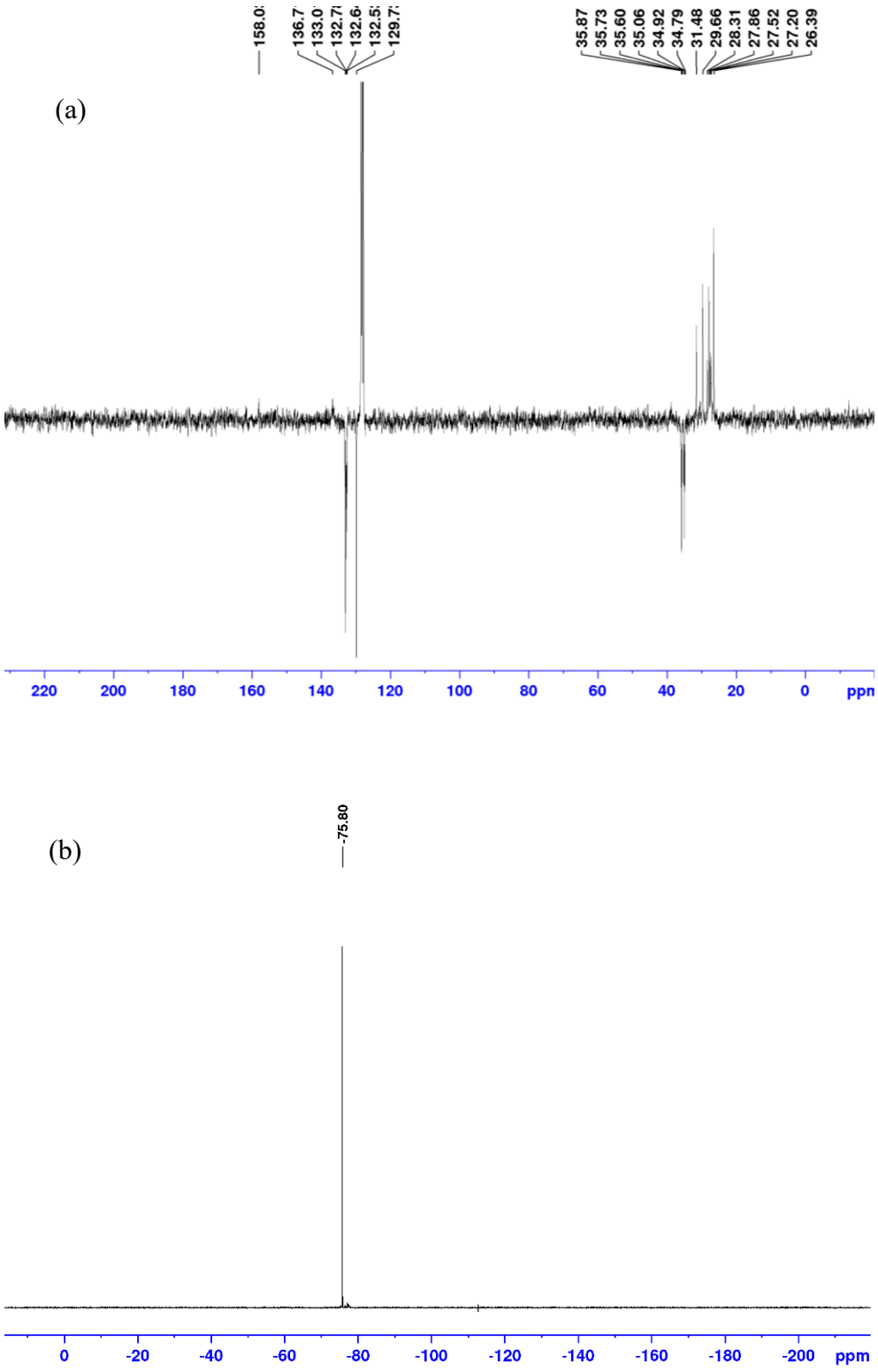

Figure B74. For **4-17** (a) $^{31}P\{^{1}H\}$ NMR spectrum (121.5 MHz, CD_2Cl_2). (b) ^{1}H NMR spectrum (300 MHz, CD_2Cl_2).

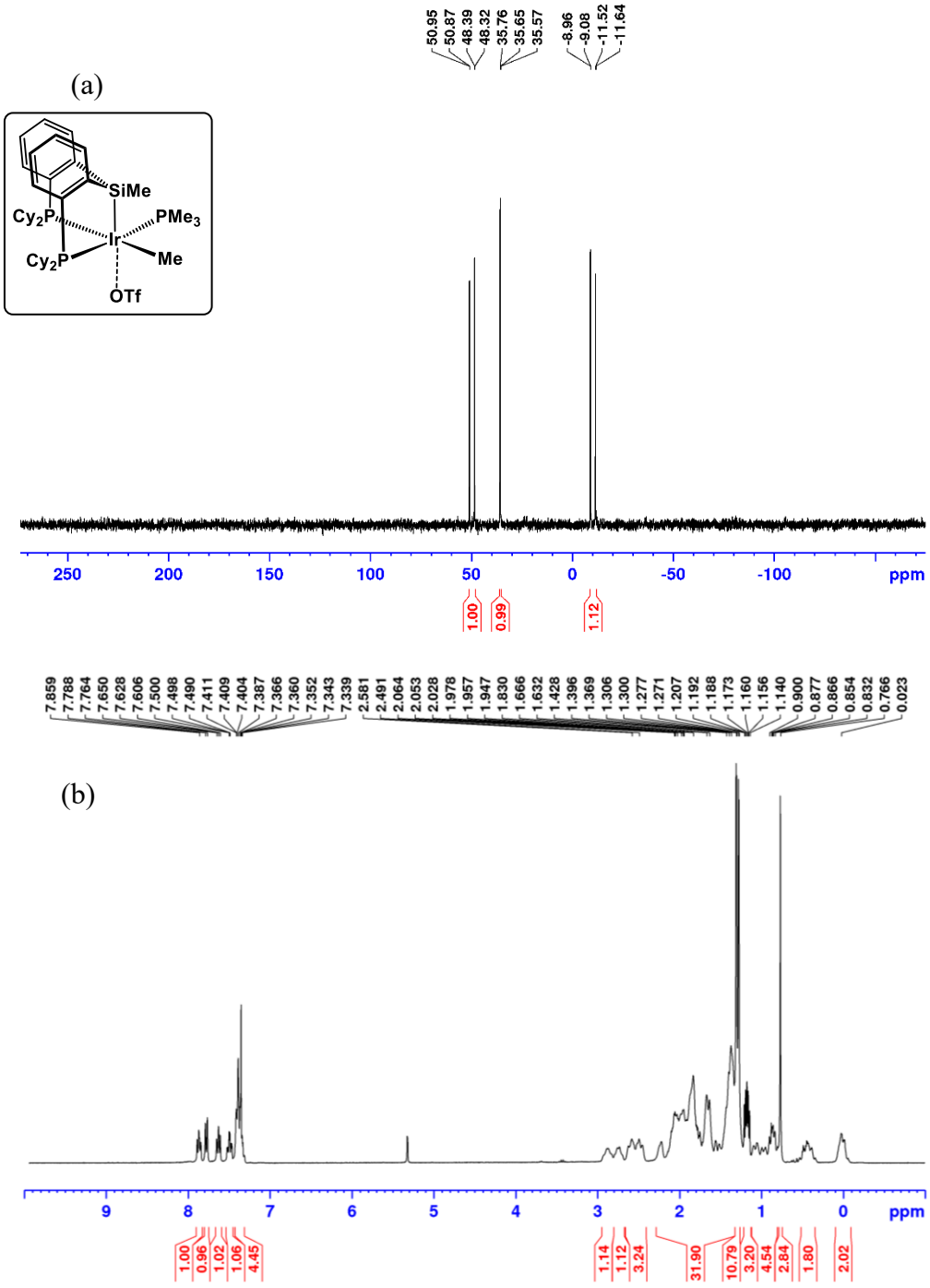

Figure B75. For **4-17** ^{13}C NMR spectrum (121.5 MHz, CD_2Cl_2).

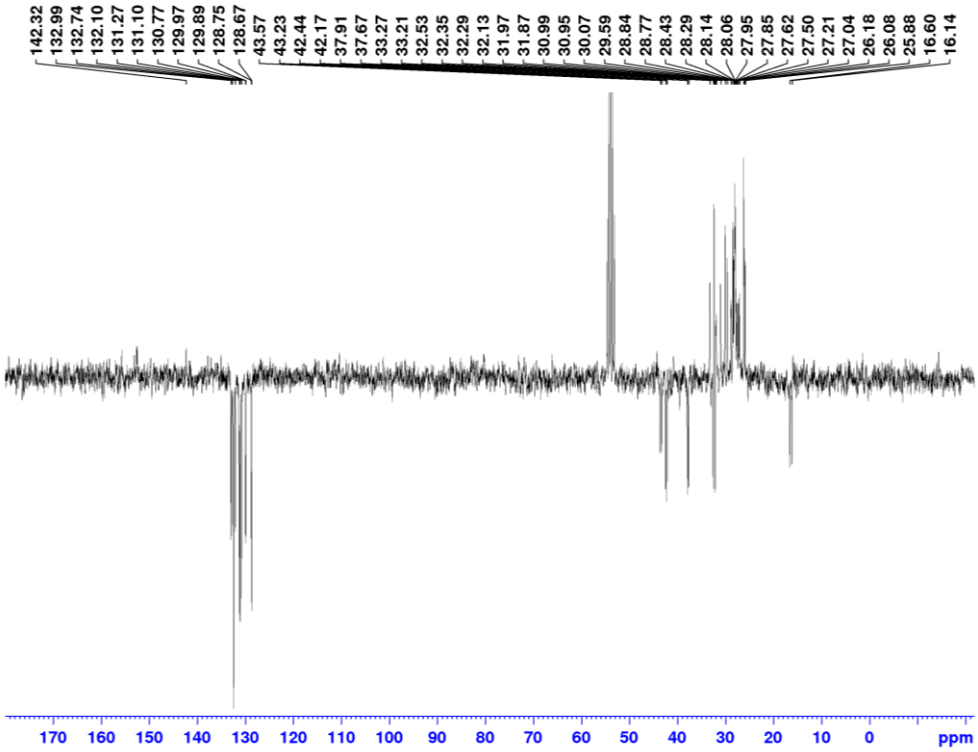

Figure B76. For **4-18** $^{31}P\{^1H\}$ NMR spectrum (121.5 MHz, C_6D_6).

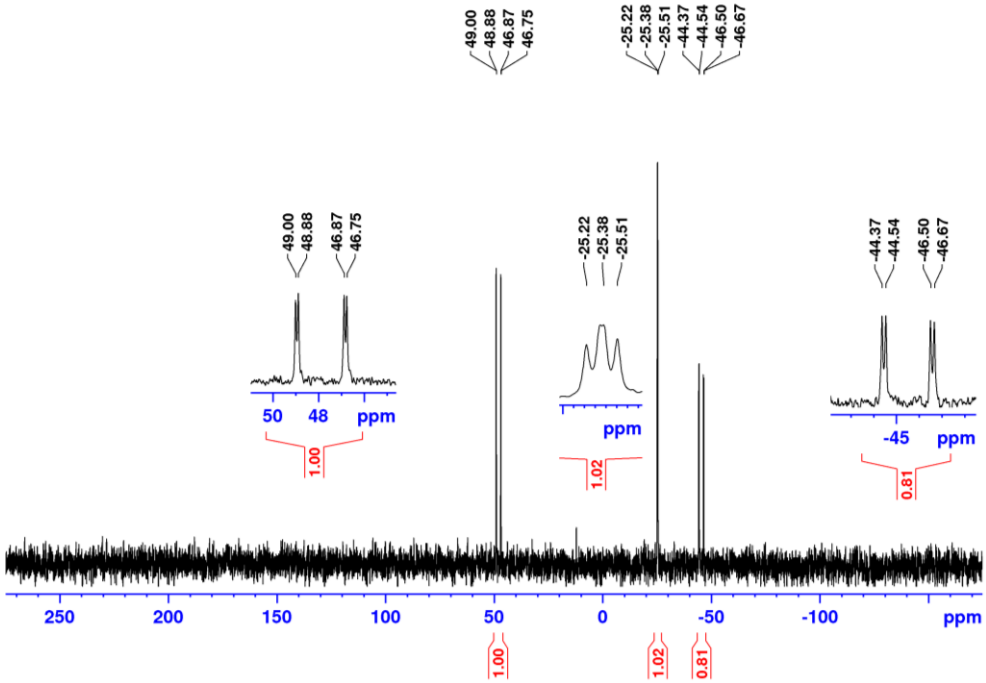

Figure B77. For **4-19** (a) $^{31}P\{^{1}H\}$ NMR spectrum (121.5 MHz, CD_2Cl_2). (b) ^{1}H NMR spectrum (300 MHz, CD_2Cl_2).

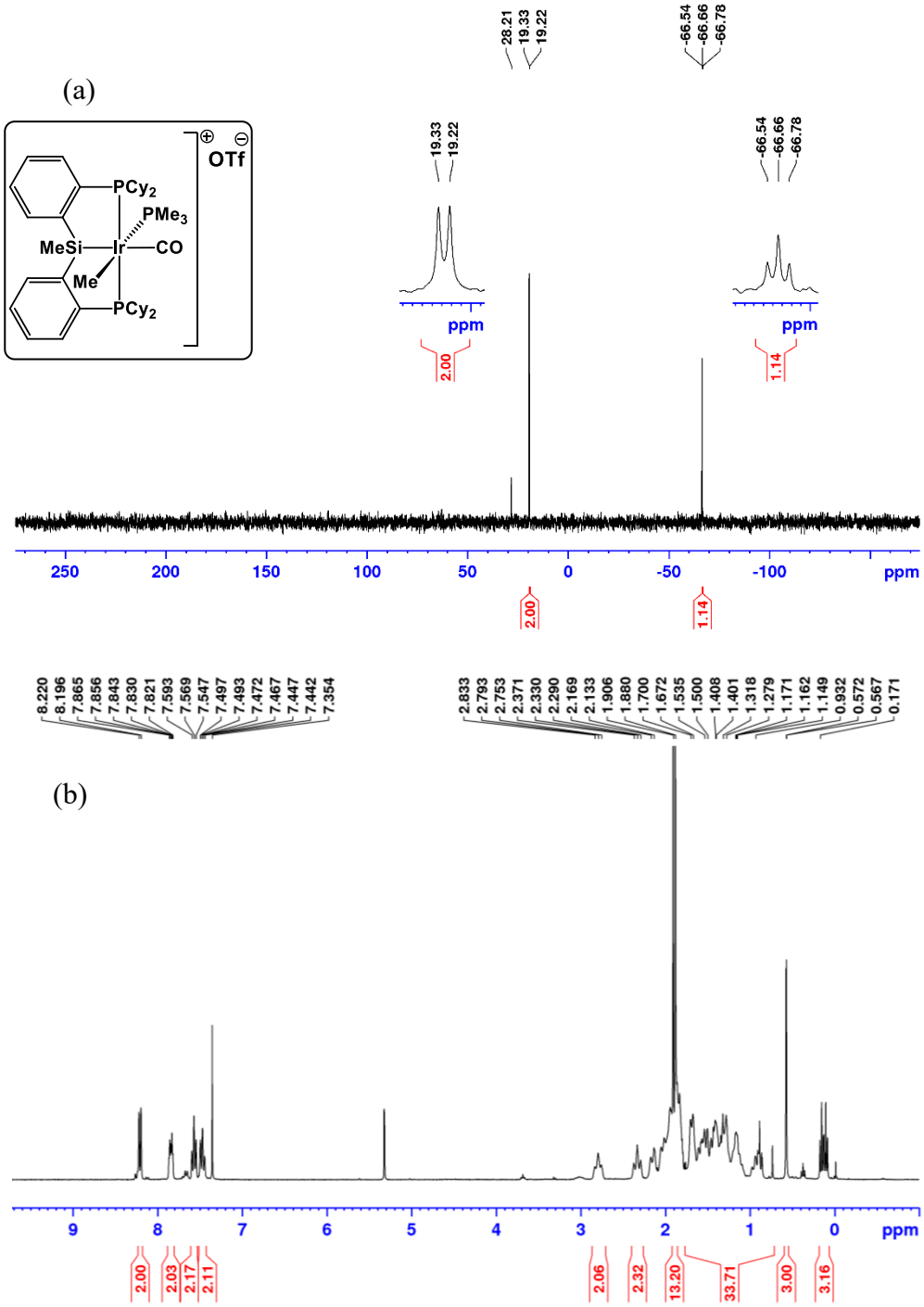

Figure B78. For **4-20** (a) $^{31}P\{^{1}H\}$ NMR spectrum (121.5 MHz, CD_2Cl_2). (b) ^{1}H NMR spectrum (300 MHz, CD_2Cl_2).

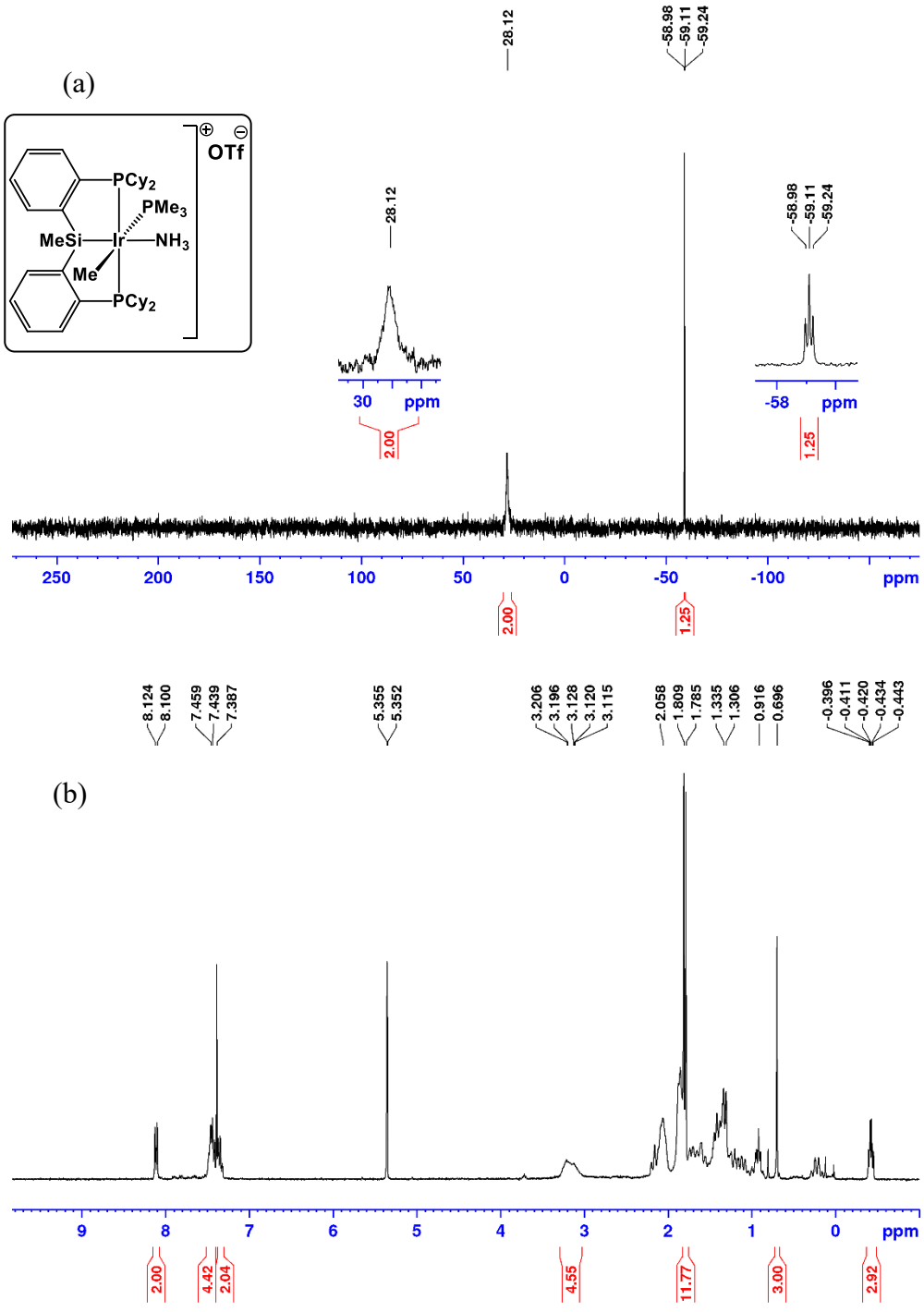

Figure B79. For **4-21** (a) $^{31}P\{^{1}H\}$ NMR spectrum (202.4 MHz, CD_2Cl_2). (b) ^{1}H NMR spectrum (500 MHz, CD_2Cl_2).

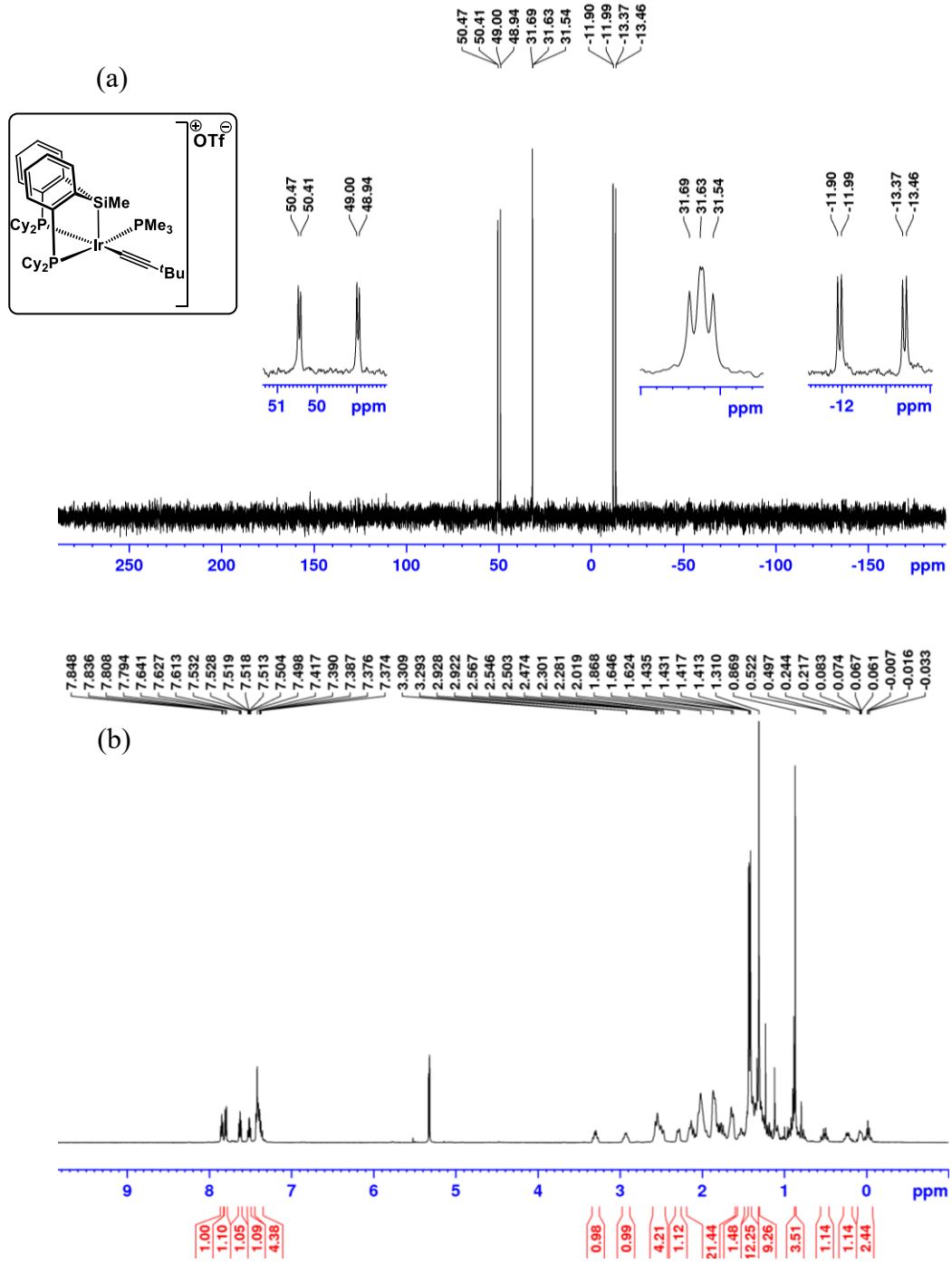

Figure B80. For **4-21** $^{13}C\{^{1}H\}$ NMR spectrum (125.7 MHz, CD_2Cl_2).

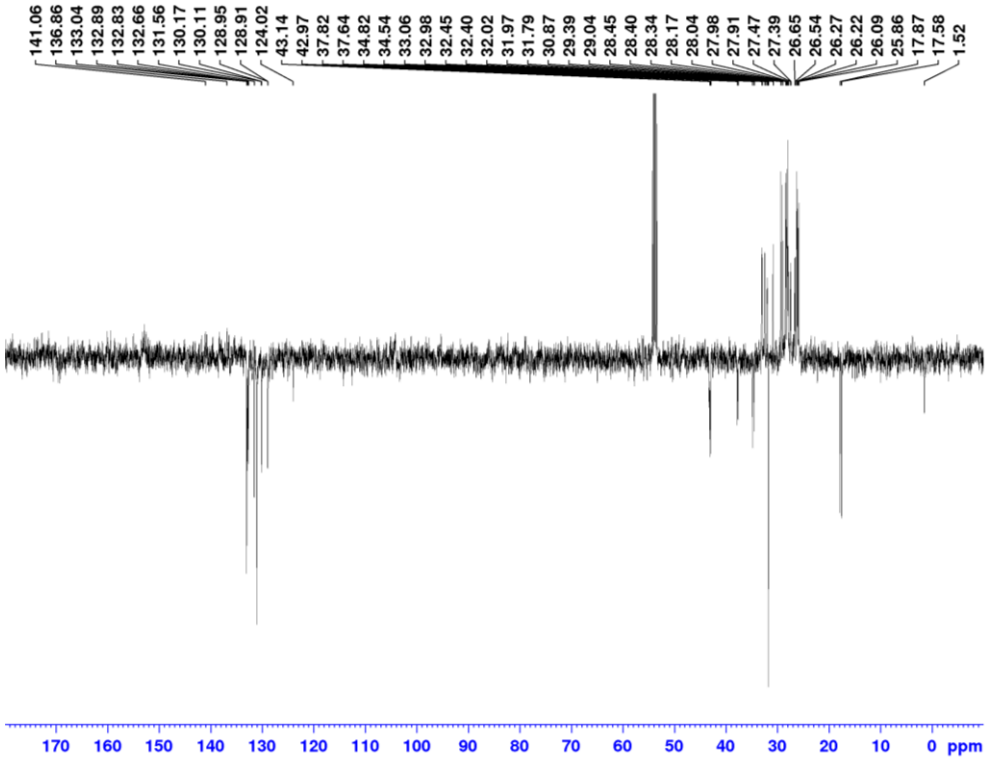

Figure B81. For **4-22** (a) $^{31}P\{^{1}H\}$ NMR spectrum (202.4 MHz, CD_2Cl_2). (b) ^{1}H NMR spectrum (500 MHz, CD_2Cl_2).

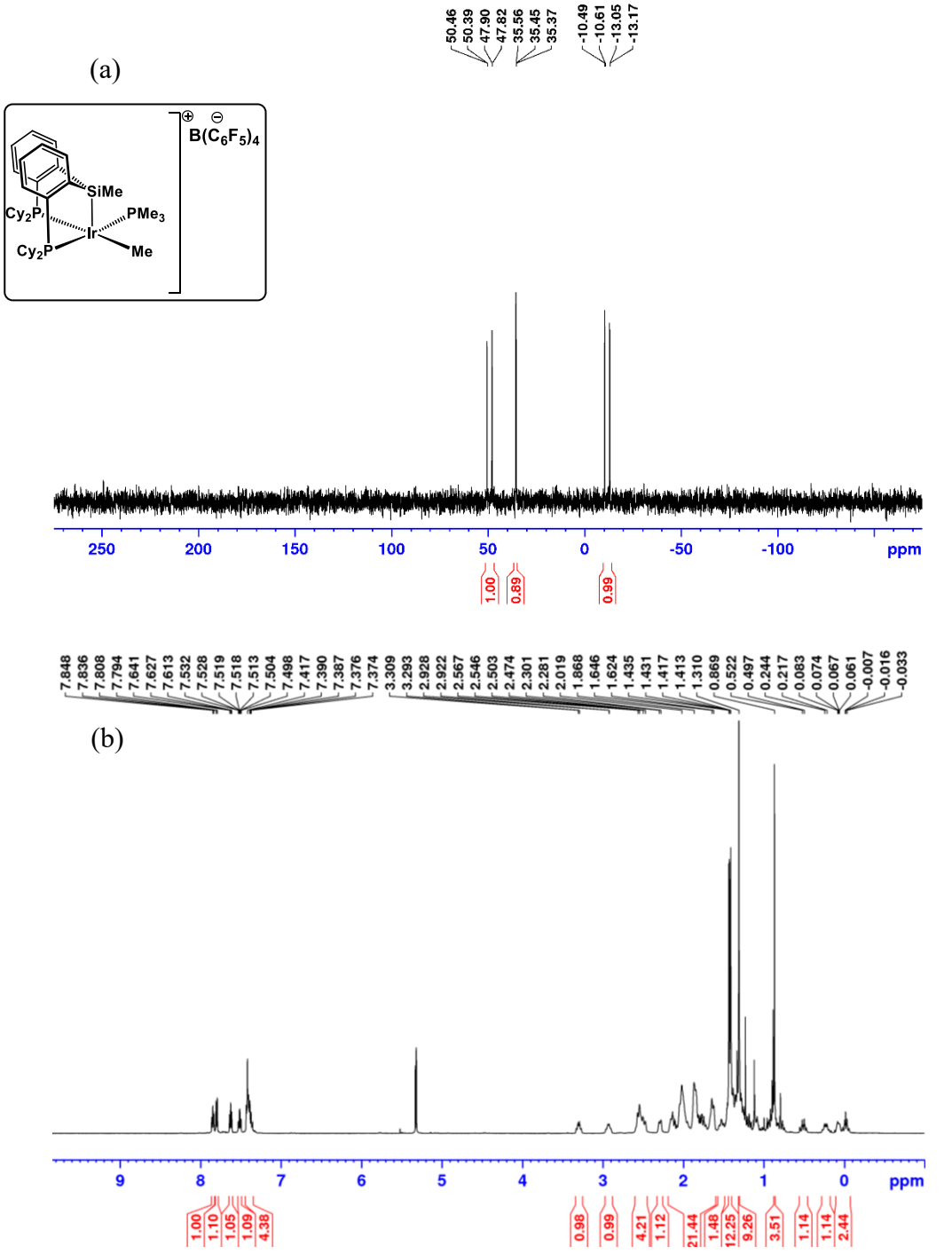

Figure B82. For **4-23** (a) $^{31}P\{^{1}H\}$ NMR spectrum (121.5 MHz, C_6D_6). (b) ^{1}H NMR spectrum (300 MHz, C_6D_6).

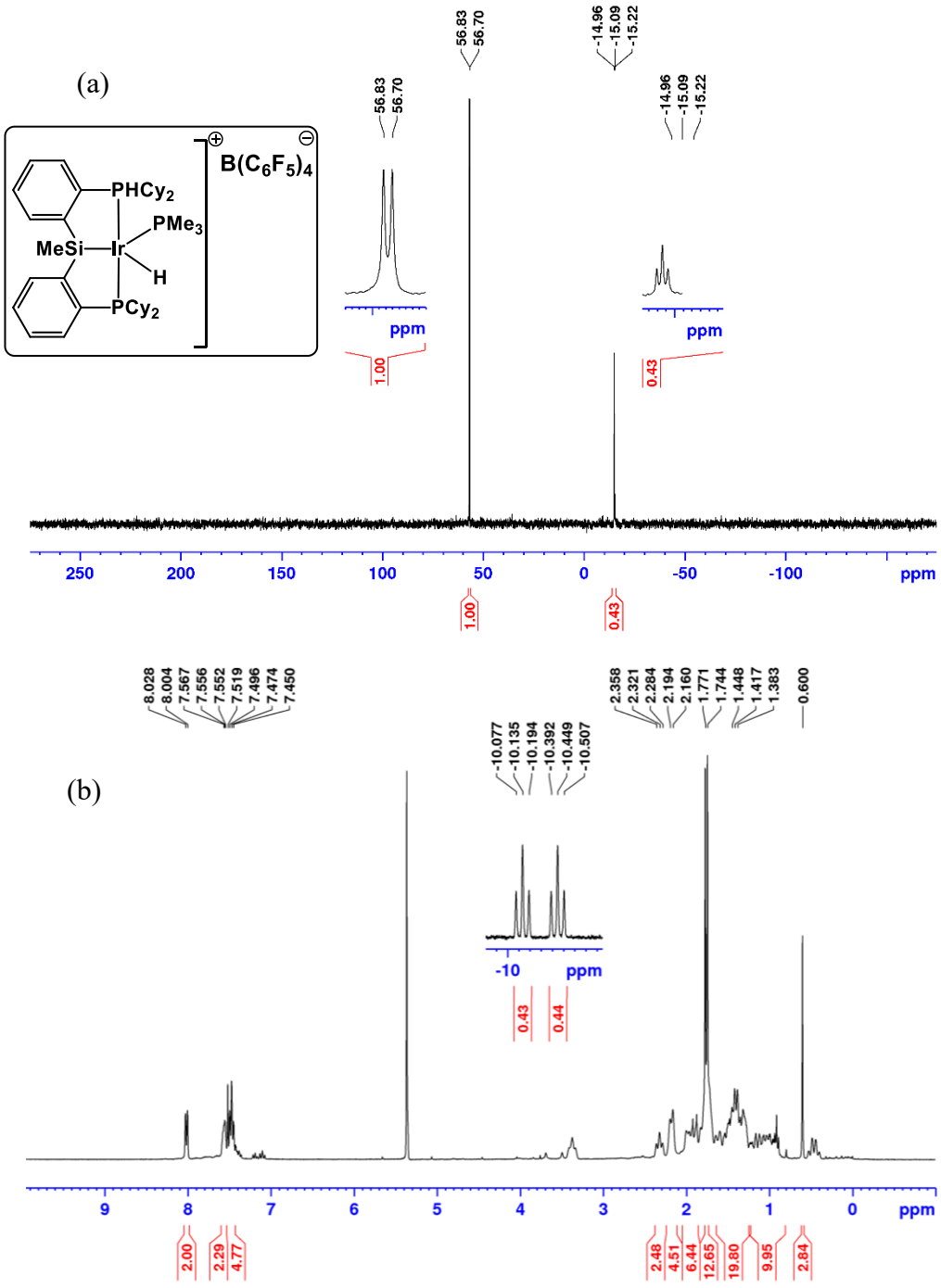

Figure B83. For **4-23** $^{19}F\{^{1}H\}$ NMR spectrum (282.4 MHz, C_6D_6).